UNIVERSITÉ DE MONTRÉAL

MACHINABILITY AND MODELING OF CUTTING MECHANISM FOR TITANIUM METAL MATRIX COMPOSITES

ROLAND BEJJANI
DÉPARTEMENT DE GÉNIE MÉCANIQUE
ÉCOLE POLYTECHNIQUE DE MONTRÉAL

THÈSE PRÉSENTÉE EN VUE DE L'OBTENTION
DU DIPLÔME DE PHILOSOPHIAE DOCTOR
(GÉNIE MÉCANIQUE)
DÉCEMBRE 2012

UNIVERSITÉ DE MONTRÉAL

ÉCOLE POLYTECHNIQUE DE MONTRÉAL

Cette thèse intitulée:

MACHINABILITY AND MODELING OF CUTTING MECHANISM FOR TITANIUM METAL MATRIX COMPOSITES

présentée par: BEJJANI Roland
en vue de l'obtention du diplôme de : Philosophiae Doctor
a été dûment acceptée par le jury d'examen constitué de :
M. LAKIS Aouni A., Ph.D., président
M. BALAZINSKI Marek, Ph.D., membre et directeur de recherche
M. ATTIA Helmi, Ph.D., membre et codirecteur de recherche
M. KISHAWY Hossam, PEng., membre et codirecteur de recherche
M. VADEAN Aurelian, Doct., membre
M. KOSHY Philip, Ph.D., PEng., membre

DEDICATIONS

To my parents: Maurice, Raymonde, Jen and friends.

ACKNOWLEDGEMENTS

This work could not have succeeded to make so many contributions to science without the support of knowledgeable and mature people who followed me all the way through this research; my professors. The support of the Aerospace Manufacturing Technology Centre, National Research Council Canada (AMTC-NRC), and the NSERC Canadian Network for Research and Innovation in Machining Technology (CANRIMT) are also acknowledged.

.

RÉSUMÉ

Les composites à matrice métallique de titane (CMMTi) sont une nouvelle classe de matériaux. Le CMMTi possède les caractéristiques des alliages de titane (légèreté, résistance et biocompatibilité) tout en ayant des propriétés physiques accrues lui conférant des avantages sur les alliages de titane. Ses nombreuses applications potentielles dans différents secteurs industriels tels l'aéronautique et le domaine biomédical en font un matériau de l'avenir. Déjà, certains fabricants de turbines montrent un grand intérêt pour de futures applications. Dans le domaine biomédical, le CMMTi offre un avantage pour les greffes osseuses présentant une action de glissement/frottement. Par contre, le CMMTi doit être usiné avant d'être utilisé comme pièce ou partie d'un assemblage, mais les particules solides de céramique ajoutées à l'alliage de titane rendent son usinage très difficile. De plus, l'intégrité de la surface du matériau après usinage est de première importance avant son utilisation dans un assemblage mécanique. La vie de l'outil est donc limitée en raison de son usure par l'action abrasive des particules dures, ainsi qu'à cause de la diffusion en raison de la température élevée de l'interface outil-matériau.

Lors de l'usinage, la durée de vie de l'outil et la rugosité de la surface de la pièce sont des préoccupations majeures pour les industriels. Trois approches ont été élaborées afin d'optimiser les paramètres d'usinage du CMMTi. La première approche expérimentale consiste en une méthode de planification d'expériences (TAGUCHI) utilisée afin d'identifier les effets des paramètres de coupe (vitesse, avance, et profondeur de coupe) sur les forces de coupe, la rugosité de surface, et l'usure de l'outil. Dans une deuxième approche, et afin de mieux comprendre le mécanisme de coupe du CMMTi, la formation de copeaux lors de la coupe a été analysée et un nouveau modèle de la bande de cisaillement adiabatique a été développé. Dans la dernière approche, et pour obtenir un meilleur outil d'analyse pour la compréhension du mécanisme de coupe, un nouveau modèle constitutif du CMMTi a été développé, en utilisant un modèle d'endommagement, à des fins de simulation. Les résultats des simulations de Modèle d'Élément Fini (MEF) ont permis de prévoir la température, les contraintes, les déformations et l'endommagement du matériau. Ces dernières informations peuvent être utilisées pour l'analyse de l'usinage ainsi que pour des applications industrielles.

Dans la littérature, il n'y a pas d'études antérieures concernant l'usinage du CMMTi. Dans la première approche expérimentale, la présente thèse est la première recherche qui a abouti à des

recommandations pratiques pour les choix des paramètres de coupe et pour l'évaluation des outils de coupe lors de l'usinage du CMMTi. À la suite de travaux expérimentaux et d'analyses, il a été trouvé que couper le CMMTi à haute vitesse est un procédé plus efficace et plus productif, puisque cela augmente la durée de vie de l'outil. Cela est en opposition avec la plupart des matériaux, où la durée de vie de l'outil diminue avec l'augmentation de la vitesse de coupe. Ce phénomène de coupe efficace à des vitesses élevées s'explique par le différent comportement des particules-outil à haute vitesse. En effet, à des vitesses plus élevées, moins de particules dures de TiC sont cassées, ce qui réduit l'usure de l'outil par abrasion. Afin d'augmenter encore plus la durée de vie de l'outil, une méthode d'usinage non conventionnelle a été utilisée. Cette méthode d'Usinage Assisté par Laser (UAL) a augmentée d'environ 180 % la durée de vie de l'outil. Pour comprendre les effets des particules sur l'usure des outils, des observations à l'échelle microscopique des particules dures par microscopie électronique à balayage (MEB) ont été effectuées, et l'interaction de l'outil-particules lors de la coupe a été identifiée. Cette dernière peut exister sous trois formes. Les particules peuvent être coupées à la surface, poussées à l'intérieur du matériau, ou même certains des morceaux des particules coupées peuvent être poussés à l'intérieur du matériau. Aucun cas d'arrachement de particules n'a été observé.

Certains alliages produisent des copeaux segmentés lorsqu'ils sont usinés. Les segmentations conduisent à la fluctuation des forces de coupe et à des vibrations possibles de l'outil de coupe, ce qui peut affecter négativement la surface finie. Étant donné que le découpage du CMMTi implique des segmentations dans les copeaux; la deuxième approche de ce projet de recherche a été centrée sur la compréhension de la formation de bandes de cisaillement adiabatique (BCA) dans les copeaux segmentés. Dans la littérature, différentes opinions existent pour le lieu de commencement des fissures dans le copeau. Pour comprendre la formation du copeau et l'initiation des fissures dans le processus de segmentation lors de la coupe du CMMTi, j'ai conçu un nouveau « Quick Stop Device» (QSD) qui a été utilisé pour immobiliser l'action de coupe. Le nouveau dispositif possède plusieurs avantages par rapport aux autres modèles trouvés dans la littérature en termes d'efficacité et de sécurité. En outre, à l'aide d'une analyse multi-échelle (macro et nano) en utilisant la microscopie électronique à balayage (MEB) et microscopie électronique à Transmission (TEM), un nouveau modèle pour l'évolution de la microstructure des grains à l'intérieur des BCA a été élaboré. Ce nouveau modèle est le premier à être développé pour le CMMTi, et est basé sur des observations des graines et des dislocations à l'échelle

atomique. Le modèle montre que des nouveaux nano-grains et sous-grains, caractérisés par une faible densité de dislocation, sont formés à l'intérieur des BCA. Cependant, aucune transformation de phase n'a été observée dans la BCA.

Dans la dernière approche du projet de recherche, une Méthode d'Éléments Fini (MEF) a été utilisée afin d'analyser les différents paramètres physiques (comme la température, les contraintes, la déformation, et l'endommagement) impliqués lors de l'usinage du CMMTi. Dans la littérature, la simulation d'usinage du CMMTi n'a jamais été réalisée, donc un nouveau modèle de comportement constitutif a été développé à l'aide de données de forces de coupe et des essais de traction. Pour simuler le processus de segmentation, un modèle d'endommagement a été ajouté. Ce modèle a donné de bonnes prédictions de la géométrie des segmentations du copeau et des forces de coupe. Afin d'avoir une meilleure compréhension de l'effet de l'UAL sur le mécanisme de coupe, la source de chaleur de l'UAL a été simulée et incorporée dans le même modèle de simulation par MEF. La simulation de copeaux segmentés avec l'UAL n'a jamais été faite auparavant pour le CMMTi, ni pour aucun autre matériau. L'analyse de la simulation par MEF a montré que l'UAL augmente la température globale du copeau, mais qu'il diminue la température maximale de l'interface outil/copeau. Cela explique l'augmentation de la durée de vie de l'outil lors de l'utilisation de l'UAL qui a été constatée expérimentalement. Une analyse plus approfondie a démontré que la température de transformation de phase n'est pas atteinte à l'intérieur les copeaux, ce qui a été également observé expérimentalement par TEM. Afin d'étudier l'endommagement et la séquence de la segmentation, une analogie a été faite entre la simulation du MEF et la formation de copeaux observée expérimentalement. Dans les deux cas, le commencement de la fissure ou de l'endommagement ne s'est jamais produit à l'extrémité de l'outil. Des analyses progressives dans la simulation du MEF ont montré que l'endommagement se produit de façon cyclique au milieu du segment, puis à la surface du matériau.

Ce projet de recherche a mené à diverses contributions en termes de résultats expérimentaux, de conception mécanique, de modèle de microstructure et de modélisation par MEF. En d'autres termes, les contributions sont: de nouvelles recommandations de coupe pour le CMMTi, le développement d'un nouveau QSD, le développement d'un nouveau modèle pour l'évolution de la microstructure de la BCA, le développement d'un nouveau modèle d'élément fini pour le CMMTi avec UAL et segmentations. Les résultats de cette recherche aideront les ingénieurs pour l'optimisation et l'analyse de l'usinage du CMMTI, et serviront également d'outil

de prédiction d’usinage. Par conséquent, cette recherche va promouvoir de nouvelles applications pour le CMMTi pour de nombreuses industries et donnera un impact favorable sur l'économie canadienne. Les résultats de cette recherche ont mené à la publication de 10 articles.

ABSTRACT

Titanium Metal Matrix composites (TiMMC) is a new class of material. The enhanced properties of TiMMC provide it with many advantages over titanium alloys. TiMMC is a material of the future and has many potential applications in the aeronautical sector, as in the turbines' cold section parts, and in biomedical applications, for example in bone transplants where a sliding/rubbing action is present. Turbine engine manufacturers already show a great interest in TiMMC for future applications. However, TiMMC requires machining in order to be used as part of an assembly, but the abrasive action of the added ceramic TiC particles, combined with the problems of cutting titanium alloys, make it a very difficult to cut material. Therefore, the tool life is limited, due to the abrasion wear from the hard particles and to the diffusion wear due to the high temperature of the tool-chip interface that characterizes the cutting of titanium alloys.

When machining, tool life, and surface roughness are major concerns for industrials. In order to optimize the machining of TiMMC, three approaches (stages) were used. First, a TAGUCHI method for the design of experiments was used in order to identify the effects of the machining inputs (speed, feed, depth) to the output (cutting forces, surface roughness). To enhance even further the tool life, Laser Assisted Machining (LAM) was also experimented. In a second approach, and in order to better understand the cutting mechanism of TiMMC, the chip formation was analyzed and a new model for the adiabatic shear band in the chip segment was developed. In the last approach, and in order to have a better analysis tool to understand the cutting mechanism, a new constitutive model for TiMMC for simulation purposes was developed, with an added damage model. The FEM simulations results led to predictions of temperature, stress, strain, and damage, and can be used as an analysis tool and even for industrial applications.

In the literature, no research studies are found on the machining of TiMMC. The first experimental approach of this current research is the only study to provide practical recommendations for determining the cutting parameters and for evaluating different cutting tools for machining TiMMC. Following experimental work and analysis, I found that cutting TiMMC at higher speeds is more efficient and productive because it increases tool life. This is in opposition to most materials, where higher cutting speeds reduce tool life. This phenomenon of efficient cutting at higher speeds was explained by the different tool/particles behavior. It was

found that at higher speeds, fewer hard TiC particles are broken, resulting in reduced tool abrasion wear. In order to further optimize the machining of TiMMC, an unconventional machining method was used. In fact, Laser Assisted Machining (LAM) was used and was found to increase the tool life by approximately 180 %. To understand the effects of the particles on the tool, micro scale observations of hard particles with SEM microscopy were performed and it was found that the tool/particle interaction while cutting can exist under three forms. The particles can either be cut at the surface, pushed inside the material, or even some of the pieces of the cut particles can be pushed inside the material. No particle de-bonding was observed.

Some alloys produce segmented chips when machined. Segmented chips lead to the fluctuation of the cutting forces and to the possible vibration of the cutting tool, both of which may negatively affect the finished surface. Since cutting TiMMC involves segmentation in the chips; the second approach of this research was aimed at the understanding of the Adiabatic Shear Band (ASB) formation in the segmented chips. In the literature different opinions exist for the location at which crack initiation occurs. To understand the chip formation and study the crack initiation in the segmentation process when cutting TiMMC, I designed a new "Quick Stop Device" which was used to freeze the cutting action. The new device has multiple advantages over other models found in the literature in terms of efficiency and safety. Furthermore, using a multi-scale (macro and nano) analysis with Scanning Electron Microscopy (SEM), and Transmission Electron Microscopy (TEM), a new model for the microstructure and grain evolution inside the ASB was developed. This new model is the first of a kind to be developed for TiMMC and is based on observations of grains and dislocations at the atomic scale. The model shows that inside the ASB, new nano-grains and nano-cells characterized by a low dislocation density are formed. However, no phase transformation was found in the ASB.

In the last approach of the research project, a FEM tool was used to analyze the different physical parameters (such as temperature, stress, strain and damage) involved when machining TiMMC. In the literature, the simulation of the machining of TiMMC has never been performed. Therefore, a new constitutive model was developed using room and high temperature cutting data, and tensile tests. To simulate the segmentation process, a damage model was added. The damage model is based on the work required in a tensile test until fracture occurs. The model gave good predictions for the geometry of chip segmentation and for the cutting forces. In order to have a better understanding of the effect of LAM on the cutting mechanism, the LAM heat

source was simulated and embedded in the same FEM simulation model. Simulations of segmented chips with LAM have never been done before for TiMMC and for any other material. The analysis of the FEM simulation gave unexpected results, and showed that although LAM does indeed increase the overall chip temperature, the peak tool/chip temperature decreases. This could explain the experimental finding of increased tool life when using LAM. Further analysis showed that the phase transformation temperature wasn't reached inside the chips. This was also shown experimentally with TEM observations. To study the damage and the segmentation sequence, an analogy was made between the FEM model and the experimental chip formation. In both cases the crack initiation, or damage, was never shown to occur at the tool tip. Analysis of incremental steps in FEM simulation showed that the damage occurs in a cyclic manner in the middle of the segment, then at the free surface.

The research project led to various contributions to knowledge in terms of experimental findings, mechanical design, microstructure model, and FEM modeling. In other words, the contributions involved new cutting recommendations for TiMMC, the development of a new 'quick stop device", the development of a new model for microstructure evolution in the ASB and the development of a new FEM model for TiMMC involving LAM and segmentation. The results of this research will serve engineers in the optimization and analysis of TiMMC machining, and can be used as a prediction tool for the machining of TiMMC. Therefore, costly trials and errors in machining experiments will be avoided. Consequently, this research will promote the applications of TiMMC for many industries, and will have a positive impact on the Canadian economy. This project led to the publication of 10 papers.

TABLE OF CONTENTS

LIST OF TABLES

LIST OF FIGURES

NOMENCLATURE AND ABBREVIATIONS

ASB	Adiabatic Shear Band
C-L	Cockcroft Latham damage model
DOE	Design Of Experiment
FEM	Finite Element Method
FIB	Focused Ion Beam
JC	Johnson Cook constitutive equation
LAM	Laser Assisted Machining
QSD	Quick stop device
SAD	Selected Area Diffraction
SEM	Scanning Electron Microscopy
TEM	Transmission Electron Microscopy
TiMMC	Titanium Metal Matrix Composite
F_c	Cutting Force
F_t	Thrust Force
F_f	Feed Force
m	Shear friction factor
T	Temperature
T_m	Melting temperature
$\bar{\varepsilon}$	Effective strain
$\dot{\bar{\varepsilon}}$	Effective strain rate
ε_{fn}	Fracture strain
σ^*	True stress
$\bar{\sigma}$	Flow stress

LIST OF APPENDICES

INTRODUCTION

Metal matrix composites (MMCs) are a new class of materials that consist of a non-metallic phase distributed in a metallic matrix, with properties that are superior to those of the constituents. The principal use of these materials is for lightweight load-bearing applications on account of their enhanced mechanical and physical properties. Metal matrix composites reinforced with ceramic particles have been developed during the last decade for applications where high wear resistance and light weight are required [1].

This research project is focused on the optimization of machining titanium metal matrix composites (TiMMC). Three approaches were used in the optimization process. First, an experimental statistical design of experiments method (TAGUCHI) was used to identify the effects of machining inputs (speed, feed, depth of cut) on the process output (cutting forces, cutting temperature, surface integrity). To enhance even further the tool life, Laser Assisted Machining (LAM) was performed. In a second approach and in order to better understand the cutting mechanism of TiMMC, the chip formation was analyzed and a new model for the adiabatic shear band in the chip segment was developed. In the last approach, Finite Element Method (FEM) was used in order to have an efficient analysis tool for understanding the cutting mechanism of TiMMC and predict the process output. A new constitutive model for TiMMC was developed for simulation purposes, with an added damage model. The FEM simulation results gave predictions of temperature, stress, strain, and damage.

The research project resulted in ten publications, nine of which as first author. Four of them are in refereed journals; the remaining six are conference papers (the publications are listed in appendix B).

Problem definition

TiMMC is a new material; therefore there is a lack of information in the literature concerning its machining. TiMMC is a very difficult to cut material and combines all the problems associated with machining titanium alloys and MMCs. Titanium alloys are considered as difficult to cut materials and are characterized by a high tool/chip interface temperature and a

strong affinity to many tool materials [2]. The ceramic particles in the MMCs improve its wear resistance properties, but also cause high abrasive wear on the cutting tool during machining [3]. This results in a very poor tool life and inconsistent part quality and thus limits the use of TiMMC in many applications.

TiMMC and CermeTi® MMCs, which are developed by Dynamet Technology, Inc., consist of a non-metallic phase TiC (10% in weight) distributed in a titanium or titanium alloy matrix [4]. The main advantages of TiMMC are their higher room and high temperature tensile strength, increased modulus of elasticity, better creep strength, good fracture toughness, high wear resistance and other benefits typical of titanium alloys (lightweight, corrosion resistance, etc.) [4]. As shown in Table 1, most of their physical properties are superior to those of their base matrix.

Most MMCs consist of an aluminum matrix reinforced with hard ceramic particles such as silicon carbide, alumina or boron carbide [3]. Some machining data can be found in literature for aluminum MMCs, however no substantial research has been done on TiMMC machining. An intensive literature review and gap analysis for the machining of titanium and aluminum MMC led to important findings, which were used for the experimental design of experiments (Figures 1-2). Therefore, this research will aim at providing value to the fundamental understanding of cutting TiMMC, as well as by supplying practical recommendations related to machining TiMMC.

Table 1- Physical properties of TiMMC [4]

Material	Yield Strength (MPa)	Tensile Strength (MPa)	Elastic Modulus (GPa)	Shear Modulus (MPa)	Fracture Toughness ($MPa/m^{1/2}$)
TiMMC	**1014**	**1082**	**135**	**51.7**	**40**
Ti-6Al-4V	**862**	**965**	**116**	**44**	**80**

Identifying the wear process associated with machining MMCs:

The process of tool abrasion wear while cutting MMCs is somewhat different from the standard process in cutting metals. In fact, due to the high abrasive nature of the material itself both two-body and three-body models have been generally accepted as the dominant abrasion

wear mechanisms. Figure 1 shows the issues associated with two-body and three-body abrasive wear mechanisms when machining MMCs; as well as, issues when machining titanium alloys. In two-body wear mode, the hard reinforcements penetrate into the cutting tool's surface and scrape out material. In three-body wear, the trapped hard reinforcements may roll and slide on the tool, resulting in surface wear [5]. Figure 2 is a cause and effect chart which depicting the causes of tool life reduction.

Understanding of the effects of controlled parameters on tool wear in cutting TiMMC

For a better understanding of tool wear mechanisms, the effects of controlled and uncontrolled variables should be studied. For that purpose, a newly developed quick stop device (QSD) was designed and used to freeze the cutting process in order to understand the initiation of the cutting phenomenon at different cutting speeds. One of the advantages of TiMMC is that its microstructure is composed of titanium Alpha and Beta phases, and of hard particles of TiC. Therefore, in the presence of plastic strain, it results in the breaking of the hard particles, and in the displacement and/or change of these phases. This means that studying the formed chip will provide information on the displacement and on the plastic strain of each zone of the chip profile. Following this thorough study of chip initiation, a new model for chip formation will be developed. Since abrasion is the dominant wear mode when machining MMCs, the effect of heat will be evaluated. Heating the workpiece softens the material and therefore decreases the cutting forces. This reduces the abrasion load of the particles on the tool. Moreover, the softer material may affect the particles' de-bonding, and may even help the particles to be pushed into the material while machining. On the other hand, the heat might raise the tool's temperature, which may lead to a softer tool, meaning that less energy is required for tool abrasion. All these issues are addressed, and Figure 3 presents a chart of the objectives for the understanding of chip morphology and the effect of heat in machining.

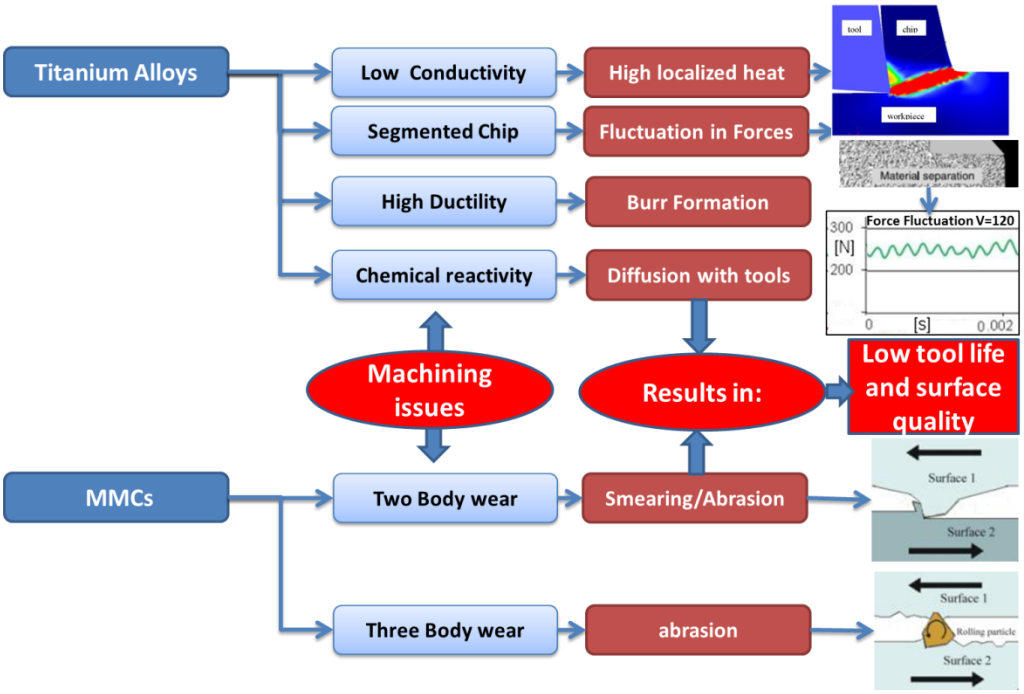

Figure 1-Wear issues associated with MMC and titanium alloys

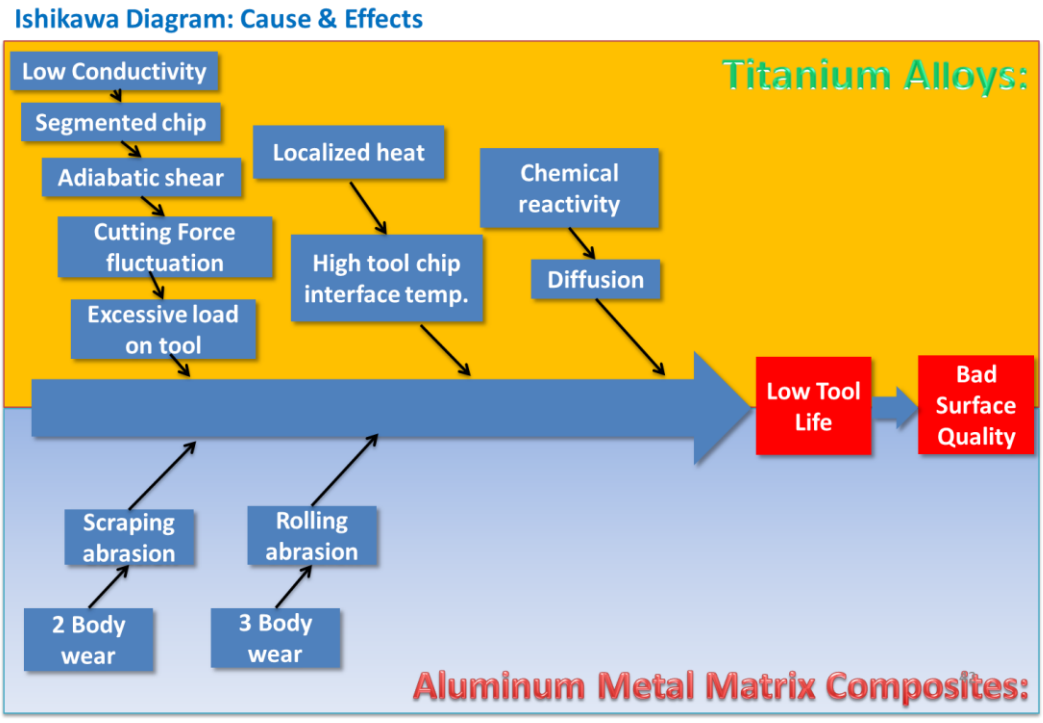

Figure 2- Aluminum MMC and titanium machining issues leading to low tool life

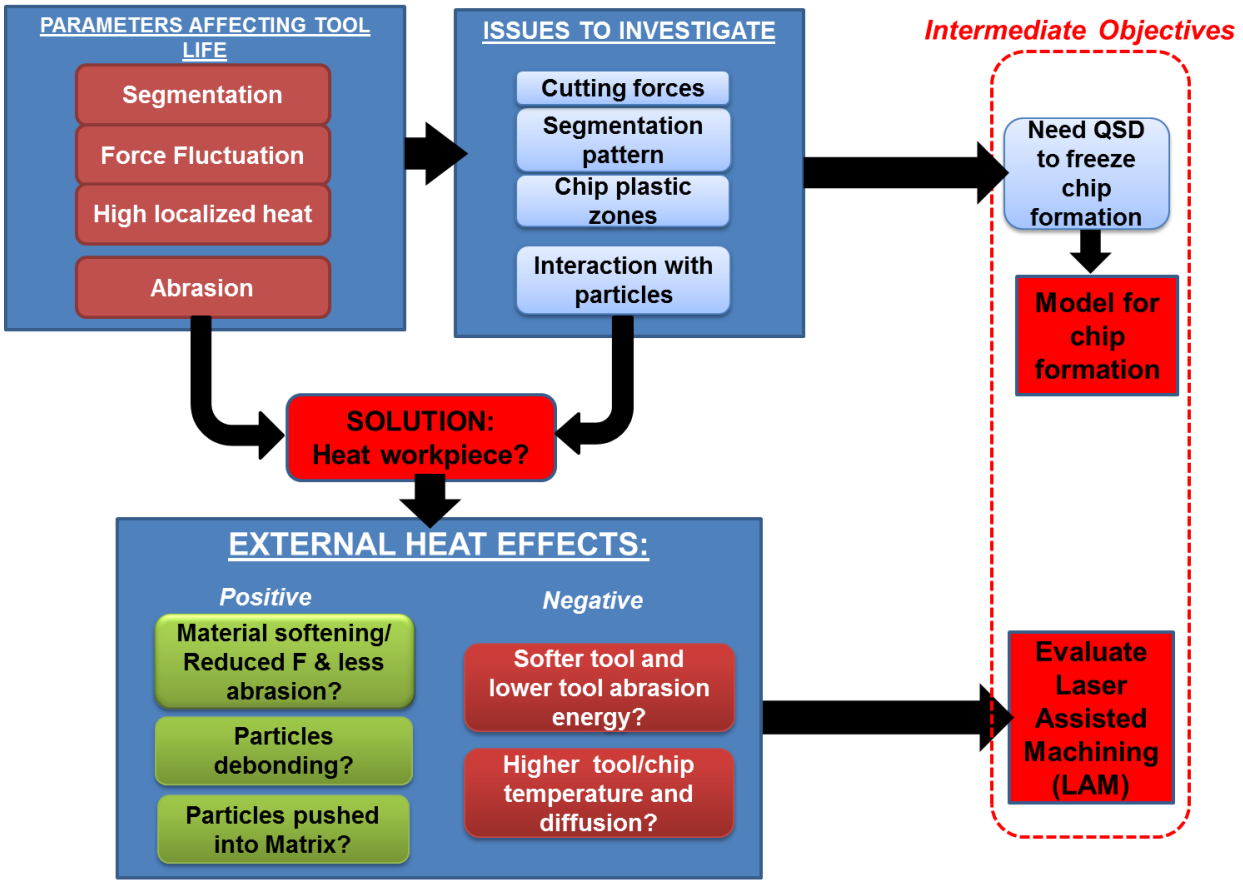

Figure 3-Chip morphology, LAM and QSD objectives

Research objectives

The first phase of this research was based on experimental investigations in order to provide practical and optimum cutting parameters for turning TiMMC. Furthermore, since this material is made near to net shape, only finishing operations were considered. The main output parameters to optimize were: surface roughness, cutting forces and tool life. Subsequently, the data obtained from the machining experiments were analyzed. To further enhance the tool life, Laser Assisted Machining (LAM) was performed and studied. At a later stage, Finite Element Method (FEM) for turning TiMMC was performed. The FEM model was used as a tool for predicting the strain, stress, strain rates, temperature and damage in the chip formation when cutting TiMMC.

Specific objectives

1. Experimental investigation of the turning process of TiMMC with different state-of-the-art tools in order to find the optimum cutting conditions. The main optimum parameters considered are: surface roughness, cutting forces and tool wear.
2. Assessment of machining with controlled laser heat source and evaluation of the effect of Laser Assisted Machining (LAM) on the tool/particles interaction. Furthermore, effort is to be made to evaluate if this enhances the already found optimum conditions.
3. Developing a model for the chip formation of TiMMC using the data from the chip morphology and the chip root obtained with the newly designed Quick Stop Device (QSD).
4. Development of an Adiabatic Shear Band (ASB) microstructure evolution model for the segmentation phenomenon and study of the crack initiation in the chips.
5. Development of a constitutive equation for TiMMC (dependence of flow stress on strain, strain rate, and temperature) and conduction of a FEM (Finite Element Method) simulation with the DEFORM software in order to simulate chip formation. The FEM simulation is to be validated using the experimental results for turning TiMMC with and without laser assisted heating.

Hypothesis statements

1. **Segmented** chip is typical for Ti alloys. No machining research has been done before on TiMMC; however, we expect to have segmentation and the problems associated with it.
2. **Abrasion** wear is the main mode of tool wear in aluminum MMC. Although, diffusion wear is common in Ti Alloys, we expect that abrasion wear is still the dominant wear mechanism for TiMMC.
3. With aluminum MMC, increasing the cutting **speed** increases the tool wear rate. This is also expected with TiMMC. Otherwise, a different cutting phenomenon occurs at high speeds.
4. Adding an external source of **heat** while machining TiMMC (as LAM) will make the material softer, and easier to cut. However when cutting titanium, high localized temperature will

occur at the tool tip which may cause diffusion wear. Therefore the additional heat source may accelerate the tool diffusion wear.

CHAPTER: 1- LITERATURE REVIEW

Metal Matrix Composites have emerged as an important class of material. They are being more and more used nowadays. However, their application in certain fields is limited due to the difficulties in machining them. The principal machining parameters that control machinability are intrinsic (such as cutting speed, feed rate, depth of cut and type of tool), and extrinsic parameters (such as particulate size, volume fraction and type of reinforcement) [6, 7].

1.1 Applications of Metal Matrix Composites (MMCs)

In recent years, the application of composite materials is among the most important developments made in material engineering. Metal matrix composites are now used in various engineering applications such as aerospace, marine, automotive and turbine compressors. The main advantages they have are their light weight, high strength, high stiffness and high temperature resistance.

Most often, some machining is required to produce a finished part. For industrial applications, when machining MMCs, a major concern is the selection of the appropriate cutting tool material and optimization of cutting speeds and feeds, which are related to the wear rate of the tool and the quality of the machining surfaces.

MMCs have great potential applications in the near future [8]; however, the hard particles inside the MMC makes machining a challenge to manufacturers. Many types of MMCs exist such as aluminum alloys, magnesium alloys, copper alloys and zinc alloys. The hard reinforcement can be silicon carbide (SiC), titanium carbide (TiC), aluminum oxide (Al_2O_3), silimulite or fibre glass. Soft reinforcements such as graphite, fly-ash and tale, are also used.

- *Brake rotors for German high speed train ICE-2*

Brake rotors for German high speed train ICE-2 made from a particulate reinforced Aluminium alloy ($AlSi_7Mg$+SiC particulates), supplied by Duralcan are shown in Figure 1.1. Compared to conventional parts made

Figure 1.1-Brake Rotor [9]

out of cast iron, these parts weigh 76 kg instead of the standard 120 kg per piece. Therefore, the MMC rotor offers an attractive weight saving potential. Moreover, an important reduction of the undamped mass is attained with MMC [9]. Figure 1.2 shows other applications in disk brakes [9].

- *Cylinder liner*

Porsche AG has developed the LOKASIL-composite technique (Figure 1.3). It is in use as a cylinder liner in the Porsche Boxter engine block. The MMC used is composed of $AlSi_9Cu_3$ alloy. The MMC contains 25% Si and is made with the squeeze casting technique. Figure 1.3 shows other applications in disk brakes [9].

Figure 1.2-W8LESS Rotor for motorbikes: AlMMC [9]

Figure 1.3- Cylinder liner [9]

- *Aerospace application: F–16 Ventral Fins*

Due to their high specific stiffness and strength, the F16 ventral fins are made from an MMC: 6092/SiC/17.5p rolled powder metal produced by DWA Composites. Previously they used 2024-T4 Al (Figure 1.4). The benefits are a decreased deflection, which provides a projected 4-fold increase in fin life and a reduction in maintenance, inspection and downtime [10].

Figure 1.4-F16 Ventral fins [10]

1.2 Applications of Titanium Metal Matrix Composites (TiMMC)

- *Knife blades*

Titanium metal matrix composites are used in a variety of components that take advantage of their unique combination of properties. For example, titanium composite knife blades (Figure 1.5) are harder, stiffer, and significantly more wear resistant than titanium knife blades manufactured with conventional titanium alloys. In fact, TiMMC has superior sharpness retention compared with high-performance steel knife blade materials [4].

Figure 1.5- Knife blades [4]

- *Military Vehicles*

The need to produce lightweight military vehicles for easy transportation by air has led to an interest in titanium for wheeled and track armored vehicles. However, in order to surpass the properties of commercial titanium alloys, which exhibit very poor wear resistance in non-lubricated metal-to-metal contact, TiMMC arose some interest. The US Army Tank-Automotive and Armaments Command (TACOM) is evaluating the possible usage of CermeTi® (TiMMC), mainly due to its light weight, strength, fracture toughness, higher modulus and significantly increased wear resistance [4].

- *Automotive Components*

There has been a general interest in MMCs in recent years for automotive applications (Figure 1.6); mainly TiMMC since it offers a combination of high strength and lower density than steel which permits the design of light weight components. The use of TiMMC in engine components such as valves, connecting rods and piston pins leads to fuel economy, reduced emissions, noise, vibration and harshness. Titanium-carbide (TiC) reinforced matrix offers additional advantages over conventional titanium alloys due to its higher modulus of elasticity, elevated temperature strength,

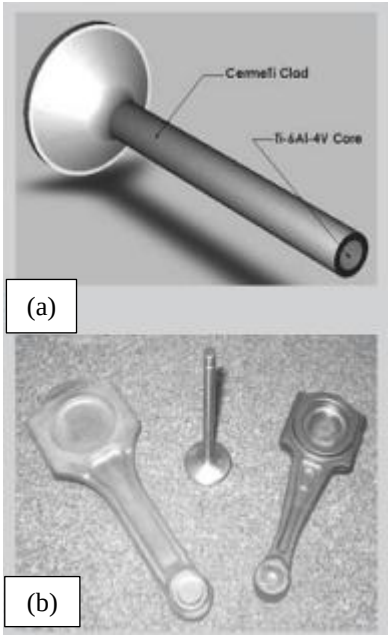

Figure 1.6- (a) valve, (b) connecting rods [4]

creep resistance and wear resistance. Furthermore, the powder metal of titanium composites is cheaper to process than the conventional manufacturing methods used for titanium materials. Comparing TiMMC with AlMMC for connecting rods, titanium matrix composites have increased absolute and specific strengths, better fatigue properties, and a higher elevated temperature strength. Moreover many steel parts can be substituted with TiMMC parts without a major redesign. A TiMMC connecting rod weighs 40% less than a high-strength steel rod and has a specific acoustic behaviour, resulting in a significantly quieter engine [4].

- *Orthopaedic Implant Applications*

Figure 1.7- Orthopaedic implants [4]

In biomedical load-bearing applications, such as in hip components, titanium alloys are the current material of choice. However, Ti alloys have poor wear resistance with formation of debris and cannot be used for articulating surfaces. Ceramic-on-ceramic applications appear to eliminate the wear debris, but may be prone to failure at a much higher rate due to a lack of toughness. TiMMC and CermeTi® materials combine the advantages of metals and ceramics and are currently under evaluation for such metal-on-metal orthopaedic implants (Figure 1.7). Moreover, spinal devices that offer articulating motion are being developed and tested. In that case, materials such as cobalt-chrome or stainless steel are undesirable due to their tendency to obscure soft-tissue imaging, as in magnetic resonance imaging [4].

- *F16 Lower Drag Brace*

Figure 1.8-Lower drag brace, F16 [9]

SP Aerospace (Netherlands) accomplished the world's first flight of an MMC primary structural landing gear component (Figure 1.8). On the F16 main landing gear, a lower drag brace was developed in titanium Matrix Composite, consisting of monofilament SiC fibres in a Ti matrix [9].

1.3 Effect of process parameters on the machinability of MMCs

The process parameters when machining MMCs can be classified in two categories; intrinsic parameters such as cutting speed, feed rate, depth of cut and type of tool, and extrisinc parameters such as particulate size, volume fraction and type of reinforcement [6].

- *Effect of cutting speed:*

The peak to valley height roughness (R_t) and the roughness average (R_a) are better at high cutting speeds [6]. When machining Al/Sic-MMC, if the speed is tripled the value of R_a is decreased by 46% at the same feed. However, when using carbide tools, low cutting speeds give better R_a values than carbide tools coated with TiC or Al_2O_3. When using Polycrystalline Diamond (PCD) inserts, the best surface quality is obtained when the tool is slightly worn. The tool wear is the most important factor influenced by cutting speed. When using uncoated carbide tools, the flank wear increases 2-fold when the speed is doubled. Moreover, when cutting aluminum MMC the tool wear is dependant on the particulate size and on the weight fraction [6]. It is worth noting that at lower cutting speeds, the soft aluminum MMC has a strong tendency to form a stable built-up-edge (BUE) on the tools' rake face [11].

- *Effect of feed rate:*

The values of the roughness parameters (Ra and Rt) increase with an increase in feed rate [6]. From experimental observations, when the feed rate is tripled, the value of R_a increased by 40 % at the same cutting speed [6]. Aditionally, the feed rate has less influence on tool wear than on surface finish. In fact, a high feed rate can reduce tool wear due to the improvement of heat conduction from the cutting zone to the workpiece [6]. Davim [12] reported that when machining Al/SiC-MMC at low speeds, high feed rates are recommended to enhance tool life. It is worth noting that the feed force and the cutting force increase with an increased feed rate. In general, high feed rates are preferred since they tend to soften the matrix, making the removal of hard SiC particles easier and therefore reducing tool wear [11].

- *Effect of the depth of cut:*

The depth of cut has a proportional influence on tool wear. When doubling the depth of cut, the wear doubles when machining aluminum MMC [6]. Furthermore, the depth of cut does not seem to affect the quality of the surface [6].

- *Effect of the tool types:*

Primary and secondary flank wear are the dominant tool wear modes, and this is due to abrasion by the hard SiC particles [11]. Coated P15 carbide tools are more effective at lower speeds. However, coating with less hardness than SiC has little benefits. Triple coated inserts with a top layer of TiN give good results in terms of wear, but result in poor surface quality. In general, HSS and WC are not suitable for machining MMC. However, diamond and CBN tools are best suited for such machining. Rhombic fixed tooling is most effective for machining MMCs at high speeds and low depth of cut. The ultrasonic vibration turning process showed a much lower cutting force as compared to the common turning process [6]. In general, the PCD inserts last ten times longer, even with five times the cutting speed, when compared to CVD coated tools [6]. Coarse grained PCD inserts were found to be the best in terms of tool wear and surface roughness [11]. Tomac and Tonnessen [7] compared the performance of the following types of coatings: TiN, Ti(N,C) and Al_2O_3. Tool wear was shown to increase rapidly with all coated inserts. Only PCD tools are better and are usually more suitable for machining aluminum MMC, and this is true in both terms of surface quality and tool life. Ceramic tools showed poor performance for the machining of Al/SiC MMC [6].

Medium cutting speed (from 200 to 450 m/min) are recommended for carbide and coated carbide tools. For higher cutting speeds it is recomended to use PCD inserts. Feed rate has the most influence of the surface finish. The recommended feed rates are 0.05~0.4 mm/rev for coated carbide tools and 1~2 mm/rev for PCD tools. The depth of cut has less influence on surface finish; however, the recommended range is 0.25~1 mm [6].

- *Effect of the particle reinforcement type:*

The particle reinforcements are considered as an intrinsic parameter. As the reinforcement particle size increases, the surface roughness increases, as does the wear rate of the tool. As the

volume fraction (volume % of SiC) increases, the surface roughness also increases. Ceramic-graphite reinforced composites can be cost effectively rough machined even with carbide tooling [6].

- *General comparison of the data available in the literature and obtained in experiments performed at École Polytechnique*

Previous research on drilling AlMMC has been performed at École Polytechnique [13]. Table 1.1 summarizes the main features of the research performed at École Polytechnique and from the literature. Note that no direct comparison can be made between the two sets of data since the research at École Polytechnique was for drilling; whereas the data from the literature is for turning.

Table 1.1-Parameters affecting the machining of AlMMC.

Parameters, cutting conditions	Observations from the literature (Turning)**[6, 7, 11]**	Observations made at École Polytechnique (drilling)**[13]**
Low cutting speed and R_a using carbide tools	Better R_a	**Worse R_a for low Rpm (4000) (but better for ISCAR)**
Cutting speed and wear	Speed x 2 =>wear x 2	**NA**
Feed and R_a	Feed x 3=>R_a x 1.4	**Ra better with high feeds (at 4000rpm)**
Feed and wear	High feed, less wear	**NA**
Feed and force	Both increase	**NA**
Carbide tools	Effective at low speed	**Medium speed chosen (6000rpm)**
Uncoated/Coated carbide and R_a	Uncoated : better R_a	**Firex coating : better R_a**
HSS and WC	Not good	**Not good**
Recommended cutting speed for Carbide	200-450 m/min	**6000 rpm**
Recommended feed for Carbide	0.05~0.4 mm/rev	**0.2mm/rev**

1.4 Machinability of titanium alloys

Titanium alloys are considered as difficult-to-cut materials. Extensive information can be found in the literature concerning the machining of such materials. Che-Haron [2] noted that increased wear rate was detected with the increase in cutting speed. Furthermore, flank wear at

the tool tip seems to be the limiting factor that controlled the tool life in all cases. The predominant wear mechanism is dissolution-diffusion, especially at high cutting speeds. In fact, at high speed, the higher temperature generated at the tool tip causes the tools to lose their strength, which subsequently increases wear.

Machining Ti-6Al-4V led to a number of observations [14]. The combination of the low thermal conductivity and a very thin chip results in very high cutting temperature concentrated in a small area at the tool-chip interface. The high temperature combined with the strong chemical reactivity of titanium results in its high affinity for almost all tool materials at cutting temperatures above 500°C. It was also noted that tool life is affected by feed; that is, as feed increases, tool life decreases when machining titanium alloys. Furthermore, titanium alloys have a low modulus of elasticity which can cause chatter, deflection and rubbing action. The cyclic segmentation in chip formation results in a large variation of the forces acting on the tool tip. This will in turn increase the possibility of chatter and tool chipping.

Arrazola *et al.* [15] studied the machinability of Ti-6Al-4V and Ti555.3 and recommends to machine these alloys with a maximum speed of 90 m/min. They also noted that diffusion is the most dominant wear mode.

1.5 Laser Assisted Machining (LAM)

Previous work done at the National Research Council of Canada - Aerospace Manufacturing Technology Centre (NRC-AMTC) on the machining of inconel showed a reduction of forces and tool wear when using Laser Assisted Machining (LAM) [16]. Abrasion tool wear is always a major concern when cutting TiMMC. In an attempt to further enhance the lifetime of the cutting tool LAM was performed. The results would help identify the effects of adding an external heat source on the mechanism of chip formation and on the tool wear. Care should be taken when using LAM on Ti alloys. The Ti alloy should be kept below a transformation temperature (800 °C) to avoid Alpha to Beta transformation [17]. Anderson *et al.* [18] showed that tool wear VB decreases as speed increases in LAM. Many problems, such as the diffusion of carbide tools (the cobalt binders), are encountered while machining titanium. The problems arise when the already

high temperature of the tool/chip interface is further increased by the heat from the laser beam. Figure 1.9 summarizes the effects of local and external heat on the tool life.

Reflectivity can be a problem with LAM, mainly when machining aluminum. Therefore, some form of coating is sometimes used on the surface of the machined material. However, with Ti alloys usually no coatings are used.

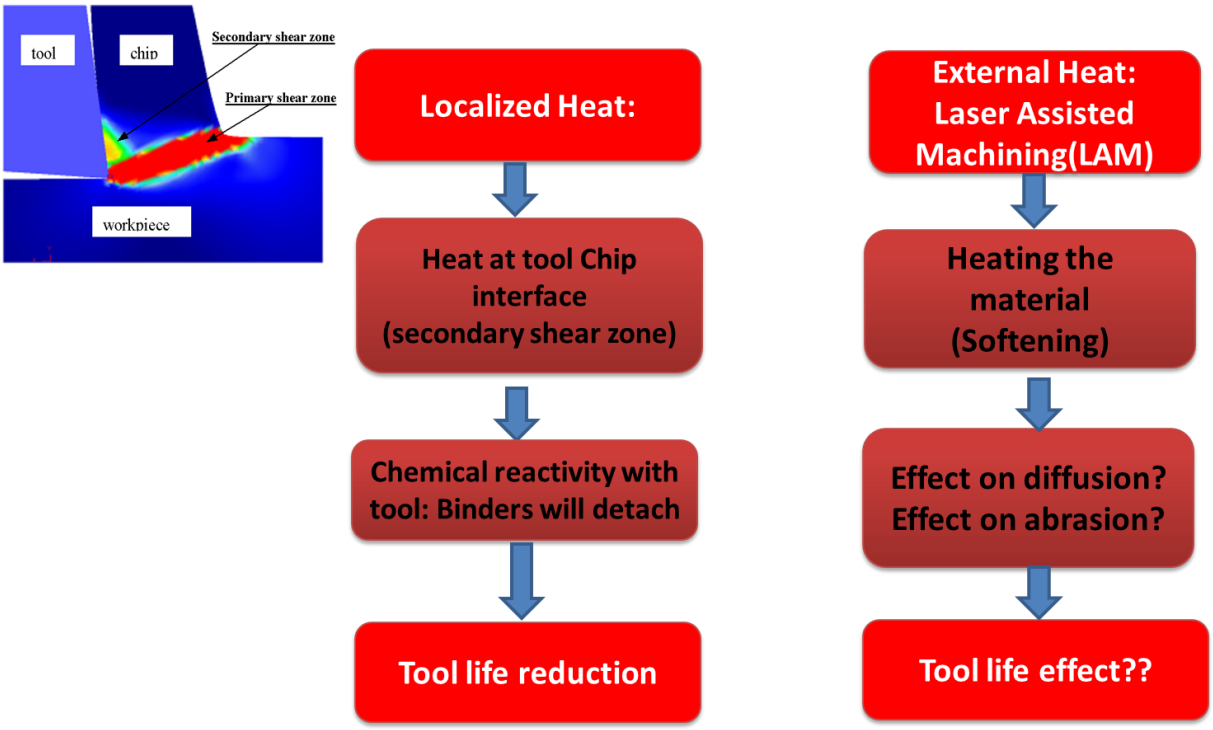

Figure 1.9-Localized and external heat effects

Localized heat (from secondary shear zone) was identified to be a major cause of diffusion wear in titanium machining. However, this should be differentiated from the localized heat of the laser source away from the cutting zone when using LAM.

Sun [19] addressed the issue of chip segmentation in Ti alloys when using LAM and found that the surface material temperature has a determining effect on chip segmentation. He noted the following: as the temperature increases, the chip segmentation is sharper and shows adiabatic shear bands. Furthermore, if the cutting speed is increased with LAM, it results in the same segmentation characteristics as observed during conventional cutting at lower speed, with a geometry ratio ‘r’ smaller than 1, where ‘r’ is the ratio between the undeformed length in the chip

to the machined length. Also, when using LAM at low speed, the chip's teeth are sharper, with geometry ratio r > 1.

1.6 Literature review of segmented chip formation

Segmented chip formation has led to many controversial theories in the past, and it is still an unclear phenomenon. Recht [20], in the 50's, studied high strain rates in some metals and observed the presence of "adiabatic shear bands". Briefly, when the increase in shear strength (τ) due to high strain (ε) is overcome by softening due to heat (θ), adiabatic shear bands can form. Such a condition can be expressed by the following relationship [20]:

$$0 \leq \frac{\frac{\delta\tau}{\delta\varepsilon}}{-\frac{\delta\tau}{\delta\theta}*\frac{\delta\theta}{\delta\varepsilon}} \leq 1 \qquad [1\text{-}1]$$

That is, if the above ratio is between 0 and 1, the material will shear catastrophically. A ratio superior to 1 indicates that strain hardening is the dominant factor, and that the shear will be distributed throughout the material. A negative ratio indicates that the material hardens with temperature and that the shear deformation will be distributed.

Adiabatic shear band formation while machining has been investigated and three leading researchers: Shaw, Nakayama, Komanduri, revealed important findings:

- *Chip formation according to Shaw [21]:*

Shaw [21] suggested that shear bands are formed due to an inside crack and void propagation. This crack forms near the tool (or at the free surface). However, due to heat and high normal stress, the sheared band will weld again.

- *Chip formation according to Nakayama [22]:*

Nakayama [22] studied crack initiation in chip formation and suggested that the crack occurs at the free surface, at the point where it starts having an angle. The angle of the crack is in the direction of the highest shear stress; therefore at 45 degree angle from the surface. Figure 1.10 shows the point at which the crack initiates. At this free surface, the stress is zero, therefore in a

Mohr circle this corresponds to the maximum shear stress, which is at a 90 degree angle from the tensile stress and therefore at 45 degree angle from the free surface.

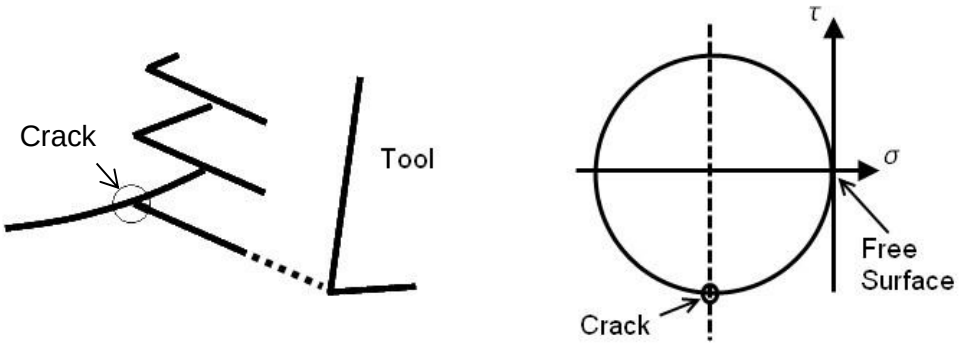

Figure 1.10- Nakayama's Model [22]

- *Chip formation according to Komanduri:*

Komanduri [23] developed a model showing the process of segmented chip formation. He suggested that a thermoplastic instability occurs within the primary shear zone, where the sheared surface originates from the tool tip and continues to the free surface (Figure 1.11). The shearing starts below the conventional shear line in an arc like shape ("A" in Figure 1.11) and then deforms outwards forming a straight line.

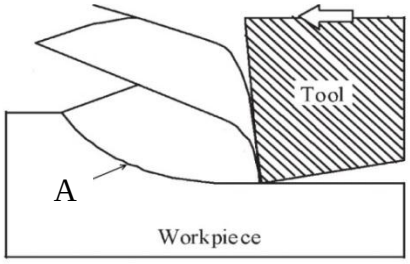

Figure 1.11-Chip formation from Komaduri's model [23]

1.7 ASB formation in segmentation and microstructure evolution

Most researches on adiabatic shear banding (ASB) in the literature derive from high speed impact or ballistic tests, and research on this phenomenon during machining is still limited. This current study attempts to fill this gap.

FEM has been successfully used in the past years for simulating machining. However, in cases where segmented chips are produced, the FEM model needs to take into account the

physical changes and the phenomenon occurring inside the ASB in order to improve the prediction of the machining simulation accuracy. This requires a complete understanding of the ASB phenomenon.

Different explanations exist for the root cause of ASB formation. Catastrophic shear instability, accumulated damage during machining, lack of ductility and shear cracks generated on the free surface of the workpiece material are some of the mechanisms proposed in the literature to explain the formation of segmented chips. In experiments resulting in a fractured surface with a presence of ASB and crack initiation, it is often uncertain whether the crack initiated the ASB, or if it resulted from the ASB phenomenon. In ballistic experiments, ASB have been clearly identified as precursors to fracture; therefore underlining the importance of identifying the criteria of ASB formation [24].

It was suggested that Rotational Dynamic Recrystallization (RDX) is responsible for the formation of micro grains in the ASB with no evidence of the "avalanche dislocation", in which the catastrophic release of dislocation pile-up, causes localized heating on the slip plane [24]. Some recent investigations show, however, that phase transformation also occurs in the deformed bands [24].

1.8 Finite Element Method (FEM) for the simulation of segmented chips

In recent years, FEM is gaining more and more importance in machining especially with the availability of powerful software such as DEFORM. FEM is of major importance since it leads to the simulation of machining and to the determination of the cutting forces, chip formation, material temperature, and chip morphology and segmentation. The methodology used in FEM involves many steps. Some of the main steps involve the development of a constitutive equation, the selection of an appropriate damage model and the definition of a tool/chip interface friction model.

FEM for segmented chips can be found in the literature. However, simulation of LAM with segmented chips has never been performed before. Below is a typical example of a FEM for turning, involving segmented chips. In order to simulate segmentation, a damage model or a specific constitutive equation is embedded in the simulation model. An example of a modified Johnson-Cook (JC) constitutive equation for titanium alloys was developed by Calamaz [25].

$$\sigma = \left(A + B\varepsilon^{n}\left(\frac{1}{\exp(\varepsilon^{a})}\right)\right)\left(1 + C\ln\frac{\dot{\varepsilon}}{\dot{\varepsilon}_0}\right) \times \left(1 - \left(\frac{T - T_r}{T_m - T_r}\right)^{m}\right)\left(D + (1 - D)\tanh\left(\frac{1}{(\varepsilon + S)^{c}}\right)\right) \quad [1\text{-}2]$$

With:

$$D = 1 - \left(\frac{T}{T_m}\right)^{d}, \quad S = \left(\frac{T}{T_m}\right)^{b}$$

Where, *a*, *b*, *c*, *d*, *m*, *n*, *A*, *B*, *C* are material constants, and σ is the effective stress, $\dot{\varepsilon}$ the effective strain rate, ε the effective strain and *T* the temperature. Figure 1.12 shows the simulated segmented chips using the conventional JC and the modified *tanh* constitutive equation.

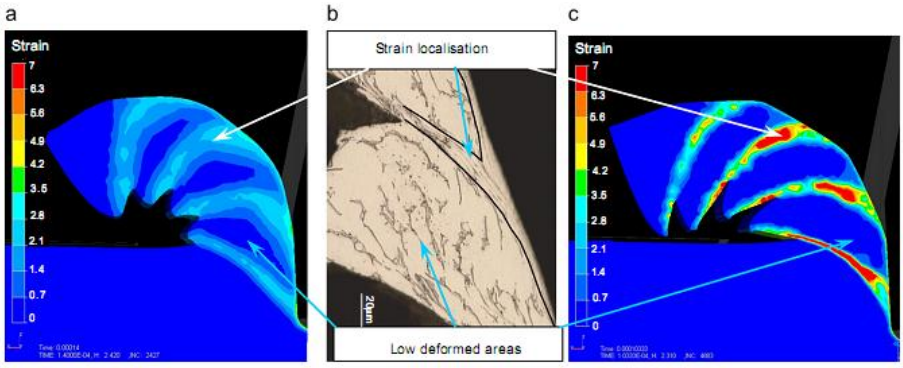

Figure 1.12 - Strain fields of predicted (a and c) and experimental chips (b) using: (a) JC and (c) *tanh* models with a cutting speed of 180 m/min and a 0.1 mm/rev feed [25]

1.8.1 Damage models

A damage criterion can be used in the FEM for simulating the chip segmentation. Among the different damage models available in the literature, McClintock [26] developed a damage model based on void initiation, growth and coalescence. The model consists of an array of elliptical cylindrical voids extending in one direction, and the condition for fracture is satisfied when each void touches the neighboring ones. The Cockcroft-Latham model uses the fracture energy in a tensile test and was shown to be constant for many alloys. This can be represented by the area under the stress-strain curve, which remains constant [27].

CHAPTER: 2- SYNTHESIS OF THE RESEARCH PROJECT

2.1 Methodology

Three approaches were used in the research plan**;** experimentation, chip formation with microstructure evolution, and FEM of cutting TiMMC, as explained in Figure 2.1. In the first experimental approach, the TAGUCHI Design of Experiment (DOE) was used in order to observe the trend effect of the input (cutting speed (v), feed (f) and tool type) on the output (cutting force (F_c), tool wear (VB_{bmax}) and surface roughness (Ra)) and therefore to define the optimum cutting conditions. Knowing these trends, hypothesis #3 was tested (effect of speed on tool wear). In order to further enhance the tool life, LAM was performed using the set optimum conditions, and new optimum conditions were defined, taking into consideration the cutting speed and the heated surface's temperature.

In the second approach, the chip formation mechanism and the microstructure evolution were experimentally examined using the Quick Stop Device (QSD), and Transmission Electron microscopy (TEM). Based on the analysis of the QSD experiments, a new chip formation model was presented. To better understand the segmentation phenomenon, the effect of the Adiabatic Shear Band inside the chips was studied by TEM, and a new model for microstructure evolution was presented. Analysis of the chip microstructures provides a basis for the understanding of the tool/particle interaction, as well as its effect on tool life.

In the last approach (FEM simulation), the data from the turning and tensile tests were used to generate the constitutive data which was used to develop a homogenous equivalent constitutive equation for TiMMC. Subsequently, a damage model was incorporated into the FEM in order to simulate the segmentation process. At a later stage, LAM was simulated by adding an external heat source to the simulation model. The FEM results were validated with experimental tests. Furthermore, the simulation results were used to determine the effect of the machining conditions (in conventional and LAM) on the tool/chip interface temperature, as well as the stress, strain and strain rate in the formed chip. Using the simulation results, hypothesis #4, which addresses the effect of an added heat source on tool life, was tested.

2.1.1 Work organization

The thesis is organized according to the described methodology which was explained in the previous section. Each main section is based on published papers. However, many additional details incorporated in the following sections were not included in the published papers. Furthermore, since the details included in the subsequent section are not a repetition of the entire content of the published papers, it will be more convenient for the reader to consult the papers in the Appendix ‘A’ when they are referred to in the text before continuing reading. The main sections are stated below:

- *Experimental investigation in conventional turning*
- *Development of a QSD for studying the chip morphology*
- *Laser Assisted Machining*
- *Chip formation model*
- *Microstructure evolution model in the ASB*
- *FEM (Finite element Method); simulation of chip formation*

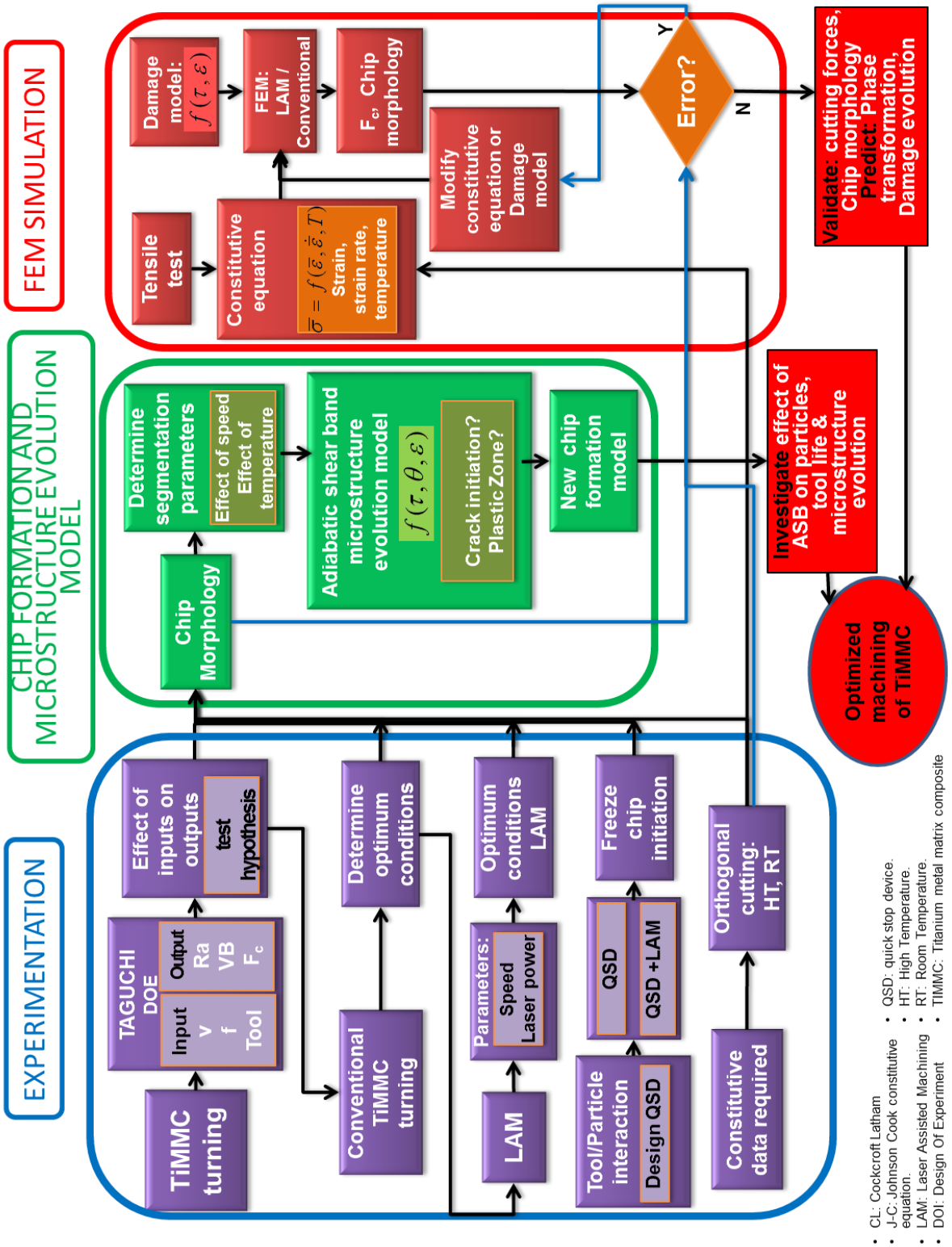

Figure 2.1 - Detailed methodology

2.2 Experimental investigation in conventional turning

Turning experiments were performed on TiMMC, using a TAGUCHI DOE (Design of experiments) for efficiency purposes and to reduce the number of experiments.

Appendixes C1 and C2 show some experimental details, and the TAGUCHI method respectively.

2.2.1 Optimum cutting parameters for turning TiMMC, testing hypothesis #3

The section below is based on the papers in the appendix [A1] with the title below:

A1- R. Bejjani, M. Balazinski, B. Shi, H. Attia, H. Kishawy, *"Machinability and Chip Formation of Titanium Metal Matrix Composites"*, Int. J. of Advanced Manufacturing Systems, IJAMS, vol. 13, "1" , 2011.

2.2.1.1 Design of experiments

One of the goals of this study was to find the optimum conditions for machining TiMMC. For this, an effective statistical tool was needed to study the effects of the cutting parameters, and tool types on the tool life, and surface roughness.

The most common way used for designing of experiments is the factorial type DOE (Design Of Experiments). However, in order to be more efficient and reduce the costly number of experiments an approach, known as Taguchi Parameter Design, was used. As a type of fractional factorial design, Taguchi Parameter Design is similar to traditional DOE methods in that multiple input parameters can be considered for a given response. The Taguchi Parameter Design uses the non-linearity of a response parameter to decrease the sensitivity of the quality characteristic to variability. Furthermore, Taguchi Parameter Design maximizes the performance of a naturally variable production process by modifying the controlled factors [28].

More details on Taguchi method, and the text matrix followed in this study can be found in Appendices C1 and C 2.

2.2.1.2 Chip morphology

- *High Speed Camera (HSC)*

In an attempt to observe and compare the cutting phenomenon at low and high cutting speeds of 230 and 120 m/min, a high speed camera was used. The use of the camera helps to identify the chip initiation and to validate the proper function of the newly developed QSD. The camera used is a Photron Camera with 500 frames/s and a shutter speed of 1/2000 s. After analyzing different frames taken by the high speed camera, it was observed that in some cases, particles are expelled and ignite when they are away from the tool (Figure 2.2).

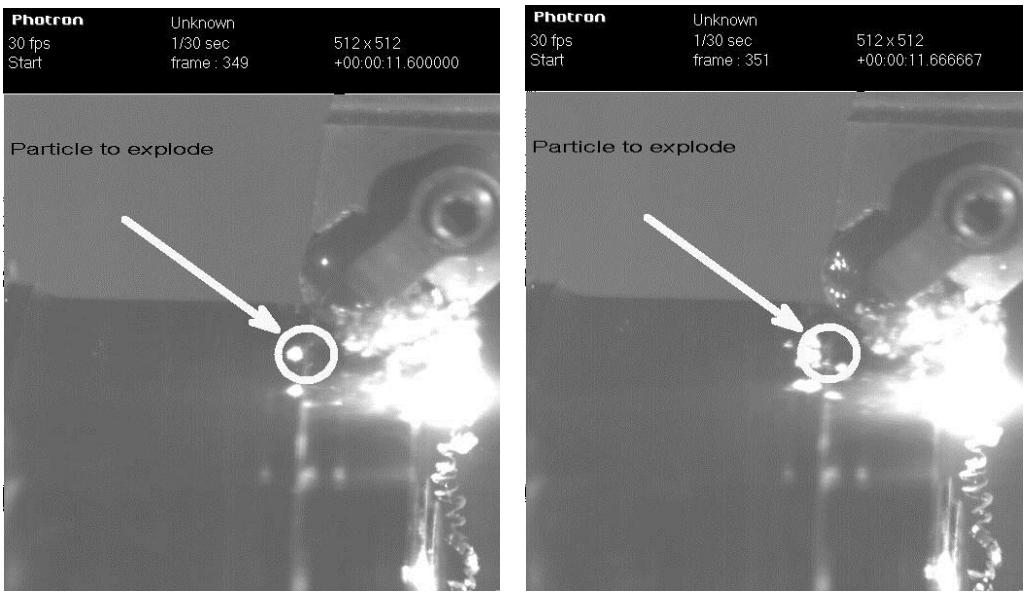

Figure 2.2- Igniting chips recorded with a high speed camera

- *Fire limit*

The following cutting parameters were critical in terms of safety and igniting chips:

- With PCD tools, at 230 m/min, 0.1 mm/rev feed, the chips caught fire as soon as they formed. However, when the feed was increased to 0.2 mm/rev, no fire was observed.
- With Carbide tools, at 120 m/min, the tool tip was badly worn and the chips caught fire. It was not possible to machine the complete length needed.

- *Chip microphotograph*

After noticing a positive change in the machining results in terms of forces, surface roughness and tool wear as the speed was increased; chips formed at two different cutting speeds were collected, sectioned and analyzed. Figure 2.3 shows the difference between chip morphology at high and low speed and the following observations can be made:

- At lower cutting speeds (100 m/min):

  - The segments were characterized by highly deformed grains indicating high strains.

  - More smashed particles were observed. However, at high speed they just seemed displaced or cut.

  - The grain boundaries inside the material were more elongated and deformed compared to those at higher speeds.

- At higher cutting speeds (230 m/min):

  - The grain boundaries were shorter and less deformed. The material seemed to have been cut without high strains in the material.

  - The shear angle was steeper.

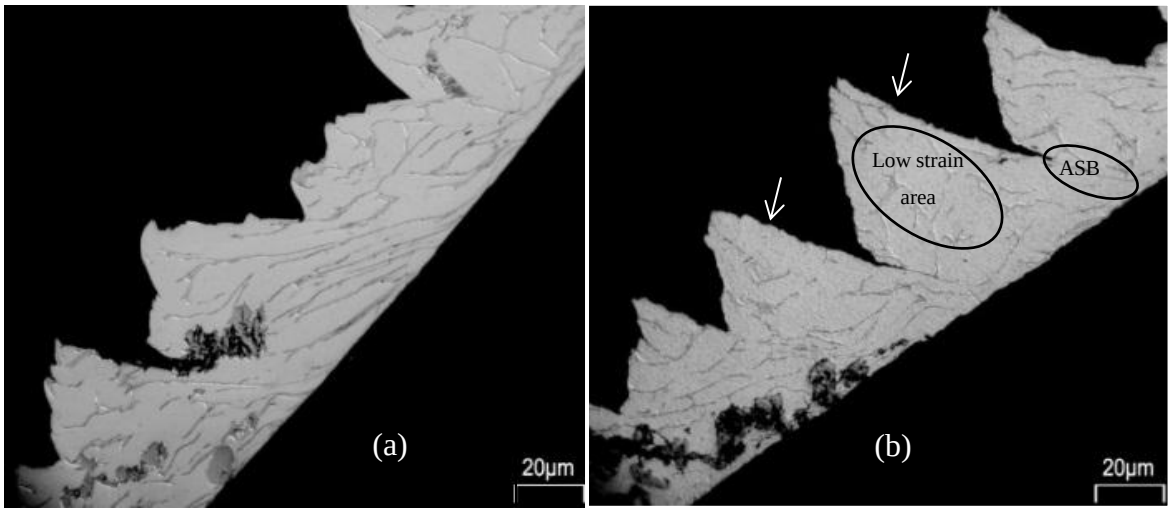

Figure 2.3- Chip morphology at low speed of 100 m/min (a) and high speed of 230 m/min (b)

2.2.1.3 Results and discussions for the turning experiments

The experiments performed on TiMMC showed that PCD tools are more suitable than carbide tools, as expected. However, only with PCD tools, it was possible to attain higher cutting speeds. The experiments showed that the optimum machining results occurred at higher cutting speeds, where tool life was the longest and surface roughness was best. This unexpected result is in contradiction with the data found in the literature for machining aluminum MMC [6]. This is an unusual phenomenon, especially since all MMCs are very abrasive and tend to wear the tool rapidly at higher speeds. Other interesting conclusions are listed below:

- It is more suitable to machine TiMMC at higher speeds. With a high speed of 170 m/min, tool wear is less than when machining at a lower speed of 100 m/min. This is unexpected and different from when machining other metals. This is also in contradiction with **hypothesis # 3**.
- TiMMC produces segmented chips, and abrasion is the main tool wear mode, confirming **hypotheses # 1 and 2.**
- The optimum speed for the least tool wear and best surface roughness is 170 m/min when using PCD tools and 90 m/min for carbide tools.
- Under optimum conditions for both tools, their respective maximum cutting lengths are 250 mm for PCD tools and 50 mm for carbide tools.
- The chip morphology was clearly different at low and high speeds.
- At higher speeds (above 180 m/min), there seems to be a different cutting mechanism where cutting force and tool wear are reduced and surface roughness is improved. Therefore, for machining TiMMC, it is much more suitable to use higher speeds. Even with a higher feed; a high speed of 170 m/min causes the cutting forces to be much more stable with no signs of alarming peaks. However, this can only be done with PCD tools, because carbide tools wear rapidly at such speeds.
- For PCD tools, cutting speed has a greater impact on surface roughness than feed.

- With PCD tools, the surface roughness is much less, compared to carbide tools. This can be attributed to the round shape of the PCD tools.
- The effect of worn tools on R_a is different for each tool. R_a is better with a worn carbide tool; however this does not apply for PCD tools. This might be due to the fact that the carbide tip wears very rapidly and becomes flat. The flat tool surface may contribute to fewer fluctuations in the machined surface height.
- There is a fire hazard with cutting speeds higher than 180 m/min and should therefore be avoided.
- Using carbide tools, the cutting force starts low and then peaks when the tool is worn. It even surpasses the maximum force attained when using PCD tools.

More informations can be found in the paper in appendix [A1], and reference [29].

2.3 Development of a Quick Stop Device (QSD) for studying chip morphology

The section below is based on the paper in the appendix [A2] with the title below:

A2- R. Bejjani, H. Attia, M. Balazinski, B. Shi, *"A NEW DESIGN OF QUICK STOP DEVICE FOR RESEARCH ON CHIP FORMATION"*, Trans. of NAMRI/SME, vol. 38 pp.269-274, 2010.

Quick stop devices (QSD) have been frequently used for studying the chip formation mechanisms. However, most quick stop devices previously designed involved a complex design, unsafe operation, and/or are difficult to use in practice. In this research, a newly developed quick stop device was designed. This QSD can be used as an alternative to the conventional explosive shear pin design. This can be useful in machine shops where usage of explosives is prohibited, as is in our case. This new quick stop device has the advantages of easy usage, high repeatability, and short set-up time.

Investigation of the chip formation mechanism of TiMMC is essential for further understanding and modeling the plastic deformation process in the primary and secondary shear zones under conditions of very high strain, strain rate and temperature. The quick stop device is a research device which freezes the cutting process instantly and allows sample collection of the chip root area that contains the primary and secondary deformation zones. With the QSD, one can

examine the adhesion of the workpiece material to the tool face, the separation of hard particles that result in three-body abrasion of the cutting tool, as well as the thickness of the primary shear zone [5].

The most common type of QSDs is the shear pin design. Shear pin-QSDs can have numerous types of actuation mechanisms. Hasting [30] developed an explosive type of shear pin QSD. Regardless of the design of the QSD, to work properly, it should meet the following requirement: the distance traveled by the tool in the material after the actuation of the QSD should be very small, in other words the separation time between the tool and the material should be minimal.

2.3.1 Description and function of the new QSD

Figure 2.4 shows the components of the new QSD. The insert (A) goes into the tool holder (E). A hardened pin (D) is inserted at the opposite end of the tool holder. The pin rests on a small flat surface (C). In normal running condition, the pin (D) will be held between the two plates (F). The tool holder is free to rotate around the tube (B).

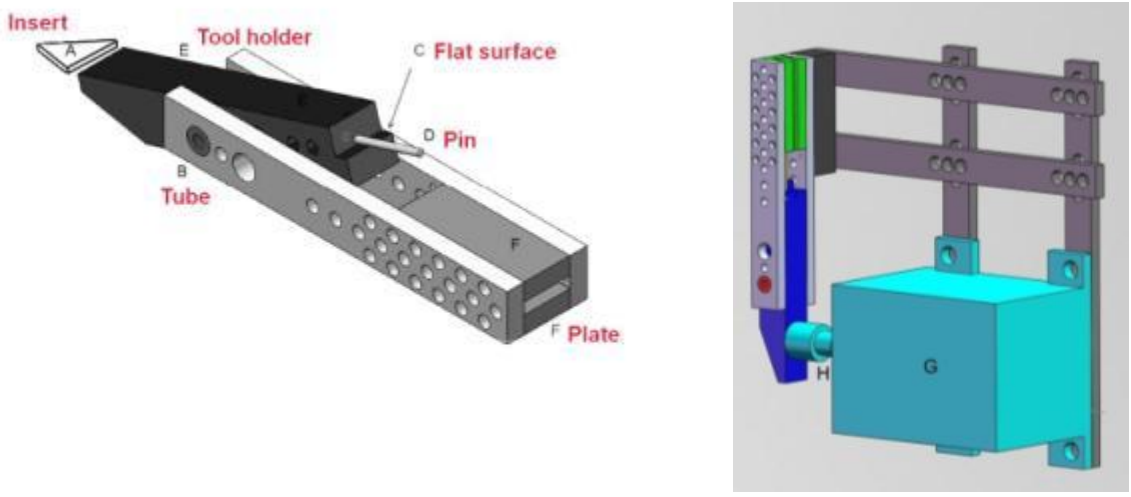

Figure 2.4- Detailed drawings of the new Quick Stop Device

Under normal machining operation, the whole assembly is fixed to a frame attached to the turret of the CNC turning centre. During machining, the pin (D) will retain the tool holder from rotating. When desired, the air cylinder (G) will be actuated with the help of a solenoid valve, causing the piston rod (H) to extend and acquire enough kinetic energy to break the hardened pin (D) when it hits the tool holder. This causes the tool holder to move away of the machined part. Figure 2.5 shows the QSD attached to the lathe.

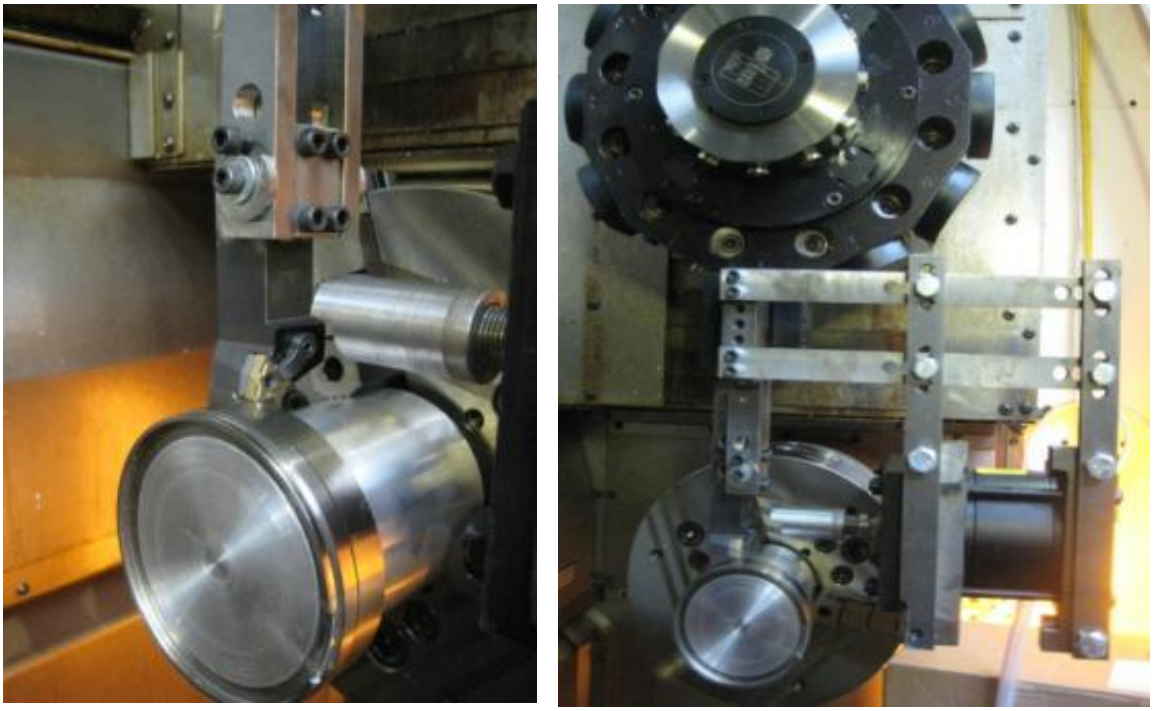

Figure 2.5-The Quick Stop Device installed in CNC lathe

The photomicrograph in Figure 2.6 shows clearly the root of the chip attached to the machined material. The segmentations of the chip can be clearly seen as well. This phenomenon is commonly observed in titanium machining and is known as adiabatic shear banding. It can be explained by a high strain rate and strain hardening combined with thermal softening in a low conductive material [31]. Figure 2.7 shows QSD tests performed at different speeds, with each test showing a unique characteristic.

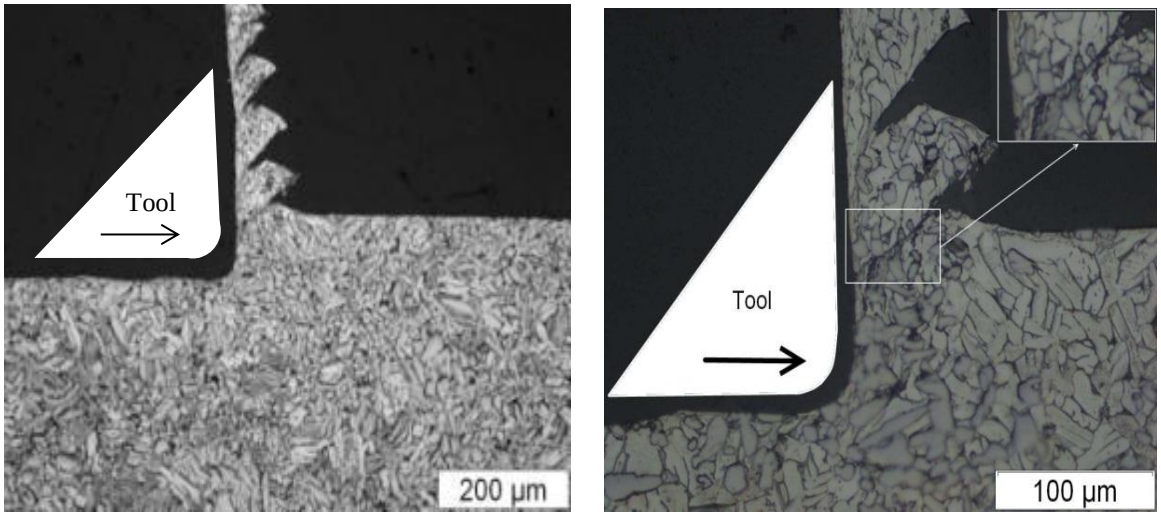

Figure 2.6- Chip formation microstructure obtained by using the QSD. Cutting conditions used: cutting speed: 70 m/min, feed: 0.2 mm/rev, and depth of cut: 0.15 mm

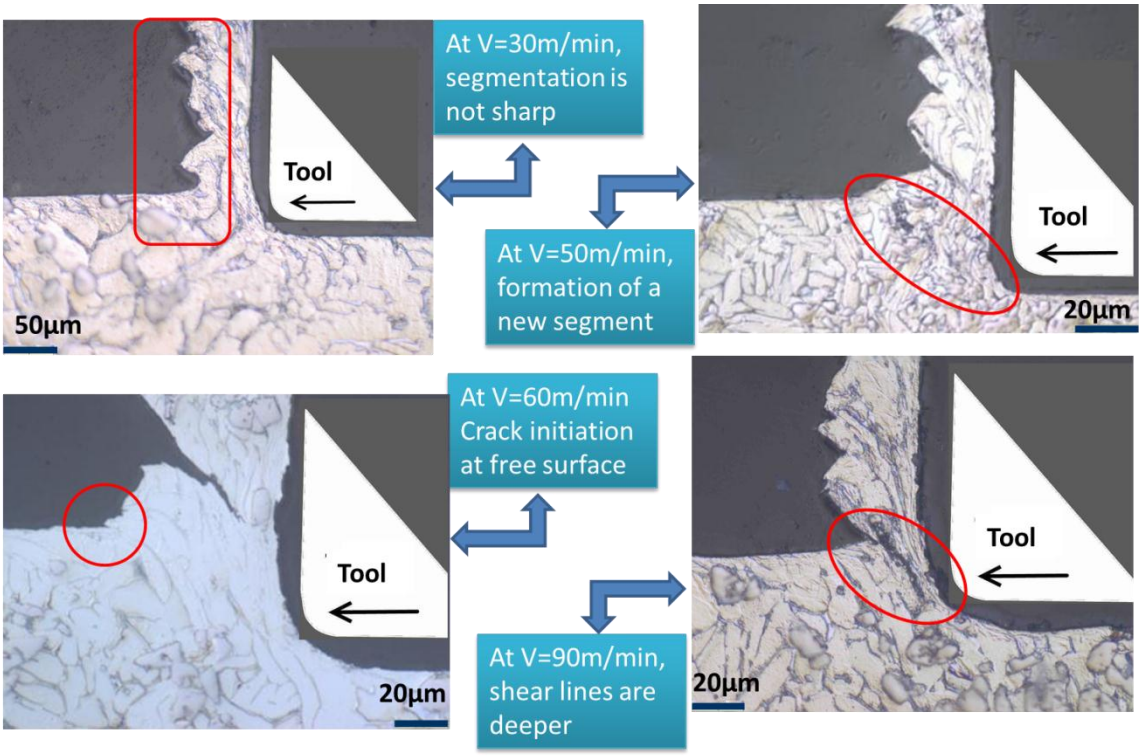

Figure 2.7- Quick Stop Device tests performed at different speeds, a) at 30 m/min, b) at 50 m/min, c) at 60 m/min, d) at 90 m/min

2.3.2 Operating results and advantages of the new QSD

The new QSD was tested extensively and was proven to have the following features and advantages over other designs:

- The QSD met our requirements.
- Safe operation: no explosives are used.
- Repetitive and reliable operation: a successfully frozen chip was formed in more than 90 % of the tests.
- Remote actuation; the operator does not have to be nearby.
- Fast set up time and easy to use; each test can be completed in less than 10 minutes.
- Rigid and chatter free operation.

More information can be found in the published paper in appendix: [A2].

2.4 Laser Assisted Machining (LAM)

The section below is based on the paper in the appendix [A3] with the title below:

A3- R. Bejjani, B. Shi, H. Attia, M. Balazinski,*" Laser assisted turning of Titanium Metal Matrix Composite"*, CIRP annals, vol. 60, "1", pp.61-65, 2011.

TiMMC is an extremely difficult to cut material mainly due to the rapid abrasion of the tools, which reduces their lifetime. In this research work, an attempt was made to enhance tool life and productivity using Laser Assisted Machining (LAM). This machining process has never been tried before for TiMMC. In preliminary orthogonal tests under laser heating, it was noticed that the tool life was much longer than in tests done at room temperature. In our previous conventional machining tests, longer tool life was achieved when cutting at higher speeds. As commonly known, higher cutting speeds will increase the tool/chip interface's temperature, which in turn may reduce the tool life. Adding an external source of heat (the laser beam) may increase even more the tool/chip interface's temperature; therefore, hypothesis #4 (possible reduction of tool life with LAM) can be tested.

Figure 2.8 shows the approach used for the LAM experimentation. Process optimization is essential since LAM does not always lead to better results [32]. In LAM, the laser beam increases the temperature of the material and makes it softer; however tool diffusion wear may be severe due to this elevated temperature.

Using the TAGUCHI design of experiment, the optimum conditions for minimum forces, minimum tool wear, and best surface roughness were determined for conventional machining. Using these optimum cutting conditions as a starting point, LAM was performed at different surface temperatures.

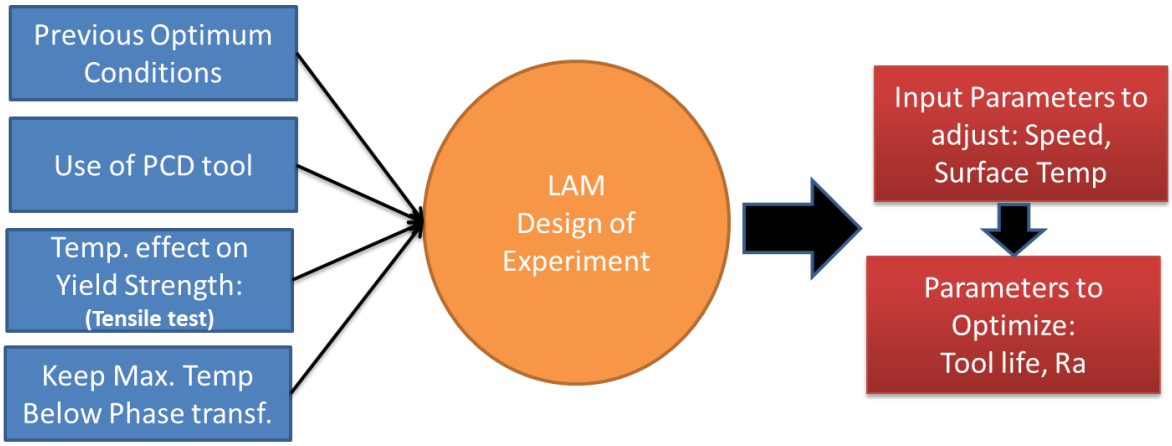

Figure 2.8-Identification of main parameters for LAM

2.4.1 Experimental set-up

Figure 2.9 shows the LAM set up. To avoid the burning of chips, the laser is adjusted to hit the surface at a distance of around 2 cm from the tool edge. Additionally, an air pipe with compressed air was used to keep the chips away from the laser area (Figure 2.10).

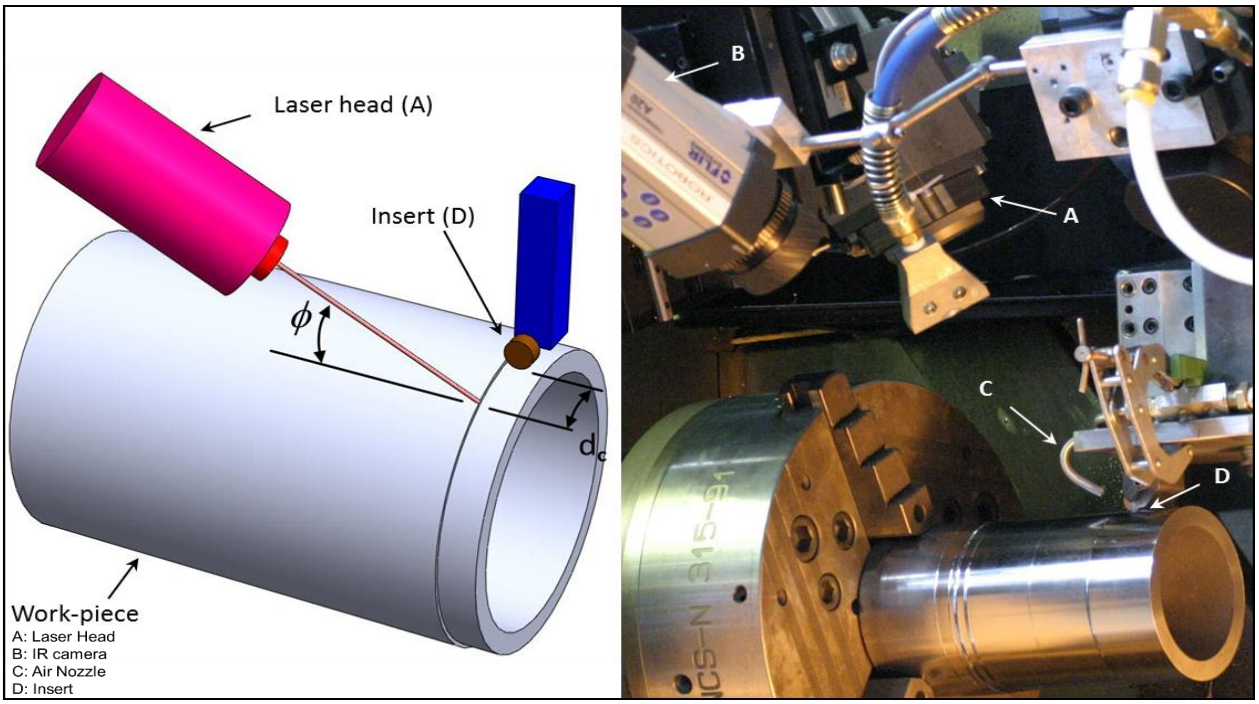

Figure 2.9-The laser beam (in red) hits the material surface just before cutting

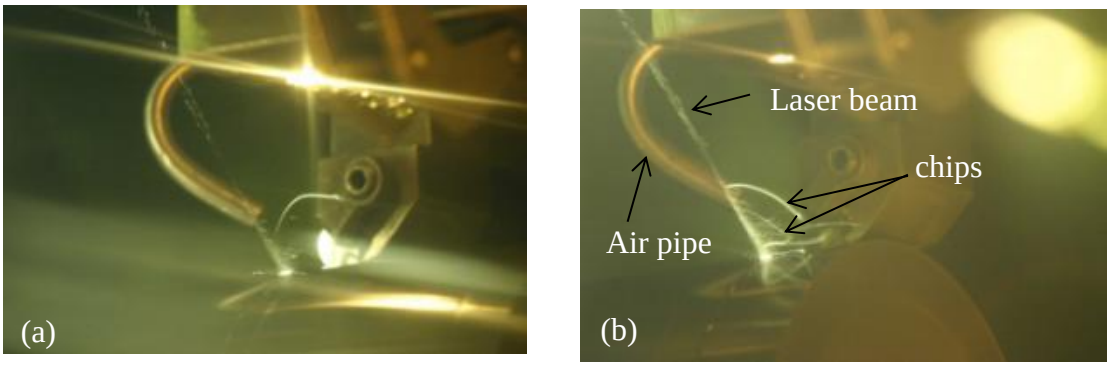

Figure 2.10- a) Laser beam hitting the surface to be machined, b) Laser beam hitting some chips causing them to ignite

2.4.2 Results and discussion

The cutting parameters used in these experiments were based on the previously found optimum conditions in conventional cutting conditions. The workpiece's surface temperature was limited to a maximum of 500°C in order to avoid reaching the phase transformation temperature of the matrix (around 850°C). The following speeds were used: v= 170 m/min and 100 m/min. The feed was kept constant at 0.2 mm/rev. and the depth of cut at 0.15 mm. The surface temperatures used were 300 and 500°C.

Effect on cutting forces

Figure 2.11 shows the effect of LAM on the machining forces. As can be seen, the greatest impact of LAM is on the thrust force (F_t). The highest difference is when machining at low speed and high temperature. The cutting (F_c) and feed forces (F_f) were not affected as much.

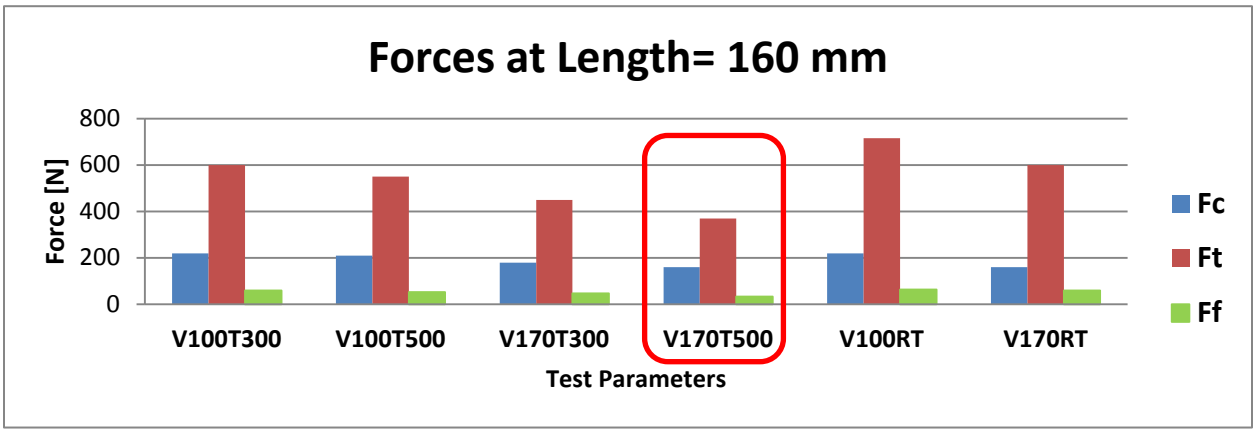

Figure 2.11- Effect of Laser Assisted Machining on cutting forces in different cutting conditions

Figure 2.12 shows the instantaneous effect of LAM on the turning forces. As the laser beam is actuated, a sudden drop in the machining forces can be seen. Again the thrust force was the most affected force. A close to 25% decrease in Ft can be seen.

Tool life

Similar to what was observed in conventional turning experiments, the uncommon effect of increased tool life when increasing the speed was also observed in the LAM experiments. The effect of LAM was shown, however, to be quite beneficial, as the tool life increased substantially as seen in Figures 2.13 and 2.14. The cutting tests were stopped when the tool wear reached a uniform flank wear criterion of 0.3 mm according to ISO 3685-1993 [33].

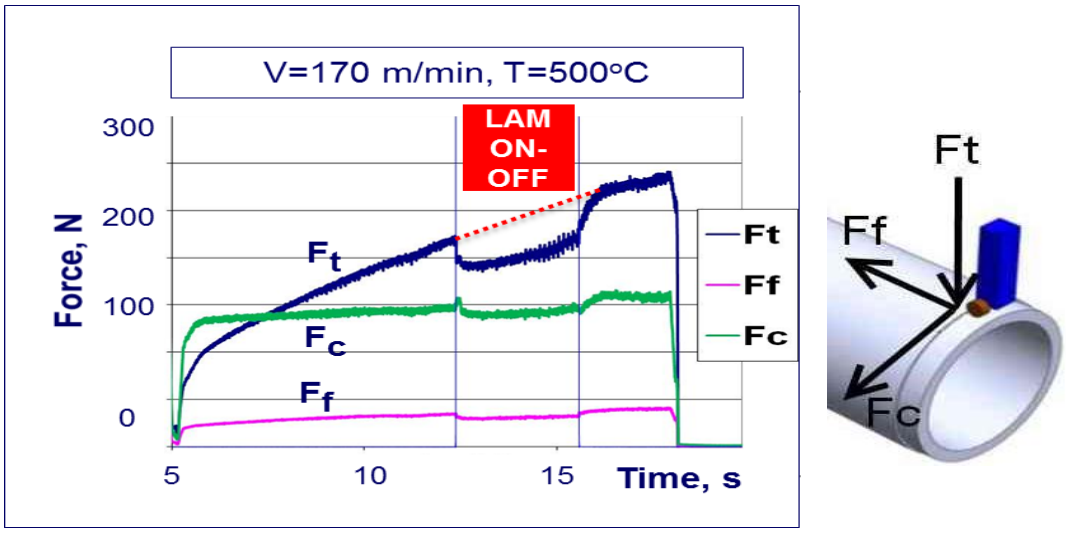

Figure 2.12- Direct effect of Laser Assisted Machining on cutting forces

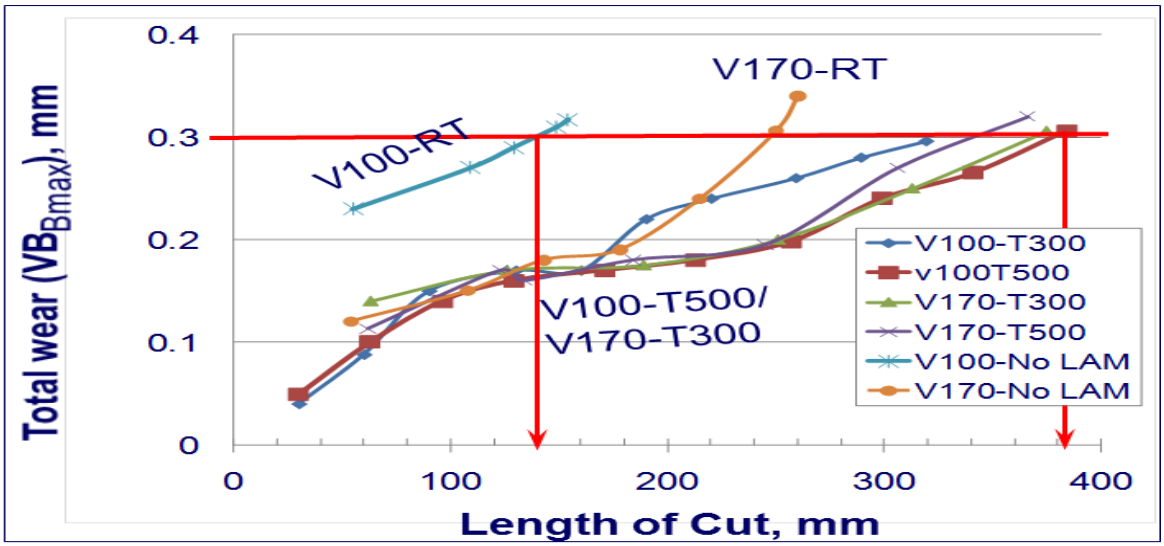

Figure 2.13- Effect of Laser Assisted Machining on tool life in each tested condition

2.4.3 Examination of chip morphology

A QSD test has never been used with LAM before. In this research, the use of a QSD in LAM can lead to a better understanding of the laser softening effect on the material and the effect on plastic deformation. Below are some main findings.

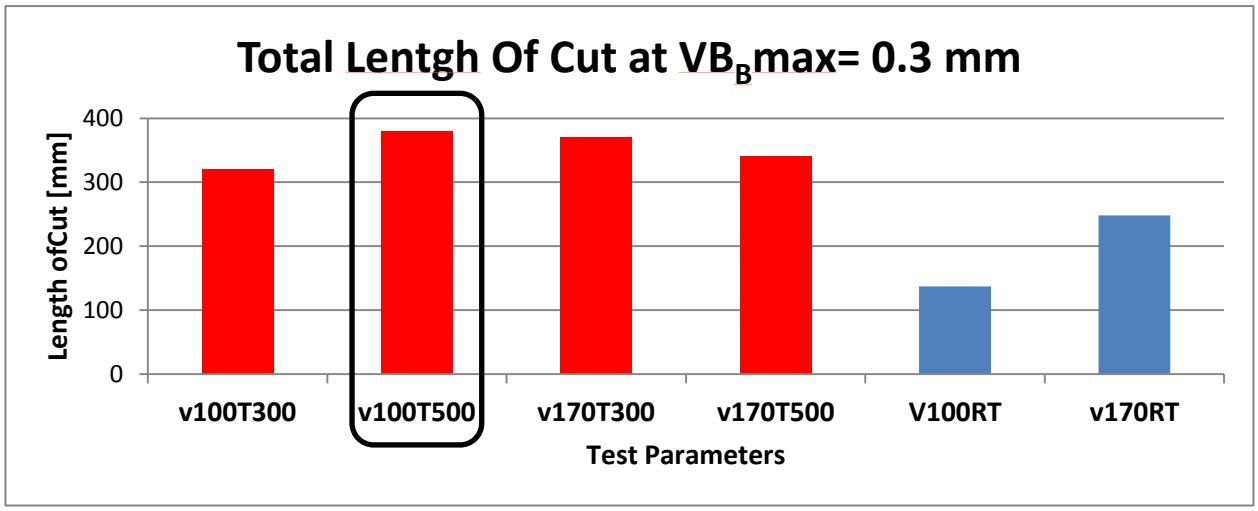

Figure 2.14-Effect of Laser Assisted Machining on the length of cut

Figure 2.15 shows the morphology of chip formation when LAM is used. One can observe that the chip formation is different from the conventional QSD test (Figure 2.6). In LAM conditions, the chip segments are more random and do not exhibit a uniform pitch. Since the matrix material had two phases (alpha, and beta), the different contrast in the beta (β) structure in the right box of Figure 2.15 shows elongated grains, which are an indication of a plastically deformed surface.

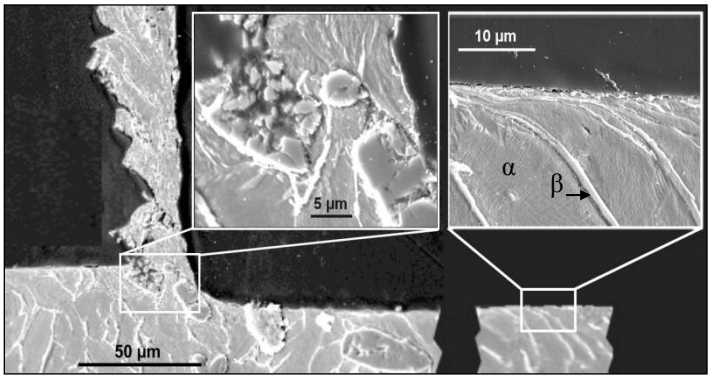

Figure 2.15- The first quick stop test ever done with Laser Assisted Machining was performed on TiMMC with v = 70 m/min and a surface temperature of 500°C

Effect of LAM on tool life, testing hypothesis #4

To understand the effect of temperature on machining and tool life, a test at a very high surface temperature of 1000°C was performed with a cutting speed of 100 m/min. This allowed

the understanding of the enhancement of tool life with LAM. Figure 2.16 shows the chip morphology of this test. We can see that the morphology changed in the titanium matrix. Also, the particles were observed to be much less broken; they seem displaced in the softer matrix. Therefore, there is less contact at the tool face, which results in reduced abrasive tool wear. The increase of tool life observed with LAM is in contradiction with hypothesis #4.

Figure 2.16- Chip morphology when the surface temperature is at 1000°C

Limitation of LAM on tool wear

Although LAM can enhance tool life, there is a limitation in LAM if high temperatures and high cutting speeds are used. As previously mentioned, abrasion wear is the main wear mode when machining MMCs. However, increasing the temperature and the cutting speed results in additional diffusion wear. Diffusion wear arises from extremely high temperatures at the chip/tool interface. Figure 2.17 shows the worn PCD tool with signs of diffusion wear.

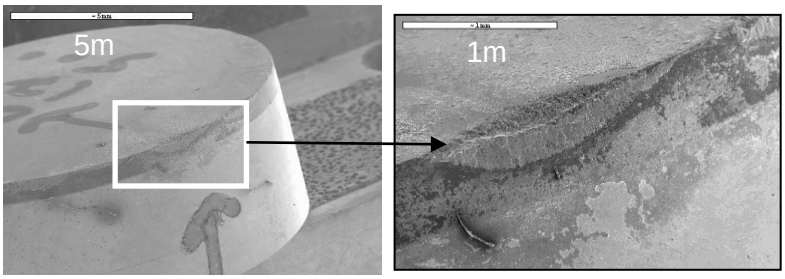

Figure 2.17- Signs of diffusion wear at 170 m/min, and high surface temperature (500°C)

2.4.4 General summary of LAM

LAM was shown to be an excellent solution for the issue of short tool life when cutting TiMMC. Tool life was increased up to 180% with a cutting speed of 100 m/min and a surface temperature of Ts = 500°C. An explanation of the increased tool life with LAM has been related to the tool/particle interaction, where the particles displace in the softer matrix instead of breaking and contributing to additional abrasion wear. LAM did not produce a change in surface morphology, or a phase transformation (at a temperature up to 500°C). While abrasion wear remains the dominant wear mode, signs of diffusion wear also appeared in LAM at high speeds and high surface temperature. Therefore, there is a limit, above which further increase in surface temperature will increase the tool/chip interface temperature and will promote tool diffusion wear. Figure 2.18 shows a summary of the results in four cases:

- Case 1: The lowest tool life occurred at a low speed of 100 m/min when cutting at room temperature.
- Case 2: A better tool life occurred when the speed was increased to 170 m/min (high speed).
- Case 3: The best tool life was achieved when using LAM with a low speed of 100 m/min.
- Case 4: When the speed is increased to 170 m/min, a reduction of tool life was observed due to the combination of abrasion and diffusion wear modes.

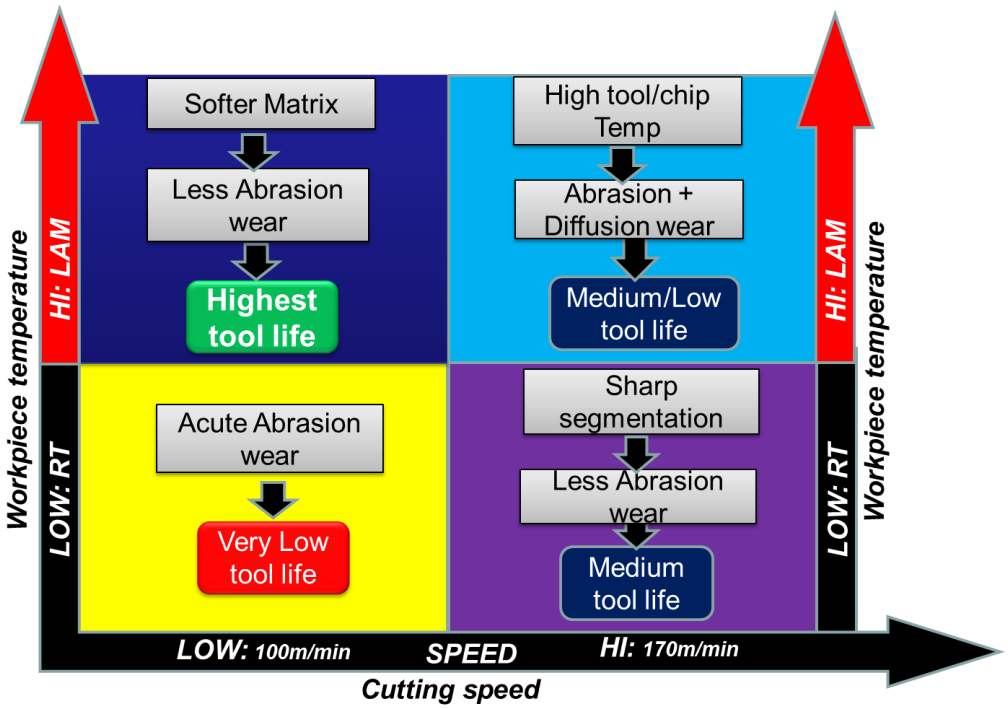

Figure 2.18- Summary of the effects of Laser Assisted Machining and speed on tool wear

More information can be found in the published paper in appendix [A3].

2.5 Chip formation model when machining TiMMC

The section below is based on the papers in the appendix [A1, A4] with the titles below:

A1- R. Bejjani, M. Balazinski, B. Shi, H. Attia, H. Kishawy, *"Machinability and Chip Formation of Titanium Metal Matrix Composites"*, Int. J. of Advanced Manufacturing Systems, IJAMS, vol. 13, "1" , 2011.

A4- R. Bejjani, M. Balazinski, H. Attia, G. L'Espérance,*" On The Adiabatic Shear Banding And Microstructure Evolution When Machining Titanium Metal Matrix Composites",* (submitted in June 2012, ASME, Journal of Manufacturing Science and Engineering, REF: MANU-12-1170).

The chips formed when machining TiMMC were observed to have segmentations. This type of chips is characterized by the formation of an adiabatic shear band and seems to be a particularity of TiMMC. Therefore, a new chip formation model was proposed. When turning conventional materials at high speeds, higher temperature at the tool tip are expected, resulting in

tool life reduction. However, our experiments showed that tool life increased with an increase of cutting speed. This uncommon phenomenon will be further investigated.

The raw material morphology shows distinctive titanium alloy phases (Alpha and Beta) and hard TiC particles. The benefit of having such a material is that the particles and different phases leave a trace after plastic deformation. Furthermore, the hard particles are brittle, therefore they can only crack and not deform. Studying the chip formation using quick stop tests' samples led to the observation of a "dual zone" chip formation shown in Figures 2.19 and 2.20.

Zone 1: This zone is characterized by very high plastic strains. This zone is shared with previous segments. Observing the grain boundaries' elongations, it was noticed that due to the high strains the grain boundary lines end up being parallel to the tool's rake face. It was also observed that traces from the shear lines of many previous segments are still apparent.

Zone 2: This zone is characterized by very low plastic deformation. The material seems to be just displaced into the chip without high strain deformation.

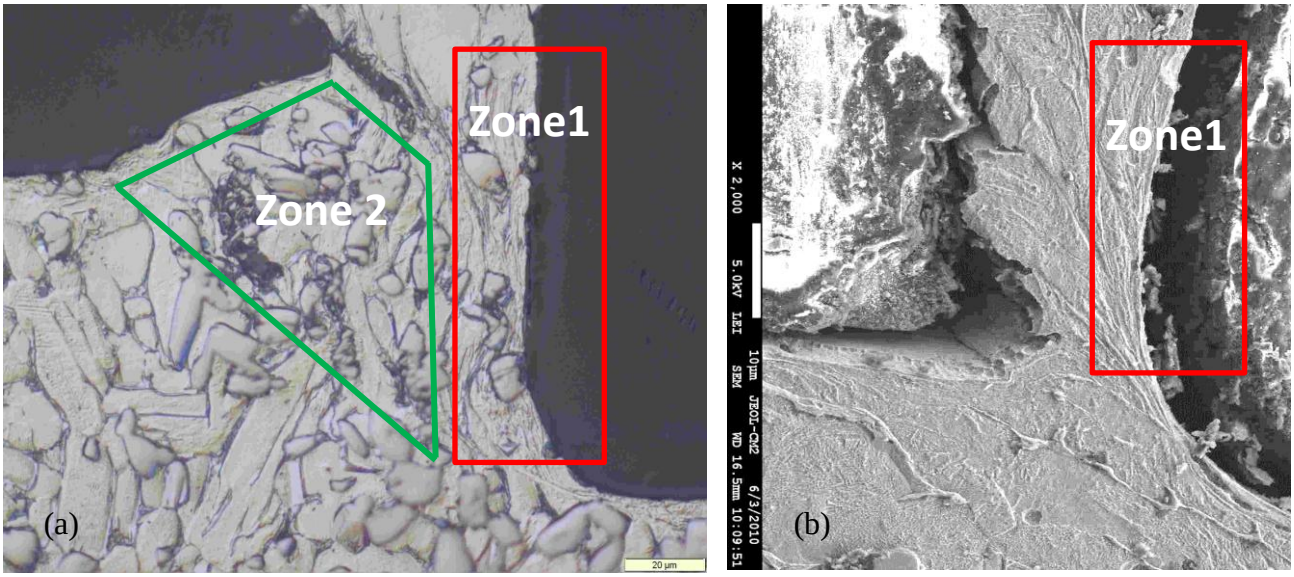

Figure 2.19- Different zones in chip formation at the speed of 50 m/min (a), 150 m/min (b)

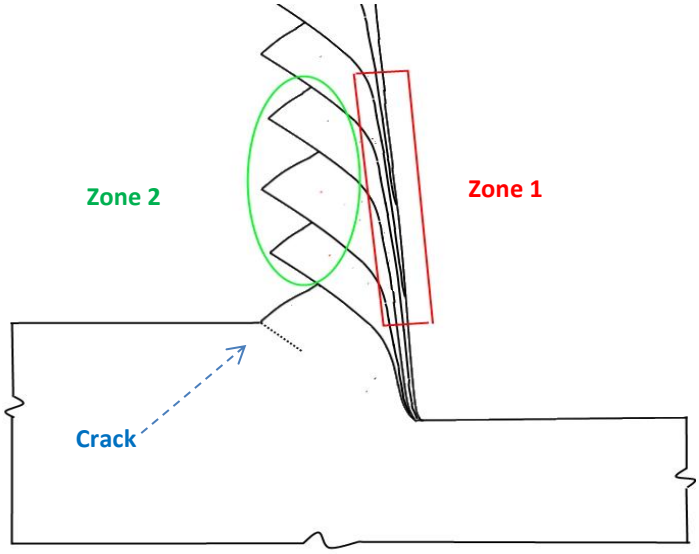

Figure 2.20- Chip formation model for TiMMC

The chip formation in Figure 2.20 has some similarities to previous models suggested by Nakayama and Komanduri [22, 23]. The shear angle seems to be close to 45 degrees, as described by Nakayama [22]. The shear line seems to be a straight line and not shaped as an arc as described by Komanduri [23]. Multiple tests using the Quick Stop Device (QSD) were performed to study crack initiation. Figure 2.21 shows evidence that the crack starts at the free surface. The crack may initiate at irregularities in the machined surface or at grain boundaries. The elongated grains observed in the ASB region in Figure 2.21 indicate that the ASB is still not fully formed, as the grain boundaries do not show close and parallel lines. This is in favor of the theory that the crack first initiates at the free surface before the formation of a clear ASB.

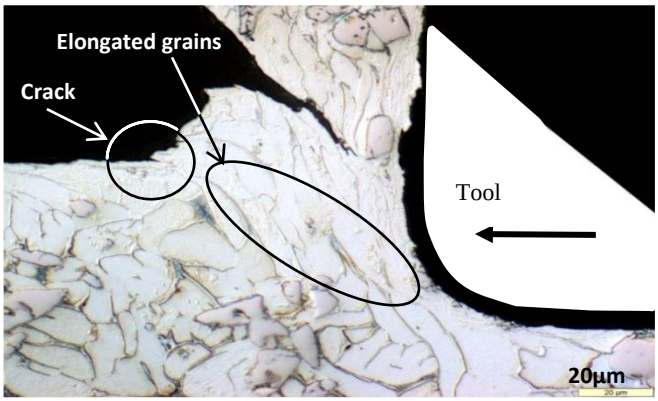

Figure 2.21-Photomicrograph showing a crack initiation at the free surface at the speed of 60 m/min

Figure 2.22 shows the path the particle took after breaking (from A to B). This particle was first in line with the adiabatic shear band, and then was sheared and displaced. The figure also shows the length of the displacement which the particle incurred after breaking.

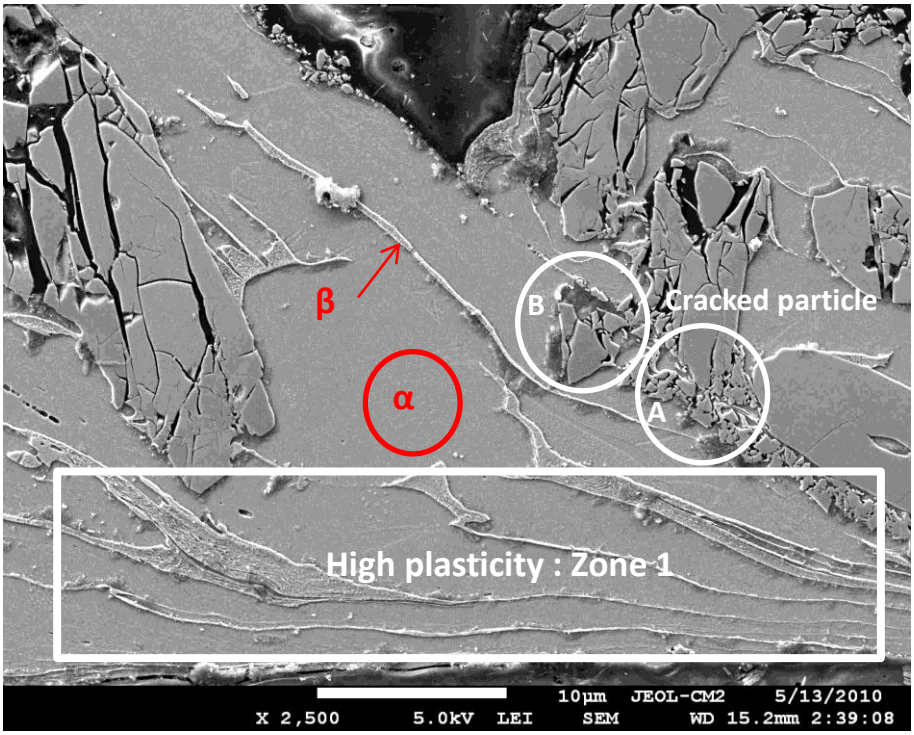

Figure 2.22-Photomicrograph showing a particle broken and displaced from position ‘A’, to position ‘B’ (at the cutting speed of 180 m/min)

2.5.1 Free surface and sheared surface

The formed chip shows that there are two surfaces on the chip free side. The surface which was originally the free surface is shown as ‘A’ in Figure 2.23, and the surface formed by the adiabatic shear band is shown as ‘B’. Close examination of this surface reveals a dimple structure. This structure is typical of ductile fractures in metals, where voids will nucleate, then grow and coalesce during shear deformation, generating a sheared surface.

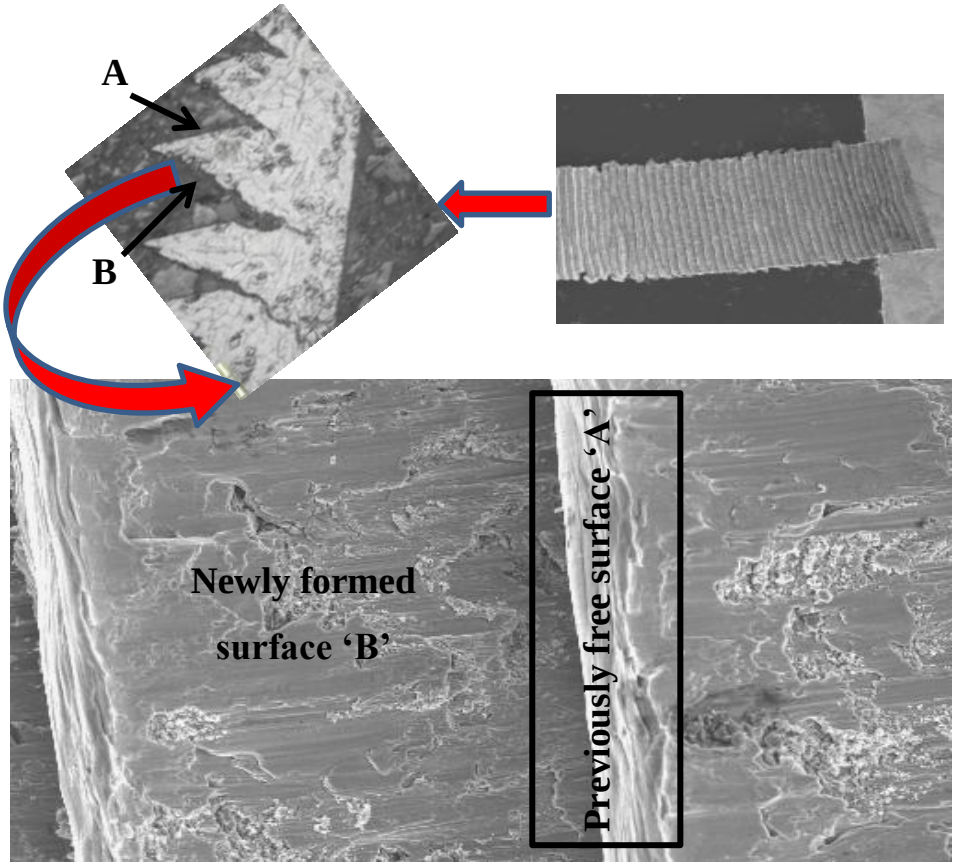

Figure 2.23-The two different surfaces 'A' and 'B' on the segmented face of the chip (at the speed of 50 m/min)

Effect of the cutting speed on tool life, testing hypothesis # 3

From the chip formation model and the previously observed chip morphologies, a thorough analysis was carried out in order to identify the relationship between the tool life and the cutting speed. It was observed that, fewer particles were broken in the chips when cutting at high speeds. In general, if a particle is located inside the segment's bulk, and not in-line with the shear band, then this region of low plastic strain will not induce high enough stresses to break the particle. Therefore, since the particle will be just displaced and not broken, it will result in less abrasion wear on the tool. This is in opposition to hypothesis # 3. Figure 2.24 shows the particle's behavior at different speed.

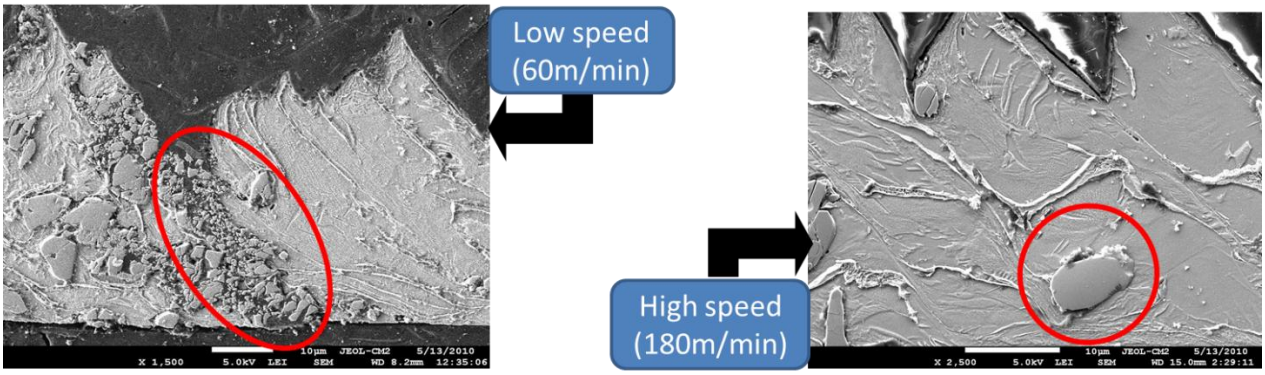

Figure 2.24- Particle behavior at different cutting speeds

For more information see the papers in appendix: [A1,A4], and reference [34].

2.6 Microstructure evolution in the ASB of the chips

The section below is based on the paper in the appendix [A4] with the title below:

A4- R. Bejjani, M. Balazinski, H. Attia, G. L'Espérance,*" On The Adiabatic Shear Banding And Microstructure Evolution When Machining Titanium Metal Matrix Composites",* (submitted in June 2012, ASME, Journal of Manufacturing Science and Engineering, REF: MANU-12-1170).

As indicated previously, machining TiMMC produces segmented chips which have been attributed to "plastic instability". The segments are characterized by adiabatic shear bands (ASB). In this research, samples were extracted from different specific locations inside the chips for subsequent observation. The objectives were to study the initiation of the ASB and the effect of the hard TiC particles on the ASB formation, and to observe the microstructure inside the ASB as well as in the vicinity of the ASB. Moreover, a model describing the microstructure evolution at different stages of the ASB formation is proposed.

Transmission Electron Microscopy (TEM) observations were performed at the atomic scale, and lattice dislocations were identified. For producing a TEM sample, thin films of specimen have to be prepared. The specimen has to be very thin in order to be electron transparent. The Focused Ion Beam (FIB) technique was used to prepare the TEM specimen. FIB preparation is a long process; however it has advantages over other techniques, such as electropolishing.

TEM is a good tool for the identification of dislocations. During plastic deformation, dislocations usually originate at the grain boundaries. With increasing strain and work hardening, dislocation interaction by cross slip and dislocation multiplication may occur sooner in high stacking fault energy materials [35]. Selected Area Diffraction (SAD) was performed on different regions inside the ASB as indicated by circles in Figure 2.25 (d). All lattice structures inside the ASB were indexed and found to correspond to alpha (h.c.p.) phase. The beta (b.c.c.) or alpha prime (martensite) phases were not found. Therefore phase transformation within the Adiabatic Shear Band (ASB) is unlikely. The orientation angles were all within 2 degrees, indicating that these microstructures are sub-grains. Some grains show, however, a remarkable difference in their orientation angles, indicating that some recrystallized grains have also been formed.

Figure 2.25 (a, b, c) shows the new model that the authors proposed for the sequence of microstructure evolution occurring in the ASB: (a) Random dislocation distribution in large grains, (which is not a low energy configuration), (b) The random dislocation distribution gives way to elongated cells (i.e. dynamic recovery) and the misorientations increases. Subsequently, dislocations accumulation and rearrangement lead to the formation of sub-grain boundaries (c).

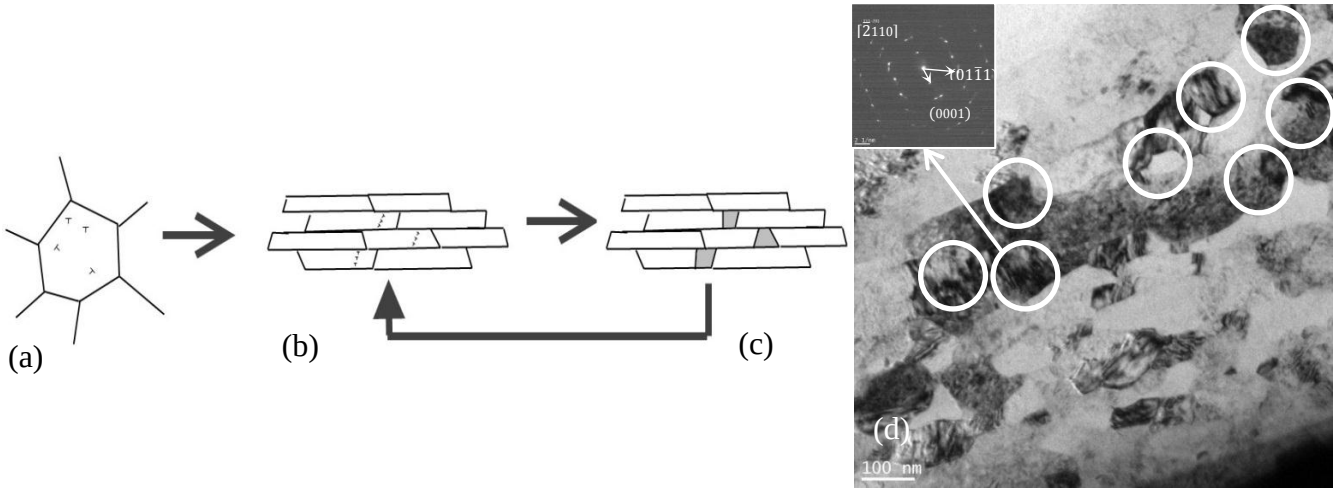

Figure 2.25- Proposed evolution sequence for the formation of nano-grains, a) Random dislocation in large grains, b) Elongated cells, and redistribution of dislocations, c) Formation of some equiaxed nano-grains. d) Actual TEM showing nano-cells inside the ASB

2.6.1 Main results and discussions

Based on Transmission Electron Microscopy (TEM), observations at the atomic scale were made and lattice dislocations were identified. The microstructure inside the ASB is composed of elongated nano-grains, with a presence of some equiaxed nano-grains. The new proposed microstructural evolution model attributes the resulting microstructure to Rotational Dynamic Recrystallization (RDX). The combination of very small grains and cells in proximity with a low dislocation density, leads to the possibility of the following chain of events: plastic strain results in grain elongation, and high dislocation. Elongated cells break-up, forming new recovered sub-grains with some recrystallized nano-grains characterized by a low dislocation density, and high misorientation. The process may repeat itself, resulting in a smaller scale of grain size.

The temperature inside the ASB was estimated to be close to the recrystallization temperature, however no martensite was observed, and no b.c.c. reflection was identified, indicating the unlikelihood of phase transformation inside the ASB. The fractured surface of the ASB was observed to be a dimpled and smeared surface. Melting with re-welding of the ASB was shown to be unlikely due to the insufficient temperature inside the ASB. This is also confirmed by the morphology of the microstructure in the ASB since solidification would have most probably produced columnar grains in the vicinity of the ASB matrix [36]. The formation of the segmentation mechanism was observed to start with a crack on the machined surface, and not from the tool tip.

TEM studies of ASB for TiMMC have never been done previously for machining applications. The results obtained here can provide valuable information on the understanding of ASB and can improve future FEM simulations involving segmentation.
More information can be found in the paper in appendix [A4], and the references [34, 37-39].

2.7 Finite element Method (FEM); simulation of chip formation

The section below is based on the papers in the appendix [A5] with the titles below:

A5- R. Bejjani, B. Shi, H. Attia, M. Balazinski*," Simulation of Segmented Chip Formation in Laser Assisted Machining of Titanium Metal Matrix Composite",* (submitted in Sept. 2012, International Journal of Machine Tools and Manufacture, Ref: IJMACTOOL-D-12-00567).

In recent years, FEM is gaining more and more importance in machining simulation processes since it allows for the prediction of cutting forces, chip formation, material temperature and chip segmentation. The methodology used in FEM involves many steps (Figure 2.26). In this research, a damage model and a newly developed constitutive equation were used and then validated with experimental data. The developed constitutive equation is an equivalent homogenous equation and describes the relationships between the stress, strain, strain rate and temperature of the TiMMC's constituents as a whole. To the author's best knowledge, no previous work aiming at modeling the segmented chip formation using LAM for TiMMC or any other material has been carried out before.

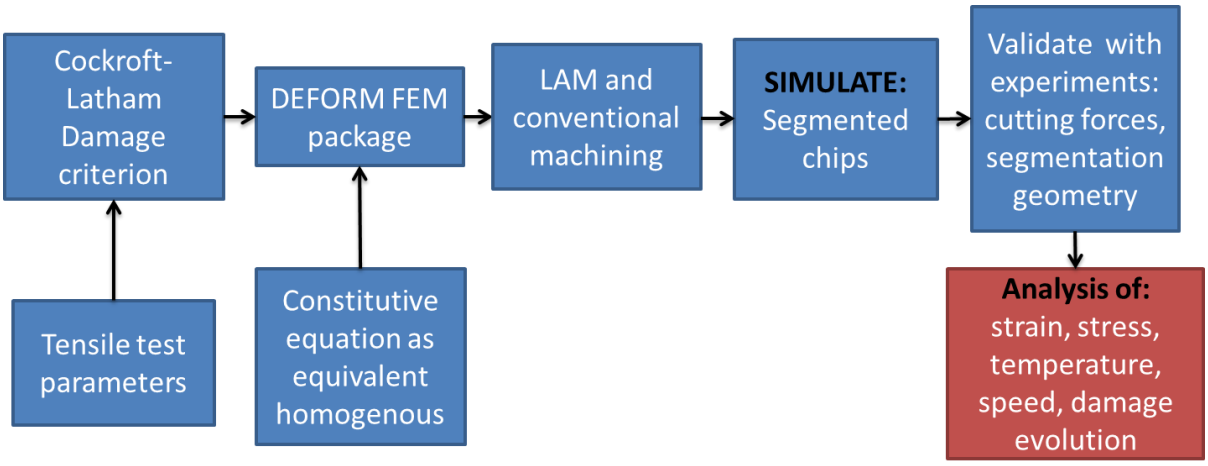

Figure 2.26-FEM simulation flowchart

2.7.1 Identification of the constitutive equation

The identification of the constitutive equation is based on the Distributed Primary Zone Deformation (DPZD) model developed at the NRC and shown in figures 2.27 and 2.28 [40, 41]. The model describes the plastic deformation in the primary deformation zone and integrates it into a methodology in order to identify the material's constitutive law in machining. Figure 2.27 shows the chip with the primary shear zone. The workpiece moves towards the cutting tool at a cutting speed (V) and the cutting tool, with the rake angle γ, is stationary. When the tool passes through the workpiece, the workpiece material, with the undeformed chip thickness (t_u), is deformed and a chip, with a thickness (t_c), is formed. The plastic deformation is assumed to start at the straight line CD (inlet boundary), inclined to the free surface at an angle corresponding to the shear angle (ϕ), and to end at the straight line EF (outlet boundary). The two boundaries are

assumed to be parallel to the shear plane AB. The distributions of the stress, strain, strain rate and temperature in the primary shear zone are shown in Figure 2.27 (b).

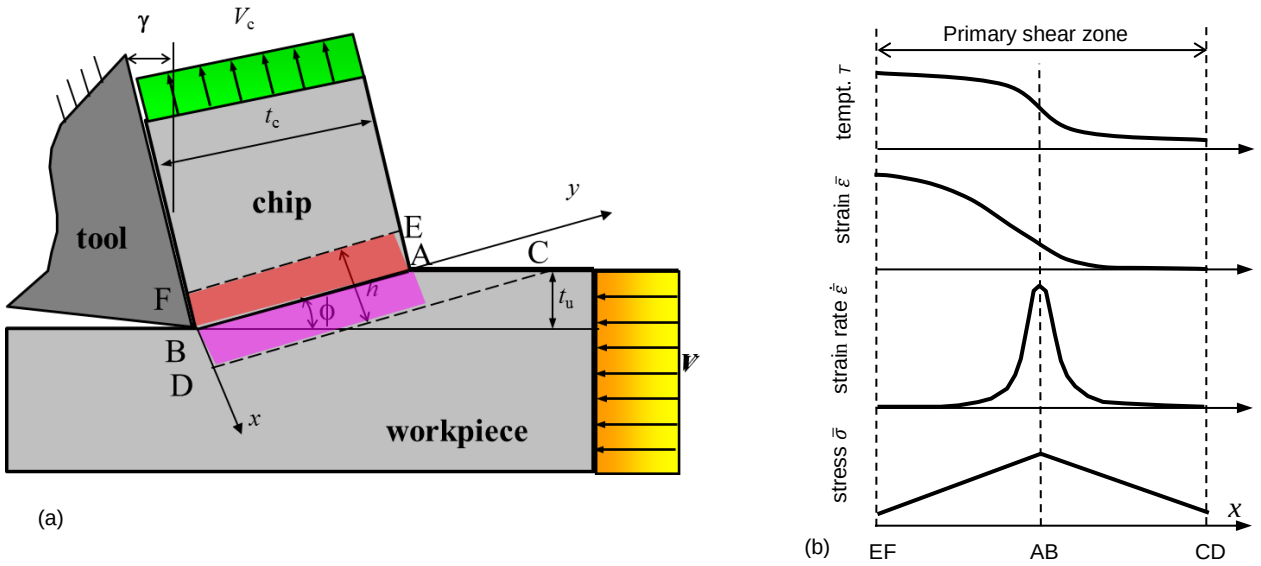

Figure 2.27- a) Parallel-sided shear zone model, b) Typical distributions of $\bar{\sigma}$, $\bar{\varepsilon}$, $\dot{\bar{\varepsilon}}$, and T [40]

2.7.2 The FEM model

The DPZD model mainly uses an analytical approach which, in combination with F_c, F_t, and t_c measured from orthogonal cutting tests, is used to predict the distributions of effective stress (or flow stress) $\bar{\sigma}$, effective strain $\bar{\varepsilon}$, effective strain rate $\dot{\bar{\varepsilon}}$, and temperature T (Figure 2.28). Quasi static tensile test performed at room and high temperatures are also added. All this data is combined, then compiled and a curve fitting technique is used to identify the constitutive law. The Johnson Cook (JC) model with five material coefficients (A, B, n, C, m) was used as

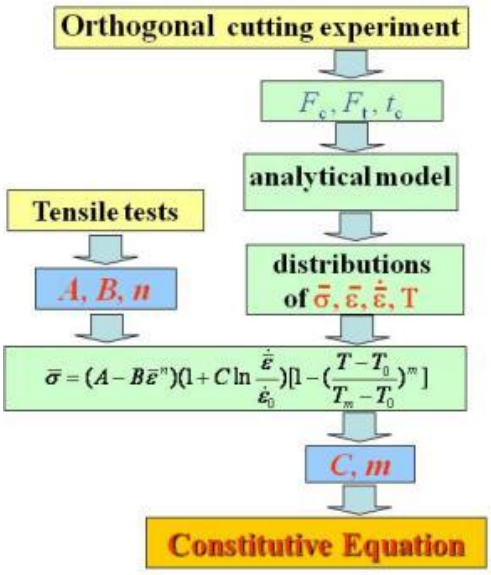

Figure 2.28- Development of the constitutive equation [40]

constitutive law, where strain hardening and adiabatic softening are taken into consideration.

.

$$\bar{\sigma} = \left(A + B\bar{\varepsilon}^{n}\right)\left(1 + C\ln\frac{\dot{\bar{\varepsilon}}}{\dot{\varepsilon}_0}\right)\left[1 - \left(\frac{T - T_0}{T_m - T_0}\right)^{m}\right] \qquad [2\text{-}1]$$

Where $\dot{\bar{\varepsilon}}_0 = 10^{-3}\,1/\mathrm{s}$, T_0 = room temperature, T_m = melting temperature. The first term in the equation describes the strain hardening effect, the second is the strain rate effect, and the third term is the temperature softening effect.

The constitutive equation constants' were determined by inputting the cutting force measurements, the tensile test data given in Table 2.1 and the physical properties of the material given in Table 1 into the DPZD model [40]. Figure 2.29 shows a 3D representation of the constitutive model of TiMMC.

JC constants for TiMMC:

A= 1150 MPa, *B*= 442 MPa, *n*= 0.86, *C*= -0.00626, *m*= 1.1

Table 2.1- Tensile tests performed at different temperatures

Sample #	Temp	Yield Stress	Strain at 0.2% offset	True Stress	Ultimate & Fracture stress	Strain at fracture	True stress
	°C	Mpa	mm/mm	Mpa	Mpa	mm/mm	Mpa
1	RT	1170	0.008	1179	1190	0.011	1203
2	RT	1150	0.0085	1159	1180	0.011	1192
3	RT	1100	0.0085	1109	1130	0.011	1142
4	500	590	0.0075	594	675	0.013	683
5	420	640	0.0125	648	725	0.021	740
6	200	780	0.0075	785	875	0.009	882

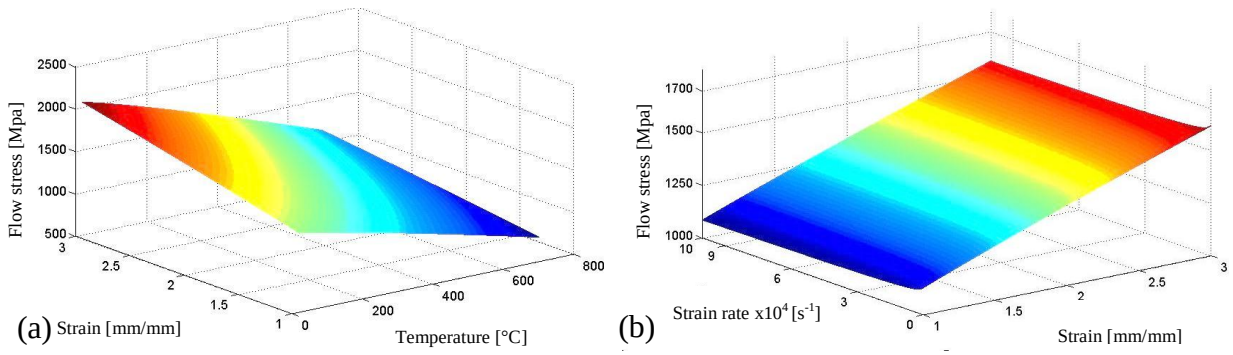

Figure 2.29- 3D representations of flow stress, a) At the strain rate of 104/s, b) At 400°C

2.7.3 Damage criterion

In order to initiate chip segmentation, a damage model has to be integrated in the FEM. The CL (Cockcroft Latham) model has been used in this case. This relatively simple model is based on the observation that the fracture energy, represented by the area under the stress-strain curve, remains constant [27]. This is true also for different temperatures of the material. In other words, as the temperature is increased, the material's ductility increases and therefore the strain is increased. The yield stress is decreased, however, due to temperature softening. Therefore, the area under the stress-strain curve remains constant. Figure 2.30 shows samples of tensile tests until fracture.

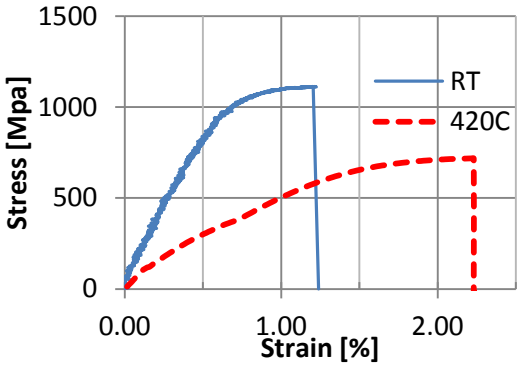

Figure 2.30- Sample of a tensile test performed at different temperatures

The CL constant can be calculated from a tensile test, where the true stress σ^* is integrated until the fracture strain ε_{fn} in the tensile test.

$$\int_0^{\varepsilon_{fn}} \sigma^* \, d\varepsilon = C \qquad [2\text{-}2]$$

2.7.4 Friction model

Since there is no universal consensus on a general friction model, multiple preliminary simulation tests were performed using a shear friction model. Since cutting at high speeds (considered here to be speeds above v = 50 m/min) generates higher temperatures, a lower value of the shear friction 'm' generated simulation results which conform better to the experimental results. Consequently, the formula below was generated for the shear friction factor, where the value of 'm' is related to the cutting speed.

$$m = 0.2i + 0.4 \begin{cases} i = 1 \text{ for } v \leq 50 \text{ m/min} \\ i = 0 \text{ for } v > 50 \text{ m/min} \end{cases} \quad [2\text{-}3]$$

2.7.5 FEM simulations results and discussion

Very little work has been performed on Finite Element Method (FEM) simulation with Laser Assisted Machining (LAM), and no work has addressed the simulation of segmented chips during LAM. The FEM simulations were validated experimentally where the cutting force and chip segmentation's pitch and thickness were validated with actual experimental tests.

High strains values were shown to be present in the adiabatic shear bands (ASB) and secondary shear zone. Furthermore, the effect of high cutting speed, as well as, LAM resulted in a reduction of the cutting forces.

The Cockcroft-Latham model was shown to be well adapted to machining with high temperatures and high strain rate conditions. In FEM simulations, the highest damage values were found along the primary shear zone and close to the free surface. The quick stop tests confirmed this prediction and showed that the segmentation is initiated by a crack at the free surface before the full formation of an adiabatic shear band.

Diffusion wear is a main issue when machining titanium alloys. Using the FEM temperature profiles; a possible reason for the increased tool life when using LAM was explained (Figure 2.31). Unexpectedly, adding a heat source to the workpiece's surface, resulted in a reduced peak temperature at the tool/chip interface, even though the overall average temperature of the chip is increased. The reduced peak temperature of the tool/chip interface reduces the diffusion wear

effect, which can increase tool life. This is in contradiction to hypothesis #4 where a drop in tool life was expected with LAM.

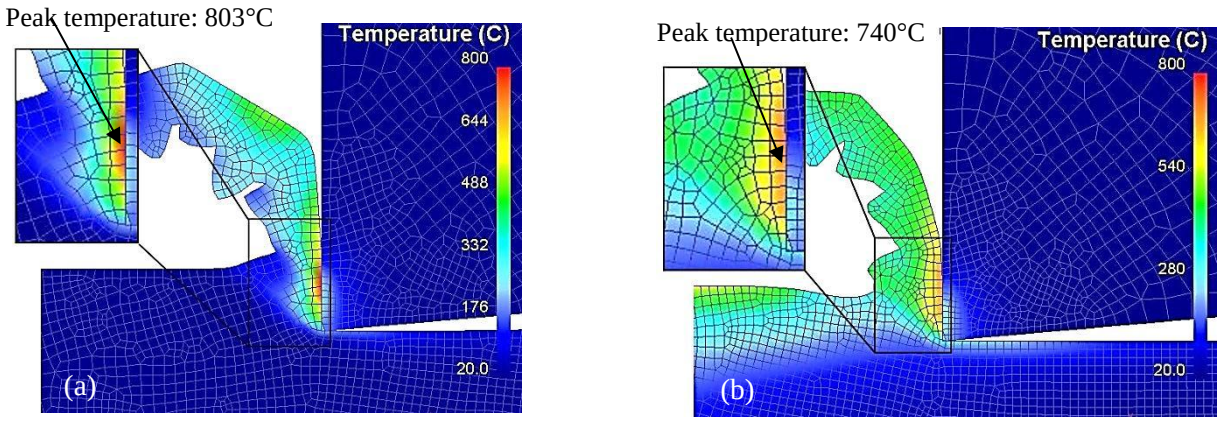

Figure 2.31- Temperature profiles at v = 150 m/min using conventional cutting (a) and LAM (b)

More information can be found in the paper in appendix: [A5].

CHAPTER: 3- ADDITIONAL RESULTS: DAMAGE EVOLUTION

Many alloys produce segmented chips when machined. TiMMC is one of them. The segmentation is characterized by an ASB. Experimentally, a crack initiation occurs when a segment is produced [21-23]. In the literature, there is no general agreement on the location of the crack initiation; however, most researches mention that the crack initiates either at the free surface or at the tool tip [21-23]. To gain a better understanding of the segmentation process; experimental tests and FEM simulations aiming at investigating the crack initiation process and damage evolution in chips were performed. The damage value 'C' corresponds to the criterion shown in equation [2-2]. This work is to be published soon.

3.1 Damage precursor and development: analysis with FEM

3.1.1 Investigation of damage across the segment: precursor of segmentation

When there is a sharp increase in the maximum principal stress combined with an increasing effective strain (which results in strain hardening), the accumulated damage peaks, and therefore generates the precursor of segmentation (Figure 3.1 step 206, which corresponds to the segmentation initiation). This is followed by an increase in temperature, which favors a reduction of stress and an increase in strain in the next simulation steps. However, after the peak of the accumulated damage (Figure 3.1 step 216), a decrease in the total accumulated damage is observed, leading to the end of the segmentation process.

3.1.2 Investigation of damage along the segment: precursor of crack initiation

Figure 3.2 shows the damage profile along the segment starting from the tool edge to the free surface. The highest value of damage starts building up at the tool tip area in step 180 (which is the step just before the segmentation initiation). However, the damage value is not high enough to cause element deletion (or the equivalent of crack initiation in FEM). The maximum accumulated damage starts in the middle of the segment, and element deletion is initiated in the FEM in step 206. This is followed by damage at the free surface. The damage value follows a cyclic pattern of peaks inside the middle of the segment (step 206), then at the free surface (step 216). The process repeats itself several times until the completion of the segment. It can be

concluded that the combination of a peak maximum principal stress with a high cumulative effective strain contributes to the damage peak, and to the beginning of element deletion.

The comparison with the QSD experimental test is shown in Figure 2.21, where a crack appears at the free surface with an elongation of the grains in the middle of the segment. Crack initiation at the free surface works concurrently with high effective strain values in middle of the segment, until a completed segment is formed.

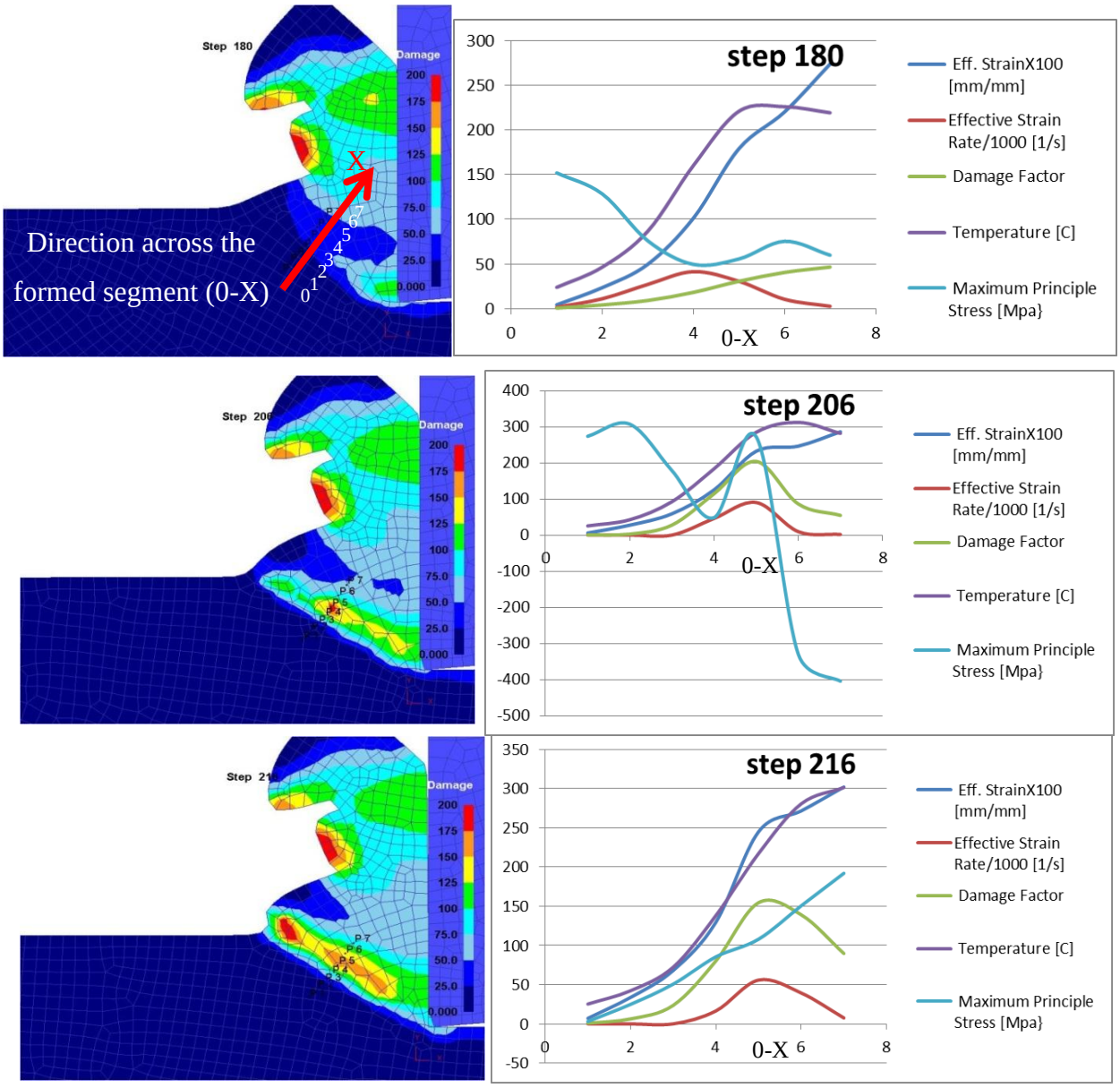

Figure 3.1- Evolution of damage across the Adiabatic Shear Band

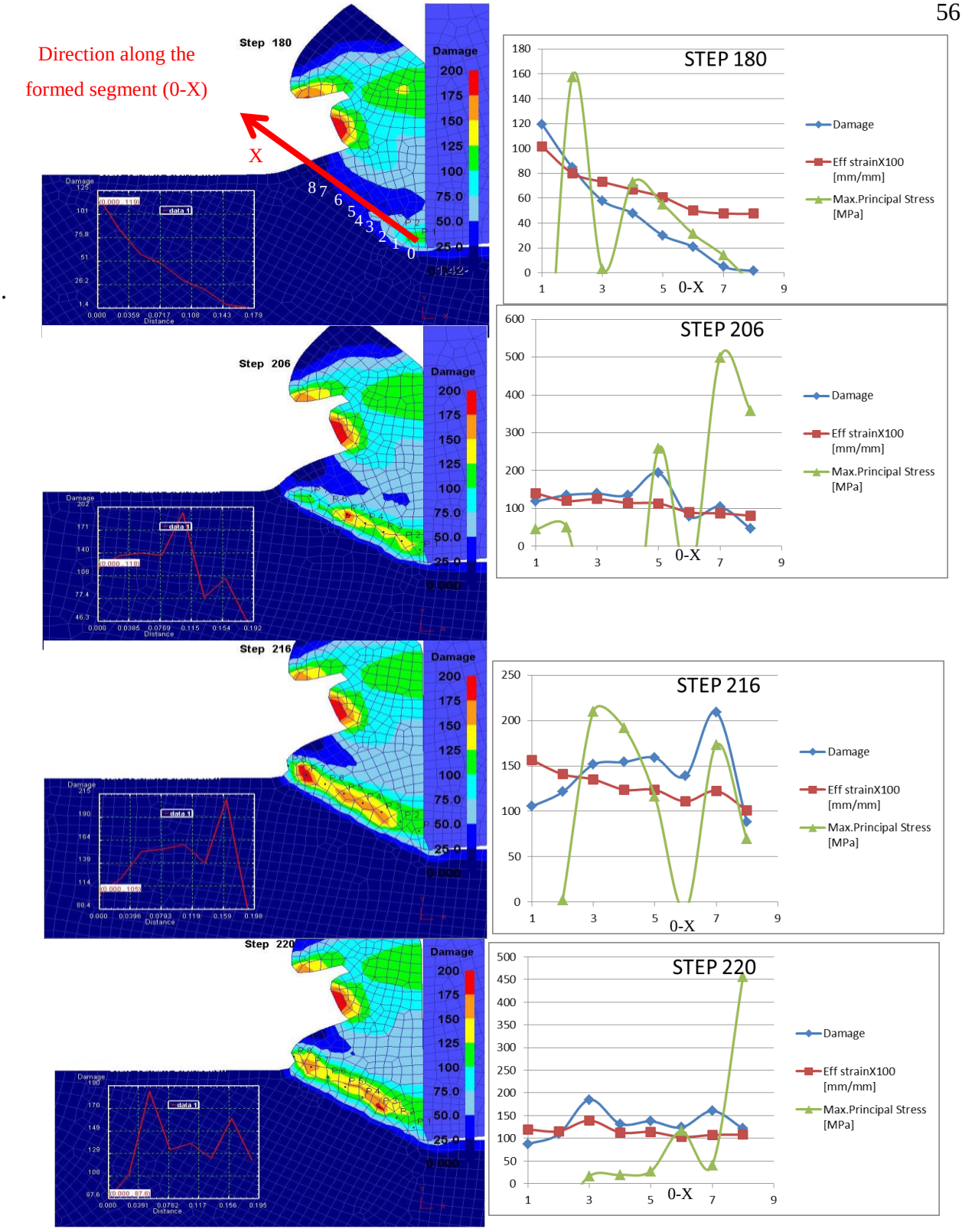

Figure 3.2- Evolution of damage along the Adiabatic Shear Band

3.2 Discussion of results in damage evolution

In the FEM simulation model, the combinations of stress and strain can lead to damage. The damage in FEM simulation is analogous to the segmentation development. Experimentally, it is very difficult to capture each moment during the segmentation process; however a step by step analysis with FEM made it possible.

The FEM simulation observations across the ASB show that the precursor of damage is a peak of maximum principal stress combined with an increase in accumulated effective strain. When the accumulated damage reaches the critical damage value, element deletion occurs. The damage stops when there is a drop in the maximum principal stress. This is favored by the increase in temperature, and therefore a decrease in material yield strength.

The FEM simulation along the ASB shows that the increase of strain in the middle of the segment can lead to an increase of damage at the same location, and then later at the free surface. The process will keep alternating with peaking damage in the middle of segment then at the free surface until the completion of the segmentation process. The simulation shows also that, even though the damage value starts building up at the tool edge, it will never reach the critical value necessary to cause element deletion.

An analogy can be made with the results obtained experimentally in the QSD tests, in which crack formation was observed at the free surface with a high strain at the location in the middle of segment. Furthermore, in these experiments no crack occurred at the proximity of the tool tip.

CHAPTER: 4- GENERAL DISCUSSION

Three approaches were used in this research study as presented in Figure 2.1. The first experimental approach with TAGUCHI DOE, was used mainly to identify the optimum cutting parameters for the best tool life and surface roughness. The second and third approaches aimed at identifying the phase transformations in the chips, chip formation with ASB evolution, and FEM. All three approaches were used for the understanding of the tool/particles behavior and for the assessment of the effect of speed and LAM on tool life. The three approaches used throughout this project are summarized below.

In the first experimental approach, this thesis is the first of its kind to seek practical recommendations for defining the cutting parameters and evaluating different cutting tools when machining TiMMC. Following the experimental work and the analysis of results, it was found that cutting TiMMC at higher speeds is more efficient and productive since tool life is increased. This is in opposition with most materials and to the Taylor's tool wear curve.

SEM microscopy was used to explain the particle behavior in the chips under high stress and strain conditions. The phenomenon of efficient cutting at higher speeds (in terms of enhanced tool life) was explained by the different tool/particles behavior where, at higher speeds, fewer hard TiC particles are broken resulting in reduced tool abrasion wear. In order to further increase the tool life, laser assisted machining was performed. LAM was shown to increase tool life by approximately 180% and to be a good solution for machining TiMMC.

Using SEM microscopy, it was found that the tool/particle interaction during cutting can exist under three forms. The particles can either be cut at the surface, pushed inside the material, or even some of the pieces of the cut particles can be pushed inside the material. No particle de-bonding was observed.

In the second approach that was followed in this research, a thorough understanding of the Adiabatic Shear Band (ASB) formation in the segmented chips was required. To understand the chip formation and the crack initiation in the segmentation process when cutting TiMMC, a new concept of a "Quick Stop Device" was designed and used to freeze the cutting action. The new device has multiple advantages over other models found in literature, in terms of efficiency and safety. Subsequently, using a multi-scale (macro and nano) analysis with Scanning Electron Microscopy (SEM), and Transmission Electron Microscopy (TEM), a new model for the

microstructure and grain evolution inside the ASB was developed. This new model is the first to be developed for TiMMC. The model showed that inside the ASB, new nano-grains and cells are formed and characterized by a low dislocation density. However, no phase transformation was found in the ASB.

In the last approach of this research project, an FEM model was developped in order to analyze the different physical parameters (as temperature, stress, strain, damage) involved when machining TiMMC. This required the development of a new constitutive model for TiMMC. To simulate the segmentation process a Cockcroft-Latham (CL) damage model was defined for the TiMMC material. The damage model is based on the work required in a tensile test until fracture. The model gave good predictions for chip segmentation geometry and cutting forces. In order to have a better understanding of the LAM effect on the cutting mechanism, the LAM heat source was simulated and embedded in the same FEM simulation model. Simulations of segmented chips with LAM have never been performed before for TiMMC or for any other material. The results were unexpected and contrary to our hypothesis, in which a higher tool/chip temperature was expected to reduce tool life when using LAM. The analysis of the FEM simulations showed that although LAM increases the overall chip temperature, the peak tool/chip temperature decreases. This could explain the experimental finding that tool life increases when using LAM. To have a better fundamental understanding of the FEM damage and the segmentation sequence, a comparison was made between the FEM model and the experimental chip formation. In both cases the crack initiation, or damage, was shown to never occur at the tool tip. The precursors of damage were determined using stress and strain profiles along and across the Adiabatic Shear Band. Analysis of incremental steps in FEM simulations showed that the damage occurs in a cyclic manner in the middle of the segment, then at the free surface.

4.1 Originality of work and contribution to knowledge

TiMMC is a new material and practically no references can be found in literature concerning its machining. Therefore, this research has many new aspects and provides the main contributions to knowledge listed below:

- Identification of optimum conditions for turning (no data is available for cutting TiMMC) in terms of tool life and surface roughness, **(OBJECTIVE 1, HYPOTHESIS 1).**
- For a fundamental understanding of chip formation, a Quick Stop Device (QSD) was designed and tests were performed. The new QSD has numerous advantages over other designs in terms of ease of use, safety and reliability.
- TiMMC has a segmented chip pattern; using the new Quick Stop Device (QSD) and chip morphology micrographs, the tool/particles interactions were explained. Moreover, experiments using Laser Assisted Machining (LAM) and QSD were performed for the first time, **(OBECTIVE 3).**
- An unexpected phenomenon of improved tool life at high cutting speed was revealed. Using QSD tests and chips photomicrographs, explanations were provided in relation to the different tool/particles interactions, **(HYPOTHESIS 2&3).**
- Explanation of the positive effect of LAM on tool life by the identification and analysis of the tool/particle behavior. LAM has never been used on TiMMC; however, our results showed that it is an effective solution for machining TiMMC as tool life was increased by 180%. This is an unprecedented achievement, **(OBJECTIVE 2, HYPOTHESIS 4).**
- Development of a new constitutive equation for TiMMC. FEM modeling of segmented chip formation has never been performed before for TiMMC, in conventional, as well as, in LAM. The proposed damage model was shown to be valid for simulating the segmentation process, **(OBJECTIVE 5).**
- Using FEM simulations, an additional explanation of increased tool life with LAM was attributed to the reduced peak tool/chip temperature with LAM leading to less diffusion wear, **(OBJECTIVE 2, HYPOTHESIS 4).**
- Phase transformation is unlikely to occur in the formed chips of TiMMC. The FEM simulation showed that the phase transformation temperature was not reached. This was confirmed by Transmission Electron Microscopy (TEM) observations in which no reflections of ‘beta’ were observed.

- Development of a new model for the Adiabatic Shear Band (ASB) microstructure evolution and explanation of the formation of new recovered sub-grains with some recrystallized nano-grains characterized by a low dislocation density, **(OBJECTIVE 4).**
- Development of a fundamental understanding and analysis of the crack initiation and segmentation phenomena in the chip formation during machining of TiMMC. The FEM simulations showed that the precursor of damage (or beginning of the segmentation process) is a combination of the peak in the maximum principal stress and of the increase in accumulated strain.

GENERAL CONCLUSIONS

TiMMC is a new material with a huge potential. To our knowledge, no research can be found in the literature on the machining of such a class of material. Therefore, this research provides an essential contribution to knowledge. Mainly, it delivers guidelines to end users for how to optimize and predict the machining behavior of TiMMC. The research also provides new and effective solutions for Laser Assisted Machining (LAM) of TiMMC.

The research project led to a number of contributions in terms of experimental findings, mechanical design, microstructure modeling and FEM modeling. In other words, the contributions involved the identification of the optimum cutting conditions for TiMMC, the development of a new 'quick stop device", the development of a new model for microstructure evolution in the Adiabatic Shear band (ASB), and the development of a new FEM model for TiMMC involving LAM and segmentation.

Experimentally, PCD tools were shown to give the best results and performed better at higher speeds. LAM enhanced the tool life by 180 %. The reduced tool wear at high cutting speeds was attributed to the reduction of broken particles in the chips, resulting in less abrasive wear. The higher tool life with LAM was explained by the different tool/particles behavior at high temperature. Using the FEM model, the increased tool life was also explained by the reduction of the peak tool/chip temperature with LAM. Furthermore, an analysis of damage propagation and evolution was performed using the FEM model.

Using Transmission Electron Microscopy (TEM), observations were made at the atomic scale and lattice dislocations were identified. Additionally, a new microstructure evolution model in the Adiabatic Shear Band (ASB) was proposed. The model explains the formation of new recovered sub-grains containing recrystallized nano-grains characterized by a low dislocation density, and high misorientation. The TEM observations showed that no phase transformation occurred in the ASB. Additionally the FEM temperature results confirmed that the phase transformation temperature was not reached.

For a fundamental understanding of the crack initiation and segmentation phenomena in the formed chips, the FEM simulation was used to identify the precursors of damage. It was found that the precursor of damage (or segmentation) is a combination of the peak in the maximum principal stress and the increase in the accumulated strain. The damage evolution

indicated that the crack initiation occurs in a cyclic manner in the middle of the formed segment, then on the free side of the chip. The damage never occurred on the tool tip side as was suggested by other researches. This was confirmed by the QSD tests in which crack initiation was shown to start at the free surface.

The results of this research will aid engineers for the optimization and analysis, and could be used as a prediction tool for the machining of TiMMC. Therefore, costly trial and errors in machining will be avoided. Consequently, this research will promote the application of TiMMC for many industries, and will have a positive impact on the Canadian economy. This research led to the publication of ten papers, nine of which as first author, and four in refereed journals (see Appendix B).

REFERENCES

[1] J. Bell, T. Stephenson, A. Waner, and V. Songmene, "Physical properties of graphitic silicon carbide aluminum metal matrix composites," *SAE Paper* vol. No. 970788, 1997.

[2] C. H. Che-Haron, "Tool life and surface integrity in turning titanium alloy," *Journal of Materials Processing Technology,* vol. 118, pp. 231-237, Dec 2001.

[3] V. Songmene and M. Balazinski, "Machinability of Graphitic Metal Matrix Composites as a Function of Reinforcing Particles," *CIRP Annals - Manufacturing Technology,* vol. 48, pp. 77-80, 1999.

[4] S. Abkowitz, S. M. Abkowitz, H. Fisher, and P. J. Schwartz, "CermeTi (R) discontinuously reinforced Ti-matrix composites: Manufacturing, properties, and applications," *Jom,* vol. 56, pp. 37-41, May 2004.

[5] S. Kannan, H. A. Kishawy, and M. Balazinski, "Flank wear progression during machining metal matrix composites," *Journal of Manufacturing Science and Engineering-Transactions of the Asme,* vol. 128, pp. 787-791, Aug 2006.

[6] S. Basavarajappa, G. Chandramohan, K. V. N. Rao, R. Radhakrishanan, and V. Krishnaraj, "Turning of particulate metal matrix composites - review and discussion," *Proceedings of the Institution of Mechanical Engineers Part B-Journal of Engineering Manufacture,* vol. 220, pp. 1189-1204, Jul 2006.

[7] N. Tomac and K. Tonnessen, "Machinability of particulate aluminium matrix composites," *CIRP Annals - Manufacturing Technology,* vol. 41, pp. 55-58, 1992.

[8] R. B. Aronson, "Machining composites," *Manufacturing Engineering,* vol. 122, p. 52, 1999.

[9] H. P. Degischer and G. Requena. (2008, january 2010). *Assessment of Metal Matrix Composites for Innovations*. Available: http://mmc-assess.tuwien.ac.at/mmc/Home.html

[10] D. B. Miracle, "Metal matrix composites – From science to technological significance," *Composites Science and Technology,* vol. 65, pp. 2526-2540, 2005.

[11] N. Muthukrishnan, M. Murugan, and K. P. Rao, "Machinability issues in turning of Al-SiC (10p) metal matrix composites," *International Journal of Advanced Manufacturing Technology,* vol. 39, pp. 211-218, Oct 2008.

[12] J. P. Davim, "Design of optimisation of cutting parameters for turning metal matrix composites based on the orthogonal arrays," *Journal of Materials Processing Technology,* vol. 132, pp. 340-344, 2003.

[13] M. Hosseiny, *Comparaison des outils Guhring et Iscar dans le perçage de composites à matrice d'aluminium* vol. Mémoire de maîtrise: École polytechnique de Montréal. Département de génie mécanique, 2006.

[14] J. F. Kahles, M. Field, D. Eylon, and F. H. Froes, "Machining Of Titanium Alloys," *Journal of Metals,* vol. 37, pp. 27-35, 1985.

[15] P. J. Arrazola, A. Garay, L. M. Iriarte, M. Armendia, S. Marya, and F. Le Maitre, "Machinability of titanium alloys (Ti6Al4V and Ti555.3)," *Journal of Materials Processing Technology,* vol. 209, pp. 2223-2230, Mar 2009.

[16] H. Attia, S. Tavakoli, R. Vargas, and V. Thomson, "Laser-assisted high-speed finish turning of superalloy Inconel 718 under dry conditions," *Cirp Annals-Manufacturing Technology,* vol. 59, pp. 83-88, 2010.

[17] C. R. Dandekar, Y. C. Shin, and J. Barnes, "Machinability improvement of titanium alloy (Ti-6Al-4V) via LAM and hybrid machining," *International Journal of Machine Tools & Manufacture,* vol. 50, pp. 174-182, Feb 2010.

[18] M. Anderson, R. Patwa, and Y. C. Shin, "Laser-assisted machining of Inconel 718 with an economic analysis," *International Journal of Machine Tools & Manufacture,* vol. 46, pp. 1879-1891, Nov 2006.

[19] S. Sun, M. Brandt, and M. Dargusch, "Effect of laser beam on the chip formation in machining of titanium alloys," in *ICALEO 2008 - 27th International Congress on Applications of Lasers and Electro-Optics, October 20, 2008 - October 23, 2008,* Temecula, CA, United states, 2008, pp. 901-909.

[20] R. Recht, "Catastrophic thermoplastic shear," *J. appl. Mech,* vol. 31, pp. 186-193, 1964.

[21] M. C. Shaw and A. Vyas, "Chip Formation in the Machining of Hardened Steel," *CIRP Annals - Manufacturing Technology,* vol. 42, pp. 29-33, 1993.

[22] K. Nakayama, "The formation of saw-toothed chip in metal cutting," in *Proceedings in the International Conference on the Production Engineering, Tokyo,* 1974, pp. 572-577.

[23] R. Komanduri and B. F. Von Turkovich, "New observations on the mechanism of chip formation when machining titanium alloys," *Wear,* vol. 69, pp. 179-188, 1981.

[24] M. A. Meyers, Y. B. Xu, Q. Xue, M. T. Perez-Prado, and T. R. McNelley, "Microstructural evolution in adiabatic shear localization in stainless steel," *Acta Materialia,* vol. 51, pp. 1307-1325, Mar 2003.

[25] M. Calamaz, D. Coupard, and F. Girot, "A new material model for 2D numerical simulation of serrated chip formation when machining titanium alloy Ti-6Al-4V," *International Journal of Machine Tools & Manufacture,* vol. 48, pp. 275-288, Mar 2008.

[26] F. A. McClintock, "Criterion for ductile fracture by growth of holes," in *ASME Meeting APM-14, Jun 12-14 1968,* 1968, p. 9.

[27] G. Cockcroft and D. J. Latham, *A Simple Criterion of Fracture for Ductile Metals*: National Engineering Laboratory, 1966.

[28] P. J. Ross, *Taguchi techniques for quality engineering : loss function, orthogonal experiments, parameter and tolerance design*. New York ; Montreal: McGraw-Hill, 1988.

[29] R. Bejjani, B. Shi, H. Attia, M. Balazinski, and H. Kishawy, "Machinability of titanium metal matrix composites," *Proceedings CIRP 2nd conf. Process Machine Interactions,* p. C12, 2010.

[30] W. F. Hastings, "New quick-stop device and grid technique for metal cutting research," *College International pour l'Etude Scientifique des Techniques de Production Mecanique Annals,* vol. 15, pp. 109-116, 1967.

[31] M. C. Shaw, A. Vyas, and Cirp, *The mechanism of chip formation with hard turning steel* vol. 47. 3001 Bern: Hallwag Publishers, 1998.

[32] G. Germain, J. L. Lebrun, T. Braham-Bouchnak, D. Bellett, and S. Auger, "Laser-assisted machining of Inconel 718 with carbide and ceramic inserts," *International Journal of Material Forming,* vol. 1, pp. 523-526, 2008.

[33] Organisation internationale de normalisation., *Essais de durée de vie des outils de tournage à partie active unique,* 2e éd. -- ed., 1993.

[34] R. Bejjani, M. Balazinski, B. Shi, H. Attia, M. Aramesh, and H. Kishawy, "Segmentation and shear localization when turning TiMMC (Titanium Metal Matrix Composites)," *26th Tech. conf., American Society of Composites,* 2011.

[35] L. E. Murr, E. A. Trillo, S. Pappu, and C. Kennedy, "Adiabatic shear bands and examples of their role in severe plastic deformation," *Journal of Materials Science,* vol. 37, pp. 3337-3360, 2002.

[36] M. A. Meyers and H.-R. Pak, "Observation of an adiabatic shear band in titanium by high-voltage transmission electron microscopy," *Acta Metallurgica,* vol. 34, pp. 2493-2499, 1986.

[37] R. Bejjani, M. Balazinski, H. Attia, and H. Kishawy, "A study on adiabatic shear banding in chip segmentation when cutting TiMMC," *1st Intl. Conf. Virtual Machining Process Tech./CIRP,* 2012.

[38] R. Bejjani, M. Aramesh, M. Balazinski, H. Kishawy, and H. Attia, "Chip morphology Study of Titanium metal matrix composites," *23rd Canadian Congress of Applied Mechanics,* pp. 499-502, 2011.

[39] M. Aramesh, M. Balazinski, H. Kishawy, H. Attia, and R. Bejjani, "A Study on Phase Transformation and Particle Distribution During Machining TiMMC Composites," *26th Tech. conf., American Society of Composites,* 2011.

[40] B. Shi, H. Attia, and N. Tounsi, "Identification of Material Constitutive Laws for Machining. Part I: An Analytical Model Describing the Stress, Strain, Strain Rate, and Temperature Fields in the Primary Shear Zone in Orthogonal Metal Cutting," *Journal of manufacturing science and engineering,* vol. 132, 2010.

[41] B. Shi, H. Attia, and N. Tounsi, "Identification of Material Constitutive Laws for Machining---Part II: Generation of the Constitutive Data and Validation of the Constitutive Law," *Journal of manufacturing science and engineering,* vol. 132, p. 051009, 2010.

[42] Y. Zhu and H. A. Kishawy, "Influence of alumina particles on the mechanics of machining metal matrix composites," *International Journal of Machine Tools & Manufacture,* vol. 45, pp. 389-398, Apr 2005.

[43] J. Z. Zhang, J. C. Chen, and E. D. Kirby, "Surface roughness optimization in an end-milling operation using the Taguchi design method," *Journal of Materials Processing Technology,* vol. 184, pp. 233-239, 2007.

APPENDIX A1: MACHINABILITY AND CHIP FORMATION OF TITANIUM METAL MATRIX COMPOSITES

R. Bejjani, M. Balazinski, B. Shi, H. Attia, H. Kishawy, *"Machinability and Chip Formation of Titanium Metal Matrix Composites"*, Int. J. of Advanced Manufacturing Systems, IJAMS, vol. 13, "1" , 2011.

IJAMS
International Journal of Advanced Manufacturing Systems

Machinability and Chip Formation of Titanium Metal Matrix Composites

Roland Bejjani, Marek Balazinski
Department of Mechanical Engineering, École Polytechnique de Montréal, 2900 boul. Édouard-Montpetit H3T 1J4 Quebec, Canada, e-mail: bejjanirol@hotmail.com; marek.balazinski@polymtl.ca

Bin Shi, Helmi Attia
Aerospace Manufacturing Technology Centre (AMTC), National Research Council of Canada, 5145 Avenue Decelles Campus of University of Montreal, H3T 2B2 Quebec, Canada, e-mail: Bin.Shi@cnrc-nrc.gc.ca; helmi.attia@nrc.ca

Hossam Kishawy
University of Ontario Institute of Technology, 2000 Simcoe Street North Oshawa, Ontario, Canada, e-mail: Hossam.Kishawy@uoit.ca

Abstract: *Titanium Metal Matrix Composite (TiMMC) is a new class of metal composite which offers superior physical properties over titanium alloys. Therefore, this material has recently been used in several applications in the aerospace and automotive industries. Although the TiMMC parts are made near net shape, a finish machining operation is often necessary to achieve the required surface finish and dimensional accuracy. In general, MMCs have been known to be difficult to cut materials, since the added ceramic hard particles are very abrasive and limit the tool life. Titanium alloys are also known to be problematic in machining; therefore, TiMMC combines both machining problems associated with MMCs and titanium alloys. Since data on the machinability of TiMMC is very limited in the open literature, this paper focuses on comparing the performance of different tools under different cutting parameters in order to find the optimum cutting conditions within the constraints of maximum surface integrity and tool life. This research revealed that Poly-Crystalline-Diamond (PCD) tools substantially outperform coated carbide tools. Moreover, chip formation has been carefully studied to understand the interaction of the added Titanium Carbide (TiC) particles with the cutting tool. Contrary to other materials, cutting of TiMMC at higher speeds was found to be more advantageous and resulted in a higher tool life. Analysis of the chip morphology also revealed that the chip formation at high speeds is clearly different from that at lower speeds, suggesting a different cutting mechanism.*

Keywords: *Titanium Metal Matrix Composites, Chip Microstructure, Machinability*

1. INTRODUCTION

Metal matrix composites reinforced with ceramic hard particles are a new class of engineered materials, which have been developed to enhance the material's physical and mechanical properties. Typical applications are in the aeronautical and automotive industries, where high wear resistance and light weight are required [1]. The most common type of MMC is the aluminum matrix reinforced with hard ceramic particles, such as silicon carbide, alumina or boron carbide [2]. The advantages

of MMC over other alloys are higher wear and fatigue resistance, higher deformation resistance, higher rigidity and better thermal shock resistance [3]. TiMMC offers a combination of high strength and lower density than steel. This generated interest in the automotive industry in recent years. For example, the use of connecting rods and piston pins made from TiMMC lead to better fuel economy, reduced emissions, noise, vibration, and harshness [4]. Titanium-carbide (TiC) reinforced Ti alloys offers additional advantages over conventional titanium alloys due to their higher modulus, elevated temperature strength, creep resistance, and wear resistance. Comparing TiMMC with AlMMC, for producing connecting rods, it was found that titanium-matrix composites have higher absolute and specific strength, better fatigue properties, and higher elevated temperature strength. Moreover, the weight of a connecting rod, made from TiMMC is 40% less than that of high-strength steel. In biomedical load-bearing applications such as hip components, titanium alloys are the current material of choice. However, Ti alloys cannot be used for articulating surfaces because they have poor wear resistance with possible formation of debris. TiMMC, CermeTi materials combine the advantages of metals and ceramics together and are under evaluation for such metal-on-metal orthopaedic implants [4].

TiMMC is made near net shape and usually requires finish machining only. As a new composite material, there is very limited information on its machinability in the open literature. The previous research achieved by the authors in [5] was a preliminary attempt on machining this material using one kind of tool. In this paper, the comparison of the performance for different tools and cutting parameters is investigated. This will provide new data on the optimum dry machining conditions of TiMMC, while maximizing tool life and surface integrity. Moreover, chip formation has been carefully studied, including the tool-chip interaction due to the presence of TiC particles. Furthermore, the effect of cutting speed on tool life has been carefully analyzed. Since machining TiMMC combines the difficulties associated with the machining of MMCs and titanium alloys, a literature review for machining the most common Aluminum MMC (AlMMC) and titanium alloys is presented first in the following section.

2. MACHINABILITY CHARACTERISTICS OF MMCS AND TITANIUM ALLOYS

2.1 Machinability of Aluminum MMC

Several machining studies have been performed previously on Aluminum MMCs. Muthukrishnan [3] noted that at low speeds the formation of built up edge (BUE) was significant, but helped protect the tool tip. When the speed is increased, the BUE did not occur and subsequently the tool life decreased substantially. It was also noted that flank wear is the dominant mode of tool failure due to abrasion action produced by the hard SiC particles. Furthermore, high feed rates are preferred since they tend to soften the matrix. Consequently, this makes the removal of the hard SiC easier and leads to a reduction in tool wear and improvement in surface finish. High cutting speeds was also found to produce smoother surfaces. Coarse grained PCD inserts were found to be the best in terms of tool life and surface quality due to their high hardness.

Songmene and Balazinski [2] reported that the abrasive nature of the hard particles when machining Aluminum MMC results in poor tool life and inconsistent part quality. This consequently limits the use of AlMMCs in many industrial applications. Tomac and Tonnessen [6] also observed that the primary wear mechanism, when machining AlMMC, is abrasive wear. They compared the performance of Polycrystalline Diamond (PCD) inserts to that of TiN, TiC/N, and

Al_2O_3 coated tools. PCD tools gave best results in terms of surface quality and had over 30 times higher tool life than carbide tools under similar cutting conditions. Kannan et al. [7] and Lin et al. [8] also confirmed that high speeds lead to a lower tool life. However, Lin et al. [8] noted that increasing the feed increases the total cut volume. Manna and Bhattacharayya [9] showed that when the speed is doubled, the flank wear also increases proportionally compared to its value at low speed.

2.2 Machinability of Titanium Alloys

As a difficult to cut material, Titanium alloys have generated considerable interest among researchers. Che-Haron [10] noted that increased wear rate was detected with the increase in speed. Flank wear at the tool nose seems to be the limiting factor that controlled tool life in all cases. The predominant wear mechanism is dissolution-diffusion, especially at high speeds, due to the higher temperature generated at the tool-chip interface.

Machinability studies of Ti-6Al-4V [11,12,13] led to the following observations. The combination of low thermal conductivity and a very thin chip results in very high cutting temperature concentrated in a small area on the tool-chip interface. The high temperature combined with the strong chemical reactivity of titanium result in high affinity to almost all tool materials at cutting temperatures over 500°C. It was also shown that tool life is affected by feed. When machining titanium alloys, as feed increases, tool life decreases. In addition, titanium alloys have a low modulus of elasticity which can cause chatter, deflection and rubbing action. The cyclic segmentation in chip formation results in a large variation of forces acting on the tool tip, which in turn increases the possibility of chatter and tool chipping [14,15].

Arrazola et al. [16] studied the machinability of Ti-6Al-4V and Ti555.3 and recommends machining these alloys up to a maximum speed of 90 m/min. It was also observed that diffusion wear is the dominant wear mode.

3. EXPERIMENTAL SET UP

Following the work of Basavarajappa et al. [17], when machining MMCs, the principal machining parameters that control machinability are intrinsic parameters (cutting speed, feed rate, depth of cut, and the type of tool), and extrinsic parameters (particulate size, volume fraction, and the type of reinforcement). In the current research, all experiments were carried out under dry cutting conditions, and the selection of the appropriate cutting tools and cutting parameters was based on previous data for machining AlMMC and Ti-alloys. Furthermore, the tool manufacturer's recommendations were taken in consideration. Machining tests were conducted on a 6-axis Boehringer NG 200, CNC turning center. Cutting forces were measured using a Kistler dynamometer, type 9121. The surface roughness of the machined material was examined after each machining test using Form Talysurf Series S4C. A high speed camera, model AOS X-Motion, was used to observe the chip formation process, and fire initiation of chips. Chips were collected for each experiment, then mounted, polished and etched for further metallographic examinations.

The tool wear progression was measured using an Olympus SZ-X12 microscope. A Scanning Electron Microscope (SEM) Jeol, JSM -840A was used for detailed studies of the chips morphology. For micro-hardness measurement, a Struer Duramin A300 was used. A specially designed and developed quick stop device (QSD) was used to examine the chip formation process and the chip morphology [18]. The material was supplied by Dynamet Technology Inc. Table 1 shows

its physical properties. The turning tests were carried out using 2.5 inches diameter cylindrical workpieces made of CermeTi®

Density	Yield Strength	Tensile Strength	Elastic Modulus	Shear Modulus	Thermal Conductivity	Specific Heat
4500 kg/m^3	1014 MPa	1082 MPa	135 GPa	51.7 MPa	5.8 W/m.ºK	610 J/kg.ºK

Table 1: Properties of Cermet Ti-C; Ti-6Al-4V, 10-12% TiC.

MMCs, which consist of a non-metallic phase TiC (10-12% by weight) distributed in a matrix of Ti-6Al-4V titanium alloy. Figure 1 shows a typical workpiece used in this study.

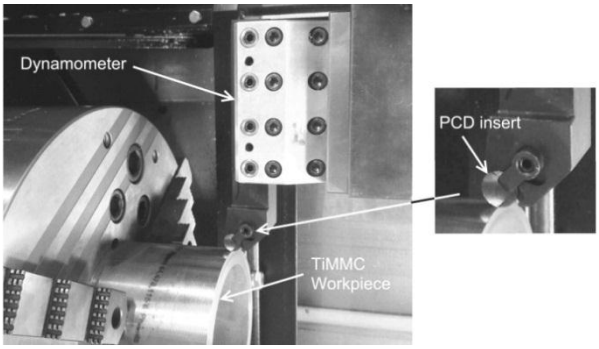

Figure 1: The TiMMC material on the CNC lathe

3.1 Cutting Tools

Based on the manufacturer's recommendations, two types of tools were used; a newly developed round 0.5" diameter Polycrystalline Diamond (PCD) insert RNMN42 from KY-Diamond, and a coated carbide tool manufactured by SECO (CNMG MF1) with a nose radius of 0.794 mm. The information on the chemical composition of the newly developed coating was kept confidential.

3.2 Design of Experiments

In order to be efficient and to reduce the costly full factorial machining tests, Taguchi Parameter Design was used in the design of experiments for this investigation. This approach considers multiple input parameters for a given response and uses the non-linearity of a response parameter to decrease the sensitivity of the quality characteristic to variability. In these experiments, for optimizing the surface roughness, 'the smaller the better' criterion was used and the signal-to-noise ratio (S/N) was plotted for each control variable [19]. The S/N ratio represents the magnitude of the mean of a process compared to its variation. The larger the S/N, the more robust is the measured variable against noise.

An L8: 4*2-Taguchi array was used with 4 speeds and 2 feeds. For the PCD tool, the speed ranged from 60 to 230 m/min, the feed was set at 0.1 and 0.2 mm/rev, and the depth of cut was kept constant at 0.15 mm. For the carbide tool, the speed ranged from 50 to 120 m/min, the feed and depth were the same as above. For each test, the total length of cut was 40 mm.

4. RESULTS AND DISCUSSION

Since some TiMMC applications can be used in critical areas as car engine parts or in aeronautics, surface roughness must be well controlled while machining. In theory, there are two main factors that affect surface roughness: the tool geometry (nose radius) and feed. This can be shown by the following formula [14]:

$$Ra=31.25\ f^2/r \qquad (1)$$

Where Ra is the arithmetic average surface roughness (in μm), f is the feed (in mm/rev), and r is the nose radius (in mm). However, in a real life situation and for TiMMC, cutting speed and tool wear cause a change in the particle-tool interactions and the chip formation process, which affect the roughness of machined surfaces.

4.1 Surface Roughness

The measurements of surface roughness were made using a Taylor Hobson Precision, Form Talysurf Series S4C. A sample of a 3D reconstructed surface profile is shown in Figure 2.

4.2 Carbide Tool

Figure 3 shows the effect of cutting conditions on surface roughness. Since the "smaller the better" was chosen in the Taguchi method, the higher the S/N ratio, the lower is the value of Ra. Figure 3 (a) shows that the feed has a much steeper slope than the speed. Therefore, the feed in this case is the dominant parameter, and has a much higher effect on Ra. In fact, Ra is better for lower feeds, as the theory predicts. As for the effect of speed, the lowest Ra was obtained at 120 m/min (Figure 3(b)). However at 120 m/min the tool flank-wear was very severe at the cutting edge, and chips caught fire. Therefore, the optimum Ra was at the speed of 90 m/min.

4.3 PCD Tool

Figure 4 (a) shows the surface roughness S/N ratio for the PCD tool. In this case, the speed has a much higher effect on Ra, and the peak S/N ratio is at 180 m/min. Moreover at lower feed, Ra is better as normally expected. In Figure 4 (b), at 230 m/min speed, the same Ra for both feeds was noticed. This suggests the possibility that at higher speed, a different cutting process might be occurring. Furthermore, one can see that an interaction exists between those two variables (speed and feed) and Ra, since the lines are not parallel. However, at 230 m/min and 0.1 mm/rev fire was observed and the test was stopped before machining the complete length.

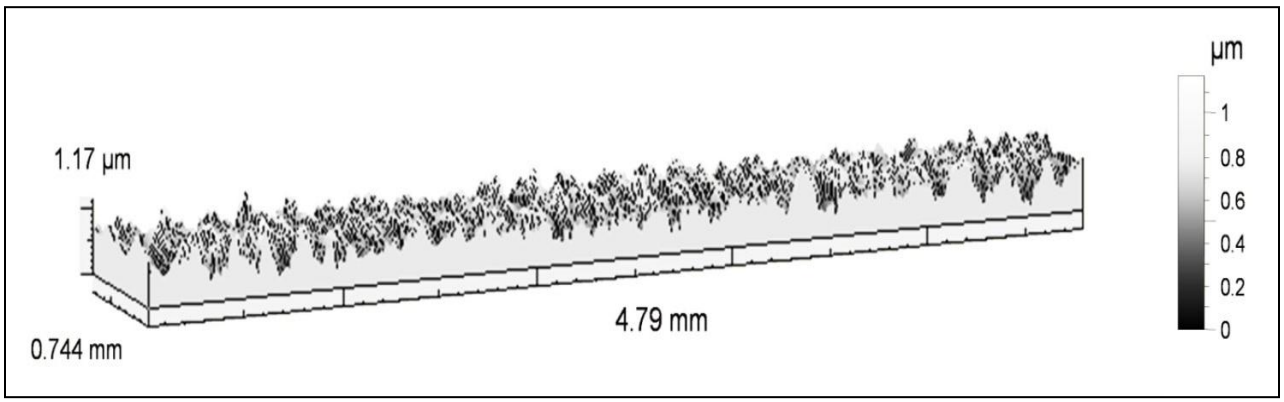

Figure 2: 3D reconstructed surface profile after cutting with a PCD tool at v=170 m/min and f= 0.2mm/rev with a mean arithmetic surface roughness Ra=0.11μm

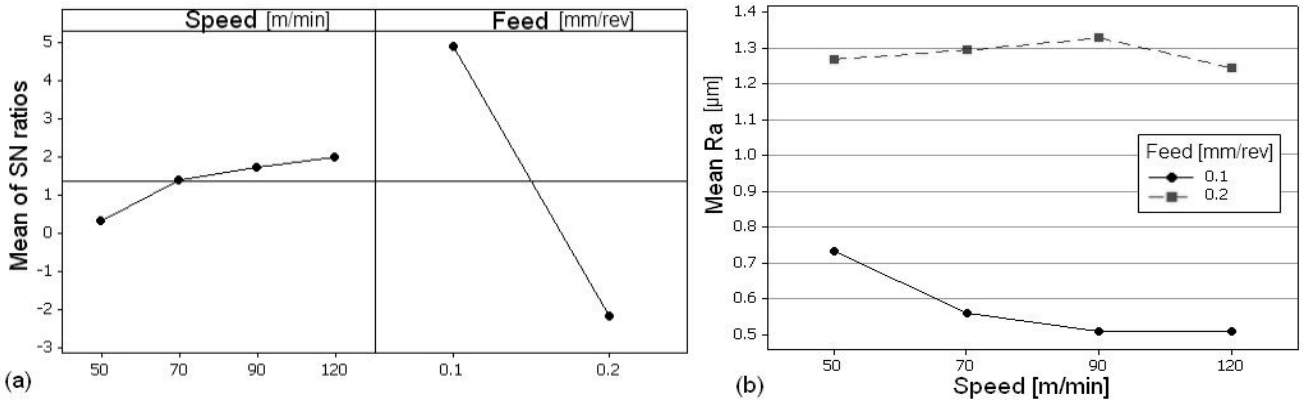

Figure 3: Surface roughness for carbide tool, (a) Sensitivity of speed on S/N ratio of Ra, (b) Ra measurements for different cutting conditions

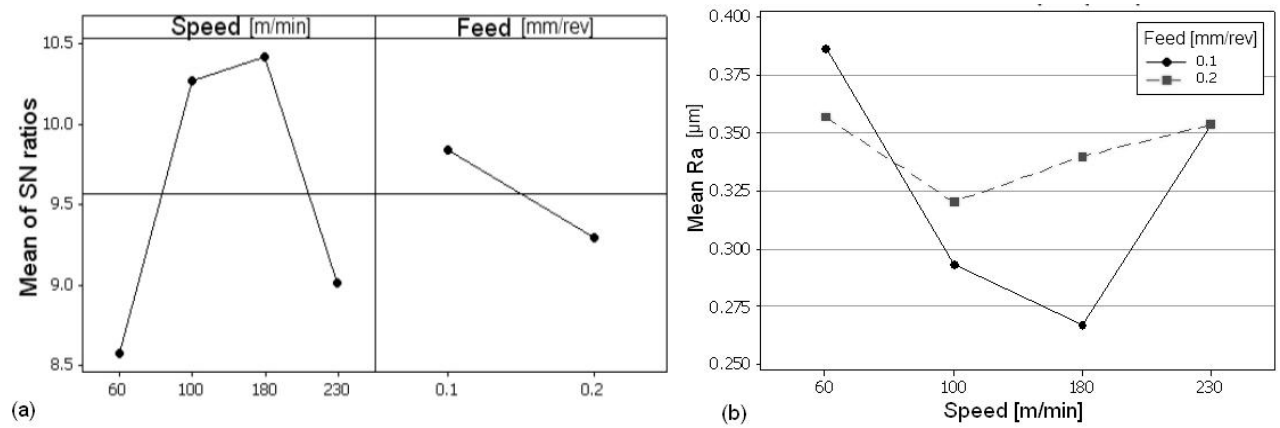

Figure 4: Surface roughness for PCD tool, (a) Sensitivity of speed on S/N ratio of Ra, (b) Ra measurements for different cutting conditions

5. CUTTING FORCES

5.1 Carbide Tool

Figure 5 (a) shows the trend of the mean cutting forces with the carbide tools for each test when the total length of cut L_c = 40 mm. As expected, the cutting force is smaller with lower feed. For speeds above 90 m/min the forces increase at a much higher rate, mainly due to the tool deterioration. The parallel lines below 90 m/min demonstrate that there is no interaction between speed and feed on Ra. Figure 5 (b) shows a typical cutting force profile when using a carbide tool. One can see that the thrust, feed and cutting forces, F_t, F_f and F_c, respectively, increase as the tool wears. However, the thrust force increases with a lesser slope than with the PCD tool (Figure 6(b)). Note that when the tool tip is severely worn, all the forces increase at a high rate. Moreover, the thrust force increases at a higher rate when the tool reaches the end of its useful life. This is in opposition to the PCD tool which wears out gradually.

5.2 PCD Tool

Figure 6 (a) shows the force profile when cutting at different speeds and feeds. As expected, the cutting force F_c decreases with higher speed. However above 180 m/min it seems to stabilize and does not decrease further. Figure 6 (b) shows a typical force profile when cutting with a PCD tool. As shown, the cutting force F_c does not vary in magnitude as much as the thrust force F_t, and

stabilizes quickly after the start of the turning operation. In other words, the thrust force increases with the length of cut, as the tool wears out. In addition, it was observed that with a higher feed, and a high speed of 180 m/min, the cutting force stabilizes and does not follow the pattern observed with the carbide tool.

6. TOOL WEAR

The abrasive wear process while cutting MMCs is somewhat different from the usual tool wear process when machining metal. In fact, due to the presence of the highly abrasive hard reinforcement particles in the material itself, both two-body, and three-body abrasion modes coexist as mechanical abrasive wear mechanisms. The two-body abrasive wear takes place when a rough and hard surface rubs against a softer one and ploughs into it. The three-body wear occurs, however, when a hard particle is introduced between two rubbing surfaces and abrades material off each of the surfaces [20]. Many researchers found that flank wear is the dominant form of tool failure when machining MMCs. This is caused by the severe abrasion of the reinforcements particles on the tool surfaces during cutting. It has been reported that

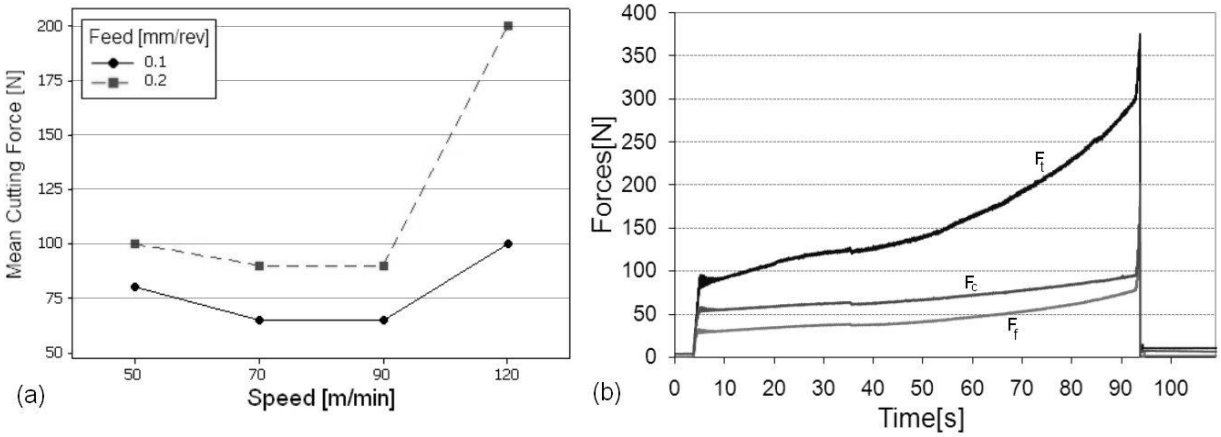

Figure 5: (a) Mean cutting force for carbide tool at different cutting conditions, (b) Forces profile at 90 m/min and 0.1 mm/rev

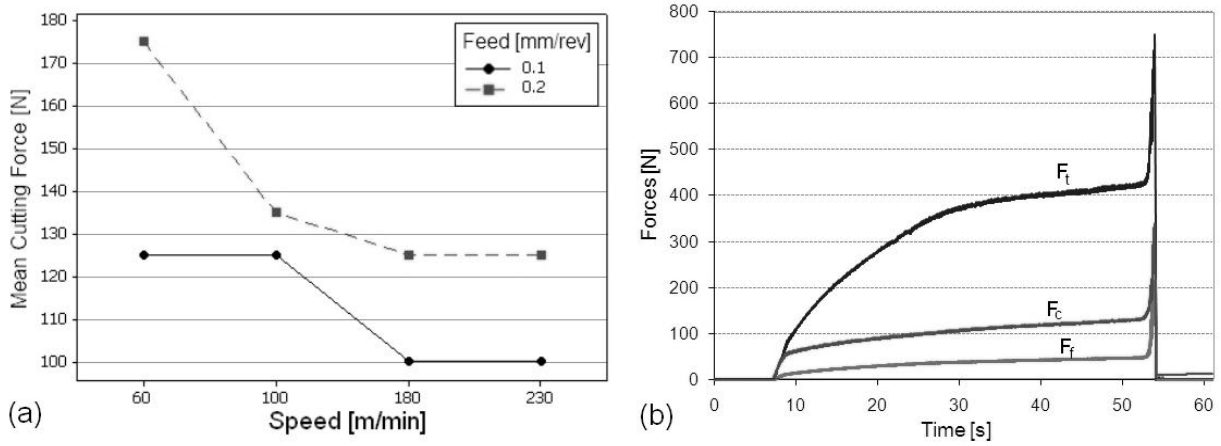

Figure 6: (a) Mean cutting force for PCD tool at different cutting conditions, (b) Forces profile at 180 m/min 0.1mm/rev

sometimes, the progression of tool wear is severe and leads to very low tool life. In some occasion, the tool lasts only a few seconds at high cutting speeds [2,6,21].

Added to the above, the problems associated with the machining of Ti alloys are also to be expected. Titanium has a combination of low thermal conductivity, and a very thin chip which results in high cutting temperature. This is to be added to the cyclic chip formation or segmentation which results in fluctuation of forces acting on the tool tip. This in turn increases the possibility of chatter.

In the current research, tool wear tests were done in a similar manner as explained previously and the tool wear was measured after a length of cut L_c = 40 mm for each set of chosen parameters.

At a later stage, another set of tool wear tests were performed using the found optimum cutting parameters. However, in those subsequent tool-wear tests, the machining was carried out until the end of the useful tool life. The tool wear was periodically measured in the course of the test, and machining was stopped once a criteria of $VB_B max$= 0.30 mm was reached. Furthermore worn tool pictures were taken for later analysis.

6.1 Carbide Tool

Figure 7 (a) shows that the effect of the cutting speed is detrimental once it reaches a value above 90 m/min. This indicates that tool wear is excessive at high speed. As expected, speed has a much greater effect than feed on tool wear. However, it is interesting to note that at the lower feed, the tool wear is slightly lower at the optimum speed of 90 m/min.

Dry machining of titanium can cause the chips to catch fire. In this research, it was observed that sparks occur at high speeds. For carbide tools, the maximum safe speed was 90 m/min, whereas it was 180 m/min for the PCD tools. As observed, the rapid tool wear of carbide tools resulted in a greater tendency of fire initiation in the chips. In order to stay on the safe side, the optimum speed was lowered from 90 to 80 m/min. Therefore the optimum machining conditions were set at a speed of 80 m/min and feed of 0.1 mm/rev. It should be noted here that 10 mm of cutting length takes around 15 seconds of machining time. Figure 7 (b) shows the tool wear progression when machining with a carbide tool at a speed of 80 m/min and a feed of 0.1 mm/rev. The maximum length of cut in the useful life of the tool was 50 mm. Two regions for wear profiles can be observed in Figure 7 (b). The first region shows a linear tool wear along the length of cut till around 40 mm. The second region has a steeper slope after 40 mm, and the wear accelerates after this point.

6.2 PCD Tool

Figure 8 (a) shows the dependence of tool wear on the cutting parameters for the PCD tool. It is interesting to see that as speed increases, the tool wear decreases. This unexpected phenomenon is in contrary to almost all other materials, and also to the test results obtained with carbide tools. This phenomenon will be analyzed in the next section when the chip morphology is identified at different cutting conditions. The optimum conditions were found to be at a speed of 180 m/min and a feed of 0.2 m/rev. Furthermore, it is interesting to see that beyond a speed of 100 m/min, feed does not seem to affects wear as much as lower speed. In fact, at a speed of 230 m/min, the wear for both feeds are the same, and relatively low. However at this speed, machining was interrupted as the chips caught fire.

For the second part of the tool life experiments, two values of speed were chosen (considered here as low and high speed). The previously found optimum speed was reduced to 170 m/min (at feed of 0.2 mm/rev) to be on the safe side. The second condition used for comparison purposes was 100 m/min and 0.2 m/rev feed. It was also safe to operate at this condition, where no fire or sparks were

observed while machining the complete tested length.

Figure 8 (b) shows the progress of tool wear with time at the two selected conditions. The figure shows that the wear pattern consists of three regions that reflect the transition from a highly-loaded tribological system (with an initial high wear rate due to the high stresses on the sharp tool edge) to a lightly-loaded system (with a reduced and uniform wear rate) and back to a highly-loaded system (with accelerated wear due to the tool temperature rise and reduced hardness) [14].

At the speed of 170 m/min the total machining length, which corresponds to the useful tool life, was 250 mm whereas it was 140 mm for v = 100 m/min. This confirms that machining at higher speed is much more advantageous, contrary to other materials. This means that machining at higher speed leads to nearly 80% additional cutting length (or cut volume). The combination of increased cutting speed and length of cut resulted in practically the same machining time. Figure 9 and 10 show samples of worn carbide and PCD tools respectively.

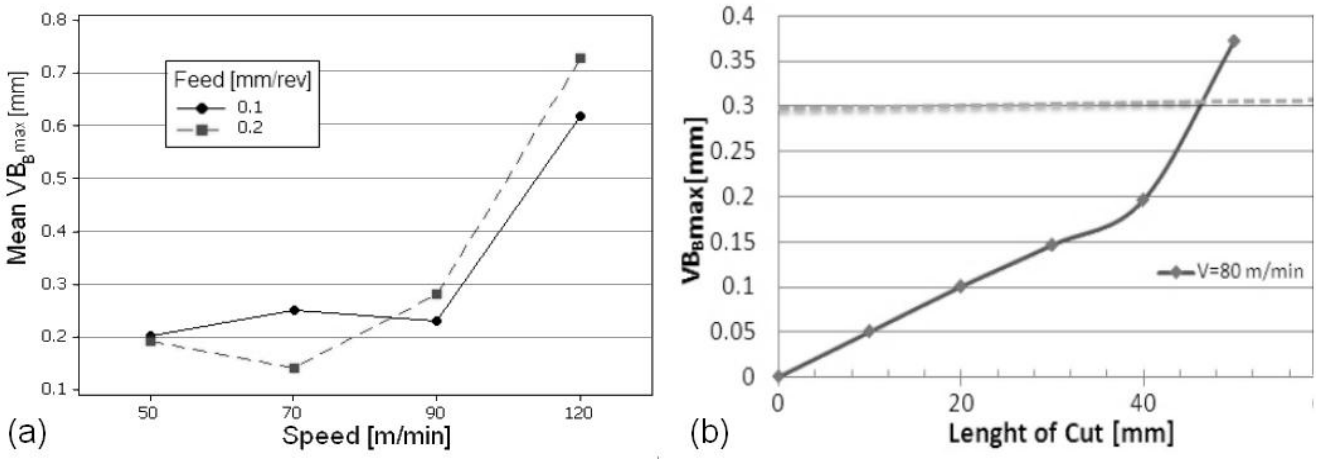

Figure 7: (a) Effect of cutting parameters on Carbide tool flank wear after L_c=40 mm, (b) tool wear progression at cutting speed=80 m/min and feed=0.1 mm/rev

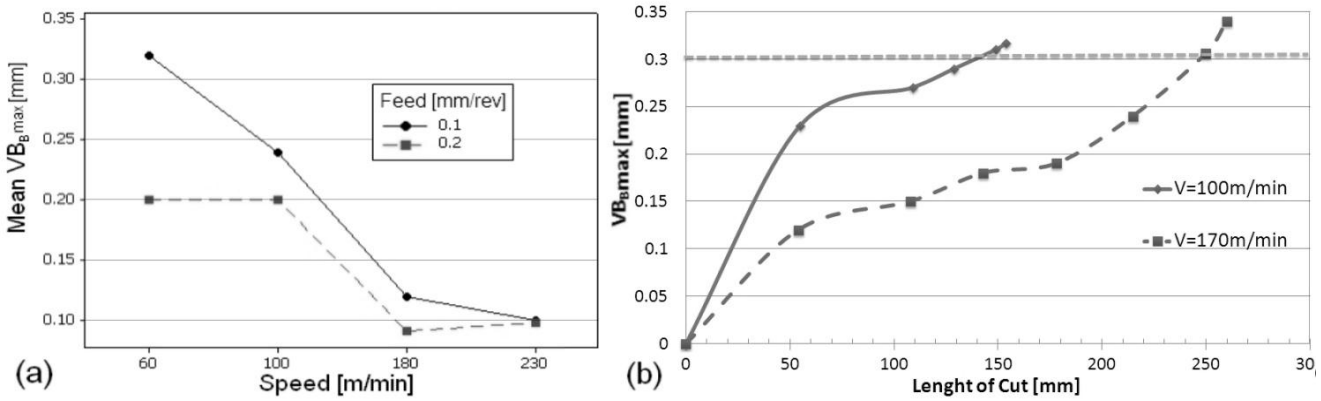

Figure 8: (a) Effect of cutting parameters on PCD tool flank wear after L_c=40 mm, (b) tool wear progression at cutting speed of 100 and 170 m/min and feed=0.2 mm/rev

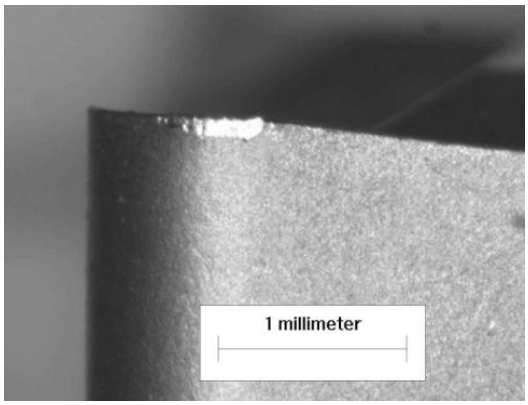

Figure 9: Flank wear on carbide tool. $VB_B max$=0.11 mm, at v=80 m/min, f=0.1mm/rev and L_c =20 mm

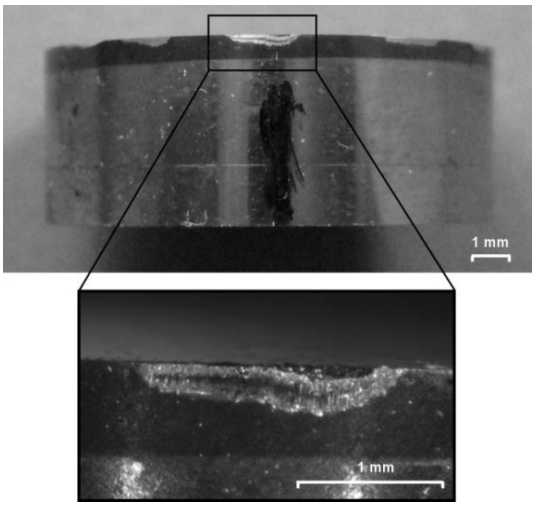

Figure 10: Flank wear on PCD tool $VB_B max$=0.3mm, at v=170 m/min, f=0.2mm/rev and L_c =250 mm

7. CHIP MORPHOLOGY ANALYSIS

Segmented chips are typical for titanium alloys. Machining TiMMC also shows a similar chip patterns. Segmentation occurs when the rate of decrease in strength resulting from a local increase in temperature equals or exceeds the rate of increase in strength due to strain hardening in the primary shear zone. Due to the low thermal conductivity of titanium, the shear energy on the shear plane increases the temperature dramatically thus softening the material, and this leads to more strain in the same shear plane [11,22]. This has been referred to as 'catastrophic or adiabatic shear' and results in a typical segmented chip pattern.

The performed experimentations results indicate that a better machining performance in terms of tool life occurs at high speed. One possible explanation of this phenomenon is that a different chip formation process occurs at higher speeds. To further investigate this, chips from different cutting speeds were analyzed. Figure 11 shows material chips at two different speeds (100 and 230 m/min). The following interesting observation can be made. At low speed, the crystalline structure of the chip is more elongated and deformed, showing high plastic deformation. At the higher cutting speed, the shear strain in the primary shear zone is reduced, as demonstrated by the larger shear angle and the smaller chip deformation. Furthermore, at higher speed, the bulk of the segment seems to be displaced with high strain at the adiabatic shear zone, and very low strain in the bulk of the segment area. It was also observed that at lower speed, more particles are smashed, while they are just displaced or cut at high speeds.

Since the shear line is not fixed in place but cyclic, the Merchant model (thin shear zone) is not applicable here. In this case, the chip formation is a cyclic segment formation with adiabatic shear lines delimiting each segment [15].

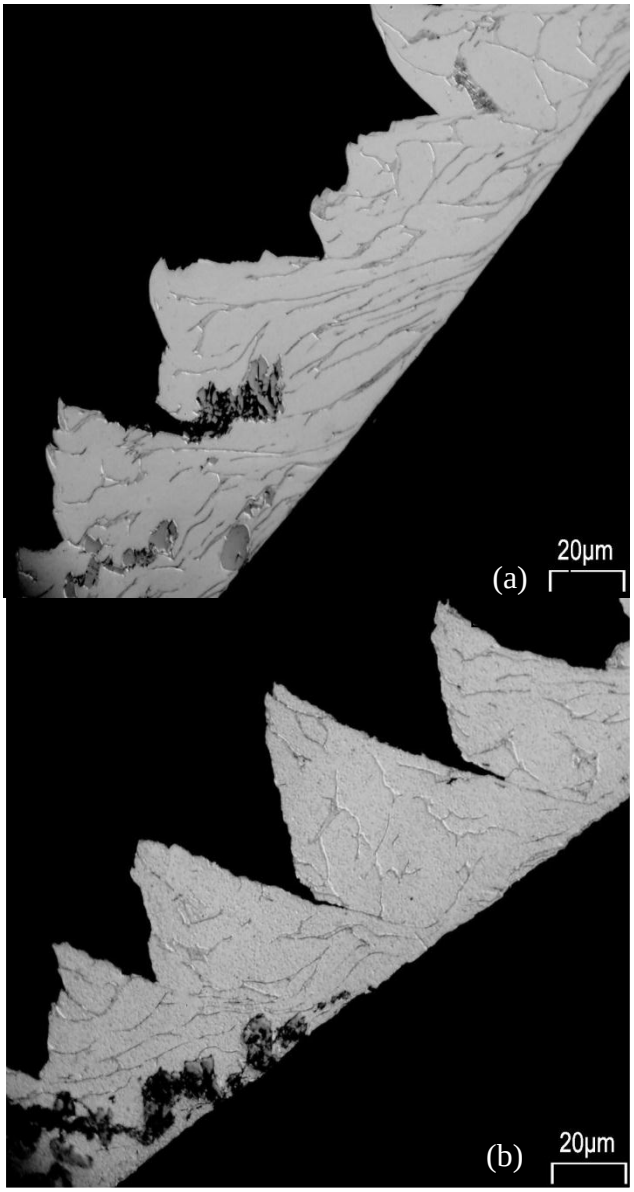

Figure 11: Chip morphology when machining with the PCD tool at (a) 100m/min and (b) 230 m/min

To analyze further the difference between chips at low and high speed, SEM pictures were taken. Figure 12 and 13 are SEM pictures of chips cross sections at 60 and 180 m/min. The zoomed part of Figure 12 is the area where a hard particle was broken. In general, at low speed the adiabatic shear is less pronounced and plastic strain exists over most of the area of the chip; therefore, inducing high stresses at the particles. When the stresses are high enough, the particles may break and smaller particles will be created. If

the proximity of those particles are close to the tool side, then "three-body wear" will occur which will increase the wear rate of the tool.

After a careful examination of the chips morphology, it was observed that in general fewer particles were broken in the chips when cutting at high speeds. Figure 13 shows an example of a particle located between two shear bands in a chip cut at high speed. In general, if a particle is located inside the segment's bulk and not in-line with the shear band (as in Figure 13), then this region of low plastic strain will not induce high enough stresses to break the particle. Therefore, since the particle will be just displaced and not broken (as in the case of Figure 12), this will result in less abrasion wear on the tool.

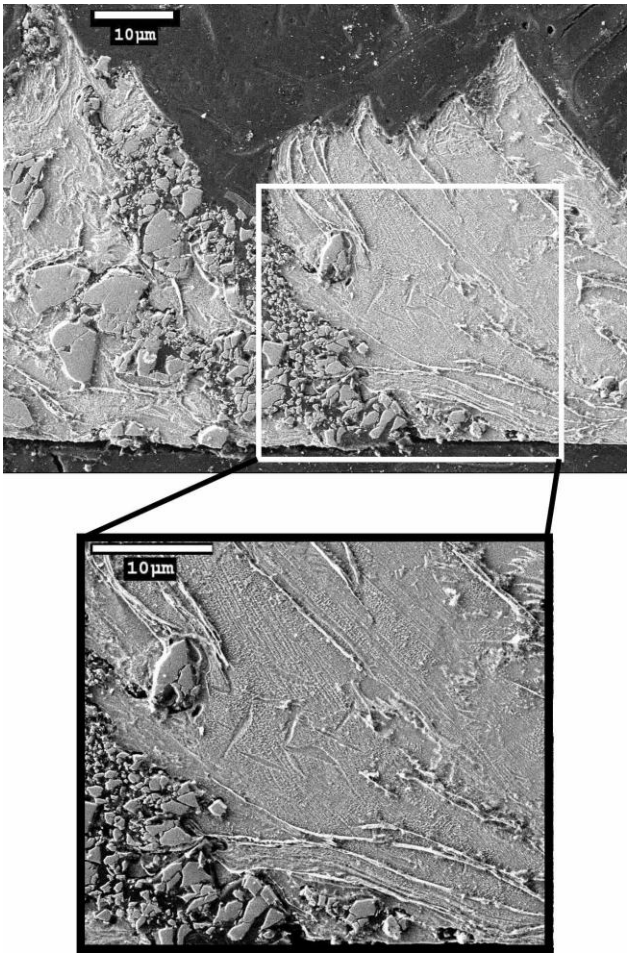

Figure 12: Chip morphology at v=60 m/min showing a particle broken into many other smaller particles

In all of the carried out experiments no built-up edge or crater wear were observed. The main wear mode is flank abrasion wear. Therefore the above reasoning might be an explanation of the lower tool abrasive wear observed when cutting at high speeds.

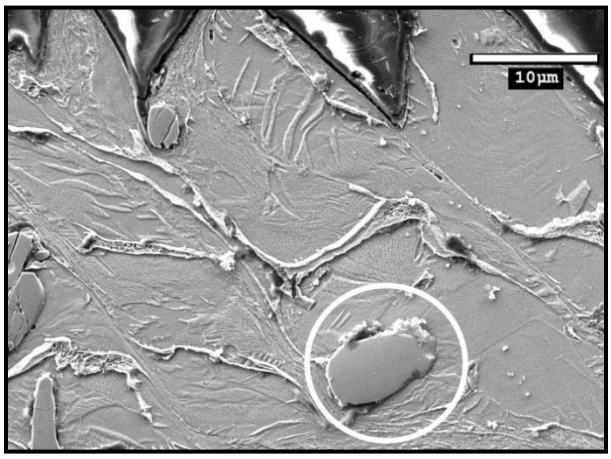

Figure 13: Chip morphology at v=180 m/min showing a particle which did not break after the chip formation

8. CHIP INITIATION CHARACTERZATION AND SURFACE INTEGRITY

With a Quick Stop Device (QSD), the process of chip formation can be frozen. Therefore, one can examine the process of chip initiation, the adhesion of the workpiece material to the tool face, the separation of hard particles that may result in three-body abrasion wear, as well as the thickness of the primary shear zone. Following this, a QSD was developed [18]. Using this QSD, samples of chip root formed during the machining of Ti-MMC were obtained and their microstructure was subsequently examined using optical and SEM microscope. The photomicrograph in Figure 14 shows the root chip interface and segmentation chip formation process.

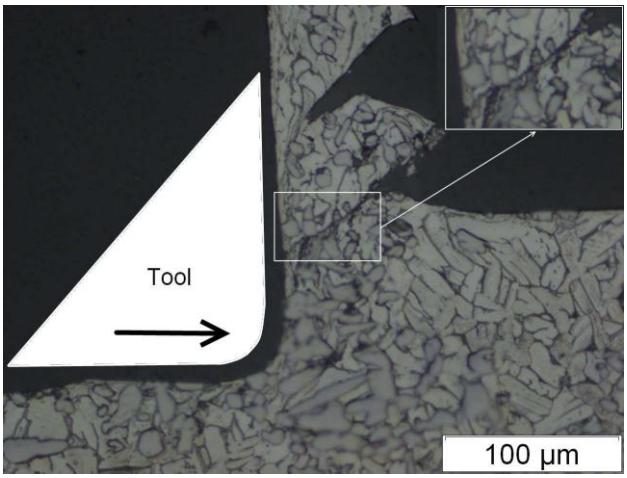

Figure 14: Chip formation using QSD. Cutting speed= 70 m/min, and feed= 0.2 mm/rev.

A close examination of the machined surface shows that no changes in α and β phase have occurred. Moreover, there was no evidence of de-bonding of hard particles. If a particle happens to be in the path of the cutting tool, then the tool will break the particle and not pull it out.

Microhardness measurements were also taken at regions near the surface and in

the bulk of material. At 20 µm below the machined surface an average of 400HV0.1 was measured, whereas the bulk hardness is 350HV0.1. This can be explained by the strain hardening occurring at the surface after the strain induced by the tool passing and removing material out of the workpiece. The depth of the strained layer was found to be approximately 70 µm.

9. OBSERVATIONS WITH HIGH SPEED CAMERA

In an attempt to see the different cutting phenomenon happening at low and high speeds, a high speed camera was used. The camera settings were: 500 frame/s, and shutter speed of 1/2000 s. After analyzing different videos with the high speed camera, while cutting at 230 m/min, at some point in time, a particle was expelled, and then sparks in the air and away from the tool as shown in Figure 15. In order to give an indication as to what extent safe machining can be performed without the hazards of fire, the following parameters were established. With PCD tools, at cutting speed of 230 m/min and feed of 0.1 mm/rev, the chips caught fire as soon as they were formed. However, when the feed is increased to 0.2 mm/rev, less fire was observed. With the carbide tool, fire was occurring at speed as low as 120 m/min. At this speed, the tool tip was worn very rapidly, which in turn promoted the danger of fire hazard.

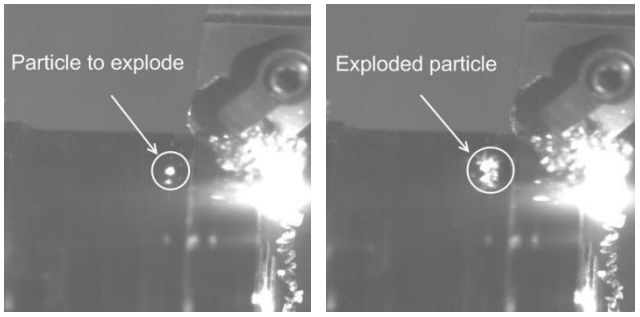

Figure 15: Chips catching fire recorded with High speed camera

10. CONCLUSIONS

The following conclusions can be drawn from this experimental investigation on finish turning of Ti-MMC using Polycrystalline Diamond (PCD) and coated carbide tools. The study showed that for the PCD tool, the cutting speed has a higher effect on surface roughness than feed. This is in opposition to the carbide tool where feed was the dominant factor. Additionally, there is a strong interaction between these two variables. Based on the range of the tested parameters, it was also found that the optimum cutting conditions were v = 170 m/min, f = 0.2 mm/rev, for PCD and v = 90 m/min, f = 0.1 mm/rev for carbide tool, where the lowest cutting force and the lowest surface roughness Ra were obtained without the danger of chips catching fire. Below are some other results:

- At higher speed (above 170 m/min) there seems to be a different cutting mechanism (less force, less wear, better Ra). Therefore, when machining TIMMC it is much more suitable to use high speed. However this can only be accomplished with PCD tools. Moreover, approximately 80% additional cut volume was achieved at the higher speed of 170 m/min compared to the lower speed of 100 m/min.
- Unlike other metals, machining TiMMC at high speeds leads to a better tool life. This unexpected phenomenon seems to be related to the change in the chip formation process that occurs at high speed. Compared to low speed cutting, it was observed that when cutting at high speed, fewer particles break. This results in less abrasion wear, and therefore leads to a higher tool life.
- Under optimum cutting conditions, the total machined length was much longer with the PCD tool (250 versus 50 mm for carbide tool). Therefore PCD tools are highly recommended if productivity is the critical parameter to be considered.

- When cutting with PCD tools, the surface roughness is better than with carbide tools, however one of the reasons might be the shape of the PCD tool which has a much larger nose radius since it is a round insert. It should also be noted that with PCD tools, at higher feeds and speeds, the arithmetic mean roughness Ra was more stable with less variation in magnitude.

REFERENCES

[1] Bell, J.A.E.; Stephenson, T.F.; Waner A.E.M.; Songmene, V.; "Physical Properties of Graphitic Silicon Carbide Aluminium Metal Matrix Composite", *SAE Paper* No. 970788, 1997.

[2] Songméné, V.; Balazinski, M.; "Machinability of Graphitic Metal Matrix Composits as a Function of Reinfoncing Particles" *CIRP Annals* Vol. 48/1. 1999, pp 77-80.

[3] Muthukrishnan, N.; Murugan M.; Prahlada Rao K.; "Machinability issues in turning of Al-SiC metal matrix composites". *Int. J. Adv. Manuf. Technol.*-2008, 39:3 pp. 211-218.

[4] Abkowitz, S., H. Fisher, Schwartz, P., "CermeTi® discontinuously reinforced Ti-matrix composites: Manufacturing, properties, and applications.", 2004, *JOM Journal of the Minerals, Metals and Materials Society*, 56, 37-41.

[5] Bejjani, R.; Shi, B.; Attia, H.; Balazinski, M.; Kishawy, H.; "Machinability of titanium metal matrix composites."; *Proceedings CIRP 2nd conf.* Process Machine Interactions; 2010; C12.

[6] Tomac, N; Tonnessen, K; "Machinability of particulate aluminium matrix composites", *Annals of the CIRP*, Vol. 41/1, pp.55-58, 1992.

[7] Kannan, S.; Kishawy, H.; Balazinski, M.; "Analysis of Abrasive Wear During Machining Metal Matrix Composites" *in Jahazi M., Elboudjaini M. and Patnaik, P., Aerospace Materials and Manufacturing Processes; proc. of the 3rd Int. Symp. of CIM*, COM 2006, 1-4 Oct., pp.227-236.

[8] Lin, J. T., Bhattacharyya, D., Lane, C., "Machinability of a silicon carbide reinforced aluminum metal matrix composite.", 1995, *Wear*, 181-183, 883-888.

[9] Manna, A., Bhattacharayya, B., "A study on machinability of Al/SiC-MMC."; 2003, *Journal of Materials Processing Technology*, 140, 711-716.

[10] Che-Haron, C. H., "Tool life and surface integrity in turning titanium alloy.", 2001, *Journal of Materials Processing Technology*, 118, 231-237.

[11] Machado, A.R.; Wallbank, J.; "Machining of Titanium and its alloys-a review"; Proceedings of the institute of mechanical engineers Part-B: *Journal of Engineering Manufacture* 204, pp53-60, 1990.

[12] Yang, X.; Liu C. Richard; "Machining Titanium and its Alloys"; *Machining Science and Technology*, 3:1, 107-139, 1999.

[13] Kahles, J.F., Field, M., Eylon, D., Froes, F.H., "Machining Of Titanium Alloys", 1985, *Journal of Metals*, 37, 27-35.

[14] Shaw M.C. ; "Metal Cutting Principles" Second edition, *Oxford University Press*, 2005.

[15] Komanduri, R.; "Some clarifications on the mechanics of chip formation when machining titanium alloys.", 1982, *Wear*, 76, 15-34.

[16] Arrazola, P. J., Garay, A., Iriarte, L. M., Armendia, M., Marya, S., Le Maître, F., "Machinability of titanium alloys

(Ti6Al4V and Ti555.3)", 2009, *Journal of Materials Processing Technology*, 209, 2223-2230.

[17] Basavarajappa, S.; Chandramohan, G; Narasimha Rao, K V; Adhakrishanan, R; Krish, V.; "Turning of particulate metal matrix composites - review and discussion", *Proceedings of the Institution of Mechanical Engineers*; Jul 2006; 220, B7; Wilson Applied Science & Technology Abstracts, pp. 1189.

[18] Bejjani, R.; Balazinski, M.; Attia, H.; Shi, B.; "A New Design of Quick Stop Device for Research on Chip Formation."; *transactions NAMRI*-SME; 2010; V38; pp 269-274.

[19] Ross, Phillip J.; "Taguchi techniques for quality engineering" ; *McGraw-Hill*, 1988.

[20] Rabinowicz, E., "Friction and wear of material"; *John Wiley*, USA, 1965.

[21] Zhu, Y; and Kishawy, H. A; "Influence of alumina particles on the mechanics of machining metal matrix composites*", International Journal of Machine Tools and Manufacture*, Vol. 45/4-5, pp. 389-398, 2005.

[22] Shaw, M.C.; Vyas, A.; "The Mechanism of Chip Formation with Hard Turning
Steel", *Annals of the ClRP* Vol. 47/1/1998.

ACKNOWLEDGEMENT

The authors wish to acknowledge Dynamet Technology Inc., for providing the Ti-MMC material used in this investigation. The support of the Aerospace Manufacturing Technology Centre (AMTC), Institute for Aerospace Research (IAR), National Research Council Canada (NRC), where the experimental work was carried out, and the Canadian Network for Research and Innovation in Machining Technology (CANRIMT).

APPENDIX A2: A NEW DESIGN OF QUICK STOP DEVICE FOR RESEARCH ON CHIP FORMATION

R. Bejjani, H. Attia, M. Balazinski, B. Shi, *"A NEW DESIGN OF QUICK STOP DEVICE FOR RESEARCH ON CHIP FORMATION"*, Transactions of NAMRI/SME, vol. 38 pp.269-274, 2010.

A NEW DESIGN OF QUICK STOP DEVICE FOR RESEARCH ON CHIP FORMATION

Roland Bejjani and Marek Balazinski
Department of Mechanical Engineering
Université de Montréal, Polytechnique
Montreal, Quebec

Bin Shi and Helmi Attia
Aerospace Manufacturing Technology Center
National Research Council Canada
Montreal, Quebec

KEYWORDS

Quick stop device, Chip formation, Metal Matrix Composite, Chip root microstructure.

ABSTRACT

Quick stop devices (QSD) have been frequently used for studying the chip formation mechanisms and the plastic deformation processes in shear zones. However, most QSD involved complex design, unsafe operation, and/or are difficult to use. This paper presents a newly developed QSD which can be used as an alternative to conventional explosive shear pin design. This QSD has the advantages of fast response, easy usage, high repeatability, and short set-up time. Safety was a major concern, and the usage of any form of detonation was avoided. This new QSD uses a piston actuated by compressed air pressure. The piston is used to break a hardened pin under bending stresses. This QSD was tested and proved to have a high degree of repeatability, chatter-free operation, and short set-up time. Using this QSD, samples of chip root formed during the machining of Ti-MMC were obtained and their microstructures were examined using optical microscope.

INTRODUCTION

For our research on the machinability of a new material: Ti-MMC (Titanium Metal Matrix Composite), we needed to study the chip formation mechanism using a QSD. Ti-MMC is a relatively new material, and very limited information, if any, is known regarding its machinability. Investigation of the chip formation mechanism of this material is essential for further understanding and modeling the plastic deformation processes in the primary and secondary shear zones under conditions of very high strain, strain rate and temperature. The quick stop device (QSD) is a research device which will freeze the cutting process instantly and this will lead to sample collection of the chip root area that contains the primary and secondary deformation zones. The separation time or the time required for the tool to stop the contact with the material after the actuation of QSD is critical and should be as small as possible in order not to have an effect on the frozen chip. In our case a high speed camera was used to validate the QSD time response. The mechanism of this newly developed QSD is purely mechanical, and it does not involve any explosive charge. This can be useful in a work environment, where the usage of explosives is prohibited, as in our case. The Ti-MMC material used in this experimental work has hard particles of TiC which are very abrasive. With the QSD, one can examine the adhesion of the

workpiece material to the tool face, the separation of hard particles that result in three-body abrasion of the cutting tool, as well as the thickness of the primary shear zone. The latter is required for identifying the material constitutive equation during machining, using the theory developed by Shi et al. [2008].

The most common type of QSD is the shear pin design, using numerous types of actuation methods. Hasting [1967] developed an explosive type of shear pin QSD where the pressure from the explosion acts through a piston, forcing the tool block to shear the pin, and subsequently move the tool insert away from the material. Vorm [1976] developed a QSD using a drop hammer with a large mass that is capable of breaking the pin. The pin should, however, be carefully sized in order to withstand the cutting force without shearing during machining. The QSD designed by Black and James [1981] uses a flying hammer to shear the pin and remove the tool from the material being machined. This QSD achieves a speed of up to 30 m/s. Some attempts were made in order to make a more advanced or simple devices. Satheesha [1990] developed a QSD which is based on a tensile pin rupture instead of a shear pin design. The concept was based on using the stored strain energy for retracting the tool. This QSD did not use an external form of energy, instead it uses the cutting force and the strain energy in order to rupture a tensile pin which is spring loaded. Gwo-Lianq [2004] developed a mechanical QSD, which when actuated with a lever, the spring force moves the tool away from the material. Jaspers [2001] developed a semi-explosive shear pin QSD, where an explosive charge drives a projectile, which in turn actuates the shear pin QSD. Table 1 shows a comparison of some quick stop devices found in the open literature.

Regardless of the design of a QSD, to work properly, it should meet the following requirement: the distance traveled by the tool in the material after the actuation of the QSD should be very small, in other words the separation time between the tool and the material should be minimal. For our tests where the maximum cutting speed is 150 m/min, we will set a target of 0.1 mm as max displacement for the tool head to reach the velocity of: 150 m/min (or 80 μ sec to reach this mentioned speed).

TABLE 1. PERFORMANCE AND DIFFERENT TYPES OF QSD.

Reference	QSD type	Max speed (m/min)	Use of explosives
Hasting [1967]	Explosive type	Used up to 300 m/min	YES
Jasper [2001]	Semi-explosive shear pin	Used up to 120 m/min	YES
Gwo-Lianq [2004]	Lever/spring	Used up to 45.6 m/min	NO
Black and James [1981]	Hammer-shear pin	1800 m/min (claimed)	NO
Satheesha [1990]	Tensile pin	Used up to 18 m/min	NO
Current new QSD	Air piston	150 m/min at 6 bars	NO

THE NEW CONCEPT OF QUICK STOP DEVICE

This paper describes a new concept for QSD. This device was developed in such a way to resolve many problems usually associated with QSDs, namely, the difficulty of ensuring test repeatability, the difficulty of maneuvering large masses, as in the case of flying hammers, and the unsafe conditions that may be encountered when explosive charges are used. Furthermore, the QSD has to be easy to use, with a fast set-up time, and no chatter or vibration during machining. Most importantly it should meet safety requirements, in places where no explosives should be used.

Figure 1 shows the components of the tool holder and the shear pin of the proposed QSD. The insert (A) goes into the tool holder (E). A hardened pin (D) is inserted at the opposite end of the tool holder. The pin will rest on a small flat surface (C). In normal running condition, the pin (D) will be held between the two plates (F). The tool holder is free to rotate around the tube (B).

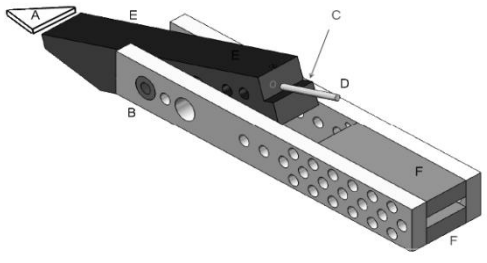

FIGURE 1. SCHEMATIC SHOWING THE MAIN PARTS OF THE TOOL HOLDER AND SHEAR PIN.

Under normal machining operation, the whole assembly will be fixed to a frame attached to the turret of the CNC turning centre. Figure 2 shows the complete QSD assembly with the piston. While machining, pin (D) (Figure 1) will retain the tool holder from rotating. When desired, the air cylinder (G) will be actuated with the help of a solenoid valve, causing the piston rod (H) to extend and acquire enough kinetic energy to break the hardened pin (D) when it hits the tool holder. This causes the tool holder to move away of the machined part.

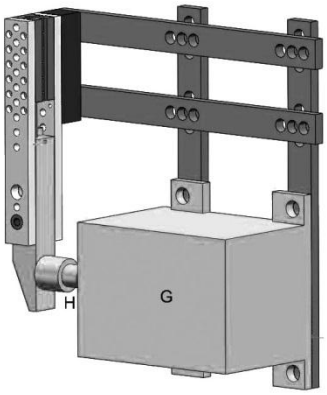

FIGURE 2. THE QSD ATTACHED TO THE AIR PISTON AND THE MOUNTING FIXTURE.

Figures 3 and 4 show the complete QSD assembly. After the piston actuation, the tool holder will tilt and therefore the chip will stay on the material as will be shown on Figure 10. It should be noted that there is no obstruction for the newly formed chip, and in our experiments we were successful in keeping the chip fixed to the material in every attempt.

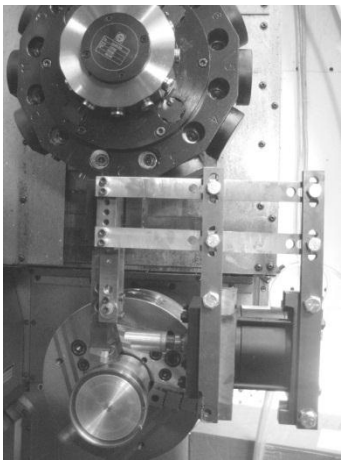

FIGURE 3. COMPLETE QSD ON THE CNC LATHE.

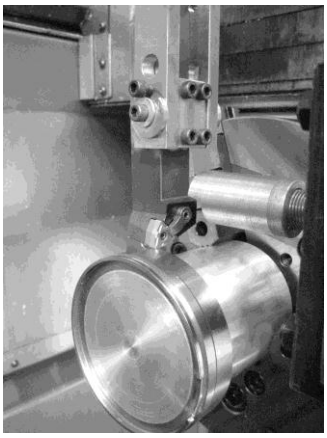

FIGURE 4. CLOSE-UP OF THE TOOL HOLDER.

Experimental Setup

Preliminary experiments were carried out to test the rigidity of the new quick stop device and to ensure that stable cutting conditions are maintained. In addition to AE (Acoustic Emissions) measurement, the surface roughness of the machined part was measured and compared to the surface roughness produced when the QSD was not used. No measurable difference was found between those tests.

The following experimental equipment is used:

- CNC Boehringer Turning Centre NG 200,
- Talysurf surface roughness and for 3D surface profile, Series S4C.
- Struer equipment for materialographic specimen preparation.
- Olympus microscope with magnification of up to 2000.
- High speed camera, model: AOS X-Motion.
- Coated carbide tool insert, SECO CNMG 432.

DESIGN CONSIDERATIONS

The following design objectives and requirements were set for the new QSD:

- Safe operation without using explosives.
- The separation speed should more than 150 m/min at the tool tip.
- Adjustable mechanism.
- Ease of use and fast setup.
- Reliable and repeatable.
- Chatter-free while machining.

As already mentioned, the success of the QSD depends mainly on its fast response. To achieve

that, many critical issues had to be carefully considered. On the pneumatic side, proper sizing of piston, air pressure, air lines and solenoid valve is essential. As for the hardened pin, the diameter, length and steel grade are also critical. When activated, the piston acquires speed as it travels; however, restrictions in the air flowing through the air lines, the solenoid valve, the piston inlet, and the piston friction will limit its speed. Furthermore, there is a limit on the pressure and the speed that the piston can safely accommodate. According to the manufacturer's specifications, the selected piston is limited to a speed of 5 m/s.

In order to size the different parts of the QSD properly, velocities were estimated by satisfying: (a) the principle of conservation of momentum, where the linear momentum of the piston at the point of impact ($P_p=m_pV_p$) is converted into angular momentum for the tool assembly ($P_t=\bar{I}_t\omega_t$), where $\bar{I}_t$ is the moment of inertia of the tool holder assembly around its pivot and ω_t is its rotational speed, and (b) the principle of conservation of energy, where the kinetic energy of the piston rod ($E= ½\ m_p\ V_p^2$) is converted to that of the tool holder ($E= ½\ \bar{I}_t\omega_t^2$). Due to the losses in the air pressure in piping system, the force and therefore the exact speed of the piston's rod at the time of impact is an approximation. To get the exact value of the tool tip speed after the impact, a high speed camera was used as will be shown later.

FEM was also carried out using DEFORM-3D® software to determine the force required to reach the fracture stress of a hardened pin made of steel AISI 52100 (~62 HRC) and has a nominal diameter of 3.175 mm. Figure 5 shows the deformed pin when the force applied is large enough to break it. As predicted, the maximum stress is at the point where the pin is touching the edge of the flat surface (C) in Figure 1. At this point (A) in Figure 5 the maximum effective stress reaches the fracture stress of 1,170 MPa.

To validate the FEM simulation, the hardened pin was tested for the maximum force it can withstand before breaking. A special fixture was constructed to hold the pin, and a dynamometer was used to measure the applied force. To check repeatability, the experiment was repeated under a wide range of conditions. Figure 6 shows one of the broken pins. All pins were fractured in a similar pattern, at the same location that was predicted by the FE analysis at location (A) in Figure 5.

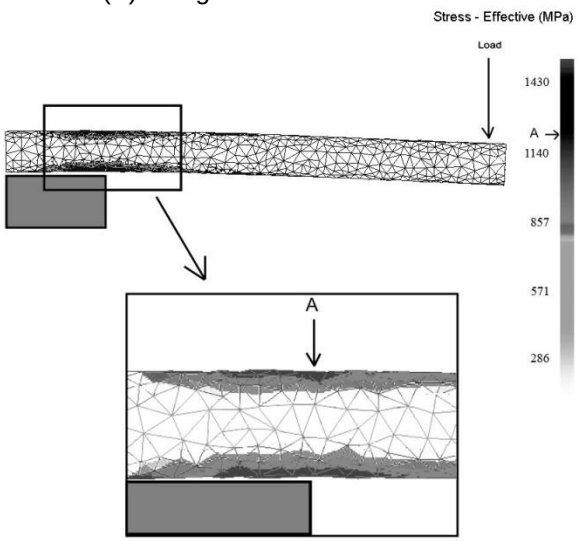

FIGURE 5. FEM SHOWING THE PIN LOADING WHEN THE MAXIMUM EFFECTIVE STRESS REACHES THE FRACTURE STRESS OF THE PIN (1,170 MPa).

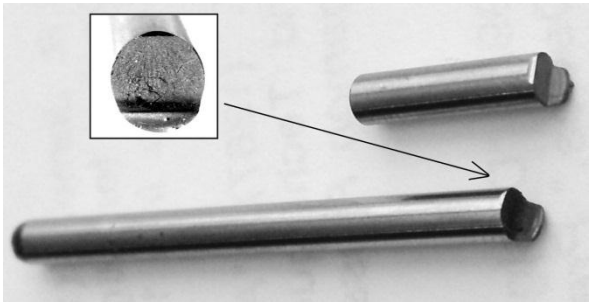

FIGURE 6. BROKEN HARDENED PIN AFTER LOAD APPLICATION.

It is worth noting that the new QSD was designed in such a way that it allows many adjustments in order to accommodate different cutting forces, different materials, and different cutting speeds.

Figure 7 shows photos taken with the high speed camera at 4,000 frames per second. Figure 7(a) shows the tool holder just before the impact, while Figure 7(b) corresponding to 10 ms after the impact. From these high speed observations, it is estimated that the tool head speed just after the impact was as high as 240 m/min. Furthermore, the displacement of the tool tip to reach a speed of 150 m/min is: 0.097 mm which is better than the target we set previously at 0.1 mm.

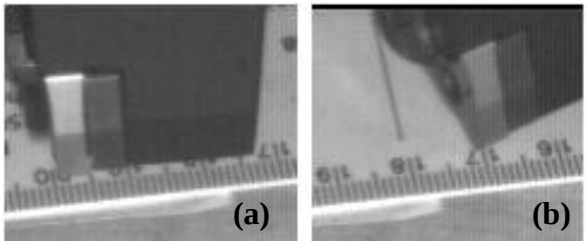

FIGURE 7. TOOL TIP POSITION BEFORE AND AFTER IMPACT USING HIGH SPEED CAMERA.

Therefore for this specific air pressure used (6 bars), the QSD could be used for cutting speeds up to 150 m/min. Moreover, in a real case situation and while machining, the cutting force will add up to the force delivered by the piston, allowing the tool head to move faster.

EXPERIMENTAL RESULTS AND DISCUSSIONS

The QSD was tested for different speeds for turning aluminum cylinder (shown in Figure 8) to check the degree of repeatability of the QSD. In each and every test, the cutting process was fully frozen with the chip attached to the workpiece.

For the material under investigation, Ti-MMC, several tests were performed using the newly developed QSD, under the following cutting conditions: Cutting speed of 70 m/min, feed of 0.2 mm/rev, and depth of cut of 0.15 mm. Each chip root was carefully removed using appropriate tools. Subsequently, the samples were molded in an epoxy solution. After a drying time of 24 hours, the chips were ground and polished to remove all the scratches. The last stage was etching with the appropriate chemical solution (KROLL).

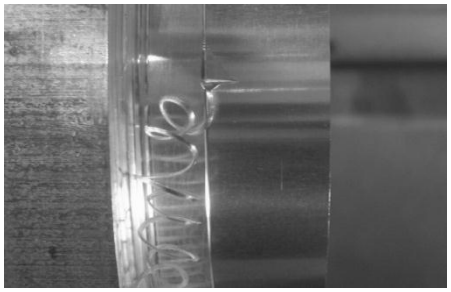

FIGURE 8. ACTUAL TEST OF QSD ON AN ALUMINUIM CYLINDER.

The samples were then examined under different magnifications, using an optical microscope. The manipulation and manual work involved in the preparation of the samples were very critical and time consuming, as any mishandling can lead to the breaking of the chip attached to the machined surface.

Figures 9 and 10 show samples of the Ti-MMC chip root observed at different magnifications in order to reveal their characteristic features. Figure 9 shows that the cutting ratio $r = p_c/p$ is greater than 1, as expected for this type of segmented saw-tooth chip that are formed by fracture [Shaw, 2005]. The figures show also the presence of gaps (g) at the roots of the chip due to the elongation of the material in the micro-crack region. The newly developed QSD also provides a means to establish the transition from a continuous chip to a segmented chip, which is familiar to most Titanium alloys. This allows deeper analysis on the deformation of the crystalline structure and the characterization of the shear zones and shear angles.

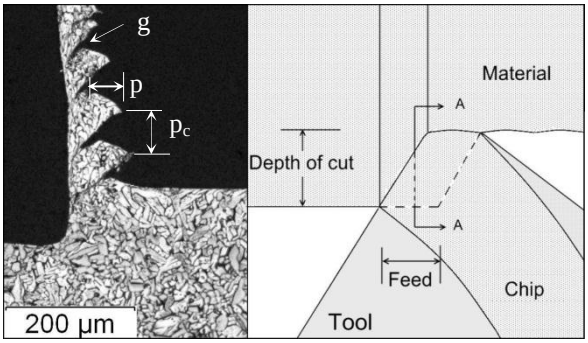

FIGURE 9. SAMPLE AT 500X MAGNIFICATION SHOWING CHIP AT SECTION A-A.

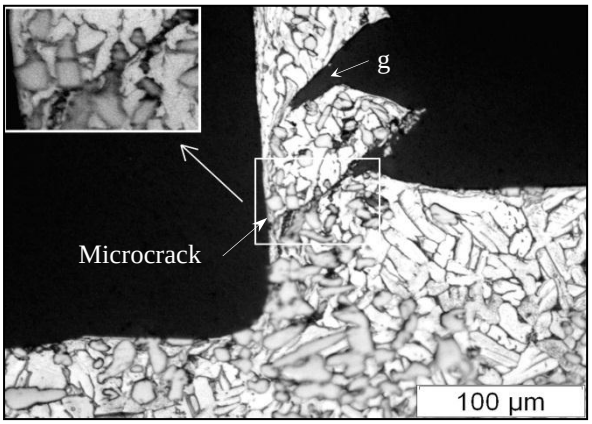

FIGURE 10. SAMPLE AT 1000X MAGNIFICATION.

CONCLUSIONS

This paper presents a new concept of quick stop device where all design objectives and requirements were met. The design and robust operation were validated for different materials and cutting conditions. Furthermore, the new QSD has the following advantages:

- Safe operation using compressed air as a source of energy, without the need for explosive charges. Unlike some types of QSD, the operator does not need to be close to the QSD, and therefore the QSD can be used in an enclosed CNC turning/machining centre, which further enhances its safe operation.
- Rigid and chatter-free operation. The QSD showed similar behavior compared to machining with the same tool and a standard tool holder.
- Repetitive and reliable operation. The QSD produced the required and predicted result repeatedly.
- Ease of operation. Once the set-up adjustments are made, only the insertion of a new pin is required for a new operation.
- Fast set-up between tests. It actually takes around one minute to make the QSD ready for a new test.
- Low operation cost.
- Adjustable mechanism. To achieve the desired speed and cutting force, the QSD can easily be adjusted.

Therefore, this new QSD is a viable alternative to the conventional explosive shear pin type, where usage of explosives is prohibited.

REFERENCES

Black J.T., C.R. James, (1981). "The Hammer Quick Stop Device for High Speed Machining and Rubbing." *J. Eng. Ind.* 103 pp. 13-21.

Gwo-Lianq C. (2004) "Development of a new and simple quick-stop device for the study on chip formation" *International Journal of Machine Tools and Manufacture*, Volume 45, Issues 7-8, June 2005, pp 789-794.

Hastings, W.F. (1967). "A New Quick Stop Device and Grid Technique for Metal Cutting Research." *Annals of CIRP, 15,109.*

Jaspers S. P. F. C. (2002) "Material behaviour in metal cutting: strains, strain rates and temperatures in chip formation." *Journal of Materials Processing Technology,* Volume 121, Issue 1, 14 February 2002, pp 123-135.

Satheesha M. (1990). "Design and Development of a Quick Stop Device." *Precision Engineering.* Butterworth-HeinemannLtd.

Shaw, M.C. (2005), *Metal Cutting Principles, 2nd edition,* Oxford University Press.

Shi, B. (2008). "Identification of the Material Constitutive Equation for Simulation of the Metal Cutting Process." *Ph.D. Thesis, McGill University*, Canada.

Vorm T. (1976). "Development of a Quick Stop Device and an Analysis of the Frozen Chip Technique." *int. J. Mach. Tool Wear Res.* 16 pp. 241-250.

APPENDIX A3: LASER ASSISTED TURNING OF TITANIUM METAL MATRIX COMPOSITE

R. Bejjani, B. Shi, H. Attia, M. Balazinski,*" Laser assisted turning of Titanium Metal Matrix Composite"*, CIRP annals, vol. 60, "1", pp.61-65, 2011.

CIRP Annals - Manufacturing Technology 60 (2011) 61–64

Contents lists available at ScienceDirect
CIRP Annals
Manufacturing Technology
Journal homepage: www.elsevier.com/locate/cirp

Laser assisted turning of Titanium Metal Matrix Composite

R. Bejjani [1], B. Shi [2], H. Attia [2](2), M. Balazinski [1](1)

[1] Mechanical Engineering Department, École Polytechnique Montréal, Montréal, Quebec, Canada
[2] Aerospace Manufacturing Technology Centre, National Research Council of Canada, Montreal, Quebec, Canada

Abstract
Although ceramic particles in Titanium Metal Matrix Composites (TiMMCs) improve its wear resistance properties, they also cause high abrasive tool wear. In an attempt to enhance tool life and productivity, Laser Assisted Machining (LAM) of TiMMC was performed under different cutting conditions, an aspect that has never been investigated before. Analysis of the results showed that LAM can significantly increase tool life by up to 180 %. The phenomenon of improved tool life at higher speeds and under LAM conditions were explained through the analysis of the chip morphology and micro-structure.

Keywords
Cutting; Laser; Metal matrix composite

1. Introduction

Titanium Metal Matrix Composite (TiMMC) is a new class of structural material which belongs to the category of MMCs. MMCs are known to have higher wear and fatigue resistance, higher deformation resistance, and higher rigidity, when compared to other alloys [1]. MMCs are, however, difficult to cut, mainly due to the added hard and abrasive ceramic particles, which limit the life of cutting tools.

As a new composite material, very limited information is available in the open literature on the machinability of TiMMC. Although parts made of TiMMC are usually produced as near net shape, finish machining is still required. The presence of the hard TiC particles in the matrix leads to both two-body and three-body abrasive tool wear mechanisms. The two-body abrasive wear occurs when a rough and hard surface rubs against a softer one and ploughs into it. On the other hand, three-body wear occurs when a hard particle is introduced between two rubbing surfaces and abrades material off each of the two surfaces [2].

Titanium alloys are considered difficult to cut materials due to their low thermal conductivity and the formation of very thin chip that result in very high cutting temperature concentrated in a small area on the tool-chip interface. In addition, the strong chemical reactivity of titanium results in high affinity to almost all tool materials [3].

Some contradictory conclusions have been reported on the effect of laser assisted machining (LAM) on tool life, when using carbide and SiAlON ceramic tools to cut Inconel 718 [4,5]. The performance of LAM on Aluminium-MMC has also been evaluated in [1]. The study pointed out the importance of the tool-particles interaction, where the particles will be more easily pushed by the tool in the heated, and therefore, softer matrix.

When using LAM on Ti alloys, care should be taken for not exceeding the phase transformation temperature of 882 °C [3]. Moreover, the heat from the laser source and the added heat from the secondary shear zone can result in severe tool diffusion wear. The present investigation is aimed at studying the effects of cutting parameters with LAM on tool life, chip morphology and surface integrity.

2. Experimental setup

The machining tests were performed on a 6-axis Boehringer NG200, CNC turning centre. The high power laser beam was generated by a 5200W IPG PHOTONICS YLR 5000 fiber laser (ytterbium) with a wavelength of 1070 nm. A schematic and a close-up of the experimental setup are shown in Figure 1. The laser head (A) is mounted on a special fixture to control the orientation of the beam ($\phi = 50^{o}$~90^{o}) and its spot size. A pressurized air nozzle (C) with a maximum pressure of 6 bars was directed at the chip area in order to remove the chips as soon as they are formed. A Thermovision A20 infrared (IR) camera (B) was used to map the temperature field near the cutting zone. Three K-type thermocouples were attached to the workpiece surface, through a high speed slip ring, to calibrate the IR camera. The cutting forces were measured using a three-component Kistler dynamometer, type 9121. The surface roughness was measured after each test, using a portable Taylor Hobson Surtronic 3+. Tool wear progression was measured using an Olympus SZ-X12 stereoscopic microscope. A Scanning Electron Microscope (SEM) Jeol, JSM-840A was used for detailed analysis of the chip morphology and the TiC particle behaviour. For micro-hardness measurement, a Struer Duramin A300 was used.

0007-8506/$ – see front matter © 2011 CIRP.
doi:10.1016/j.cirp.2011.03.086

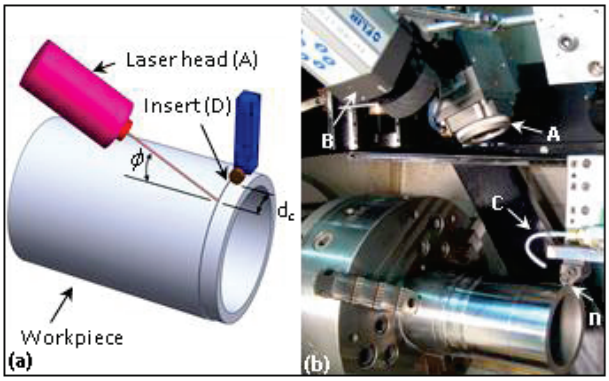

Figure 1 LAM experimental setup: (a) schematic diagram, (b) actual setup.

A specially developed quick stop device (QSD) was used to freeze the chip formation process. For safety reasons, the new QSD device is actuated pneumatically (0.6~0.7 MPa) to break a hardened pin in bending, instead of using explosives. The detailed design features of this QSD, and its performance and repeatability are described in [6]. Chips were then polished and etched for further metallographic examinations.

The turning tests were carried out using 63.5 mm diameter cylindrical workpieces made of CermeTi® MMCs, which consist of a non-metallic phase TiC (10~12% by weight) distributed in a matrix of Ti-6Al-4V titanium alloy (yield stress 1150 MPa), manufactured by Dynamet Technology. The tool used was a Poly-Crystalline-Diamond (PCD), RNMN42 round insert from KY-Diamond, with 12.7 mm diameter and 0° rake angle.

3. Experimental approach

The starting point of this study was based on the optimum conditions established by the authors in [7] for conventional turning of TiMMC. The controlled variables were the cutting speed and feed, while the optimization objective functions were the surface roughness and tool life. The optimum speed for conventional cutting was found to be 180 m/min [7]. Similar to other MMCs, the primary wear mode was abrasion on the flank face of the cutting tool.

In the present work, the selected cutting speed was reduced to 170 m/min (considered here as high speed; HS), in order to reduce the possibility that the chips catch fire. Another speed level of 100 m/min was considered for comparison purposes (considered here as low speed; LS). The feed and depth of cut were kept constant at 0.2 mm/rev and 0.15 mm, respectively.

Tensile tests at high temperature were performed, and similar to titanium alloys, the yield stress was found to be greatly dependant on temperature, and was reduced by approximately 50% at 500 °C. The maximum surface temperature, when using the laser heating source, was limited to 500 °C (considered here as high temperature; HT) in order to prevent the phase transformation in the matrix. The other surface temperature used in the present study was 300°C (considered here as low temperature; LT). Furthermore, room temperature (RT) conventional machining tests were conducted to establish a reference point. The measurement errors of various parameters were estimated and are represented in the results, shown in section 4, as error bars.

4. Analysis of results and discussions

4.1. Laser beam optimization and parameters control

The laser system used in this study has a focal length L_f = 220 mm, and the beam spot diameter on the workpiece was adjusted to d_L = 2 mm. The laser beam was oriented at an angle $\phi = 70^o$ with respect to the workpiece (Figure 1 (a)). To avoid any interference of the chips with the laser beam and the risk of catching fire, the beam was adjusted to hit the surface at a distance d_c = 23 mm away from the cutting tool.

The dependence of the surface temperature T_s (at the distance d_c from the center of the laser spot) on the laser power and the cutting speed were established. The laser power was varied from 840 to 1,875 W for each speed. Figure 2 shows that at a higher speed, more power is needed to reach the required T_s, since less time is available to raise the material temperature. Furthermore, the heat loss by convection is increased at higher turning speeds.

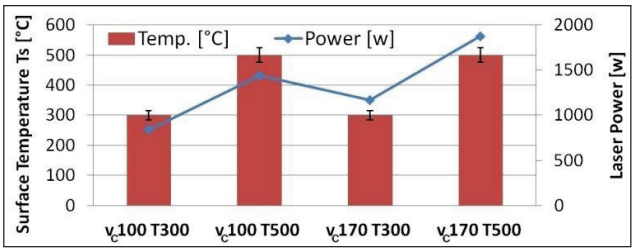

Figure 2 Effect of laser power and cutting speed on surface temperature. The speed v_c is in [m/min] and the temperature T_s in [°C].

4.2. Effect of laser power and cutting speed on surface roughness

Figure 3 shows the effect of cutting speed and surface temperature T_s on the average arithmetic surface roughness R_a. The lowest values of R_a were obtained when cutting at room temperature (RT). The increase of T_s to 500 °C, when using LAM, led to an average increase of R_a by only 15%. This suggests that the softening of the matrix affects the tool-particle interaction and the mechanism of chip formation.

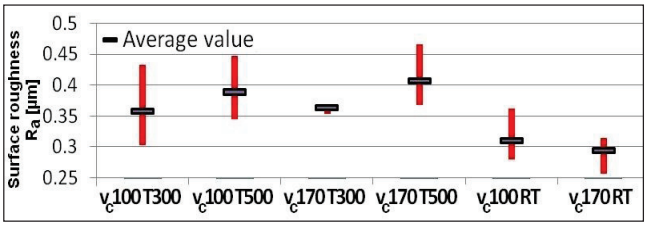

Figure 3 Effect of speed and surface temperature on surface roughness R_a.

4.3. Effect of laser power and cutting speed on cutting forces

Figure 4 (a) shows the direct effect of the material softening by LAM on reducing the cutting forces, as the laser beam was activated ON and then OFF. As expected, round inserts produce relatively large thrust forces (F_t). It was noted that LAM has the highest effect on F_t, reducing it by approximately 25% in this case. Figure 4 (b) shows the effect of different cutting parameters on the cutting forces after cutting a fixed length of 160 mm in the feed direction. As expected, the lowest forces were obtained for the highest cutting speed v_c and highest T_s. Here also, F_t has the highest sensitivity to the combined effects of v_c and T_s.

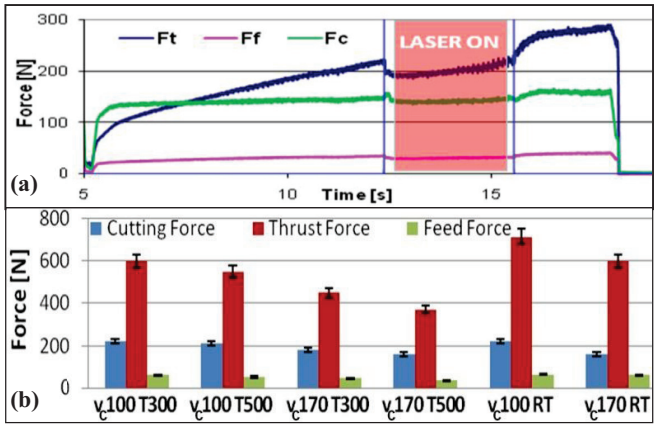

Figure 4 Cutting forces: (a) direct LAM effect on cutting forces when T_s=500°C and v_c= 170 m/min, (b) forces at length of cut= 160 mm.

4.4. Effect of laser power and cutting speed on tool wear

Figure 5 shows the maximum length of cut (L_c) in the feed direction achieved for different cutting conditions, with a tool wear criterion of VB_{Bmax}= 0.30 mm. In all conditions, LAM resulted in increased tool life and total cut volume. The largest length of cut L_c = 380 mm was obtained for the combination of low speed and high surface temperature (LS/HT). This represents a 180% increase in the total length of cut, compared to RT test at the same speed. At high speed and low surface temperature (HS/LT), however, the length of cut L_c is slightly reduced to 370 mm, and if both the material removal rate and the tool life are considered as the objective functions, then this combination of HS/LT represents the optimum cutting condition.

Similar to previous work by the authors in [7] on conventional machining of TiMMC, cutting at high speed resulted in an unexpected increase of tool life. An explanation of the effect of T_s and v_c on tool life will be discussed in section 4.6, in relation to the tool-particle interaction.

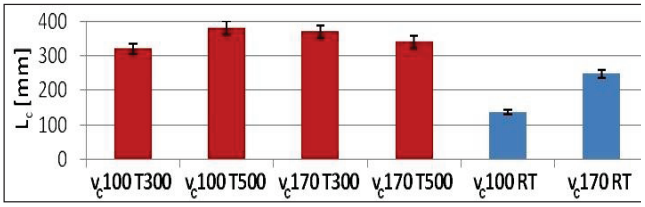

Figure 5 Cutting conditions effect on total cut length L_c at VB_{Bmax}= 0.3 mm.

Even though the use of LAM is beneficial with respect to tool life, the combination of high surface temperature T_s and high speed (HT/HS) does not lead to the maximum tool life. To understand the interaction between T_s and v_c, SEM examination of worn tools was carried out. Similar to other MMCs, abrasion wear on the tool flank was the dominant wear mode for all tests conditions, except for the condition of HT/HS, where both flank and crater wear were present, as shown in Figure 6 (a) and (b).

Tool diffusion wear is a common problem when cutting Ti alloys since they have a strong adherence to the tool in the contact area [8]. However, the adhered material limits the diffusion of the tool constituents to the newly formed chip material. The adhered material was also shown to react with carbon from the PCD tool, forming a TiC hard protective layer. Since diamond is pure carbon, then this process is promoted [8]. Energy-dispersive-spectrometry (EDS) taken on the flank area

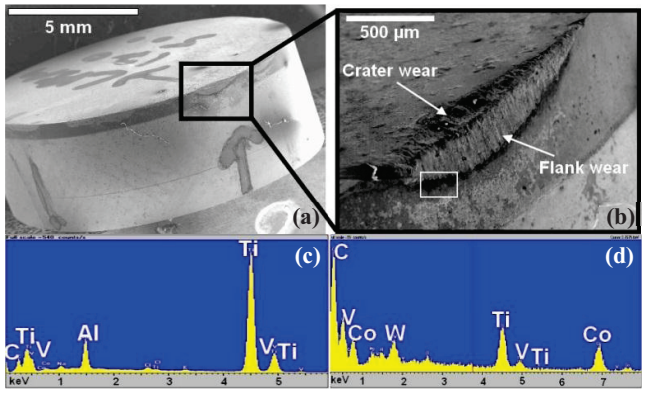

Figure 6 Worn tool at high speed/high temperature (HS/HT): (a) PCD tool, (b) close up, (c) EDS on the flank wear surface, (d) EDS on boxed area.

confirms the adherence of Ti, Al, and V from the matrix of the workpiece material to the tool, as shown in Figure 6 (c). EDS of the boxed area in Figure 6(b), which is located on the edge of the flank wear, is shown in Figure 6(d). The peaks presence of Ti and C confirms the possibility of the TiC protective layer formation.

4.5. Chip formation and surface integrity

The microstructure and the morphology of the chips were studied under different test conditions (Figure 7). The analysis showed that LAM affects the segmentation pattern, because adiabatic shear banding is mainly a thermal process (boxed areas, Figure 7) [3]. In general, the chips formed with LAM have a highly irregular segmentation pattern, characterized by larger fluctuations in segment height (h) and pitch (p) when compared to chips formed under conventional machining conditions.

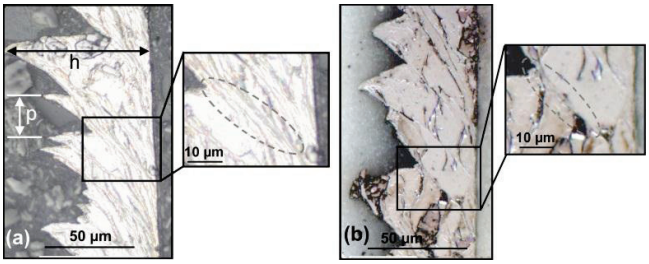

Figure 7 Chip morphologies, (a) with LAM, v_c = 100 m/min, T_s = 500°C, and, (b) conventional machining, v_c= 100 m/min, RT.

To further investigate the chip formation process, a quick stop (QS) test with LAM was carried out (v_c= 70 m/min, f= 0.15 mm/rev, T_s=500 °C). Figure 8 shows the formation of a new chip

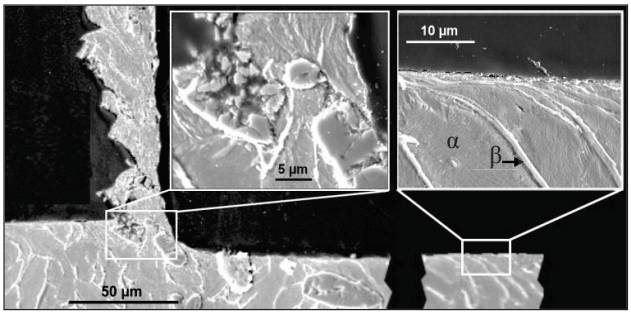

Figure 8 Quick stop test with LAM at T_s=500 ° C, v_c= 70 m/min.

segment, where a TiC particle was broken due to the plastic deformation of the matrix from the cutting action. Also shown (right box), are the elongated grains, which are an indication of a plastically deformed surface. This resulted in strain hardening, and a higher machined surface hardness of 430 HV0.1, compared to the base material (368 HV0.1). The depth of this strained layer is approximately 70 µm. Furthermore, there was no noticeable difference in the hardness and the depth of the strained region when compared to RT tests. Comparison with the bulk material also indicated that no phase transformation took place within the machined surface retaining the same alpha-beta (α-β) structure.

4.6. Tool-particle interaction behaviour

Examination of the TiC particle behaviour indicated that no particle debonding took place. However, in some cases, when the particle is embedded inside the matrix and is in the path of the cutting tool, three possible cases of tool-particle interaction can be encountered: (1) The particle is broken and a part of it is kept inside the matrix (Figure 9 (a)), (2) Parts of a broken particle are pushed back into the matrix (Figure 9 (b)), and (3) Non-broken particles are pushed into the matrix (Figure 9 (c)), where strain deformation lines in the matrix could be seen below the pushed particles. The last two cases are especially promoted by LAM, since the matrix is softer due to the increased temperature. Therefore, the broken particles can be more readily pushed by the tool into the softer matrix. This may also explain why moderately higher values of R_a are obtained with LAM.

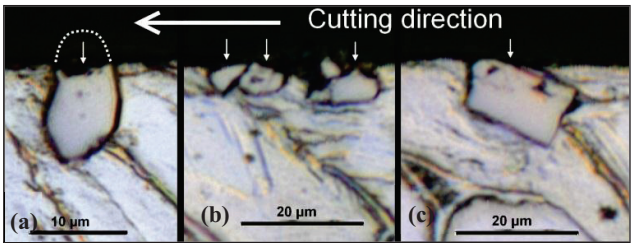

Figure 9 Particles behaviour with v_c=70 m/min and T_s=500 ºC, (a) broken particle, (b) broken pieces pushed into matrix, (c) particle pushed into matrix.

To further investigate the tool-particle interaction and to provide an understanding of the positive effect of high surface temperature on tool life, an additional LAM experiment was performed at a much higher temperature; T_s = 1000°C and v_c= 100 m/min. Figure 10 (a) shows a chip formed at these conditions. Compared to the chips shown in Figure 7, there is a noticeable difference in the microstructure of the chip, suggesting that the chip material underwent a phase transformation. This was also suggested by the increase of the matrix hardness in the chips to 500 HV0.1, compared to 445 HV0.1 in the RT tests. Careful examination of the chips revealed that most of the particles inside the chip did not break; but they were just displaced inside the matrix (compared to the RT test in Figure 10 (b)). The high temperature in LAM made the matrix softer, resulting in stresses on the particles that are below the level required to break them. This means that if fewer particles are broken, then consequently less abrasion wear occurs. It should be kept in mind that while machining, broken particles can be entrapped between the flank face and the material, resulting in three-body abrasion wear. Figure 10 (c) shows that a similar effect is observed at higher speed of 170 m/min, where an increase in cutting speed is associated with fewer broken particles.

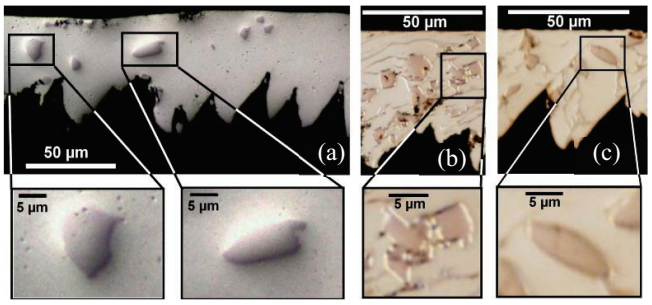

Figure 10 Chip morphologies, (a) particles not broken at T_s=1000°C, v_c= 100 m/min with LAM, (b) broken particles at RT v_c= 100 m/min, (c) particle not broken at RT, v_c= 170 m/min.

5. Concluding remarks

This study is the first attempt for laser assisted machining of TiMMC, which proved to be a practical solution for enhancing tool life. At v_c=100 m/min and T_s= 500°C, the total cut volume increases by 180%, compared to conventional machining at the same cutting speed. This substantial increase could not be achieved otherwise. An explanation of the increased tool life with LAM has been related to the tool-particle interaction, where the particles displace in the softer matrix instead of breaking and contributing to additional abrasion wear. LAM, however, may increase moderately the surface roughness by up to 15%.

While abrasion wear is still the dominant wear mode, signs of diffusion wear also appeared in LAM at high speeds and high surface temperature. Therefore, there is a limit, above which further increase in surface temperature will increase the tool chip interface temperature and will promote tool diffusion wear.

The unexpected phenomenon of increased tool life at higher cutting speeds was consistently observed in all machining conditions and was related to fewer broken particles and consequently less abrasion wear. The exception was when machining at high speed, high temperature, where tool diffusion wear was observed.

References

[1] Wang, Y., Yang, L.J., Wang, N.J., An investigation of laser-assisted machining of Al2O3 particle reinforced aluminum matrix composite, 2002, Journal of Materials Processing Technology, 129: 268-272.

[2] Kishawy, H.A., Kannan, S., Balazinski, M., 2005, Analytical Modeling of Tool Wear Progression during Turning Particulate Reinforced Metal Matrix Composites, Annals of the CIRP, 54:55-58.

[3] Machado, A.R., Wallbank, J., 1990, Machining of Titanium and its alloys-a review, Proceedings of the institute of mechanical engineers Part-B: Journal of Engineering Manufacture 204: 53-60.

[4] Germain, G., Lebrun, J.L., Braham-Bouchnak, T., Bellet, D., Auger, S., 2008, Laser-assisted machining of Inconel 718 with carbide and ceramic inserts, Int. J. Mater. Form. 1:523-526.

[5] Attia, H., Tavakoli, S., Vargas, R., Thomson, V., Laser-Assisted High Speed Finish of Superalloy Inconel 718 under Dry Conditions, 2010, Annals of the CIRP, 59: 83–88.

[6] Bejjani, R., Balazinski, M., Attia, H., Shi, B., 2010, A New Design of Quick Stop Device for Research on Chip Formation, Transactions NAMRI-SME, 38:269-274.

[7] Bejjani, R., Shi, B., Attia, H., Balazinski, M., Kishawy, H., 2010, Machinability of titanium metal matrix composites, Proceedings CIRP 2nd conf. Process Machine Interactions, C12.

[8] Hartung, P.D., Kramer, B.M., 1982, Tool Wear in Titanium Machining, Annals of the CIRP, 31:75-80.

APPENDIX A4: ON THE ADIABATIC SHEAR BANDING AND MICROSTRUCTURE EVOLUTION WHEN MACHINING TITANIUM METAL MATRIX COMPOSITES

R. Bejjani, M. Balazinski, H. Attia, G. L'Espérance,*" On The Adiabatic Shear Banding And Microstructure Evolution When Machining Titanium Metal Matrix Composites",* (submitted in June 2012, ASME, Journal of Manufacturing Science and Engineering, REF: MANU-12-1170).

On The Adiabatic Shear Banding And Microstructure Evolution When Machining Titanium Metal Matrix Composites

Bejjani Roland[1], Balazinski Marek[1] , Helmi Attia[2], Gilles L'Éspérance[1]
[1]École Polytechnique, Campus Université de Montréal
2900 boul. Édouard-Montpetit Montreal, Qc, Canada.
[2]National Research Council Canada

Abstract: Titanium Metal Matrix Composite (TiMMC) is a new class of material, which has high potential applications in the aeronautical and biomedical sectors. Like Titanium alloys, TiMMC produces segmented chips when machined. The segmentations in the chips are characterized by Adiabatic Shear Bands (ASB), and result in fluctuation in the cutting forces. Furthermore, the induced tool vibration affects negatively the machined surface's roughness.

Since analytical solutions cannot describe the thermo-mechanical nature of the process accurately, Finite Element Method (FEM) is the preferred method for deriving the cutting forces, strain, strain rate, temperature and stresses resulting from machining. FEM has been successfully used in the past years, however, when segmented chips are produced, the FEM model should also involve the physical changes and the phenomenon occurring inside the ASB in order to improve the prediction accuracy. This requires a complete understanding of the ASB phenomenon.

Different explanations exist for the root cause of ASB formation. Catastrophic shear instability, accumulated damage during the machining, lack of ductility and shear cracks generated on the free surface of workpiece material are some of the mechanisms proposed in the literature to explain the segmented chip formation.

Most researches in the literature on the adiabatic shear banding (ASB) are for high speed impact or ballistic tests, and research on this phenomenon when machining is still limited. This current study will aid to fill this gap. In this paper, the initiation of the ASB is studied, and its effects on microstructural evolution of the matrix material are discussed. Transmission Electron Microscopy (TEM) observations were performed in the atomic scale and lattice dislocations were identified. Furthermore, the sheared surfaces as well as the effects of the hard TiC particles on the ASB formation were investigated. TEM observations using thin foils prepared by Focused Ion Beam (FIB) inside the ASB on TiMMC were never carried out before. The main advantage of the FIB process is the ability to accurately position the specimen in the area of interest. This work can lead to a better understanding of chip formation and can assist in future FEM predictions.

Keywords: Titanium, chip-formation, shear-band, microstructure, metal-matrix-composites

1. INTRODUCTION

Titanium Metal Matrix Composite (TiMMC) is a new type of metal composite. It has superior physical properties over Titanium alloys. Therefore, this material has potential applications mainly in the aerospace, biomedical and automotive industries.

Reinforcement of conventional Titanium alloys with Titanium Carbide (TiC) particles improves the material modulus of elasticity, elevated temperature strength, creep resistance, and wear resistance.

Titanium alloys are the current material of choice for some biomedical applications such as load-bearing hip replacement components. TiMMC materials combine the advantages of metals and ceramics together and are under evaluation for such metal-on-metal orthopaedic implants [1].

Machining TiMMC produces segmented chips which have been attributed to "plastic instability". However their cause and mechanism are not well understood for cutting processes. The segments are characterized by adiabatic shear bands (ASB). The mechanism of deformation in a localized shear band, is one in which the rate of thermal softening exceeds the rate of strain hardening. This is usually referred to as an ''adiabatic shear process'' [2]. This phenomenon has been the object of intensive research for the last sixty years, since the early work of Zener and Hollomon [3]. However, deeper studies including theoretical and experimental investigations began around the early seventies. Most of the studies were based on high speed impact or ballistic experiments [4]. In experiments resulting in a fractured surface with a presence of an ASB, and a crack initiation; it is often uncertain whether the crack initiated the ASB, or if it resulted from the ASB phenomenon. In ballistic experiments, ASB have been clearly identified as a precursor to fracture; therefore the importance of identification for the criterion of the phenomenon [5].

Meyers [6] calculated the onset of instability of ASB in relation to shear strain (γ). A value of $\gamma = 1$ was determined for pure Titanium. Culver predicted the thermal instability shear strain to be 1.15 for the same material [7]. However, Meyers [6] indicates that strain up to 5 were found in impact test of Ti6Al4V alloy.

Two different theories on the mechanism of generation of segmented chips are found in literature; namely, "crack initiation", and "thermo-plastic instability". The main difference between the two theories is the mechanism of catastrophic failure in the primary shear zone which occurs with the deformation at the incipient segment directly ahead of the cutting tool. Shaw [8] postulated that shear bands form due to inside microfractures, and void propagation. However, due to heat and high normal stress the sheared band will weld again. The crack initiation occurs near the tool (or at the free surface) and propagates to complete the segment.

Nakayama et al. [9], Shaw and Vyas [10], Konig [11], among others, suggested that the catastrophic failure is initiated first by a crack at the free surface ahead of the tool, which propagates toward the tool tip and forming a segment. Kommaduri et al. [12], Davies et al. [13] suggested however, that a thermoplastic instability occurs within the primary shear zone. Komanduri [14] has identified two important stages in the formation of the segments in segmented chips. The first stage of segment formation involves upsetting of the wedge shaped volume of material immediately ahead of the tool (the beginning of segment formation). Once a critical shear strain is attained, thermo-plastic instability occurs and further shear strain is accommodated within the 'failed' shear zone. This leads to the formation of a segment. However, no full explanation of the thermo-plastic instability was included. As shown in Figure 1, the failure occurs in an arc like shape (A in Figure 1) and the sheared surface originates from the tool tip to the free surface. After the thermo-plastic instability and while the segment is being formed, the arc will end up forming a segment which becomes a line parallel to previous segments.

When machining Titanium alloys, Komanduri [14] noted a possible additional feature of shear localization where a phase transformation from the low-temperature hexagonal close packed (h.c.p.) structure to the body centred cubic (b.c.c.) structure with a corresponding increase in the number of available slip systems. This phenomenon can further localize the shear strain. The h.c.p. to b.c.c. phase transformation results from the temperature increase which accompanies plastic deformation.

Nakayama [15] investigated the initiation of crack in chip formation, and observed that the crack occurs at the free surface where the free surface starts bending (Figure 2). The angle of crack is in the direction of the highest shear stress, therefore at 45 degrees from this surface.

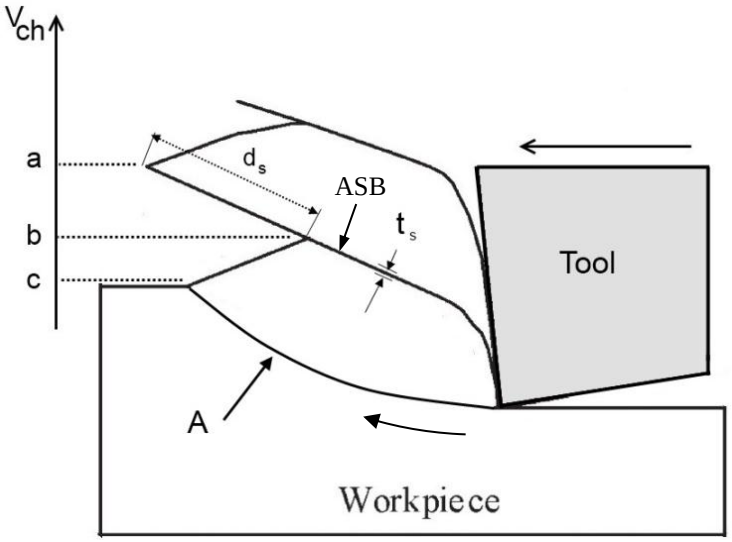

Figure 1; Chip formation sequence, where d_s is the displacement in the ASB, t_s is the ASB thickness, v_{ch} is the chip speed.

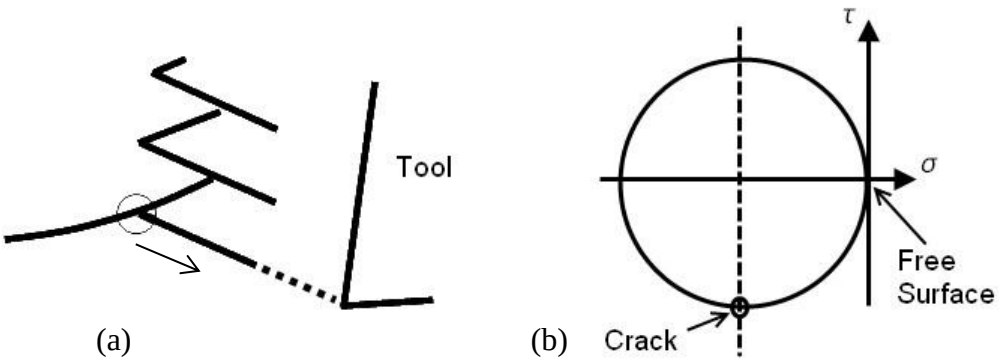

Figure 2; a) Crack initiation shown by the circle, b) Mohr circle at the crack location [15].

1.1. Conditions for ASB occurrence, and temperature rise

Segmented chip formation lead to many controversial theories in the past, and it is still a phenomenon where research is still active. In dynamic torsional loading, a sudden drop in the stress-strain curve was attributed as catastrophic failure due to localised shearing [16]. For the last two decades, the criterion for ASB formation has been based on a combination of mechanical instability with a thermal model. Later, based on thermoplastic instability, linear perturbation analysis was carried out suggesting a maximum load required for ASB formation [17]. Bai [18] predicted that the condition for ASB should include both stress and strain rate.

Recht [2] studied high strain rates in some metal and developed a criterion for the "adiabatic shear bands". For a strain ε; adiabatic shear occurs when the thermal softening effect from the temperature θ is higher than the added strain hardening strength τ.

$$0 \leq \frac{\frac{\delta\tau}{\delta\varepsilon}}{-\frac{\delta\tau}{\delta\theta}*\frac{\delta\theta}{\delta\varepsilon}} \leq 1 \qquad (1)$$

That is, if the above ratio is between 0 and 1, the material will shear catastrophically. Values larger than 1 indicate that strain hardening is the dominant factor, and the shear will distribute throughout the material. A negative value indicates that the material becomes harder with temperature, which is usually uncommon.

In order to estimate the temperature rise inside the ASB, the shear strain, and the shear strain rate had to be calculated. For segmented chips, the shear strain γ can be calculated using [19]:

$$\gamma = \frac{d_s}{t_s} \qquad (2)$$

Where d_s is the displacement within the shear band and t_s is the ASB thickness (Figure 1). For estimation of the temperature in the ASB, a simple equation can be used [20]:

$$\Delta T = \frac{\beta\ \tau\gamma}{\rho C} \qquad (3)$$

Where β is a thermal conversion factor, generally taken as 0.9, τ is the shear stress, γ is the shear strain, ρ is the density, and C is the heat capacity of the material.

1.2. Phase transformation and white etching bands

White etching bands have been reported in the literature in the ASB. Li *et al.* [21] classified the ASB in two types: deformed, and white etching bands. They proposed that the deformed bands will become white etching bands with increasing strain. Rogers [22], on the other hand, classified the bands into 'deformed' and 'transformed' types. For the latter type, the intense heat evolution and rapid cooling after deformation can be responsible for phase transformation of the material.

Me-Bar and Shechtman [23] reported that the high temperature generated in the ASB might cause a phase transformation from alpha to beta in the Ti-6Al-4V alloy. The white etching bands, which are referred to as "transformed" bands, have received much attention because phase transformations occur in the band. This suggests that phase transformation temperature has been reached [3]. The evidence for the occurrence of phase transformation in the ASB of steels rises from the well-defined width of the white band which has a very high hardness compared to the matrix. Meyers [24] indicates, however, that the shiny appearance of this "transformed" band is the result of a fine recrystallized structure resulting in increased resistance to etching; hence the name "white etching bands". These features have been mistakenly identified as phase transformation products [24]. In other words, the white etching bands are an unlikely indication of phase transformation. Meyers also noted the absence of b.c.c. reflections in the ASB; therefore the h.c.p.-b.c.c. transformation did not occur [6]. It was suggested that Rotational Dynamic Recrystallization (RDX) seems to be responsible for the micro grain formation in the ASB and there was no evidence of the "avalanche dislocation concept", where the catastrophic release of dislocation pile-up causes localised heating on the slip plane [5].

Some recent investigations show, however, that phase transformation occurs also in the deformed bands [5]. Moreover, α_2 phase (Ti_3Al) has been reported in the ASB of Ti-6Al-4V [20]. Also, parallel martensite plates showing α' (h.c.p.) platelets have been identified in the ASB of Ti-6Al-4V formed in ballistic experiments [25].

1.3. Recrystallization, superplacticity and super high strain rates

Super high strain rates were observed to occur in the ASB. Xue *et al*. [26] reported that the strain rate within the bands for Al-Li alloy was $1x10^6 s^{-1}$. Some investigations reveal that 'super-plastic flow' occurs for polycrystalline material with high strain rate sensitivity [27]. If recrystallization occurs in ASB, the new grain size will be lower than 0.1 μm. Also, the temperature within the shear band may reach more than 0.4 times the melting temperature on the absolute scale; providing appropriate conditions for super plastic deformation [20].

Meyers [24] studied the recrystallized microstructure in the ASB and calculated the theoretical grain size in case migrational recrystallization occurred during the cooling time after deformation. The results were found to be one order of magnitude smaller than the actual experimental results. Also, the calculated time, during which deformation occurs, was one order of magnitude lower than the actual cooling time. This suggests that migrational mechanism for recrystallization cannot occur alone in deformation during cooling. Therefore Meyers concluded that a Rotational Dynamic Recrystallization (RDX) was responsible for the observed microstructure in the ASB.

Most studies about ASB in the open literature are for high speed impact tests. Since the ASB is characterized by very small grains in the microstructure, Transmission Electron Microscopy (TEM) can be a useful investigation tool. In this technique, a thin foil of electron-transparent sample must be used. Different methods can be used for making a TEM sample. Eletropolishing is a common method; however it has limitations mainly due to the fact that the exact location of the area to be examined cannot be controlled. With the Focused Ion Beam (FIB) method, one can extract the exact location of interest; therefore it is a preferred method, since ASB are usually very narrow.

Research on ASB in machining experiments is very limited, and the present authors could not find any thorough ASB study using TEM with FIB specimens. This is the first study of ASB using an FIB sample of TiMMC chips. A deeper understanding of the ASB will give valuable input to the understanding of the physics behind the phenomenon, which can be applied in the future in FEM simulations to increase their prediction's accuracy. On the material aspect, the ASB results in the formation of nano-grains which have superior physical characteristics compared to the base material. Understanding the ASB may give an input to the design and enhancement of the material development.

In this research, samples were extracted from different specific locations inside the chips for subsequent observation. The objectives are to study the initiation of the ASB, the effect of the hard TiC particles on the ASB formation, the observation of the microstructure inside the ASB, as well as in proximity of the ASB. Moreover, a model describing the microstructure evolution at different stages of the ASB formation is proposed.

2. EXPERIMENTAL SETUP

Machining tests were conducted on a 6-axis Boehringer 200 CNC turning center. Chips were collected for each experiment, mounted, polished and etched for further metallographic examinations. Uncoated carbide tools with 0°rake angle were used.

The chips microstructures were identified using an Olympus SZ-X12 microscope. A Scanning Electron Microscope (SEM) Jeol, JSM -840A was used for detailed studies of the chips morphology. For micro-hardness measurement, a Struer Duramin A300 was used. A specially designed and developed quick stop device (QSD) was used to examine the chip formation process and the chip morphology [28]. For FIB sample making, Hitachi FB 2000A was used. A

TEM Jeol, JEM 2100F was used for detailed studies of the chips morphology and microstructures.

The turning experiments were carried out using 2.5 inches diameter cylindrical workpieces made of TiMMC. The material consists of a non-metallic phase TiC (10-12% by weight) distributed in a matrix of Ti-6Al-4V Titanium alloy. The following machining parameters were used: cutting speed of 30, 50, 100, 150, and 230 m/min, with a feed of 0.1 or 0.2 mm/rev.

3. RESULTS AND DISCUSSIONS

3.1. Chip morphology

The chip morphology and segmentation process shows different characteristics at different speeds (Figure 3). At low cutting speed of 100 m/min, the grain microstructure of the chip is more elongated and deformed, showing high plastic deformation as shown in Figure 3(a). At the higher cutting speed of 230 m/min shown in Figure 3(b), the shear strain in the primary shear zone is reduced, as demonstrated by the larger shear angle and the smaller chip deformation. Furthermore, at higher speed, the bulk of the segment seems to be displaced with high strain at the adiabatic shear zone, and very low strain in the bulk of the segment area.

The free side of the chip along the ASB is the fractured area formed after the occurrence of the ASB shown by the arrows in Figure 3(b). Fractured surfaces have been studied in Split-Hopkinson Tension Bar (SHTB) [17]. Interrupted tests of SHTB shows a sudden drop in stress strain curve suggesting that the fracture is caused by initiation and coalescence of voids in micro-cracks. The localized shear promotes even further the nucleation and growth of voids and therefore accelerates fracture along the ASB [17].

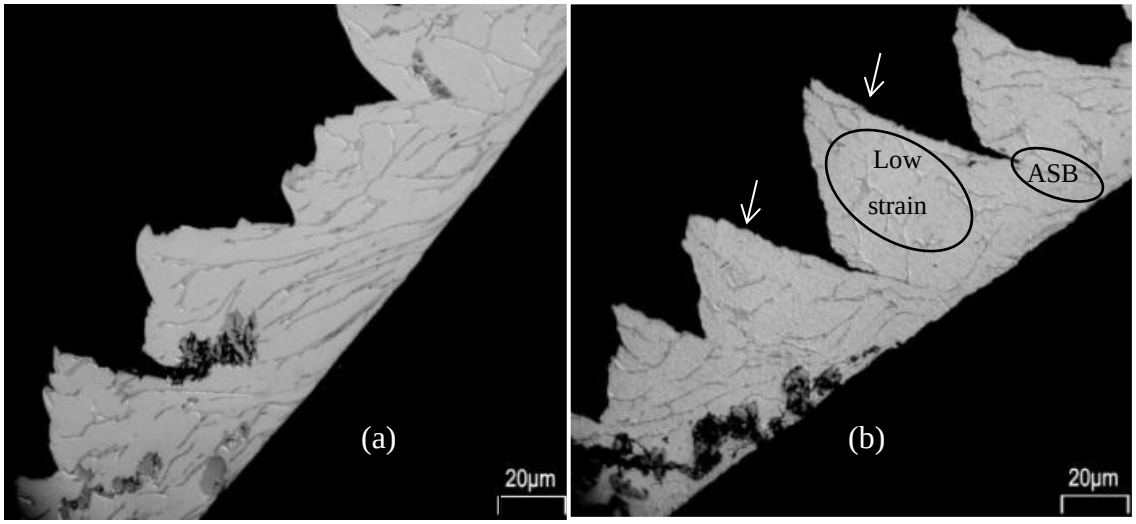

Figure 3; Chip formation, a) At a speed of 100 m/min, b) At a speed of 230 m/min, arrows showing the formed ASB surface.

In order to investigate the formed shear surface; different experiments have been conducted during orthogonal cutting of TiMMCs. Figure 4 shows different chip characteristics with cutting speeds of 50 and 150 m/min. The observations of the chips cut at different speeds show that the

segmentation distance decreases with the increase of cutting speed. The average distances between segments are 150 µm and 90 µm for the speeds of 50 and 150 m/min respectively.

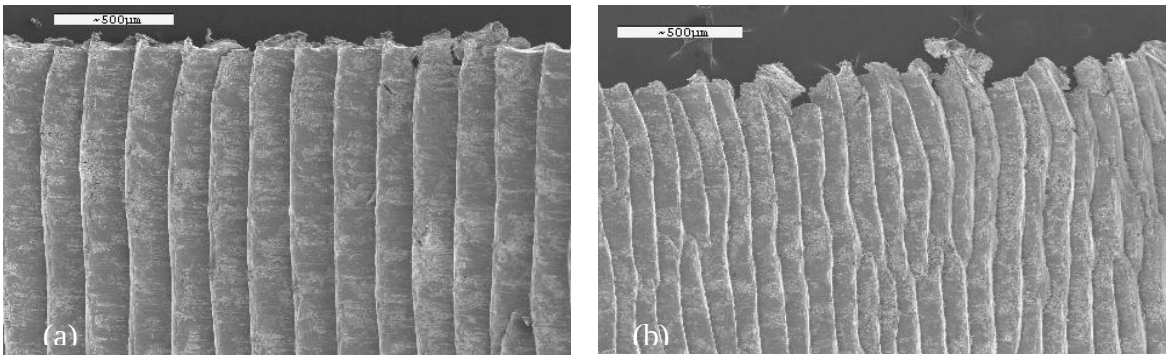

Figure 4; SEM image showing the free side of chip, a) At a speed of 50 m/min, f =0.1 mm/rev, b) At a speed of 150 m/min, f=0.1 mm/rev.

As noted in [29] as cutting speed increases, the strain required to overcome material bonding and development of initial cracks, decreases. Following this, the periodicity of cracks initiation increases, leading to smaller segmentation distances.

3.2. Strain Characterization In Chips

The TiMMC base matrix material with an alpha+beta microstructure has equiaxed grains with random orientation. After cutting and chip formation, the random grain structure will achieve a particular pattern inside the chips. Figure 5 shows an SEM picture of a polished chip showing the ASB in the material. The elongated grain boundaries near the ASB suggest a very high strain. Grains in proximity of the ASB, have elongated grain boundaries parallel to the ASB. Similar elongated grains can be seen in the secondary shear zone, also indicating high strains.

The thickness of the ASB t_s is around 3 µm. The shear lines indicated by the elongated grain boundaries show a continuation from the ASB to the secondary shear zone, indicating an unlikely possibility of fracture and welding in the ASB (Figure 5).

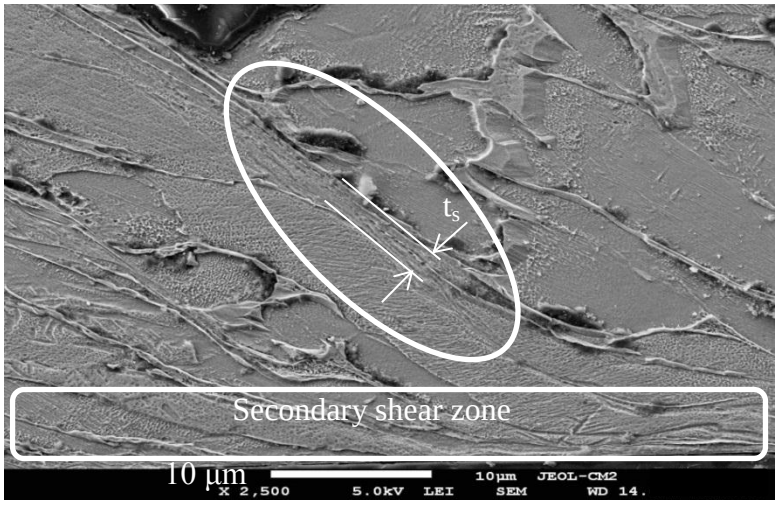

Figure 5; Microstructure of chip showing the adiabatic shear band and its thickness (v=100 m/min f = 0.2 mm/ rev.).

It is interesting to observe the particles behaviour inside the chips and their interaction with the ASB phenomenon. Figure 6 shows two cases of a particle which was located in line with a formed ASB. Under the shearing action, the particle was split and displaced. This shearing action reveals the magnitude of the high strain involved in the ASB. Furthermore, the matrix material further away from the ASB still has the equiaxed structure indicating a lower strained area (shown in bottom of Figure 8).

Following many observations of the particle behaviour inside the chips, it was found that the particles are not hindering the ASB formation. If a particle happens to be aligned with an ASB, it will shear and the ASB will continue its path while forming.

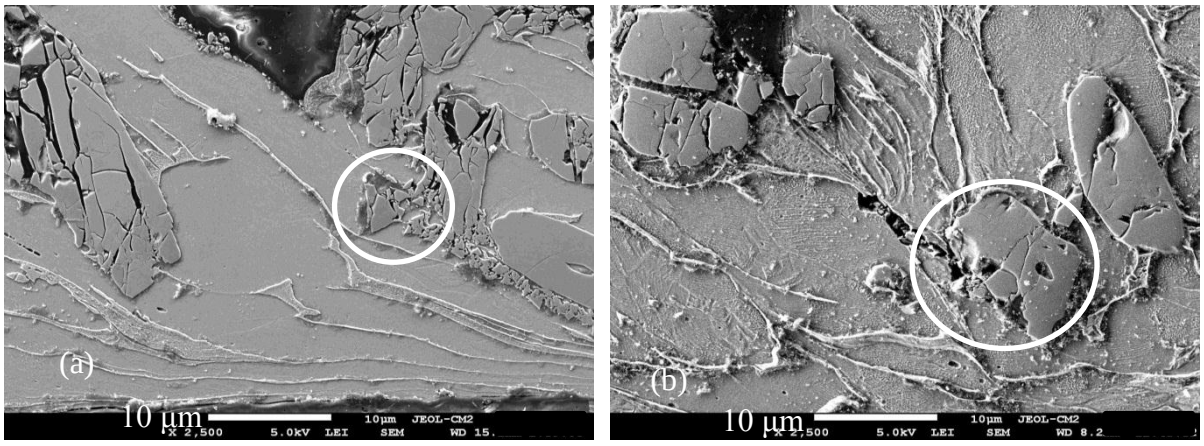

Figure 6; (a),(b), Microstructure of chip, circles showing particles aligned with an ASB. (v= 60 m/min, f= 0.2 mm/rev.).

3.3. Fractured Surfaces in ABS

The undersides of the chips segment were examined as shown in Figure 7. This fractured surface is the surface where the ASB occurred and then resulted in a sheared surface area. Closer examination of this fractured surface reveals a dimple and smeared appearance, which is a characteristic of low conductivity alloys such as Titanium alloys. These features are present in the chips at the speed of 50 m/min in Figure 7. This appearance is similar to rubbing experiments, and indicates that the surfaces moved past each other after fracture [30]. However, as will be shown later, no signs of melting were observed. The dimple structure is typical of ductile fracture in metals, where voids will nucleate, then grow and coalesce during shear deformation generating a sheared surface. This is in opposition to brittle fracture which is characterized by cleavage structure.

A closer look at the sheared surface shows the hard particles, which were sheared while the ASB was formed. Figure 7 shows a particle (A) which was sheared in the ASB. Furthermore traces of sheared grain boundary can be observed. A closer look at those boundary lines show trails, indicating ductility and high strains before fracture.

Some attempts were made to calculate the critical cutting speed for the occurrence of ASBs in machining Ti–6Al–4V and was found to be v_c= 0.15 m/s [31]. At higher cutting speeds, higher shear strain rates within the primary shear zone will favor the propagation the adiabatic shear band further to the free surface. High strains at locations close to the ASB are attained due to a high level of ductility resulting from thermal softening. Komanduri [14] suggested a possibility of alpha-beta transformation inside the ASB.

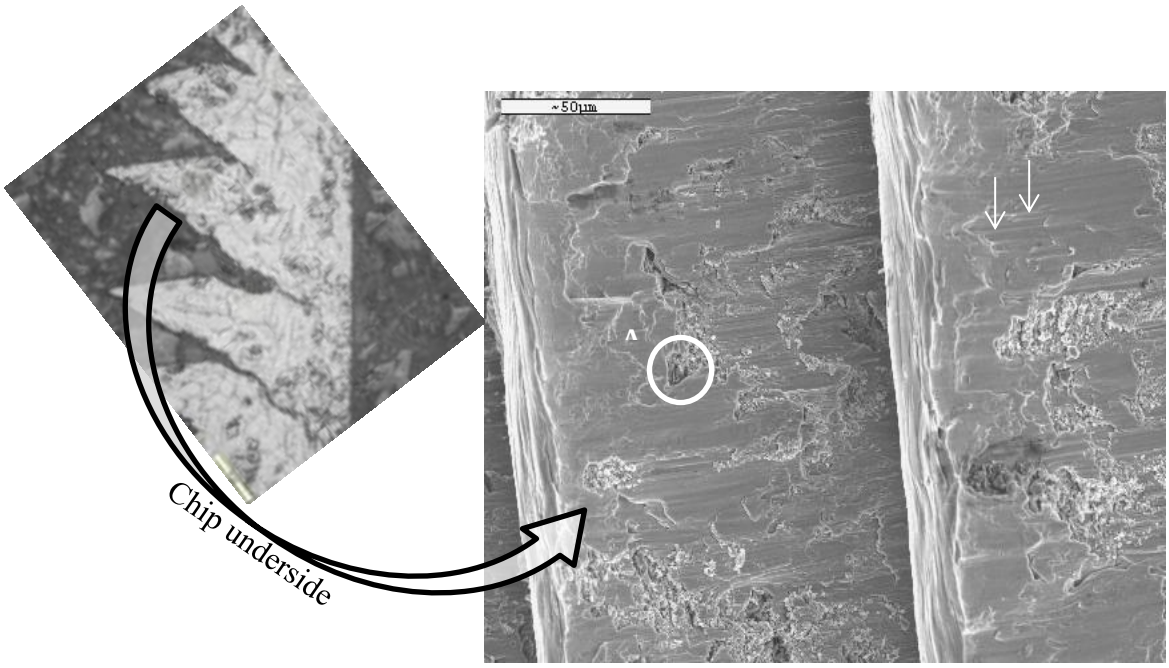

Figure 7; Top view of sheared surface of the segment of chip, circle showing a broken particle (v= 50 m/min, f = 0.1mm/ rev), arrows showing trails.

3.4. Quick Stop (QS) test

Some observations of QS tests on hardened steel [32], showed that the initiation of adiabatic shear at the tool tip is related to a decrease in the shear angle in adjacent areas to the tool tip; requiring higher shear strains and higher shear strain rates compared to those within the upper region of the primary shear zone. Furthermore, the initiation of the ASB is also related to the presence of an additional heat source at the secondary shear zone.

To further investigate on the segmentation and ASB formation in TiMMC, a Quick Stop Device (QSD) was developed and used in order to freeze the process of chip formation and to examine the process of chip initiation and propagation. The details of the QSD can be found in [28]. Furthermore, since TiMMC includes TiC particles, the effects of the hard particles on the segmentation process can also be investigated.

Using this QSD, samples of chip root formed during the machining of TiMMC were obtained and their microstructure was subsequently examined using a Scanning Electron Microscope (SEM). Since the process of chip initiation cannot be synchronized with the QSD triggering, multiple quick stop tests were performed in order to detect the initial crack formation. The photomicrograph in Figure 8 shows the root chip interface taken at a speed of 60 m/min, where an evidence of a crack seems to be initiating at the free surface. The crack seems to occur before the formation of the ASB which will eventually initiate the formation of a new segment in the chip.

A close examination of the machined surface shows a similar alpha-beta ($\alpha + \beta$) phase pattern as in the base material. In addition, the micro-hardness in these deformation zones were measured. The hardness inside the ASB was found to be 475HV0.1. Inside the lightly strained area inside the chip segment the microhardness is 420HV0.1, compared to the hardness of the base matrix material which is 368HV0.1. The increased hardness can be the result of strain hardening, even a possibility of phase transformation, or microstructural changes in the form of grain refinement as will be shown later.

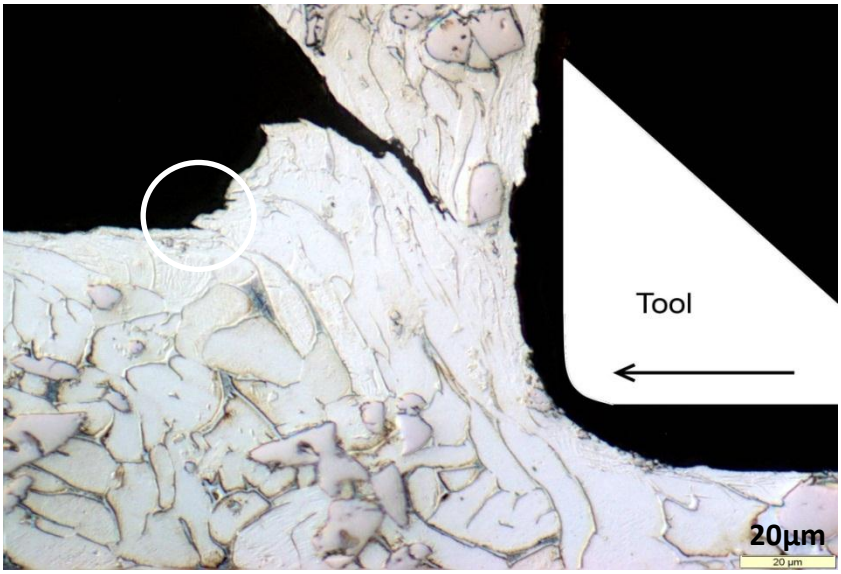

Figure 8; A quick stop test showing the chip formation. Inside the circle, a crack seems to initiate at the free surface (v= 60 m/min).

3.5. Shear strain, strain rate and temperature rise in the ASB

Figure 1 shows a typical chip formation sequence with an ASB. In order to estimate the temperature rise inside the ASB, the shear strain, and the shear strain rate had to be estimated. For segmented chips, the shear strain γ can be calculated using equation (2). Calculation of γ for different cutting speeds show that the shear strain is 5.1 for a speed of 30 m/min and 7.5 for the speed of 150 m/min. Those values are comparable to those reported in [19] for machining Titanium.

The time during which the ASB occurred was estimated using the volume constancy of the removed chip material. Point ‘c’ indicates the location of the segment to be formed (Figure 1). Points ‘b’ and ‘a’ were coincident before the formation of the chip segment; therefore, the ASB caused this same location to be separated into two points ‘a’ and ‘b’. The chip volume was estimated from the chip photomicrographs. Since all the material removed from the workpiece will form the chips, the average vertical speed of chips was calculated. The distance on the vertical axis (V_{ch}) from point ‘a’ to ‘c’ corresponds to the formation of one complete segment. The time interval from point ‘a’ to ‘b’ is the time during which the ASB is formed. For the cutting speed of 150 m/min for

example, the time interval for the ASB formation was estimated to be $1.5x10^{-5}$s. Therefore, the shear strain rate was $4.5x10^{5}s^{-1}$. This high value is comparable to shear strains in ballistic impact tests.

Estimation of the temperature in the ASB can give valuable information, since the material strength, material microstructural changes associated with phase transformation and recrystallization are related to temperature. The temperature that marks the onset of thermal recovery or recrystallization in metals is generally described as [17]:

$$T = (0.4 \sim 0.5)\, T_m \quad (4)$$

Where, T_m is the melting point of the matrix on the absolute scale. Taking the melting point of the matrix as 1660°C [5] gives a recrystallization temperature range of 500 ~ 690° C. Temperature has a major influence of the formation of the ASB. Due to the difficulty of measuring the temperature in the ASB experimentally, equation (3) can be used. For the matrix material: τ = 650 MPa at high strain rates in the range close to $10^{5}s^{-1}$ [33], the average estimated value of γ was 6, $\rho = 4.43$ g/cm^3, $\beta = 0.9$, and C = 454 J/kg.K.

In the course of this investigation, tensile tests were performed on this material, and it was noted that the tensile yield strength is reduced by 50% as the temperature is increased from the room temperature to 500°C. Assuming a von Mises yield criterion in plain strain conditions, the shear stress will be linearly related to the tensile yield strength. Taking this into consideration and correcting the shear stress by assuming a linear relation with temperature, equation (3) gives an estimation of temperature rise inside the ASB of 585°C. For a room temperature of 25°C, the temperature inside the ASB will be of 610°C. This value is close to range of the recrystallization temperature, indicating that the microstructure inside the ASB could reveal a recovered or recrystallized texture.

For Ti-6Al-4V tested under impact, shear strains of 5 were found, and temperature inside ASB could have reached 883°C [6]. Furthermore Meyers reported that the absence of reflection of b.c.c. is indicative that no transformation has occurred in the ASB [6]. Titanium undergoes a phase transformation (from h.c.p. to b.c.c.) at 883°C and melts at 1669°C [6]. Therefore melting of the material is unlikely to occur.

3.6. Transmission Electron Microscopy (TEM) observations

3.6.1. Focused Ion Beam (FIB) preparation for TEM

To fully understand the ASB phenomenon, it is critical to identify the microstructural changes inside the ASB and relate it to the base material. The ASB are typically only few micrometers wide which makes it a difficult task to study. Consequently, transmission electron microscopy (TEM) has been the principal tool for investigation purposes.

For producing a TEM sample, thin films of specimen have to be prepared. The specimen has to be very thin in order to be electron transparent. The Focused Ion Beam (FIB) technique was used to prepare the TEM specimen. FIB preparation is a long process; however it has advantages over other techniques as electropolishing. Using FIB, one can exactly locate and extract the area of interest for the specimen making. To prepare the samples, the chips were mounted, polished and then etched. Figure 9 shows the location of the extracted FIB specimens. Using the cut sample, a rectangular area was selected where the "lift-off" technique was used for specimen extraction. The steps involved in the "lift-off" technique are as follows (Figure 10): (a) Identification of the area of interest. The selected area was taken across the ASB, and another specimen was taken in the lightly strained area inside the segment where grain boundaries are present. This was followed by the deposition of Tungsten on the selected rectangular area of~ 17 μm length, and ~ 4 μm width. This layer of Tungsten will act as a protective layer for the

specimen as the milling will be performed around it. (b) Ion milling using the Gallium ion beam. The first milling step is to create a staircase in front of the area of interest. (c) This is followed by milling around the area of interest as deep as the staircase. Only a small bridge is kept to hold the area of interest. The sample is then tilted to 45° so that the bottom of the area of interest can be milled. At this stage the specimen will still have a small part attached to the base material. (d) A micro-manipulator is welded to the area of interest using the Tungsten deposition system. Later on, the bridge will be milled and the area of interest will be lifted off and transferred to a TEM grid. The specimen will be further ion milled to a final thickness of ~ 100 nm, which is an electron transparent thickness. The final specimen attached to the grid will be used later for TEM examination.

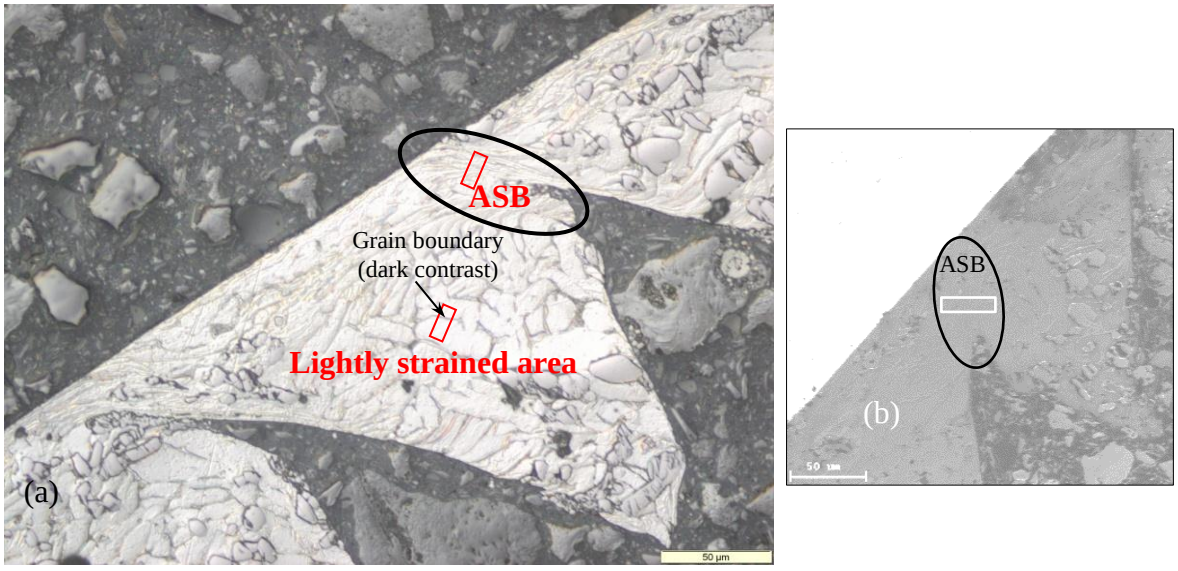

Figure 9; Location of FIB, a) FIB samples location for illustration purposes. Grain boundary crossing the lightly strained specimen, b) Actual FIB location in ASB.

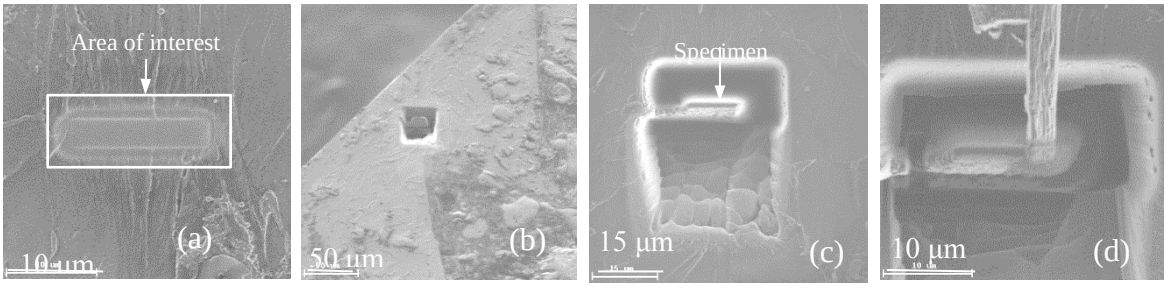

Figure 10; FIB sequence in a segment of chip formed at the speed of 50 m/min, a) Location of rectangle in ASB, b.c) After ion milling, d) Extraction with micro-manipulator.

3.6.2. TEM observations in the lightly strained area

A sample from the lightly strained area shown in Figure 9 was observed with the TEM. The sample was intentionally taken at the boundary of two grains. This boundary which has a dark contrast in Figure 9 (a) is shown in Figure 11(a) as a darker band compared to the surrounding matrix. Selected Area Diffraction (SAD) was performed on the dark band which has a different texture and was indexed as beta (b.c.c.), whereas the surrounding material was indexed as alpha (h.c.p.). This is in accordance with the matrix material which has an alpha-beta matrix type. Furthermore, Energy Dispersive Spectroscopy (EDS) on this dark band show that it is richer in Vanadium content. However, the matrix was richer in Aluminum content, which is to be expected since Vanadium is a beta stabilizer and Aluminum is an alpha stabilizer. Figure 11(b) shows the microstructure of two large grains. These grains with an average diameter of 25 µm are considered large compared to the nano-grains usually found in the ASB. Both grains were identified as alpha by SAD indexing. SAD of those grains revealed a high misorientention angle, indicating that they are two separate grains, and not sub-grains.

Two main types of dislocation exist: screw and edge. Dislocations found in real materials are typically mixed and have the characteristics of the two types. Usually when a material is strained plastically, the dislocation density increases as in "cold working" conditions. Unlike an optical microscope, TEM allows the observation of dislocations. Dislocation lines have different diffractive properties than the regular lattice within a grain and therefore reveal a different contrast effect (usually seen as dark lines in a clearer matrix). Ballistic experiments show that grains inside the ASB are characterized by low dislocation densities. However, in areas where low strains occurred as in our selected sample, high dislocation densities are expected as indicated by the arrows in Figure 11(c).

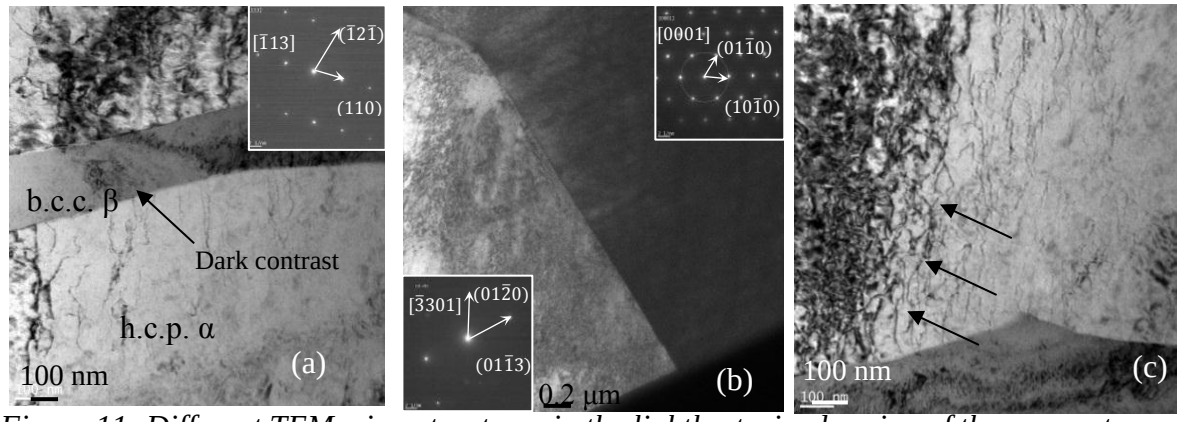

Figure 11; Different TEM microstructures in the lightly strained region of the segment, a) Darker contrast band with SAD indexed as beta. This corresponds to the grain boundary dark contrast shown in Figure 9 (a), b) Two different grains with their respective SAD, c) Arrows showing high density dislocations.

3.6.3. TEM observations inside the ASB

Figure 12 shows TEM, and Scanning Transmission Electron Microscopy (STEM) pictures, showing the microstructure of the sample inside the ASB. The Selected Area Diffraction (SAD) in Figure 12 (a) shows a spotty ring pattern with some brighter dots, indicating a general misorientation of grains with a preferred orientation of some grains. The grains are much smaller compared to the previous sample in the lightly strained region. The grains show generally an elongated structure with typical dimensions of 100 x 400 nm. The grain orientation

seems to be parallel to the edge of the FIB sample. However, some equiaxed grains with high angle boundaries are also found and can be classified as very small, sometimes in the range of 25 nm (Figure 13).

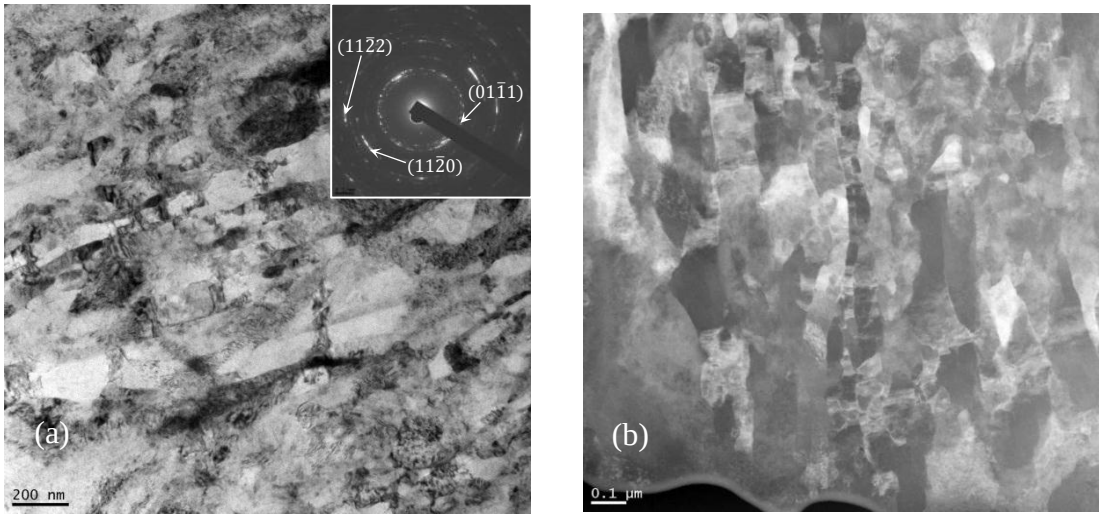

Figure 12; a) TEM inside the ASB with corresponding SAD, b) STEM inside the ASB.

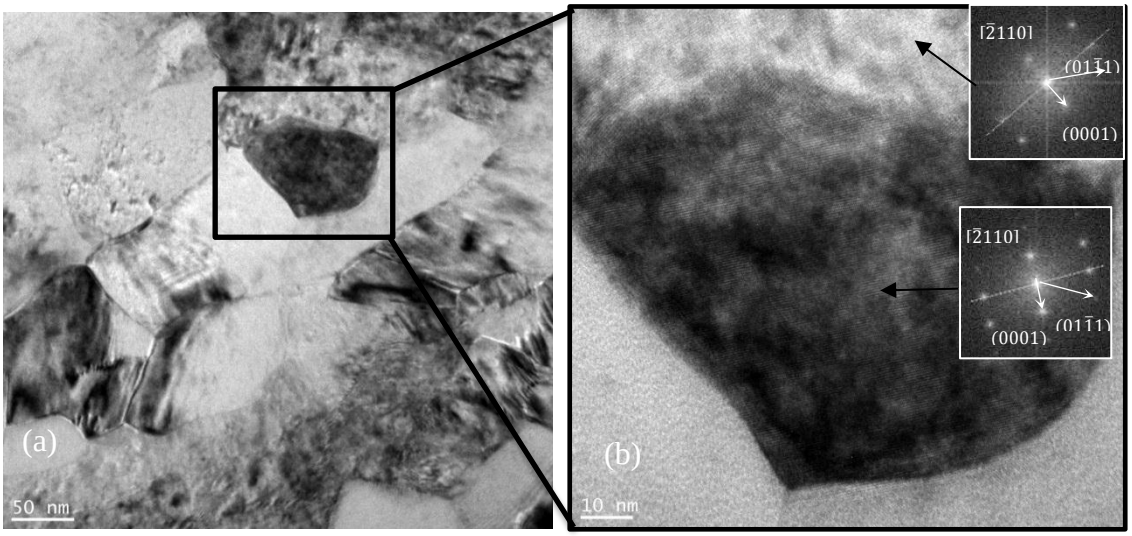

Figure 13; a) Nano grain inside the ASB, b) High resolution TEM from the dark contrast grain. FFT showing a 15° misorientation between the grain and upper surroundings.

All lattice structures inside the ASB were indexed and found to correspond to alpha (h.c.p.) phase. The beta (b.c.c.) or alpha prime (martensite) phases were not found. Therefore phase transformation within the Adiabatic Shear Band (ASB) is unlikely. However the initial matrix base material has a more dominant alpha phase; therefore one should not exclude the possibility that beta structure was not initially in the FIB sample.

To study the new grains, and determine if they are sub-grains or new Recrystallized (RX) grains, a sample area was chosen where a multitude of grains (or sub-grains) are apparent. The

SAD was directed on a grain area, and then the sample was tilted and oriented toward the zone axis. Dark field imaging was performed as in Figure 14 (a), where the light contrast areas show low grain misorientations. Bright field imaging was performed for the same sample with the previously oriented zone axis. The SAD was performed on different regions as indicated by circles in Figure 14 (b). The orientation angles were all within 2 degrees indicating that those microstructures are sub-grains.

Some grains show, however, a remarkably higher difference in orientation angles as the grain shown in Figure 13 (b) with a misorientation of 15 degrees, indicating that some recrystallized grains were also formed.

Murr *et al.* [34] indicated that the notion that "recrystallization usually involves the development of high angle boundaries", is not always true since it violates the second law of thermodynamics. The preferred recrystallization microstructures would consist of low angle interfaces, with a preference for elongated structures, where the maximum number of structures have been eliminated. Therefore it is possible that recrystallized grains exhibit very small misorientations or a mixture of misorientations as high angle boundaries. Murr *et al.* [34] also indicated that the designated recrystallized grains, implicitly accommodate the complex interplays between recovery and recrystallization. Consequently, there are regimes in ASB formation, where recovery, recrystallization and grain growth can occur in a complex and simultaneous manner. This explains the very low misorientation angle found sometimes between the elongated and equiaxed grains formed in the ASB.

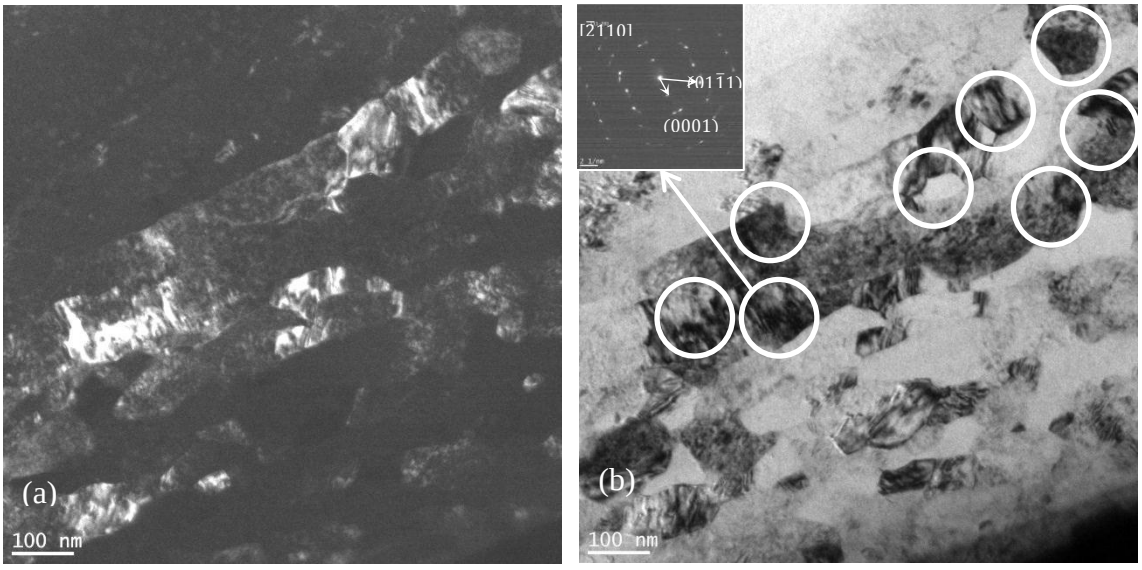

Figure 14; a) Dark field imaging , b) Bright field imaging showing sub-grains inside the ASB. The circles show the location of the various SAD patterns, and the inset is the SAD of the arrowed cell.

During plastic deformation, dislocations usually originate at the grain boundaries. With increasing strain and work hardening, dislocation interaction by cross slip and dislocation multiplication may occur sooner in high stacking fault energy materials [34].
High stacking fault energy material as alpha Titanium [35] are difficult to work harden, but easier to dynamically recover due to cross slip.

In the ASB, where large strains are encountered, Murr [34] indicated that at some critical strain, the plastic strain energy saturates and recovery or recrystallization occur, allowing for extensive grain refinement which facilitates large shear strain by grain sliding.

Using high resolution TEM analysis and Fast Fourier Transform (FFT), for the grain shown in Figure 13 (b), different areas inside the equiaxed grain show the same orientation angle. Furthermore, no signs of dislocation were found inside the grain, which indicates that the grain has already undergone recovery or recrystallization. Following a large strain, some randomly aligned dislocations formed on the cell walls without forming distinct boundaries (Figure 15). Wide cell boundaries were observed using high resolution imaging as shown in Figure 15 (b), and on the atomic scale, dislocations were found at the cell boundaries in Figure 15 (d). In order to better show the dislocations, FFT was performed in the interest area of the boundary, subsequently an inverse FFT reveals clear dislocations in Figure 15 (c). Loose tangles rearrange themselves and transform into dislocation walls by annihilation of dislocations with opposite signs, separating dislocation free subgrains. With increasing plastic strain, the thickness of dislocation walls will be narrower, forming sharper grain boundaries. This grain refinement suggests the involvement of dynamic recovery of stored dislocations [36]. The metal flow confined in the narrow ASB creates a complex stress state with high levels of hydrostatic and deviatoric stresses. Such high pressures usually prevent or delays fractures, allowing high strains [36].

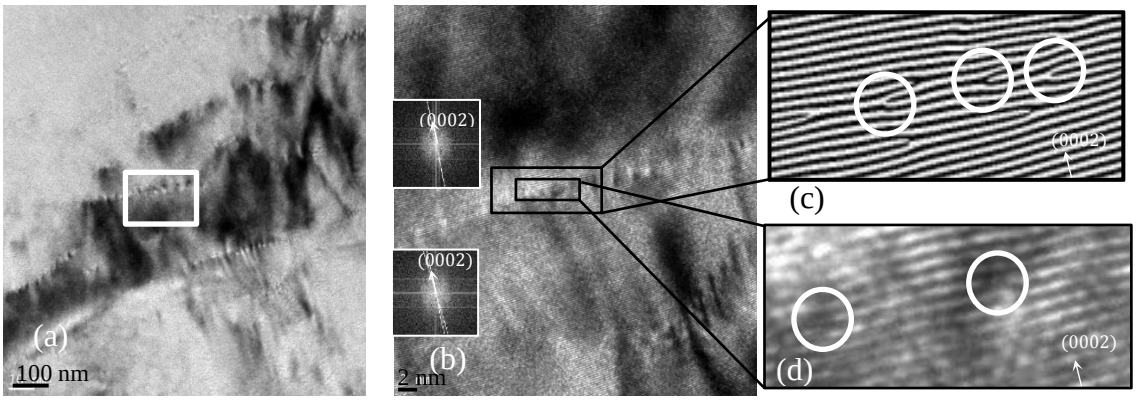

Figure 15; a) Sub-grain boundaries, b) Inset region of (a), at the atomic scale, the FFT shows a 5 degrees difference between the region above and below the inset region, c) Inverse FFT of inset region in (b) showing dislocations inside the circles. The black lines show the (0002) planes, d) Enlarged inset showing atomic scale and dislocations.

It was shown that the grains morphology did not change significantly across the width of the FIB sample compared to the center of the ASB, indicating that the material did not melt. Melting and then solidification would have mostly probably produced columnar grains in the vicinity of the ASB matrix interface [6].

Figure 16 shows the present author's proposed sequence of microstructure evolution occurring in the ASB: (a) Random dislocation distribution in large grains, (which is not a low energy configuration), (b) The random dislocation distribution gives way to elongated cells (i.e. dynamic recovery) and the misorientations increases. Subsequently, dislocations accumulation and rearrangement lead to the formation of sub-grain boundaries. One should note here that grain boundaries are defects forming easy diffusion paths. The effect of strain will lead to grains elongation with an increase in dislocation density and an increase in the entanglement of dislocations. This high dislocation density leads to an increase in the stored energy. The stored energy is a driving force for transformation which can be regarded as a pressure that causes boundaries to move. Plastic deformation requires movement of dislocations under the strain from the applied and internal stresses. The saturation strain state is attained in the presence of significant strain hardening and dynamic recovery. (c) As the deformation is increased, some of the sub-grains break up, leading to smaller equiaxed grains. The sequence will repeat itself each time lowering the scale of the grain sizes which explains the observed nano-grains. A similar behavior has been found in the ASB of high speed impact tests [6, 22].

Dislocations can climb by diffusion and move to different planes, by absorbing or emitting vacancies which can occur at high temperature. This is called polygonization.
During recovery, dislocations become mobile at higher temperature, then eliminate or rearrange themselves to give polygonization walls. Higher temperatures can lead to recrystallization, and the recrystallized grains will be free of dislocations.

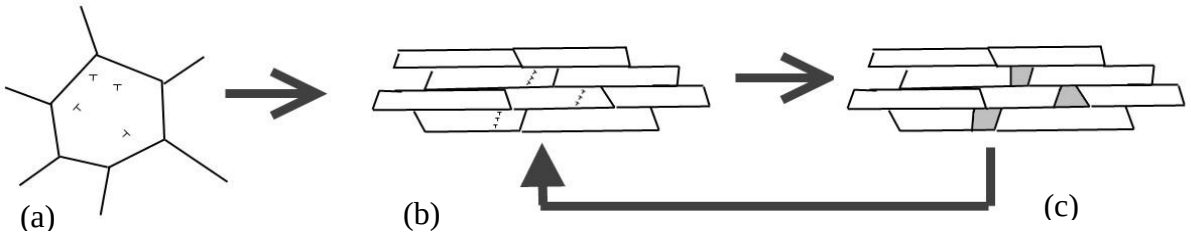

Figure 16; Proposed evolution sequence for the formation of nano-grains, a) Random dislocation in large grains, b) Elongated cells, and redistribution of dislocations, c) Formation of some equiaxed nano-grains.

3.6.4. Rotational Dynamic Recrystallization (RDX):

Derby [37] classifies dynamic recrystallization in two types, rotational, and migrational recrystallization. Migrational recrystallization occurs when the strain reaches a critical level; new strain-free grains nucleate and grow within the deforming material. In rotational recrystallization; a dynamically recovered substructure undergoes a gradual increase in misorientation, leading to the transformation of cell boundaries into high angle boundaries. If the recrystallized structure forms after deformation, a migrational mechanism is required, because of the absence of mechanical strain.

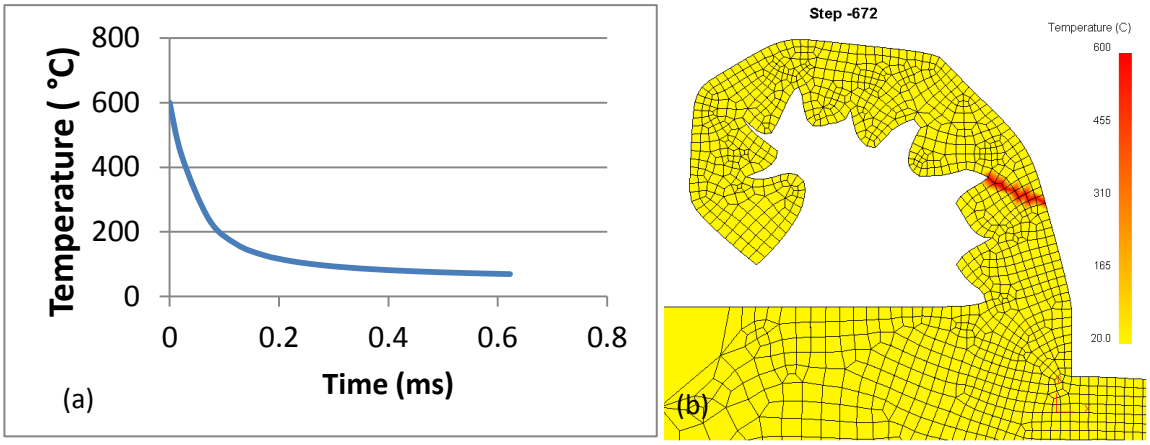

Figure 17; ASB cooling time simulation, a) FEM cooling time curve, b) Location of the ASB in the simulated chip (in red).

It is instructive to calculate the time during which the ASB is formed. During this time, only a portion of it will be above the recrystallization temperature. The cooling temperature can be calculated by FEM simulation of a chip where the initial temperature condition inside the ASB is the previously calculated temperature in the ASB (610 °C). The cooling time is calculated as the heat is dissipated in the chip and in the surrounding air. The software DEFORM was used to simulate the cooling time. Complete details of FEM machining simulation leading to segmented chip of TiMMC will be published elsewhere. The ASB calculated temperature was assigned as initial condition inside the ASB as seen in Figure 17 (b). Figure 17 (a) shows that the cooling time is in the range of 10^{-4}s.

The previously calculated ASB formation time ($1.5x10^{-5}$s) is lower by one order of magnitude than the cooling time. The very rapid initial drop in temperature, as shown in Figure 17 (a), indicates that most probably the microstructure found inside the ASB is due to the plastic deformation and not subsequent to it. Therefore this will exclude the migrational recrystallization. It should be noted that the times for static and dynamic recrystallization differ by 7 orders of magnitude [38].

Furthermore, rotational recrystallization requires a simultaneous plastic deformation. In high speed impact tests of Titanium, the studied microstructures inside the ASB suggested that this mechanism was operational [6]. Meyers mentions that deformation takes place primarily by grain boundary sliding [6]. The geometrical constrains inside the shear band are such that sliding produces rotation of micro-grains. Inside the ASB the plastic shear strain accommodation required by rotation, does not take place by diffusion, but by dislocation generation and motion. It is suggested that the nano-grains found inside the ASB of TiMMC is also due to RDX.

CONCLUSIONS

Most studies involving Adiabatic Shear Bands (ASB) were made for impact tests and not for machining. During machining, extreme conditions of high strain, strain rate and temperature occur inside the ASB. Studying such extreme conditions can give an insight in other interesting areas in machining as the contact surface between the machined surface and the worn tool. In this

study, it was shown that in the lightly strained area, large alpha grains in the matrix have a striped band shaped beta boundary microstructure. Those grains located inside a segment are characterized by a high dislocation density; therefore they did not incur a recovery process. A possible explanation is that the temperature in this lightly strained area was less that the recrystallization temperature. This is not the case in the area inside the ASB which is a highly strained area, and where the temperature was estimated to be close to the recrystallization temperature (between 500 and 690° C).

In the ASB area, the strain, and strain rate in the ASB were estimated. Inside the ASB, the strains were up to 7.5 and the strain rates were up to $4.5x10^5\ s^{-1}$. These values are considered high and comparable to ballistic experiments.

Based on Transmission Electron Microscopy (TEM), observations down to the atomic scale were performed and lattice dislocations were identified. The microstructure inside the ASB is composed of elongated nano-grains, with a presence of some equiaxed nano-grains. A proposed microstructural evolution was proposed and the resulting microstructure was attributed to Rotational Dynamic Recrystallization (RDX). The combination of very small grains and cells in proximity with a low dislocation density, leads to the possibility that a loop of the following was occurring: plastic strain, resulting in grain elongation, and high dislocation. Elongated cells break-up, to form new recovered sub-grains with some recrystallized nano-grains characterized by a low dislocation density, and high misorientation. The process may repeat itself, resulting in a smaller scale of grain size.

The temperature inside the ASB were estimated to be close to the recrystallization temperature, however no martensite was observed, and no b.c.c. reflection were identified indicating the unlikelihood of phase transformation inside the ASB. The fractured surface of the ASB was observed to be a dimpled and smeared surface. Melting with re-welding of the ASB was shown to be an unlikely possibility due to the not high enough temperature inside the ASB, and due to the morphology of the microstructure in the ASB. The formation of the segmentation mechanism was observed to start with a crack on the machined surface, and not starting from the tool tip. Furthermore, the hard particles inside the matrix were not hindering, or retarding the ASB formation. The ASB simply sheared the particles on its way.

TEM studies of ASB for TiMMC were never done previously for machining applications. The results can give valuable information in the understanding of ASB and can improve future FEM simulations involving segmentation.

ACKNOWLEDGEMENT

The authors wish to acknowledge Dynamet Technology Inc., for providing the material. The support of the Aerospace Manufacturing Technology Centre, National Research Council Canada (AMTC-NRC), and the NSERC Canadian Network for Research and Innovation in Machining Technology (CANRIMT) are also acknowledged. Moreover, the Quebec's Nanotechnology Infrastructure (QNI), are acknowledged for their support of nanotechnology laboratories. Finally, Philippe Plamondon from the Center for Characterization and Microscopy of Materials of Ecole Polytechnique is acknowledged for the TEM observations.

REFERENCES

[1] Abkowitz, S., H. Fisher, Schwartz, P., "CermeTi® discontinuously reinforced Ti-matrix composites: Manufacturing, properties, and applications", *JOM Journal of the Minerals, Metals and Materials Society*, 56, 37-41, 2004

[2] Recht, R. F., 1964, ''Catastrophic Thermoplastic Shear,'' *ASME J. App Mech.,* 31, pp. 189–192.

[3] Zener, *C,* and Hollomon, *J.* H., "Effect of Strain Rate on the Plastic Flow of. Steel", Journal of *Applied Physics*, p. *22,* Vol. 15, 1944

[4] Yang H.J., Zhang J.H., Xu Yongbo and Marc Andre Meyers, "Microstructural Characterization of the Shear Bands in Fe-Cr-Ni Single Crystal by EBSD", *J. Mater. Sci. Tech.* 24 pp. 819-828, 2008

[5] Meyers M. A., Perez-Prado M. T., Xue Q., Xu Y., and McNelley T. R., "Microstructural Evolution In Adiabatic Shear Localization In Stainless Steel", *Acta Materialia*, pp 1307-1325, 51, 2003

[6] Meyers M.A., R. Pak H., "Observation of an Adiabatic Shear Band in Titanium by High Voltage Transmission Electron Microscopy", *Acta Met.*, 34, pp 2493-2499, 1986

[7] Culver, R.S., "Thermal Instability Strain in Dynamic Plastic Deformation*", in Metallurgical Effects at High Strain Rates, eds. RW Rohde, BM Butcher, JR Holland and CH Karnes*, Plenum, NY, pp. 519-530, 1973

[8] M.C. Shaw, A. Vyas, "Chip Formation in the Machining of Hardened Steel", *CIRP Annals - Manufacturing Technology*, Volume 42, Issue 1, pp 29-33, 1993

[9] Nakayama, K., Arai, M., and Kada, T., ''Machining Characteristics of Hard Materials,'' *CIRP Ann.*, 37(1), pp. 89–92, 1988

[10] Shaw, M. C., and Vyas, A., ''Chip Formation in the Machining of Hardened Steel,'' *CIRP Ann.*, 42(1), pp. 29–33, 1993

[11] Konig, W., Berktold, A., and Koch, K.-F., ''Turning Versus Grinding—A Comparison of Surface Integrity Aspects and Attainable Accuracies,'' *CIRP Ann.*, 42(1), pp. 39–43, 1993

[12] Komanduri, R., Schroeder, T., Hazra, J., von Turkovich, B. F., and Flom, D. G., ''On the Catastrophic Shear Instability in High-Speed Machining of an AISI 4340 Steel,'' *ASME J. Eng. Ind.*, 104, pp. 121–131, 1982

[13] Davies, M. A., Chou, Y., and Evans, C. J., ''On Chip Morphology, Tool Wear and Cutting Mechanics in Finish Hard Turning,'' *CIRP Ann.*, 45(1), pp.77–82, 1996

[14] Komanduri, R., "Some clarifications on the mechanisms of chip formation when machining titanium alloys", *Wear* 76: 15–34, 1982

[15] Nakayama, K., "The Formation of Saw-tooth Chip," *Proceedings 1st International Conference on Production Engineering*, Tokyo, Japan, pp. 572–577, 1974

[16] Marchand A., Duffy J.,"An experimental study of the formation process of adiabatic shear bands in a structural steel", J. *Mech. Phys. Solids*. 36(3), pp 251- 283, 1988

[17] Xu Y., Zhang J., Bai Y. and Meyers M. A., "Shear Localization in Dynamic Deformation: Microstructural Evolution", *Met. Trans., 39A*, 811-843, 2008

[18] Bai Y.L., "Thermo-plastic instability in simple shear", *Journal of the Mechanics and Physics of Solids*, V30, Issue 4, pp 195-207, 1982

[19] Turley, D., Doyle, E., and Ramalingam, S. "Calculation of Shear Strains in Chip Formation in Titanium", *Science and Technology*, 55(1), 45-48, 1982

[20] Xu Y., Bai Y., Meyers M.A., "Deformation, Phase Transformation and Recrystallization in the Shear Bands Induced by High-Strain Rate Loading in Titanium and Its Alloys*", J. Mat. Sci. Tech.* 22(06) 737-746, 2006

[21] Li G.A., Zhen L., Lin C., Gao R.S., Tan X., Xu C.Y.," Deformation localization and recrystallization in TC4 alloy under impact condition*", Materials Science and Engineering: A,* V395, Issues 1–2, pp 98-101, 2005

[22] Rogers. H. C., "Adiabatic Plastic Deformation," *Ann. Rev. Matls. Sci.* Vol. 9, pp. 283-311, 1979

[23] Me-Bar Y., Shechtman D., "On the adiabatic shear of Ti6Al4V ballistic targets", *Materials Science and Engineering*, V58-2, pp181-188, 1983

[24] Meyers M.A., Nesterenko V.F., LaSalvia J.C., Xu Y.B., and Xue Q., "Observation and Modeling of Dynamic Recrystallization in High-Strain, High-Strain Rate Deformation of Metals*", J – Phys. IV France*, 10, pp 9-51, 2000

[25] Murr L.E., Ramirez A.C., Gaytan S.M., Lopez M.I., Martinez E.Y., Hernandez D.H., Martinez E., "Microstructure evolution associated with adiabatic shear bands and shear band failure in ballistic plug formation in Ti–6Al–4V targets", *Materials Science and Engineering: A*, V:516:1-2, pp 205-216, 2009

[26] Xu Y.B., Zhong W.L., Chen Y.J., Shen L.T., Liu Q., Bai Y.L., Meyers M.A., "Shear localization and recrystallization in dynamic deformation of 8090 Al–Li alloy", *Mat. Sci. and Engineering A*, V 299: 1-2, pp 287-295, 2001

[27] Koch C.C., Cavin O.B., McKamey C.G., Scarbrough J.O.,"Preparation of "amorphous" Ni60Nb40 by mechanical alloying," *Appl. Phys. Lett* 43,1017–1019, 1983

[28] Bejjani, R., Balazinski, M., Attia, H., Shi, B., "A New Design of Quick Stop Device for Research on Chip Formation.", *transactions NAMRI-SME*, V38, pp 269-274, 2010

[29] Mabrouki, T., Belhadi, S., and Rigal, J.-F., " Fundamental Understanding of the Segmented Chip Genesis for Smart Machining. A Contribution in Hard Material Turning", *J. of Advances in Integrated Design and Manufacturing in Mechanical Engineering II*. 443-459, 2007

[30] Walley, S.M., "Shear Localization: A Historical Overview", *Metallurgical and Materials Transactions A*, V: 39:11, pp 2629, 2654, 2007

[31] H. Zhen-Bin, R. Komanduri, "On a thermo-mechanical model of shear instability in machining", *Ann. CIRP* 44 (1)69–73, 1995

[32] Barry J., Byrne, G, "The Mechanisms of Chip Formation in Machining Hardened Steels", *J. Manuf. Sci. Eng.* 124, 528, 2002

[33] Xue Q., Meyers M.A., and Nesterenko V.F., "Self-Organization of Shear Bands in Titanium and Ti-6% Al-4% V Alloy", *Acta Mat.*, 50, 575-596, 2002

[34] Murr, L.E., Trillo, E.A., Pappu, S., Kennedy, C., "Adiabatic shear bands and examples of their role in severe plastic deformation", *J. Mater. Sci.*37, 3337–3360, 2002

[35] Lefebvre L.P., E. Baril, "Effect of Oxygen Concentration and Distribution on the Compression Properties on Titanium Foams", *Advanced Engineering Materials* , v:10:9, pp868-876, 2008

[36] Misra, A., & Thilly, L., "Structural metals at extremes", *MRS Bulletin*, *35*(12), 965-976, 2010

[37] Derby, B., "The dependence of grain size on stress during dynamic recrystallization*", Acta. Metallurgica et Materialia*, v.39:5 , pp.955-962, 1991

[38] Andrade, U., Meyers, M. A., Vecchio, K. S., & Chokshi, A. H., "Dynamic recrystallization in high-strain, high-strain-rate plastic deformation of copper", *Science*, 42(9), 3183-3195, 1994

APPENDIX A5: SIMULATION OF SEGMENTED CHIP FORMATION IN LASER ASSISTED MACHINING OF TITANIUM METAL MATRIX COMPOSITE

R. Bejjani, B. Shi, H. Attia, M. Balazinski*," Simulation of Segmented Chip Formation in Laser Assisted Machining of Titanium Metal Matrix Composite",* (submitted in Sept. 2012, International Journal of Machine Tools and Manufacture, Ref: IJMACTOOL-D-12-00567).

Simulation of Segmented Chip Formation in Laser Assisted Machining of Titanium Metal Matrix Composite

Bejjani Roland[1], Bin Shi [2], Helmi Attia[2], Balazinski Marek[1]
[1]École Polytechnique, Campus Université de Montréal
2900 boul. Édouard-Montpetit Montreal, Qc, Canada.
[2] Aerospace Manufacturing Technology Centre, National Research Council of Canada, 5145 Avenue Decelles Campus of University of Montreal, H3T 2B2 Qc, Canada.
(rolandbejj@gmail.com, bin.shi@cnrc-nrc.gc.ca, helmi.attia@nrc-cnrc.gc.ca, marek.balazinski@polymtl.ca,)

Abstract: Titanium Metal Matrix Composites (TiMMC) is considered as a new material with potential applications in the aerospace, automotive and biomedical sectors. Similar to titanium alloys, machining TiMMC produces segmented chips at relatively high speeds. The segmentations are characterized by adiabatic shear bands (ASB). The ASB occurs when the rate of material softening due to the increase in temperature exceeds the increase in strength due to the material's strain hardening. Even though the segmented chips are easier to evacuate than continuous chips, they cause fluctuation in forces which can reduce tool life and impact negatively on the finished machined part. TiMMC is a very difficult to cut material, however, Laser Assisted Machining (LAM) was used in order to improve the machining productivity and tool life. Our previous work on TiMMC machining showed that LAM extends tool life substantially.

For process design and optimization, Finite Element Method (FEM) models can provide predictive tools for investigating process parameters. This research investigates the machining simulation and chip formation with segmentation using LAM on TiMMC. This required the development of a new constitutive equation which can predict the flow stress behavior of the material in machining under very high strain and strain rate conditions. Furthermore, an appropriate damage model was introduced to simulate the chip segmentation. The chip formation, segmentation geometry and cutting forces were validated with orthogonal cutting experiments. Strain, strain rates, material damage, crack initiation and temperature profiles were investigated and compared to experimental results. The experimental results included microstructures using 'quick stop tests' and Transmission Electron Microscopy (TEM). The results of the simulations explained possible reasons of the prolonged tool life. The possibilities of phase transformation inside the ASB were studied using the simulation temperature profiles. Furthermore, the imitation of the crack formation in the segmentation phenomenon was investigated. Only limited work has been performed previously on cutting simulation using LAM; however the simulation of the segmented chips formation with LAM was never performed previously.

Keywords: FEM simulation; laser assisted machining; shear-band; segmentation; TiMMC

4. INTRODUCTION

Titanium Metal Matrix Composite (TiMMC) is a new type of metal composite. It has superior physical properties over Titanium alloys with potential applications in the aerospace, automotive and

biomedical sectors. Machining TiMMC produces segmented chips which have been attributed to "plastic instability". However, their cause and mechanism are not well understood for cutting processes. The segments are characterized by adiabatic shear bands (ASB), whose mechanism of deformation is localized and takes place when the rate of thermal softening exceeds the rate of strain hardening [1].

Different theories exist in the literature on the mechanism responsible of generating segmented chips. The main difference between the theories is the mechanism of catastrophic failure in the primary shear zone and the crack initiation location which has been claimed to occur either at the tool tip, the primary shear zone, or at the free surface. Nakayama et al. [2] and Konig [3] suggested that the catastrophic failure is initiated first by a crack at the free surface ahead of the tool, which propagates toward the tool tip to form a segment. Shaw [4] suggested that shear bands form due to inside microfractures in the shear zone, and void propagation. Due to heat and high normal stress, the sheared band will, however, weld again. This crack forms near the tool or at the free surface and propagates to complete the segment. Kommaduri et al. [5], suggested that a thermoplastic instability occurs within the primary shear zone, where the sheared surface originates from the tool tip to the free surface. When machining Titanium alloys, Komanduri [6] noted a possible phase transformation from the hexagonal close packed (h.c.p.) structure to the body centred cubic (b.c.c.) structure with a corresponding increase in the number of available slip systems. This transformation results from the temperature increase which accompanies plastic deformation in the ASB.

In the literature, limited work involving the Finite Element Method (FEM) simulation of segmented chips was found. Marusich [7] was one of the earliest to model the chip segmentation; however, the geometrical consideration of the chip segments (segment pitch and thickness) were not validated experimentally. Guo [8] worked on crack formation in chip segmentation and found that a crack initiates in the primary shear zone, followed by another crack that initiates at the free surface, which then joins the initial one. Again, the chip geometries were not considered. Calamaz [9] developed a new constitutive model in order to induce the softening effect in the segment. In his work, the cutting and feed forces were underestimated, and the error between the simulated and experimental segment pitch was around 20% in some cases. Umbrello [20] used a damage criterion for simulating the chip segmentation. The damage constant was adapted and changed for different cutting conditions. Lorentzon [11] used also a damage criterion to simulate the chip segmentation. The cutting forces had good agreement with the experiments; however, the segment's pitch error was in some cases as high as 25%.

Laser Assisted Machining (LAM) has been considered for machining difficult to cut materials. In LAM, the laser source is used to locally heat the workpiece surface prior to cutting. The increase in the material's temperature softens it, and therefore reduces the cutting forces. Depending on the machined material, this may lead to improvement in tool life and material removal rate. The effects of LAM on machinability of Inconel 718 were investigated by Attia et al. in [12]. It was found that LAM can increase tool life by 40%. The authors of the present study investigated the LAM on TiMMC and observed that the tool life increased up to 180% with LAM [13]. The main tool wear modes were identified as abrasion and diffusion wear.

Very few investigations were carried out on the simulation of LAM [14,15]. In all these studies, the segmentation phenomenon was omitted. Shi et al. [14] simulated the LAM of Inconel 718 but the segmentation in chips was not investigated. Recently, Germain [15] simulated the LAM process in two steps; the first one was the simulation of the laser heating of the material, followed by another simulation of the cutting action. In his work, no geometrical consideration of the chip dimensions or segmentations were included. The constitutive data obtained from the Split

Hopkinson Bar (SHB) is often used in the literature for machining simulation. However, since SHB can only reach strain rates less than $10^4 s^{-1}$ [16], the derived equation might not be appropriate.

In the present study, a new constitutive model for TiMMC was developed, considering it as a homogeneous material. The data used for developing the constitutive equation were strain, strain rate, temperature, and stress. These data were obtained from actual machining tests and the application of the Distributed Primary Zone Deformation (DPZD) model developed by Shi et al. [16]. The advantage of this method is that the strain rates acquired are the actual high strain rates produced under machining conditions [16]. The FEM model was validated with actual cutting experiments. Following this development, a damage model was introduced, and the segmentation phenomenon was simulated and validated experimentally. In the subsequent stage, after determining the actual surface temperature experimentally at different cutting speeds, a laser beam was added to the simulation. The laser simulation was calibrated in order to obtain the actual workpiece's surface temperature measured experimentally for the different used speeds. Following this calibration, Laser Assisted Machining was simulated and the segmentation geometry and cutting forces results were validated experimentally.

The objectives of this research are to investigate the effects of LAM on the cutting process parameters (stress, strain, strain rate, temperature), and the crack initiation and propagation in the segmentation process. Using the simulation results, a possible reason of the extended tool life when using LAM was explained. The phase transformation inside the ASB was investigated using the simulation temperature profiles and Transmission Electron Microscopy (TEM). Furthermore, using the FEM damage model, the crack initiation of the segmented chips was studied and compared to the experimental Quick Stop Device (QSD) tests.

Over a hundred simulations were performed. Each simulation running time was up to 6 hours on a 2GHz dual core computer. To the author's best knowledge, no previous work was carried out before to model the segmented chip formation using LAM for TiMMC or any other material.

5. IDENTIFICATION AND VALIDATION OF THE MATERIAL CONSTITUTIVE EQUATION

To accurately describe the plastic deformation in the primary and the secondary shear zones, the material constitutive equation should cover wide ranges of strains, strain rates, and temperatures that are encountered in the cutting process [17]. In this study, the methodology developed by Shi et al. [16,18] was used to characterize the TiMMC. This methodology is based on integrating a newly developed Distributed Primary Zone Deformation (DPZD) model [16] with quasi-static tests and orthogonal cutting tests at room temperature (RT) and high temperature (HT). The quasi-static tests provide the constitutive data at very low strain rates and strains. The RT cutting tests are used to generate the constitutive data at high strain rates and strains, while the HT cutting tests are employed to capture the material properties at high temperatures. Based on the generated constitutive data, the material constitutive equation can be identified. Details of the formulation of the DPZD model are presented in [16] and [18].

A physically meaningful description of the primary zone can be represented by a parallel-sided shear zone model [19]. The DPZD model is based on several assumptions including plane strain conditions, a sharp cutting edge, and continuous chip formation. These assumptions were fulfilled as much as possible by carefully designing the experiments and choosing proper cutting

conditions. For instance, to satisfy the plane strain conditions, the width of cut was chosen to be more than 10 times larger than the undeformed chip thickness.

6. GENERATION OF THE CONSTITUTIVE DATA

6.1. Experimental set up

The orthogonal cutting tests were carried out on a Boehringer NG200 turning center. The material consists of a non-metallic phase TiC (10-12% by weight) distributed in a matrix of Ti-6Al-4V titanium alloy. Table 1 lists the TiMMC physical and mechanical properties. The machining workpieces used in the tests were prepared in the form of cylindrical tubes. An unused carbide insert: Sandvik H13A, with a 0° rake angle, and sharp edges (~20 microns) was used for each cutting condition. The machining forces were measured using a Kistler dynamometer 9272 mounted on the turret of the turning center. The average values over few revolutions, under steady state conditions, were used in the analysis.

A high power laser beam was generated by a 5200W IPG PHOTONICS YLR 5000 fiber laser (ytterbium) with a wavelength of 1070 nm. A Thermovision A20 infrared camera (IR) was used to map the temperature field near the cutting zone. For the calibration of the IR camera, and for accurate workpiece's surface temperature measurements, three K-type thermocouples spot-welded in the preheating region were used. Since the workpiece was rotating, a high-speed slip ring was installed on the rotating workpiece to connect the thermocouple extension wires to a data acquisition system. Chips were collected for each experiment, then mounted, polished and etched for further metallographic examinations. The chips morphology was identified using an Olympus SZ-X12 microscope. A TEM Jeol, JEM 2100F was also used for detailed studies of the chips and microstructures.

A quick stop device (QSD) was used to freeze the chip formation process. For safety reasons, the QSD designed by the authors is actuated pneumatically (0.6~0.7 MPa) to break a hardened pin in bending, instead of using explosives. The detailed design features of this QSD, and its performance and repeatability are described in [20].

Table 1, Physical properties of TIMMC,(Ti-6Al-4V, 10-12% TiC).

Density (kg/m^3)	Yield Strength (MPa)	Tensile Strength (MPa)	Elastic Modulus (GPa)	Shear Modulus (MPa)	Mass density (Kg/m3)	Melting temperature (K/°C)	Thermal Conductivity (W/m.K)	Specific Heat (J/kg.K)
4500	1014	1082	135	51.7	4500	1738/1465	5.8	610

6.2. Machining experiments and constitutive data generation

Orthogonal cutting was performed with the following machining parameters; cutting speeds ranging from 30, to 150 m/min, and a depth of cut (for finishing operations) of 0.10 or 0.15 mm. A transition from continuous to segmented chips was identified when machining Ti-6Al-4V, where continuous chips were observed at speeds below 50 m/min [21]. Similarly, machining TiMMC at speeds below 50 m/min produces continuous chips, with minor segmentations. Therefore, the segmentation geometries were only considered for speeds above 50 m/min and continuous chips were assumed for speeds below 50 m/min.

Both room and high temperature cutting tests were designed to satisfy orthogonal cutting conditions with quasi-continuous chip formation. In the high temperature tests, the workpiece

was preheated to 693 K (420°C) using a controlled laser beam. The cutting conditions and experimental results used for the generation of the constitutive data are listed in Table 2. For the generation of the quasi static data, tensile tests were carried out. Room and high temperature tensile tests were carried out to obtain the yield stresses at different temperatures.

Table 2, Cutting conditions and experimental results (rake angle γ=0°).

Test #	**Cutting Conditions**				**Experimental Results**	
	Cutting speed $\boldsymbol{V}$ (m/min)	Feed rate $\boldsymbol{t_u}$ (mm/rev)	Width of cut $\boldsymbol{w}$ (mm)	Initial temperature $\boldsymbol{T_i}$ (°C/K)	Cutting force $\boldsymbol{F_c}$ (N)	Thrust force $\boldsymbol{F_t}$ (N)
RT	50	0.10	2.5	20/293	575	360
HT	30	0.15	2.5	420/693	640	290

By inputting the cutting parameters and the measurements given in Table 2 and the physical properties of the material given in Table 1 into the DPZD model [16], a total of 200 sets of constitutive data ($\bar{\sigma}$, $\bar{\varepsilon}$, $\dot{\bar{\varepsilon}}$, and T) were generated for each cutting conditions. Each set of the constitutive date corresponds to one point in the primary shear zone. The data cover the rages of $\bar{\varepsilon}$ from 0.002 to 1.3; $\dot{\bar{\varepsilon}}$ from 0.001 to 2.3×10^4 s^{-1}; and T from 20 to 827 °C.

6.3. Identification of the constitutive equation

In this study, the Johnson-Cook (JC) model [22] is used to describe the flow stress behavior, which is described as,

$$\bar{\sigma} = \left(A + B\bar{\varepsilon}^{n}\right)\left(1 + C\ln\frac{\dot{\bar{\varepsilon}}}{\dot{\bar{\varepsilon}}_0}\right)\left[1 - \left(\frac{T - T_0}{T_{melt} - T_0}\right)^{m}\right] \tag{1}$$

where, $\bar{\sigma}$ is the flow stress, A, B, n, C, m are material constants; $\dot{\bar{\varepsilon}}_0$ is a reference strain rate, $\dot{\bar{\varepsilon}}_0 = 10^{-3}$ s^{-1}; and T_0 and T_{melt} are room and melting temperatures of the material, respectively. Based on the generated constitutive data from RT and HT cutting tests as well as the quasi static tests, the material constants in the JC model were identified using a nonlinear regression technique. The results are: A= 1150 MPa, B= 442 MPa, n= 0.86, C= -0.00626, m= 1.1. Figure 1 shows 3D representations of the constitutive equation.

In general, materials which exhibit a strong temperature dependent yield stress also exhibit high strain rate sensitivity. This is due to the less effective thermal activation at high strain rates. Thermal activation promotes a portion of the dislocations to cross a short range barrier of dislocation motion [23]. Strain rate sensitivity is attributed to a change in the number of moving dislocations, rather than the change of dislocation diffusion velocity [24]. In the case of metal matrix composites, the effects of the hard particles cracking under high strain rates promotes the dislocation pile-up and the adiabatic shear band formation, which results in a reduction of material strength [25]. This may explain the negligible value of C (the coefficient related to strain rate effect) in equation (1) where the strain rate hardening is counteracted by a drop in strength due to the promotion of the ASB by the hard particles.

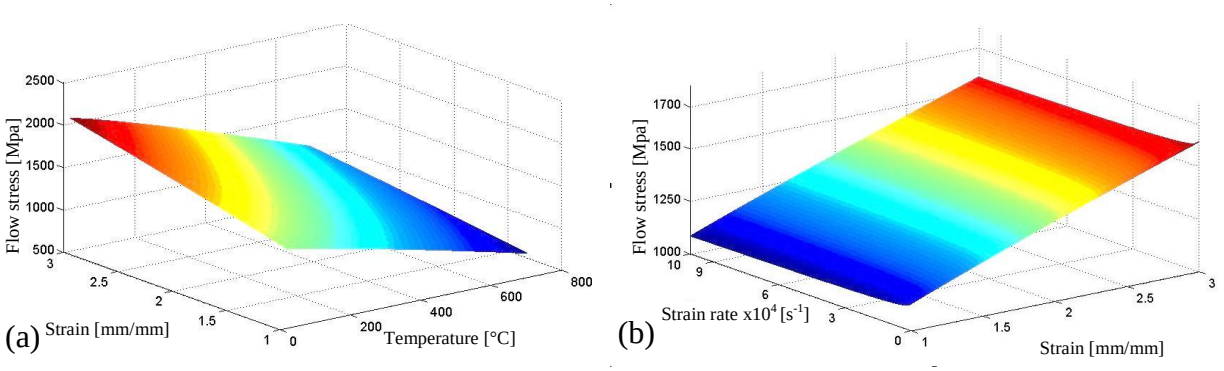

Figure 1, 3D representations of flow stress, a) At the strain rate of 10^4/s, b) At 400°C

7. MODELLING THE LASER SOURCE

In the machining tests, a laser source was used in order to heat the material's surface to the desired temperature. A relationship was determined between the laser power intensity and the workpiece speed, and the surface temperature. To simulate LAM in DEFORM® [26], the laser heat source radiation was modeled using a moving heat exchange window as shown in Figure 2. The window was synchronized to move at the same speed as the tool. For practical reasons and to avoid interference between the heat exchange window and the formed chip, the heat exchange window width and distance from the tool tip were 0.25 mm and 0.50 mm, respectively. Through interaction with the heat exchange window, the equivalent heat flux of the laser is applied, and the workpiece surface is preheated prior to cutting [14]. The heat flux applied in the simulation was calibrated for each cutting speed. Therefore, the different preheating surface temperatures used experimentally can be attained in the simulation just before the cutting action.

To reduce computational time, a dual zone mesh was used, where a fine mesh is used in the chip formation zone and the heated area, and a less dense meshing elsewhere. The remeshing module is activated when the elements are highly distorted. A new, and less distorted mesh is created, and all the constitutive parameters associated with the element will be updated into the new mesh [26].

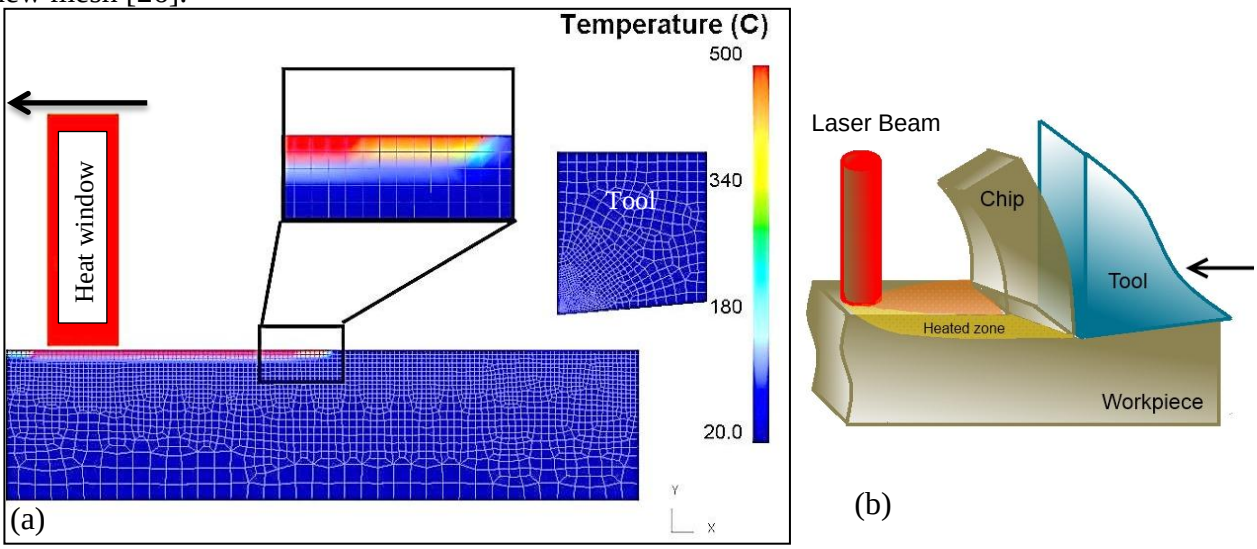

Figure 2, a) Simulation of laser source with unengaged tool, b) Illustration for a 3D representation of the LAM configuration (not to scale).

8. DAMAGE AND FRICTION MODELS

In order to simulate the segmentation phenomenon, a damage model was used for speeds above 50 m/ min. Other previous researches used different damage models in order to simulate the segmentation. Baker [27] assumed a critical strain value, below which strain hardening occurs. Above this critical strain, strain softening is assumed to occur. McClintock [28] developed a damage model, based on void initiation, growth, and coalescence. The model consists of an array of elliptical cylindrical voids extending in one direction, and the condition for fracture is satisfied when each void touches the neighboring ones.

In the present work, simulations were performed using different damage models; namely: McClintock, Brozzo, and Cockcroft-Latham (C-L). The C-L damage model [29] resulted in a segmentation behavior which agrees well with the experimental results. The model is based on the assumption that the total plastic work done per unit volume until the fracture point is a constant 'C' and can calculated from a tensile test [29]:

$$C = \int_0^{\varepsilon_f} \sigma d\varepsilon \qquad (2)$$

where ε_f is the true strain at fracture and σ is the true stress. This relatively simple model is based on the observation that the fracture energy, represented by the area under the stress-strain curve, remains constant [29]. This is true also for different material temperatures. In other words, as the temperature is increased, the material's ductility increases and therefore the strain is increased, even though the true stress is decreased. This effect is confirmed by the different tensile tests performed under room and high temperature in this research work (Figure 3).

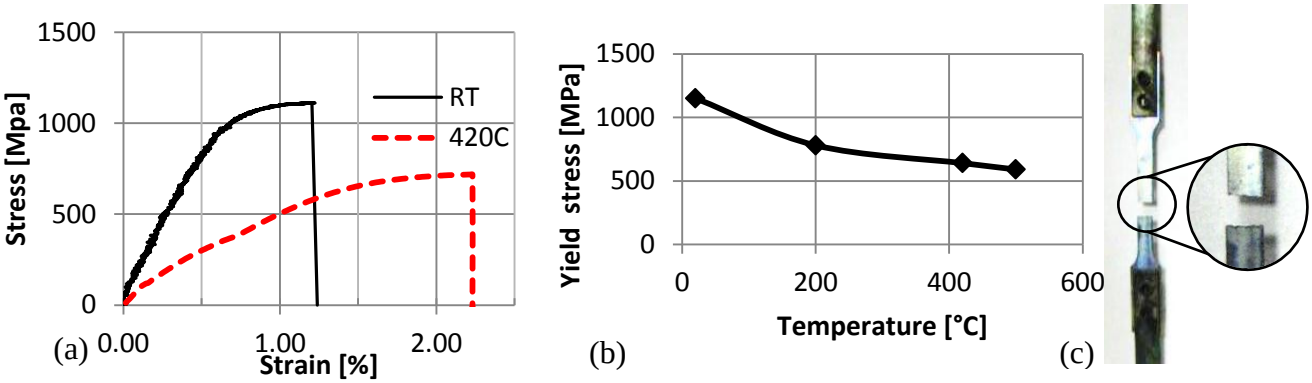

Figure 3, Tensile tests, a) at RT and 420°C, b) RT and HT tests, c) fractured specimen.

As indicated earlier, there is no general consensus whether the crack initiation occurs at the tool tip, inside the primary shear zone, or at the free surface. In DEFORM, the simulation of the crack initiation that leads to the segment formation is assumed to occur when the critical damage value C_o is reached. At each simulation step, the damage value is calculated by equation (2), and the corresponding elements are deleted once their damage values C is greater than C_0. The domain under consideration is remeshed to adjust for the voids produced by the deleted elements [26].

8.1.Tensile test:

To calculate an initial value of critical damage (C_0) using equation (2), tensile tests were performed at room and high temperature up to 500°C. The data generated from the tensile tests were combined with the machining data as mentioned previously for obtaining the constitutive data for TiMMC. Figure 3 shows some tensile tests results and a typical fractured specimen.

An average value of critical damage C_0= 10±0.2 MPa was calculated from equation (2), for all room and high temperature tensile tests. The damage value was then iteratively readjusted for the simulation to behave similar to the experimental segmentation phenomenon. The final value of critical damage constant C_0= 100 MPa was kept fixed for the entire FEM simulations of segmented chips for conventional and LAM machining.

A possible reason for the discrepancy of the critical damage values between the tensile tests and the FEM simulation validated by the machining experiments is due to the very high strains which can occur in the ASB. The high normal stress, combined with high temperature will lead to very high strains values before failure [30]. Moreover, localized superplastic deformation could exist inside the ASB. The increase in temperature in the ASB, close to the recrystallization temperature, added to the small grain size (lower than 0.1 μm) provides appropriate conditions for superplastic behavior [31]. Research on ASB showed that the shear deformation inside the ASB for Ti-6Al-4V can be extremely large [32]. Cast Ti-6Al-4V subjected to a superplasticity tensile test, achieved an elongation of 265% at fracture [33]. Considering the above, even though the tensile strength might be reduced approximately 50% at 500°C for TiMMC, the C value which is the area under the stress/strain curve, might increase more than one order of magnitude due to the increased strain at fracture. As will be shown later, once this damage value is fixed for high strain rates applications as in machining, the simulation can predict well the segmentation behavior under various conditions.

8.2.Friction model:

In FEM simulations, no general agreement on a universal friction model seems to exist for FEM numerical analysis. Lorentzon [11] revealed that an advanced friction model can influence the material flow with insignificant influence on cutting forces and chip shape. Childs [34] worked extensively on modeling the tool chip friction for medium carbon free steels, and indicated that even though advanced friction models can usually lead to better results; there are no friction models which satisfy all conditions. When machining carbon steels, Childs observed that the friction factor *'m'* decreases with increasing temperature in:

$$\tau = m\,k \tag{3}$$

where, k is the shear strength at the interface, and τ is the friction stress. As commonly known, higher cutting speeds generate higher temperature at the tool/chip interface. The higher temperature, which causes thermal softening, is believed to cause self-lubrication; thus lowering the friction effect [35].

In Karpat, Y. and Özel OK, T. [36] it was also found that the friction factor *'m'* decreases with increasing cutting speeds for Ti-6Al-4V. In Zhang, Y.C. [37] sticking friction was identified as the major friction model when machining Ti-6Al-4V and a fixed shear friction factor of m = 0.6 was used. No machining information was found for the friction of TiMMC. However, ball on disk friction and wear tests have been performed on different types of TiMMC [38]. Such tests, which are not subjected to the same conditions encountered in machining, showed that the friction factor for such material fluctuated between 0.4 and 0.7.

Since there is no universal consensus on a general friction model, multiple preliminary simulation tests were performed using a shear friction model as in equation (3). Since cutting at high speeds (which are considered here as speeds above v = 50 m/min) generates higher temperatures, a lower value of *'m'* generated results which conform better to experimental results. Consequently, the formula below was generated for the shear friction factor, where the value of *'m'* is related to the cutting speed.

$$m = 0.2i + 0.4 \begin{cases} i = 1 \; for \; v \leq 50 \; m/min \\ i = 0 \; for \; v > 50 \; m/min \end{cases} \quad (4)$$

9. RESULTS AND DISCUSSIONS:

9.1. Validation of the constitutive equation

To validate the identified JC model, a different group of cutting tests was carried out under different cutting conditions at Room Temperature (RT). The FEM simulations of these cases were conducted using the JC model and the predicted cutting forces were compared with the experimental results and are shown in part I of Table 3. The averages of peaks in the steady state region were used for comparison of forces in FEM and experimental tests.

Table 3, Experimental and FEM simulation results. The values of 'p' and 't' are the average values. The range is presented in between brackets.

					Cutting Force [N/mm]			Chip Pitch: p [mm], Thickness: t [mm]					
Speed m/min	Feed mm/rev	Pre-heat Temp °C	C-L Damage Mpa	Friction constant	FEM	Exp.	Error %	p: FEM	p: Experiment	Error %	t: FEM	t: Experiment	Error %
Part I: Conventional, continuous chips													
45	0.10	--	--	0.6	267	230	14	--	--	--	--	--	--
30	0.15	--	--	0.6	285	308	8	--	--	--	--	--	--
Part II: Conventional, segmented chips													
80	0.10	--	100	0.4	225	230	2	0.084 [0.08~0.09]	0.080 [0.08~0.09]	4	0.133 [0.12~0.15]	0.129 [0.12~0.13]	3
150	0.10	--	100	0.4	177	166	6	0.079 [0.07~0.08]	0.078 [0.07~0.09]	2	0.124 [0.11~0.13]	0.120 [0.11~0.12]	4
Part III: LAM, segmented chips													
55	0.10	415	100	0.4	175	177	1	0.100 [0.09~0.11]	0.115 [0.11~0.12]	15	0.150 [0.14~0.15]	0.170 [0.17~0.18]	13
150	0.10	415	100	0.4	160	163	2	0.096 [0.09~0.1]	0.082 [0.07~0.09]	14	0.122 [0.11~0.13]	0.126 [0.12~0.14]	3

The results show that under these cutting conditions the prediction errors for the cutting force are less than 15%. This range of discrepancy shows that the identified JC model can properly describe the plastic deformation during the cutting process. The factors that may have caused the discrepancy between the FE simulation predictions and the experimental measurements are:

- The perfectly sharp cutting edge was used in the FE simulations, while experimentally a small edge radius always exists in the cutting inserts.
- In the FEM simulations, the workpiece material was modeled as rigid-plastic, and the tool was modeled as rigid. The elastic properties were neglected.
- The plane strain deformation was applied in the 2D FE simulations. This means that there is no side flow in the simulations. However, side flow always occurs in the cutting experiments.

9.2. Chip segmentation and cutting forces

Simulations of chip formation were performed for different speeds with conventional machining and LAM. The simulated chips geometry and cutting forces were compared to the actual cutting experiments.

Table 3 Part II, and III, show a summary of conventional and LAM simulation results respectively, and a comparison with the experimental results. Figure 4 shows typical simulated and experiential chips formed under LAM conditions. For both FEM and experimental tests, an increase of the cutting speed results in a decrease of the cutting force. This can be explained by the increased thermal effects induced by an increase of cutting speed. The cutting force is reduced due to the reduction in strength due to thermal softening. Comparing the cutting force in conventional cutting at the speed of 80 and 150 m/min, a 38% reduction in cutting force is observed at the higher speed. A similar effect can be detected when using LAM where the additional heat source reduces further the material strength and therefore the cutting force. A 10% reduction of cutting force is observed when LAM is used at the cutting speed of at 150 m/min (Table 3).

In general there is a good agreement in the cutting forces and geometry of segmentations. The maximum error in the cutting force between the simulations and the experiments for segmented chips is 6%. The range of error for the segment's thickness "t" and pitch "p" is less than 15%. A similar trend was observed in FEM and experimental chips under LAM and conventional cutting. As the speed is increased the pitch "p" and thickness "t" of chips decreases. The effect of LAM increased slightly the pitch and thickness values as seen in Figure 4 (c).

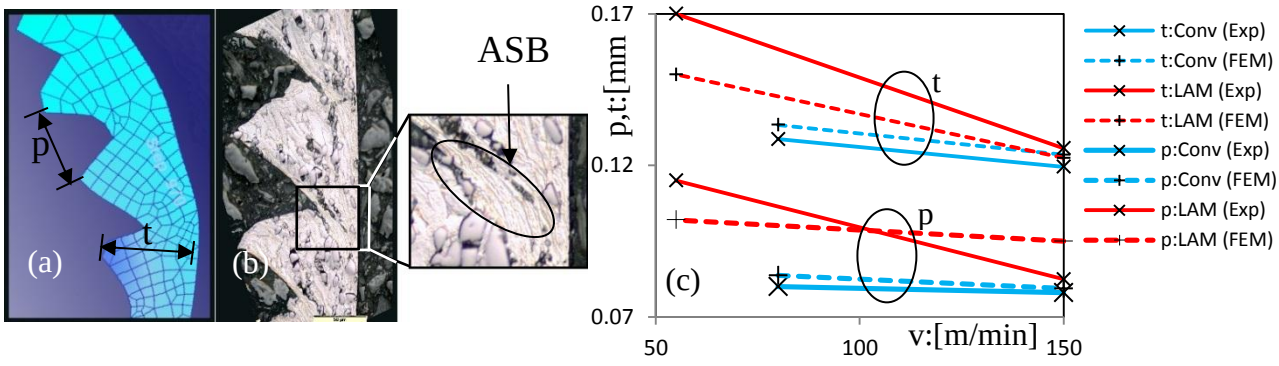

Figure 4, a) FEM, and b) experimental chip segmentation at the speed of 55 m/min, c) Chip segmentation pitch "p" and thickness "t" at different speeds.

9.3.Strain and strain rates profiles

Figures 5(a) and (b) show the simulations of the effective strain, for conventional and LAM respectively at the cutting speed of 150 m/min. Experimentally; the Adiabatic Shear Bands (ASB) and the secondary shear zone are characterized by very high strains. This can be observed in Figure 6(a), where the elongated grain boundaries indicate high strains. Similar to experimental observations, the simulations presented in Figure 5 show that the high strain locations are in the ASB and secondary shear zones. The high hydrostatic stress located partly in the primary and secondary shear zones allows an increase in strain without the formation of voids, voids coalescence, and eventually crack formation (Figure 6(b)). The simulations showed that the highest strain reached with conventional cutting at 150 m/min was 3.15, and the highest strain rate was $5x10^5$ s^{-1}. For LAM, the highest strain for the same speed was increased to 3.5, and the highest strain rate was reduced to $4x10^5$ s^{-1} (Figures 5 and 7). Note that those values are the peaks reached during the complete simulation steps. For the purpose of clarity, Figures 5 and 7 show only typical values of strain, and strain rates distribution. The increase of strain in LAM conditions can be attributed to the material softening effect under a heat source. To investigate the reduction of the maximum strain rate under LAM conditions, the width and the maximum nodal velocity inside the primary shear zone were compared (Figure 7). It was found that the width of the high strain rate zone (above 10^3/s) in the primary shear zone increased by approximately 21% with LAM; however, the maximum nodal velocity was reduced by 18% with LAM. This can be compared to the reduction of maximum strain rate by 20% with LAM.

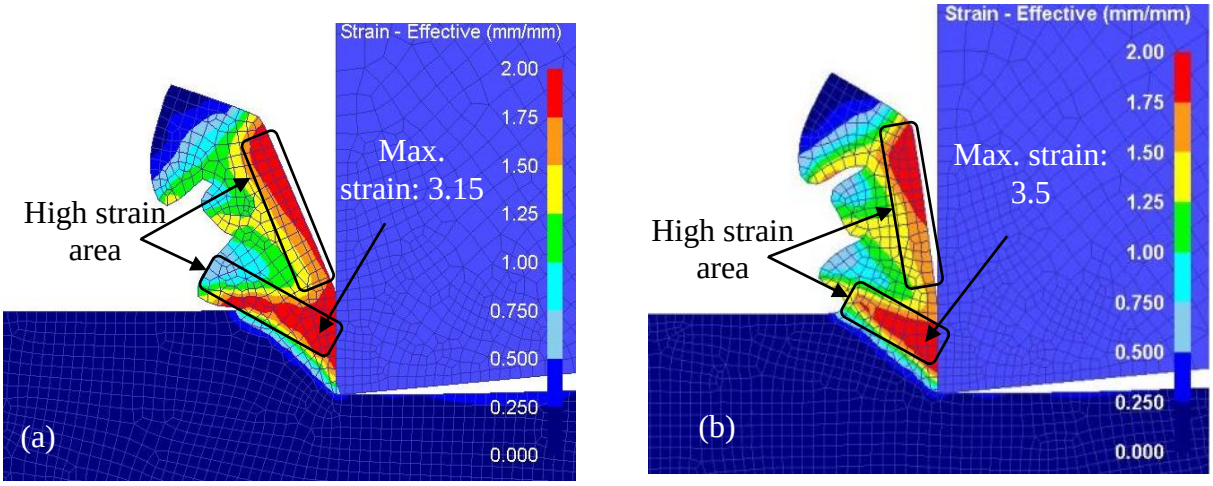

Figure 5, Effective strain at 150 m/min for, a) Conventional, and b) LAM conditions.

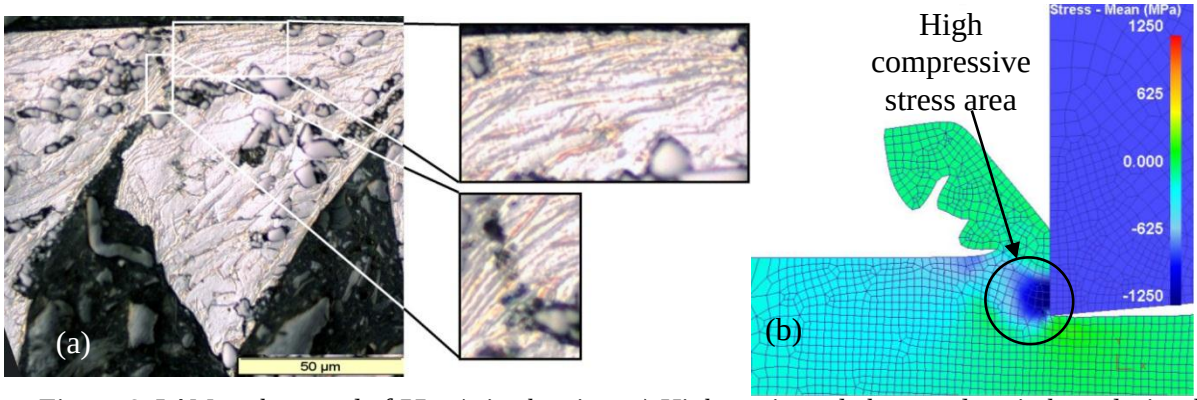

Figure 6, LAM at the speed of 55 m/min showing, a) High strain and elongated grain boundaries, b) Hydrostatic (mean) stress.

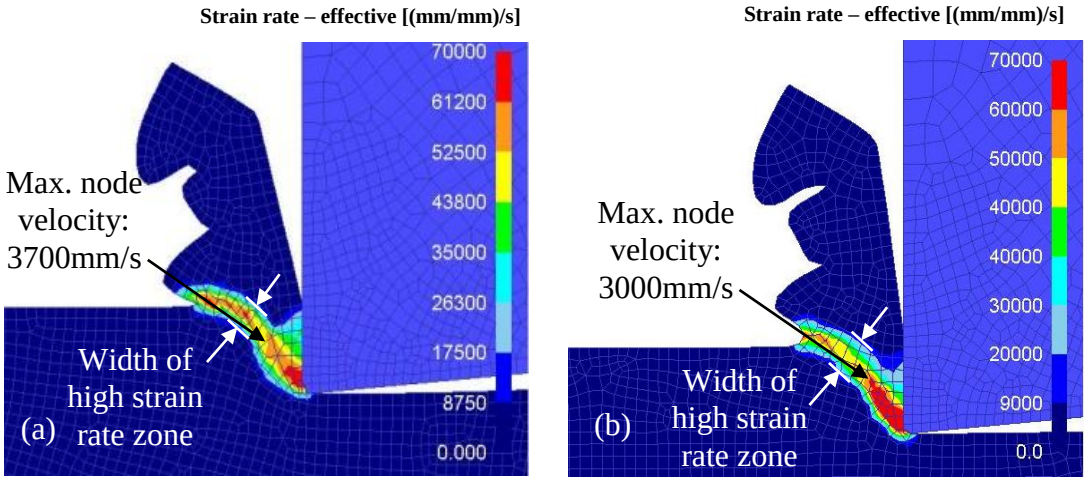

Figure 7, Effective strain rate at 150 m/min, a) Conventional, b) LAM.

9.4.Stress profiles

Figure 8 shows the effective stress profile for LAM and conventional cutting at the speed of 150 m/min. As expected, the maximum stresses are in proximity of the tool tip, extending below the tool and along the primary shear zone. Comparing conventional and LAM effective stresses profiles, one can observe that the zone of the highest effective stress is reduced when using LAM. This can be explained by the softening effect when the material is heated with the laser source.

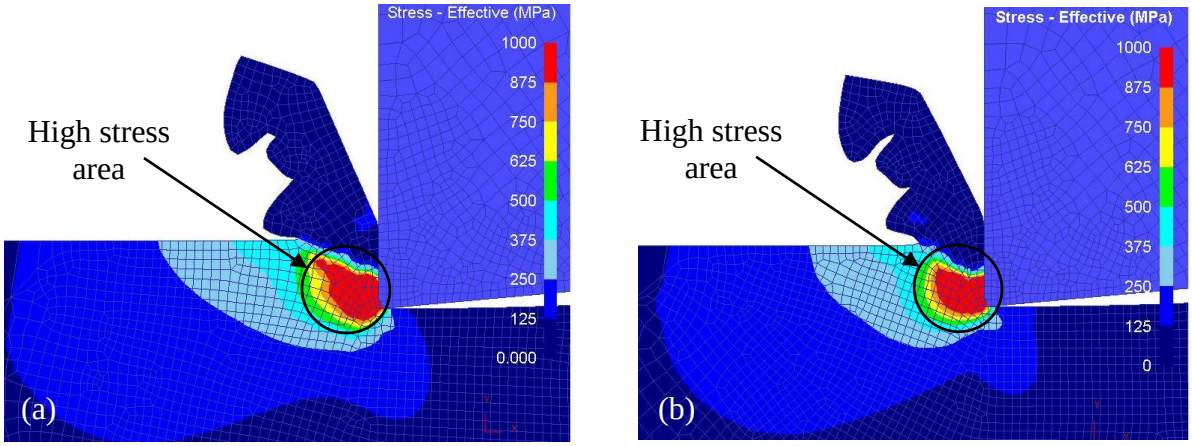

Figure 8, Effective stress with a speed of 150 m/min, a) Conventional cutting, b) LAM.

9.5.Material damage and crack initiation

To study the crack initiation with segmented chips, the Quick Stop Device (QSD) was used in order to freeze the process of segmentation. The QSD test is a long and tedious experiment which implies careful manipulation in order to observe the morphology of chip formation. Multiple QSD tests are required in order to be able to capture the exact moment of the segmentation initiation.

Figure 9 shows evidence that the crack starts at the surface. However in order for the crack to start, a material displacement is suspected to emerge from the inside of the "to be formed segment". The crack initiation may start at irregularities of the machined surface or grain boundaries. However, it is difficult to determine if the crack appeared first and then the ASB

formed, or if it is a mutual phenomenon where the crack initiation and ASB formation work concurrently and end up in chip segmentation.

The elongated grains observed in the ASB region in Figure 9 indicate that the ASB is still not fully formed, as the grain boundaries do not show close and parallel lines. This is in favor of the theory that the crack is first initiating at the free surface before the formation of a clear ASB. The conventional and LAM simulations in Figure 10 show also that the damage does not start at the tool tip as some other previous studies suggested. The highest damage values appear to be along the primary shear zone, and close to the free surface which is the region where the segmentation will occur.

This indicates that the Cockcroft-Latham (C-L) damage theory is well adapted for the simulation of the ASB formation. The C-L theory of damage was first developed for tensile tests, in a "quasi static" environment. However, once the model's constant is adjusted for conditions involving high hydrostatic stresses with high strain and strain rates, the damage criterion gave satisfactory results in machining simulations.

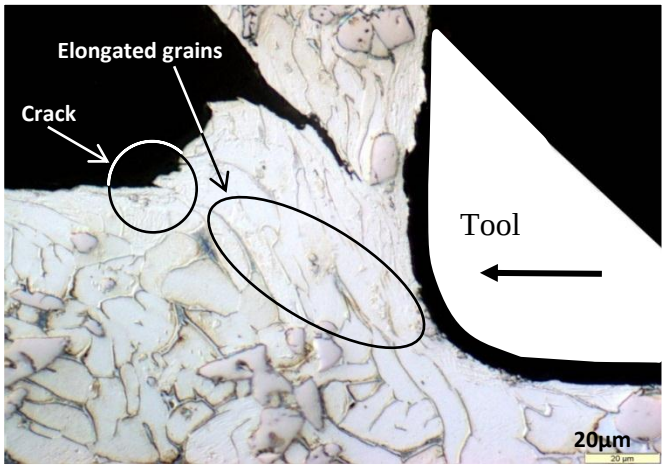

Figure 9, A quick stop test showing the chip formation and an apparent crack initiation at the speed of 60 m/min.

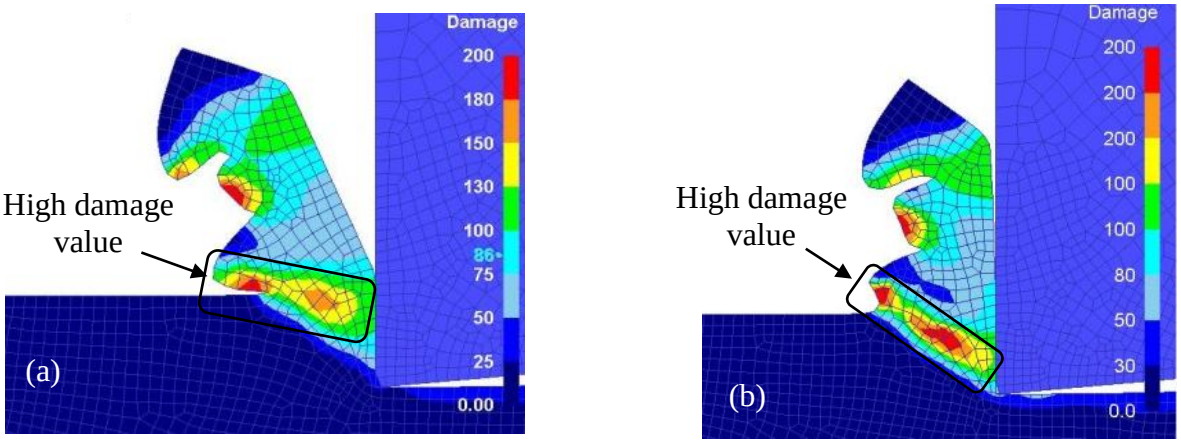

Figure 10, Damage value with a speed of 150 m/min, a) conventional, b) LAM.

9.6.Temperature profiles

Figure 11 (a) shows the temperature profile for conventional simulation at the speed of 150 m/min. As shown, the secondary shear zone is the region with the highest temperature with an average peak temperature of 803 °C and the typical average temperature inside the ASB is below 600 °C.

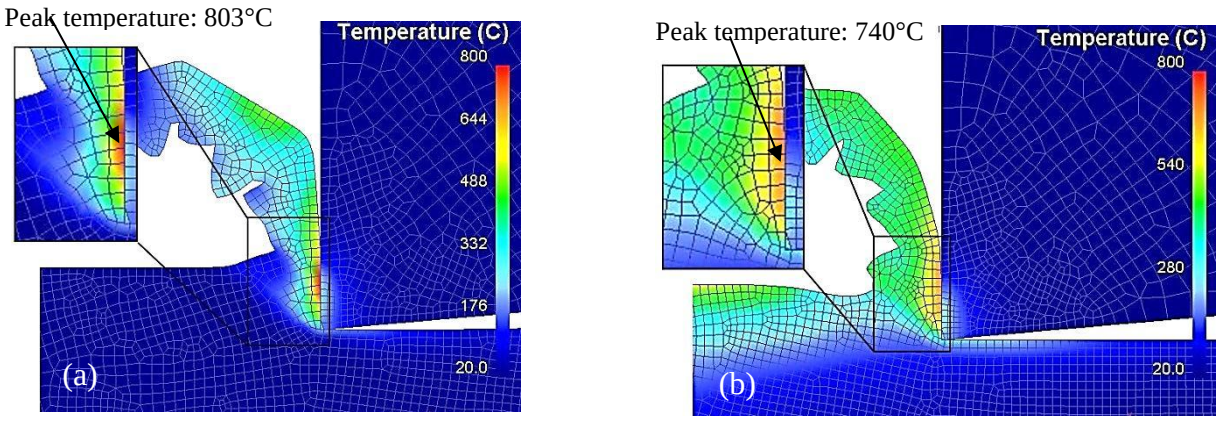

Figure 11, Temperature profile at150 m/min, a) Conventional cutting, b) LAM.

It is experimentally very difficult to measure the temperature of the ASB. However, the Titanium alloy matrix incurs a phase transformation at the temperature of 883°C [36]. To confirm if a phase transformation occurred in the ASB, a Transmission Electron Microscopy (TEM) test was performed inside the ASB. Figure 12 shows a TEM microstructure of a chip taken inside the ASB. Selected Area Diffraction (SAD) was performed on different regions as indicated by circles in Figure 12. The orientation angles were all within 2 degrees indicating that those microstructures are sub-grains. The microstructure inside the ASB is composed of elongated nano-cells, with a presence of some equiaxed nano-grains. All lattices structures for the subgrains inside the ASB were indexed and found to correspond to Alpha type. No traces of Beta or Alpha prime (martensite) were found. Therefore, phase transformation within the Adiabatic Shear Band is unlikely; which consolidate the FEM simulation results, since the temperature observed inside the ASB is lower than the phase transformation temperature of 883°C. The typical temperature inside the ASB of 600°C shown by the FEM simulations, indicates that the recrystallization temperature was reached ($T_{recrystallization}$ = 500 ~ 690° C for the matrix alloy). Experimentally this is confirmed by the TEM tests, since some grains show a remarkably higher difference in orientation angles (approximately 15 degrees), indicating that some recrystallized grains were also formed inside the ASB.

As a difficult to cut material, Titanium alloys have generated considerable interest among researchers. Che-Haron [39] noted that increased wear rate was detected with the increase in speed. For Ti-6Al-4V, the combination of low thermal conductivity and a very thin chip results in very high cutting temperature concentrated in a small area on the tool-chip interface. This high temperature combined with the strong chemical reactivity of Titanium result in high affinity to almost all tool materials at cutting temperatures over 500°C and resulted in diffusion wear which limited tool life [40].

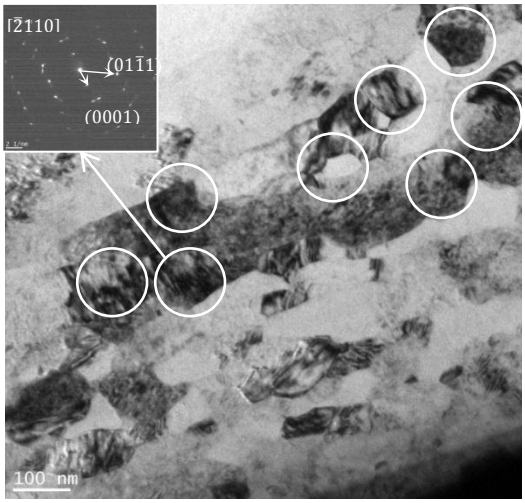

Figure 12, Bright field imaging showing sub-grains inside the ASB. The circles show the location of the taken SAD, and the inset is the SAD of the arrowed cell.

Comparing the temperature profile of LAM and conventional machining in the FEM simulation for the same cutting speed, one could project that the added surface temperature will increase substantially the chip temperature (Figure 11). In fact, the average temperature in the middle of the chip (but not inside the ASB zone) is 476°C with LAM compared to 310°C in conventional machining. However, the average peak temperature, which is located in the tool/chip interface area, appears to be lower with LAM than when conventional machining (740°C with LAM and 803°C in conventional machining).

As commonly known, most of the heat generated in machining goes into the chip. The main heat generation sources while cutting are in the shear plane and on the tool chip-interface. Under LAM conditions, the softened material will result in reduced heat generation in the shear plane due to a reduced yield stress. In addition, the reduced cutting forces with LAM will result in a reduction of friction and heat generation at the tool/chip interface.

In our previous work on LAM of TiMMC [13], it was shown that LAM can increase tool life up to 180%, since the laser heating creates a material softening effect and alters the tool-particle interaction, as well as, the tool wear mechanism. The FEM study also shows that LAM reduces the peak tool/chip interface temperature, which reduces diffusion wear and leads to a higher tool life. This observation is one probable reason for the increased tool life which was observed experimentally when using LAM on TiMMC [13].

10. CONCLUSIONS

Very little work has been performed on Finite Element Method (FEM) simulation with Laser Assisted Machining (LAM), and no work has been found before for the simulation of segmented chips with LAM. In this research, a new constitutive model for an equivalent homogenous material of TiMMC was developed and validated experimentally. To simulate the segmentation phenomenon, a damage model was introduced with a fixed value of damage constant. The FEM simulations were validated experimentally where the cutting force and chip segmentation's pitch and thickness were validated with actual experimental tests.

High strains values were shown to be present in the adiabatic shear bands (ASB) and secondary shear zone. The same observation was found by the chips' microstructure micrographs. Furthermore, the effect of high cutting speed, as well as, LAM resulted in a reduction of the cutting forces.

The Cockcroft-Latham model was shown to be well adapted to machining with high temperatures and high strain rates conditions. In FEM simulations, the highest damage values appeared to be along the primary shear zone, and close to the free surface. The quick stop tests showed that the segmentation is initiated by a crack at the free surface before the full formation of an adiabatic shear band.

Experimental Transmission Electron Microscopy (TEM) observations indicated that no phase transformation occurred in the ASB. This was also supported by the simulation of the temperature profiles inside the ASB which were less than the phase transformation temperature of 883C°.

Diffusion wear is a main issue when machining Titanium alloys. Using the FEM temperature profiles; a possible reason for the increased tool life when using LAM was explained. Paradoxically, adding a heat source to the workpiece's surface, results in a reduced peak temperature in the tool/chip interface, even though the overall chip average temperature is increased. The reduced peak tool/chip temperature diminishes the diffusion wear effect, which can increase tool life.

ACKNOWLEDGEMENT

The authors wish to acknowledge Dynamet Technology Inc., for providing the material. The support of the Aerospace Manufacturing Technology Centre, National Research Council Canada (AMTC-NRC), and the NSERC Canadian Network for Research and Innovation in Machining Technology (CANRIMT) are also acknowledged.

REFERENCES

[1] Recht, R., F., ''Catastrophic Thermoplastic Shear,'' *ASME J. App Mech.*, 31, 1964, pp. 189–192.

[2] Nakayama, K., Arai, M., and Kada, T., ''Machining Characteristics of Hard Materials,'' *CIRP Ann*., 37(1), 1988, pp. 89–92

[3] Konig, W., Berktold, A., and Koch, K.-F., ''Turning Versus Grinding—A Comparison of Surface Integrity Aspects and Attainable Accuracies,'' *CIRP Ann.*, 42(1), 1993, pp. 39–43

[4] Shaw, M.C., Vyas, A., "Chip Formation in the Machining of Hardened Steel", *CIRP Annals - Manufacturing Technology*, Volume 42, Issue 1, 1993, pp. 29-33

[5] Komanduri, R., Schroeder, T., Hazra, J., von Turkovich, B. F., and Flom, D. G., ''On the Catastrophic Shear Instability in High-Speed Machining of an AISI 4340 Steel,'' *ASME J. Eng. Ind.*, 104, 1982, pp. 121–131

[6] Komanduri, R., "Some clarifications on the mechanisms of chip formation when machining titanium alloys", *Wear*, 1982, 76: 15–34

[7] Marusich, T. D. and Ortiz, M., "Modelling and simulation of high-speed machining", *Int. J. Numer. Meth. Eng.*, 1995, 38: 3675–3694

[8] Guo Y.B., David W. Yen, "A FEM study on mechanisms of discontinuous chip formation in hard machining", *Journal of Materials Processing Technology*, V155–156, 2004, pp. 1350-1356

[9] Calamaz M., Coupard D., Girot F., "A new material model for 2D numerical simulation of serrated chip formation when machining titanium alloy Ti–6Al–4V", *International Journal of Machine Tools and Manufacture*, Volume 48, Issues 3–4, 2008, pp.275-288

[10] Umbrello D., "Finite element simulation of conventional and high speed machining of Ti6Al4V alloy", *Journal of Materials Processing Technology*, Volume 196, Issues 1–3, 21, 2008, pp.79-87

[11] Lorentzon J., Järvstråt N., Josefson B.L., "Modelling chip formation of alloy 718", *Journal of Materials Processing Technology*, Volume 209, Issue 10, 1, 2009, pp.4645-4653

[12] Attia H., Tavakoli S., Vargas R., Thomson V., "Laser-Assisted High Speed Finish of Superalloy Inconel 718 under Dry Conditions", *Annals of the CIRP*, 2010, 59: 83–88

[13] Bejjani R., Shi B., Attia H., Balazinski M., "Laser assisted turning of Titanium Metal Matrix Composite", *CIRP Annals - Manufacturing Technology*, Volume 60, Issue 1, 2011, pp 61-64

[14] Shi, B.; Attia, H.; Vargas, R.; "Numerical and experimental investigation of laser-assisted machining of Inconel 718", *Machining Science and Technology*, 12(4), 2008, pp.498-513

[15] Germain G., Dal Santo P., Lebrun J.L., "Comprehension of chip formation in laser assisted machining", *International Journal of Machine Tools and Manufacture*, Volume 51, Issue 3, 2011, pp.230-238

[16] Shi, B., Attia, H., Tounsi, N., "Identification of Material Constitutive Laws for Machining-Part I: An Analytical Model Describing the Stress, the Strain, the Strain Rate, and the Temperature Fields in the Primary Shear Zone in Orthogonal Metal Cutting". *ASME Journal of Manufacturing Science and Engineering*, Vol. 132, No.5, 2010, 051008 (11 pages)

[17] Shi, B. and Attia, H., "Current Status And Future Direction In The Numerical Modeling And Simulation Of Machining Processes: A Critical Literature Review", *Machining Science & Technology*, 2010, 14: 149-188

[18] Shi, B., Attia, H. and Tounsi, N., "Identification of Material Constitutive Laws for Machining-Part II: Generation of the Constitutive Data and Validation of the Constitutive Law". *ASME Journal of Manufacturing Science and Engineering*, Vol. 132, No.5, 2010, 051009 (9 pages)

[19] P. L. B. Oxley, "Mechanics of Machining, An Analytical Approach to Assessing Machinability", *Haisted Press, John Wiley & Sons Limited*, 1989, New York

[20] Bejjani, R., Balazinski, M., Helmi, A., Shi, B. "New Design of Quick Stop Device for Research on Chip Formation", *transactions NAMRI-SME* , 2010, *V38*

[21] Daymi, A., Boujelbene, M., Ben Salem S., Hadj Sassi, B., Torbaty S., "Effect of the cutting speed on the chip morphology and the cutting forces", *Computational Materials Science & Surface Eng.*, 1, 2, 2009, 77-83

[22] Johnson, G. R., and Cook, W. H., "A Constitutive Model and Data for Metals Subjected to Large Strain, High Strain Rates and High Temperatures," *Proceedings of the Seventh International Symposium on Ballistics*, The Hague, The Netherlands, 1983, pp. 541–547

[23] Smallman R.E., Bishop R.J., "Modern Physical Metallurgy and Materials Engineering", Sixth Edition, *Elsevier Ltd.*, 1999

[24] Adams, K. H., "Dislocation mobility and density in zinc single crystals", Dissertation (Ph.D.), *California Institute of Technology*, 1965

[25] Owolabi G. M., Odeshi A. G., Singh M.N.K., Bassim M.N., "Dynamic shear band formation in Aluminum 6061-T6 and Aluminum 6061-T6/Al2O3 composites", *Material Science & Eng.*, A, 457, 2007, 114-119

[26] Deform™ – User Manual, SFTC- Deform V9.0.1 *Scientific Forming Technologies Corporation* Ed. Columbus, OH, USA, 2006

[27] Baker M., Rösler J., Siemers C., "A finite element model of high speed metal cutting with adiabatic shearing", *Computers and Structures* 80 (5,6), 2002, pp. 495–513

[28] McClintock, F. A., "A Criterion for Ductile Fracture by the Growth of Holes", *ASME Journal of Applied Mechanics*, 1968, pp. 363

[29] Cockroft, M. G., Latham, D. J.,"Ductility and workability of metals", *Journal of the Institute of Metals* , 1968, 96:33-39

[30] Tönshoff H.K., Arendt C., Ben Amor R., "Cutting of Hardened Steel", *CIRP Annals - Manufacturing Technology*, Volume 49, Issue 2, 2000, pp 547-566

[31] Xu Y., Bai Y., Meyers M.A., "Deformation, Phase Transformation and Recrystallization in the Shear Bands Induced by High-Strain Rate Loading in Titanium and Its Alloys*", J. Mat. Sci. Tech.* 22(06), 2006, pp. 737-746

[32] Murr, L.E., Trillo, E.A., Pappu, S., Kennedy, C., "Adiabatic shear bands and examples of their role in severe plastic deformation", *J. Mater. Sci.*37, 2002, pp. 3337–3360

[33] Q. Li, E. Chen, D. Bice, and D. Dunand, "Transformation Superplasticity of Cast Titanium and Ti-6Al-4V", *Metallurgical and Materials Transactions A*, 38 [1], 2007, 44-53

[34] Childs, T. H. C., Dirikolu M.H., Maekawa K., "Modelling of friction in the simulation of metal machining" In: *24th Leeds-Lyon Symposium on Tribology*. Amsterdam: Elsevier Tribology Series, 1998, 34:337-46

[35] Childs, T.H.C., "Friction modelling in metal cutting", *Wear*, Volume 260, Issue 3, 10, 2006, pp 310-318

[36] Karpat, Y.; Özel OK, T.,"Mechanics of high speed cutting with curvilinear edge tools". *International Journal of Machine Tools & Manufacture*, 2008, 48(2):195–208

[37] Zhang, YC., "On methodologies inside two different commercial codes to simulate the cutting operation", *Advanced material research, trans tech publications Switzerland*, 2011, v:223-162-171

[38] Kim, I.Y. Choi, B.J.; Kim, Y.J.; Lee, Y.Z., "Friction and wear behavior of titanium matrix (TiB+TiC) composites", *Wear*, v 271, n 9-10, , 2011, pp 1962-5, 29

[39] Che-Haron, C. H., "Tool life and surface integrity in turning titanium alloy", *Journal of Materials Processing Technology*, 118, 2001, pp.231-237

[40] Machado, A.R.; Wallbank, J.; "Machining of Titanium and its alloys-a review"; Proceedings of the institute of mechanical engineers Part-B: *Journal of Engineering Manufacture* 204, 1990, pp53-60

APPENDIX B: LIST OF PUBLICATIONS

- **REFEREED JOURNALS PAPERS**

- R. Bejjani, B. Shi, H. Attia, M. Balazinski*," Simulation of Segmented Chip Formation in Laser Assisted Machining of Titanium Metal Matrix Composite",* (submitted in Sept. 2012, International Journal of Machine Tools and Manufacture, Ref: IJMACTOOL-D-12-00567).

- R. Bejjani, M. Balazinski, H. Attia, G. L'Espérance,*" On The Adiabatic Shear Banding And Microstructure Evolution When Machining Titanium Metal Matrix Composites",* (submitted in June 2012, ASME, Journal of Manufacturing Science and Engineering, REF: MANU-12-1170).

- R. Bejjani, B. Shi, H. Attia, M. Balazinski,*" Laser assisted turning of Titanium Metal Matrix Composite"* , CIRP annals, vol. 60, "1", pp.61-65, 2011.

- R. Bejjani, M. Balazinski, B. Shi, H. Attia, H. Kishawy, *"Machinability and Chip Formation of Titanium Metal Matrix Composites"*, Int. J. of Advanced Manufacturing Systems, IJAMS, vol. 13, "1" , 2011.

- **REFEREED CONFERENCE PAPERS**

- R. Bejjani, M. Balazinski, H. Attia, H. Kishawy*," A study on adiabatic shear banding in chip segmentation when cutting TiMMC"*, 1st Intl. Conf. Virtual Machining Process Tech./CIRP, 2012.

- R. Bejjani, M. Aramesh, M. Balazinsk, H. Kishawy, H. Attia, *"Chip morphology Study of Titanium metal matrix composites"*, 23rd Canadian Congress of Applied Mechanics, pp. 499-502, 2011.

- R. Bejjani, M. Balazinski, B. Shi, H. Attia, M. Aramesh, H. Kishawy, *"Segmentation and shear localization when turning TiMMC (Titanium Metal Matrix Composites)"*, 26th Tech. conf., American Society of Composites, 2011.

- M. Aramesh, Balazinski M., H. Kishawy, H. Attia, **R. Bejjani,** *"A Study on Phase Transformation and Particle Distribution During Machining TiMMC Composites"***,** 26th Tech. conf., American Society of Composites, 2011.

- R. Bejjani, H. Attia, M. Balazinski, B. Shi, *"A NEW DESIGN OF QUICK STOP DEVICE FOR RESEARCH ON CHIP FORMATION"*, Transactions of NAMRI/SME, vol. 38 pp.269-274, 2010.

- R. Bejjani, B. Shi, H. Attia, M. Balazinski, H. Kishawy, *"Machinability of titanium metal matrix composites"*, Proceedings CIRP 2nd conf. Process Machine Interactions, C12, 2010.

APPENDIX C1: CONVENTIONAL TURNING EXPERIMENT DETAILS

Experimental set up

Some industrial considerations were taken for machining TiMMC, therefore, all experiments were performed in dry machining conditions, and a selection of the appropriate cutting tool was based on previous data for machining Aluminum MMC. Furthermore tool manufacturer's recommendations were taken into account.

Tools used

Following the literature review, poly crystalline diamond (PCD) tools due to their higher hardness than most of the common reinforcements provide better tool life. However, because of high cost of PCD tools, other tools like cemented carbides and ceramics were also used to machine MMC materials [7].

In our tests, two kinds of tools are used, PCD (Polycrystalline Diamond) RNMN from KY-Diamond, round 0.5" diameter PCD insert. The Carbide tool is manufactured by SECO: CNMG coated carbide. The tools were recommended by the manufacturers.

Separate experiments were carried out for Carbide and PCD tools. The objective was not to compare the two tools, but more to evaluate the results and effectiveness of each tool. An L8: 4*2: Taguchi array was used; this consists of 4 speeds and 2 feeds for each tool.

The selection of cutting parameters was as below:

- For the PCD tool, the speed ranged from 60 to 230 m/min, the feed 0.1 and 0.2 mm/rev. and the depth of cut was kept: 0.15mm (Table 1).
- For the Carbide tool: the speed ranged from: 50 to 120m/min, the feed and depth same as above (Table 2).

The total length of cut of each test was 40mm. The material used has 10-12% TiC particles in matrix of Ti-6Al-4V. It is cylindrical with a diameter of around: 125mm.

The choice of optimums:

For each tool, the optimum cutting parameters gave the best Ra with the lowest VB. Also, the cases where the chips caught fire were not considered for optimum conditions.

Taguchi Array

PCD tool

Table 1- The Taguchi array used for the PCD tool

Test #	v [m/min]	f [mm/rev]	d [mm]	L cut [mm]	Ra [μm]	VB [mm]
1	60	0.1	0.15	38.65	0.386	0.32
2	60	0.2	0.15	38.65	0.356	0.2
3	100	0.1	0.15	38.55	0.293	0.24
4	100	0.2	0.15	38.35	0.32	0.2
5	180	0.1	0.15	38.25	0.266	0.12
6	180	0.2	0.15	38.15	0.34	0.091
7	230	0.1	0.15	37.95	0.353	0.1
8	230	0.2	0.15	38.05	0.353	0.098

Note here that the higher the Signal to Noise ratio (SN) the better the surface roughness is (or the lower the Ra). The measurements of surface roughness were made using a portative tool from Taly-Surf. A sample of surface profile can be seen in Figure 1.

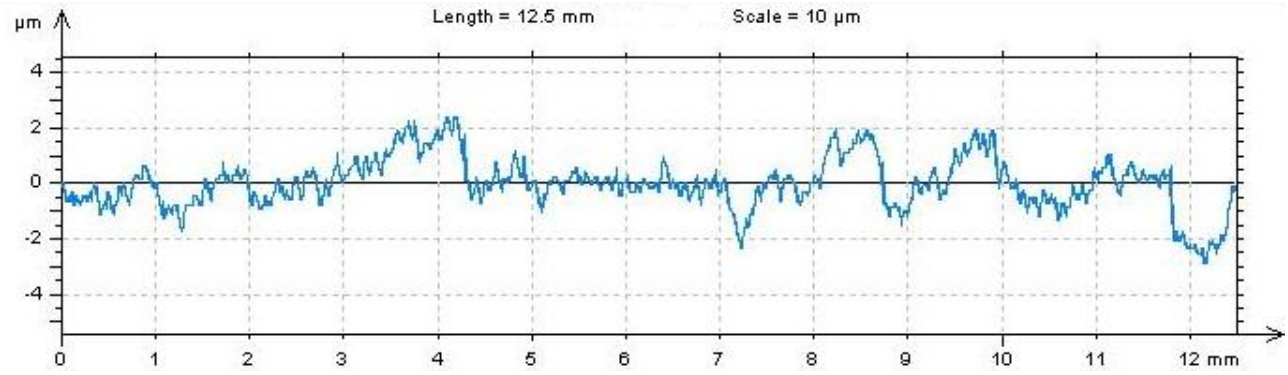

Figure 1, Surface roughness profile. Cutting parameter: speed 170m/min feed: 0.2 mm/rev.

Carbide tool

Table 2- The Taguchi array used for the carbide tool

Test #	v [m/min]	f [mm/rev]	d [mm]	L cut [mm]	Ra [μm]	VB [mm]
1	50	0.1	0.15	39.9	0.73	0.2
2	50	0.2	0.15	39.8	1.27	0.19
3	70	0.1	0.15	39.7	0.56	0.25
4	70	0.2	0.15	39.6	1.29	0.14
5	90	0.1	0.15	39.5	0.51	0.23
6	90	0.2	0.15	39.4	1.33	0.28
7	120	0.1	0.15	39.3	0.51	0.62
8	120	0.2	0.15	39.2	1.24	0.73

Tool Wear

The process of abrasion while cutting MMC is somewhat different from the standard process of cutting metal. In fact, due to the high abrasion in the material itself; both two-body and three-body models have been generally accepted as mechanical abrasive wear mechanisms [3, 7, 42]. In our experiments, the tests stopped once a value of 0.3mm was reached for $VB_{b\ max}$; subsequently, pictures of worn tool were taken by optical microscopes.

APPENDIX C2: TAGUCHI ORTHOGONAL ARRAY

Taguchi orthogonal array

The most common way of design experiments is the factorial type DOE (design of experiments); however, in order to be more efficient and reduce the costly number of experiments a good approach known as Taguchi Parameter Design was used for our experiments. As a type of fractional factorial design, Taguchi Parameter Design is similar to traditional DOE methods in that multiple input parameters can be considered for a given response. The Taguchi Parameter Design uses the non-linearity of a response parameter to decrease the sensitivity of the quality characteristic to variability. Furthermore, Taguchi Parameter Design leads to maximize the performance of a naturally variable production process by modifying the controlled factors [28].

In our case, in order to optimize the surface roughness or the lowest value of Ra, the smaller the better procedure was used (to minimize Ra).

Depending on objectives, the Taguchi method defines three different forms of mean square deviations (i.e., signal-to-noise ratios: S/N) including the nominal-the-better, the larger-the-better and the smaller-the-better. The signal-to-noise ratios can be considered as an average performance characteristic value for each experiment [28]. Figure 1 shows the basic steps using this technique [43]:

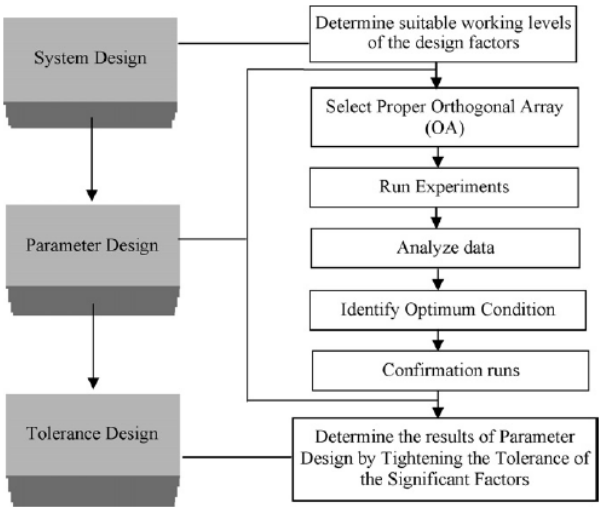

Figure 1, Taguchi method flowchart [43]

Orthogonal array:

The purpose of the orthogonal array is to efficiently determine the optimum turning operation parameters for achieving the lowest surface roughness in that range of parameters while considering a noise factor.

For example, an L9 orthogonal array will have up to 4 control variables, with 3 levels each in addition to noise Factors (Table 1). Therefore 9 runs will be needed, and this for each NOISE factor. With 2 noise factors, and 2 tools, this will sum up to: 9*2*2= 36 experiments or runs.

For our case, some of the following features were used:

- The use of an array with the fewest experimental runs possible.
- Relationships between the control parameters and the response parameter.
- The use of 2 different tools inserts (Carbide and PCD).
- Effects of the noise parameter on the response parameter.
- Optimum turning operation parameters for surface roughness, given this noise factor.

Where, the response variable is: R_a (surface roughness), and the following controlled variable can be used (with the levels for each variable):

- A: spindle speed (v), (LOW, MEDIUM, HIGH)
- B: feed rate (f), (LOW, MEDIUM , HIGH)
- C: depth of cut (d), (LOW, HIGH)
- D: tool type, (PCD or carbide)

Noise factors:

Noise factors are usually uncontrolled variables, and could be chosen as:

- X: temperature range for cutting, (LOW, HIGH)
- Y: condition of tool, (NEW , WORN)

Table 1. An example of orthogonal array.

					Outer noise array				
					X	1	1	2	2
					Y	1	2	1	2
Inner control factor array									
Run	A	B	C	D		N1	N2	N3	N4
1	1	1	1	1					
2	1	2	2	2					
3	1	3	3	3					
4	2	1	2	3					
5	2	2	3	1					
6	2	3	1	2					
7	3	1	3	2					
8	3	2	1	3					
9	3	3	2	1					

To reduce the time and cost of experiments, it was intended to allow the selection of an orthogonal array with as few runs as possible, while still allowing for a robust experiment.

Signal to noise factor

Using smaller the better equation (to minimize R_a), the signal to noise (S/N) factor was plotted for each control variable. For that, the mean R_a was calculated for each run, and the corresponding S/N used is [28]:

$$\eta = -10 \log \left[\frac{1}{n} \left(\sum y_i^2 \right) \right]$$

Where η = the S/N ratio; y_i = the individual surface roughness measurements in a run for both noise conditions; and n = the number of replications (in this case, n = 9).

Confirmation run

After choosing the optimum values (or levels) for each controlled variable, the combination of selected control parameter values was not actually carried out in the experiment.

Taguchi method selects only a small number of combinations of control variables (rather than all combinations as in the full factorial design of experiment). Due to this situation, a confirmation run is needed in order to validate the results.

The objective of the confirmation run is to determine that the selected control parameter values would produce better surface finishes than all those runs already done in the first part of

the experiment. For this, multiple runs should be done using the same parameters chosen as optimal. The confirmation run should show a R_a with a value lower or equal than all runs already done before.